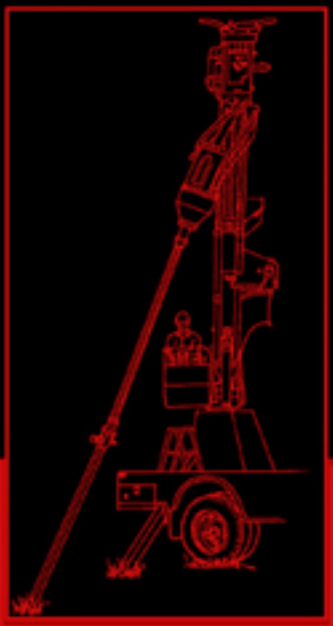

Second Edition

EARTH ANCHORS

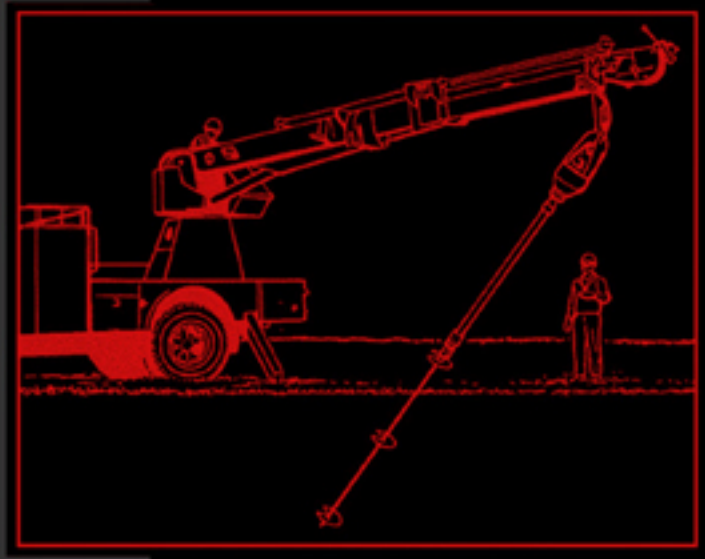

Braja M. Das
Sanjay Kumar Shukla

EARTH ANCHORS

Second Edition

Braja M. Das
Sanjay Kumar Shukla

J.ROSS PUBLISHING

ISBN 978-1-60427-077-8

Printed and bound in the U.S.A. Printed on acid-free paper
10 9 8 7 6 5 4 3 2 1

Library of Congress Cataloging-in-Publication Data

Das, Braja M., 1941-
Earth anchors / by Braja M. Das and Sanjay Kumar Shukla. — Second edition.
pages cm
Includes bibliographical references and index.
ISBN 978-1-60427-077-8 (hardcover : alk. paper) 1. Foundations. 2. Anchorage (Structural engineering) I. Shukla, Sanjay Kumar. II. Title.
TA775.D226 2013
624.1′5—dc23

2013010895

Direct all inquiries to J. Ross Publishing, Inc., 300 S. Pine Island Road, Suite #305, Plantation, Florida 33324.

Phone: (954) 727-9333
Fax: (561) 892-0700
Web: www.jrosspub.com

TABLE OF CONTENTS

PREFACE

Anchors are primarily used in the construction of foundations for earth-supported and earth retaining structures. The fundamental reason for using earth anchors in construction is to transmit the outwardly directed load to the soil at a greater depth and/or farther away from the structure. Although earth anchors have been used in practice for several hundred years, proper theoretical developments for purposes of modern engineering design have taken place only during the past 40 to 45 years or so. This book summarizes most theoretical and experimental works related to the development of proper relationships for ultimate and allowable holding capacities of earth anchors.

The first edition of this book was published with a 1990 copyright by Elsevier Science Publishers B.V., Amsterdam, The Netherlands, in the Developments in Geotechnical Engineering Series (No. 50). It was reprinted with a 2007 copyright by J. Ross Publishing in their Classics Series. Sanjay Kumar Shukla is the co-author of this second edition. The book now has a total of ten chapters. In this edition, the following major changes have been made:

- Horizontal plate anchors in sand are presented in Chapter 2 and horizontal plate anchors in clay in Chapter 3.
- Helical anchors are now presented in two chapters: anchors in sand in Chapter 6 and anchors in clay in Chapter 7. A discussion on single-helix screw anchors in sand has been added to Chapter 6.
- Two new chapters have been added: suction and caisson anchors (Chapter 9) and geo-anchors (Chapter 10).
- A summary section has been included for each chapter.

- Self-assessment multiple-choice questions, followed by answers, are given at the end of each chapter.

In all chapters, the discussions have been limited to the failure mechanisms in the soil and procedures to calculate the ultimate and allowable loads. No attempt has been made to describe the construction procedures for installation of the anchors. Modifications to the contents of the book in future editions will, of course, be necessary with future developments and changes in the state-of-the-art. We hope this book will be helpful to designers and researchers working in the area of earth anchors.

Thanks are due to Janice Das for preliminary editing and providing other help during the preparation of the text. The authors are grateful to Tom Bowling of Entura Hydro Tasmania of Australia for several meaningful suggestions during the preparation of this text. Thanks are also due to Sandy Pearlman, the project editor, who did an outstanding job in putting the entire manuscript together in a very short period of time. We truly appreciate the help of Steve Buda of J. Ross Publishing for undertaking the task of publishing this edition of the book.

Braja M. Das
Sanjay Kumar Shukla

THE AUTHORS

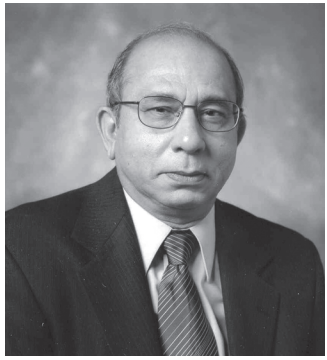

Professor Braja M. Das is Dean Emeritus of the College of Engineering and Computer Science at California State University, Sacramento. He received his M.S. in civil engineering from the University of Iowa and his Ph.D. in the area of geotechnical engineering from the University of Wisconsin. He is the author of several geotechnical engineering texts and reference books and has authored more than 250 technical papers in the area of geotechnical engineering. His primary areas of research include shallow foundations, earth anchors, and geosynthetics. He is a Fellow and Life Member of the American Society of Civil Engineers, a Life Member of the American Society for Engineering Education, and an Emeritus Member of the Chemical and Mechanical Stabilization Committee of the Research Board of the National Research Council (Washington, D.C.). He was previously a member of the editorial board of the *Journal of Geotechnical Engineering* (ASCE), a member of the *Lowland Technology International* journal (Japan), associate editor of the *International Journal of Offshore and Polar Engineering* (ISOPE), and co-editor of the *Journal of Geotechnical and Geological Engineering* (Springer, The Netherlands). Presently, he is the Editor-in-Chief of the *International Journal of Geotechnical Engineering* (Maney Publishing, U.K.).

Dr. Sanjay Kumar Shukla is an Associate Professor and Program Leader of the Discipline of Civil Engineering at the School of Engineering, Edith Cowan University, Perth, Australia. He graduated in 1988 with a first-class degree with distinction in civil engineering from the Ranchi University, Ranchi, India and received his M.Tech. and Ph.D. degrees in 1992 and 1995, respectively, in civil engineering from the Indian Institute of Technology, Kanpur, India. He is a Fellow of Engineers Australia, a Life Fellow of the Institution of Engineers (India) and Indian Geotechnical Society, and a member of the American Society of Civil Engineers and the International Geosynthetics Society. He has more than 20 years of teaching, research, and consultancy experience in the field of geotechnical and geosynthetic engineering. He serves on the editorial boards of the *International Journal of Geotechnical Engineering* and the *Indian Geotechnical Journal* and is the Scientific Editor of the *Journal of Mountain Science.* He has authored and edited 4 books and 12 book chapters. He is also an author of 117 research papers and technical articles, including 73 refereed journal publications.

1

EARTH ANCHORS: GENERAL

Earth anchors are constructed to resist the loads which cause instability to structures such as foundations, earth retaining structures, and slopes. During the last three to four decades, the experimental and mathematical research works relating to earth anchors have accelerated, and the results of those works have been published in various technical journals and conference proceedings. This chapter introduces the very basic description of earth anchors and most of their types commonly used in geotechnical engineering structures. A comprehensive review of the specific anchor types and their engineering aspects is presented systematically in the following chapters.

1.1 INTRODUCTION

Anchors used in soil and rock, commonly called *earth anchors,* are primarily designed and constructed to resist outwardly directed loads imposed on structures such as foundations, earth retaining structures, and slopes. These outwardly directed loads are transmitted to the soil and rock at a greater depth by the anchors.

Buried anchors have been used for thousands of years to stabilize structures. Tents are the oldest structures which were stabilized by using anchors or stakes. Until the middle of the 19th century, anchors were primarily used for stabilizing fairly lightweight structures. With the design and construction of large suspen-

sion bridges, very large loads were transmitted to the bridge foundations. In order to support these loads, permanent anchoring systems in rock medium were gradually developed and constructed.

With the development and construction of special lightweight structures such as lattice transmission towers and radar towers, design of special tension anchoring systems for foundations became necessary, primarily because the wind load created reactions that were greater than the self-weight of the structures.

Earth anchors of various types are now used for uplift resistance of transmission towers, utility poles, aircraft moorings, submerged pipelines, and tunnels. Anchors are also used for tieback resistance of earth retaining structures, waterfront structures, at bends in pressure pipelines, and when it is necessary to control thermal stress.

The earlier forms of anchors used in soil for resisting vertically directed uplifting loads were *screw anchors.* Figure 1.1 shows two different configurations of screw anchors. These anchors were simply twisted into the ground up to a pre-estimated depth and then tied to the foundation. They were used either singly or in groups.

In general, at the present time, earth anchors can be divided into seven basic categories: *plate anchors, direct embedment anchors, helical anchors, grouted anchors, anchor piles* and *drilled shafts, suction caisson* and *drag anchors,* and *geo-anchors.* Some authors refer to plate anchors as direct embedment anchors.

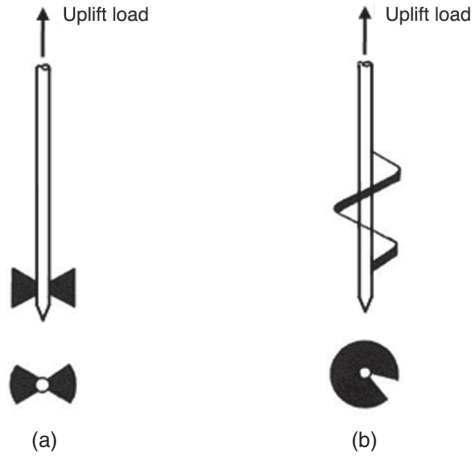

FIGURE 1.1 Two different configurations of screw anchors

1.2 PLATE ANCHORS

Plate anchors may be made of steel plates, precast concrete slabs, poured concrete slabs, timber sheets, and so forth. They may be horizontal to resist vertically directed uplifting load, inclined to resist axial pullout load, or vertical to resist horizontally directed pullout load, as shown in Figures 1.2a to 1.2c. These anchors can be installed by excavating the ground to the required depth and then backfilling and compacting with good quality soil. They may be referred to as *backfilled plate anchors* (Figure 1.3a). In many cases, plate anchors may be installed in excavated trenches, as shown in Figure 1.3b. These anchors are then attached to tie-rods, which may either be driven or placed through augered

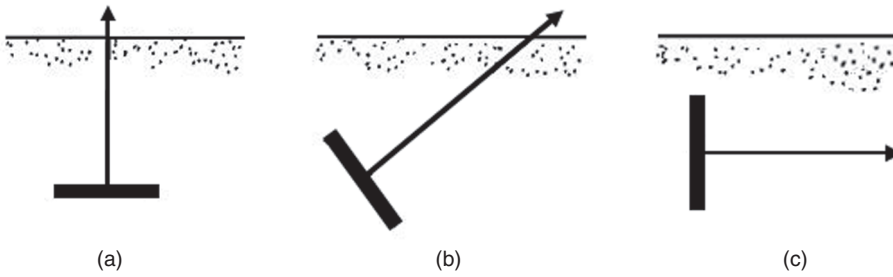

FIGURE 1.2 Plate anchors: (a) horizontal plate anchor, (b) inclined plate anchor, and (c) vertical plate anchor

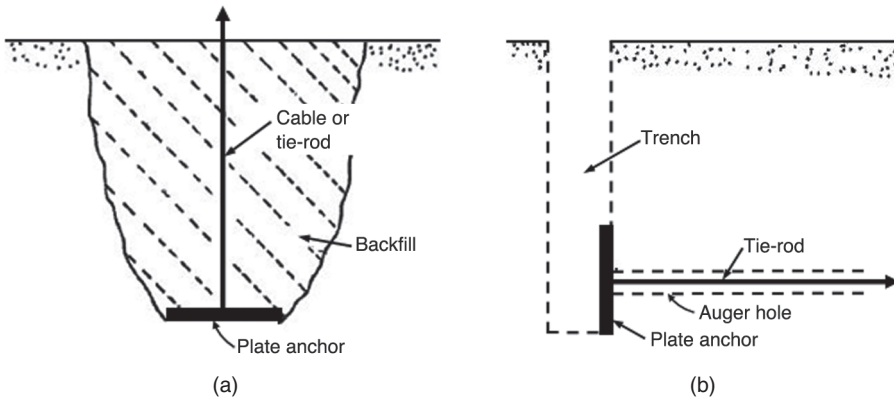

FIGURE 1.3 Installation of plate anchors: (a) backfilled plate anchor and (b) direct bearing plate anchor

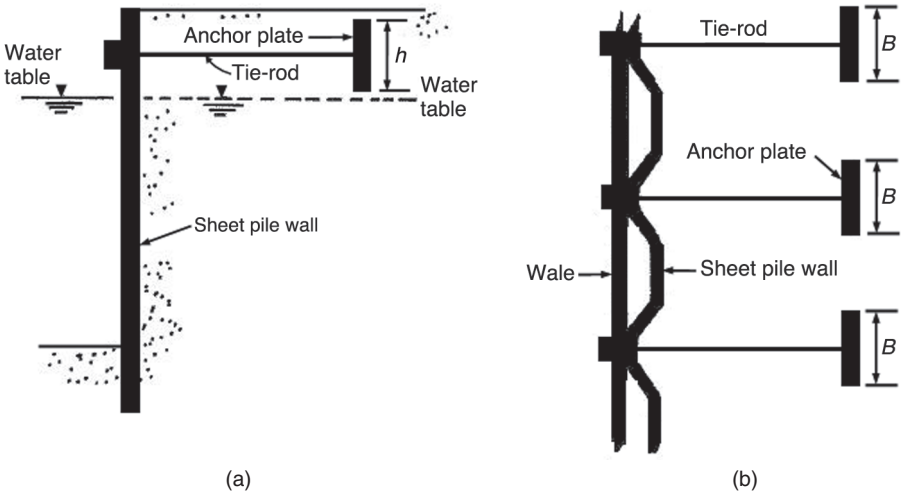

FIGURE 1.4 Use of vertical plate anchor in sheet pile wall: (a) section and (b) plan

holes. Anchors placed in this way are referred to as *direct bearing plate anchors.* In the construction of sheet pile walls, primarily used for waterfront structures, vertical backfilled or direct bearing plate anchors are common. Figure 1.4a shows the cross section of a sheet pile wall with a vertical anchor. The vertical anchors of height h and width B and spaced with a center-to-center spacing of S are tied to the sheet pile wall, as shown in Figure 1.4b.

In many cases, horizontal anchor beams along with batter piles can also be used in the construction of sheet pile walls (Figure 1.5).

1.3 DIRECT EMBEDMENT ANCHORS

Direct embedment anchors are similar in nature to direct bearing plate anchors (Figure 1.6). They may be triangular or take any other penetrative shape, and they are installed vertically by driving with a rod to a desired depth. After the desired depth is reached, the rod is withdrawn and the cable is tensioned to rotate the anchor through an angle of 90° into its final position.

1.4 HELICAL ANCHORS

Helical anchors consist of a steel shaft with one or more helices attached to it (Figure 1.7). An anchor made by suitably connecting a prefabricated steel screw

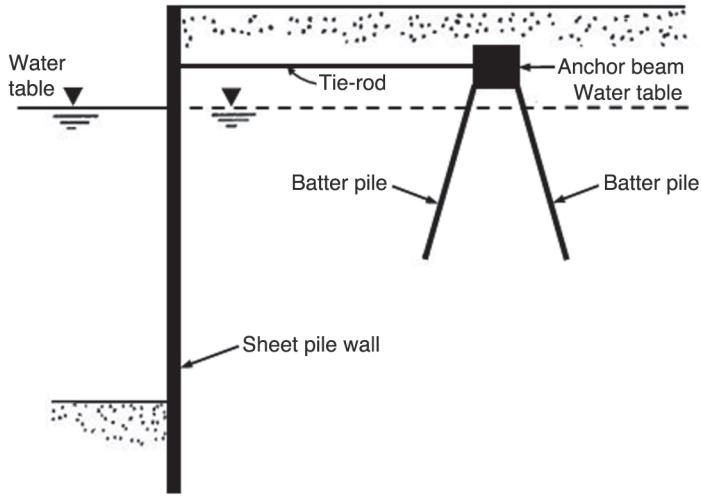

FIGURE 1.5 Use of horizontal anchor beam with batter piles in sheet pile wall

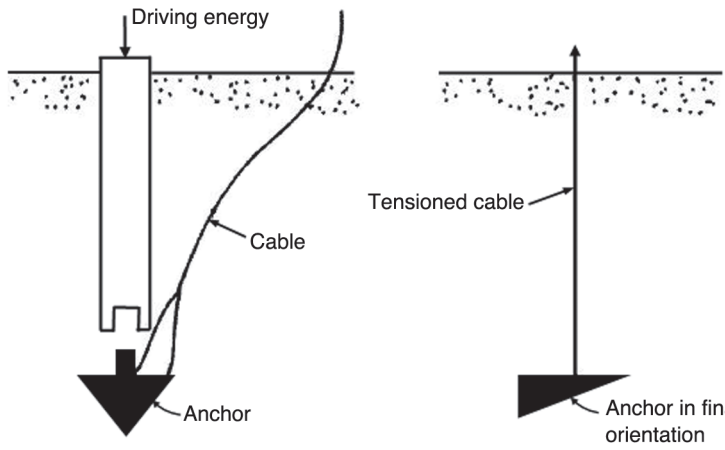

FIGURE 1.6 Direct embedment anchor (redrawn after Kulhawy, 1985)

helix element to a steel shaft is called a *single-helix (screw) anchor,* which is one form of helical anchor. A single-helix (screw) anchor can also be made as helically shaped circular steel plates welded to a steel rod. Another form of helical anchors is a *multi-helix anchor,* in which the circular plates are welded at a predetermined suitable spacing.

For multi-helix anchors, the pitch and center-to-center spacing of the helices can be varied so that the upper helices follow the lower ones. This helps reduce

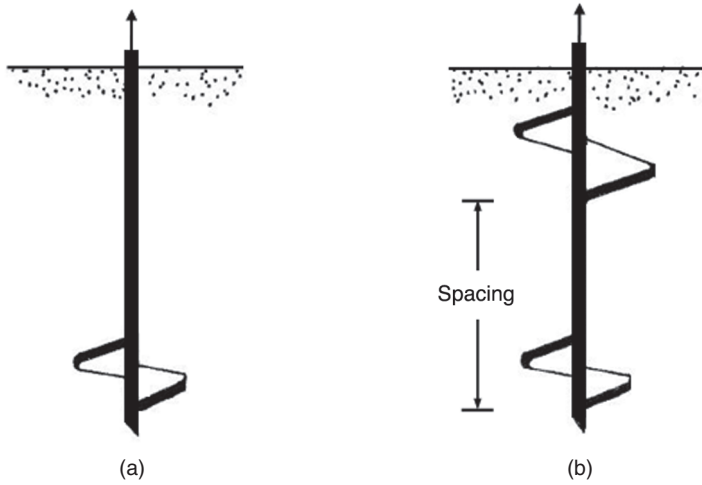

FIGURE 1.7 Helical anchors: (a) single helix and (b) multi-helix

the disturbance in the soil. Figures 1.8 and 1.9 are photographs of helical anchors with one and two helices, respectively. The schematic diagram and a photograph of the installation of a helical anchor are shown in Figures 1.10 and 1.11, respectively. These anchors are driven into the ground in a rotating manner using truck- or trailer-mounted augering equipment where the soil condi-

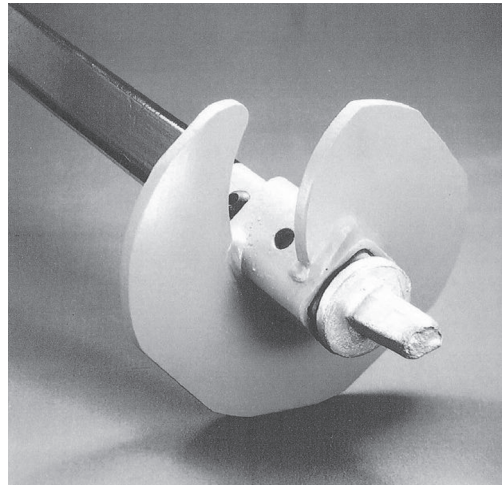

FIGURE 1.8 Helical anchor with one helix (Courtesy of A.B. Chance Co., Centralia, Missouri)

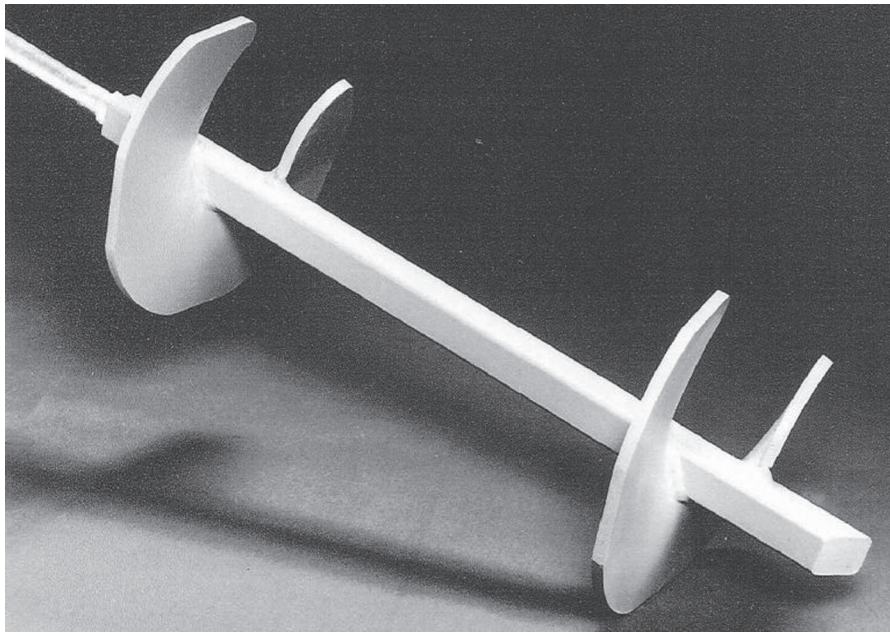

FIGURE 1.9 Helical anchor with two helices (Courtesy of A.B. Chance Co., Centralia, Missouri)

tions permit. An axial load is applied to the shaft while rotating to advance it into the ground. When installing these augers in soils mixed with gravel and large boulders, care should be taken to avoid possible damage to the helices.

Helical anchors can resist tensile loads on the foundation; however, at the same time, they can also supply additional bearing capacity to the foundation (under downward-loading condition) developed at the helix-soil interface.

Helical anchors are becoming increasingly popular in the construction of electric transmission tower foundations in the United States. They may be installed in either a vertical or an inclined position.

1.5 GROUTED ANCHORS

Grouted anchors primarily consist of placing a steel bar or steel cable into a predrilled hole and then filling the hole with cement grout. Figure 1.12 shows various types of grouted anchors, brief explanations of which are given below:

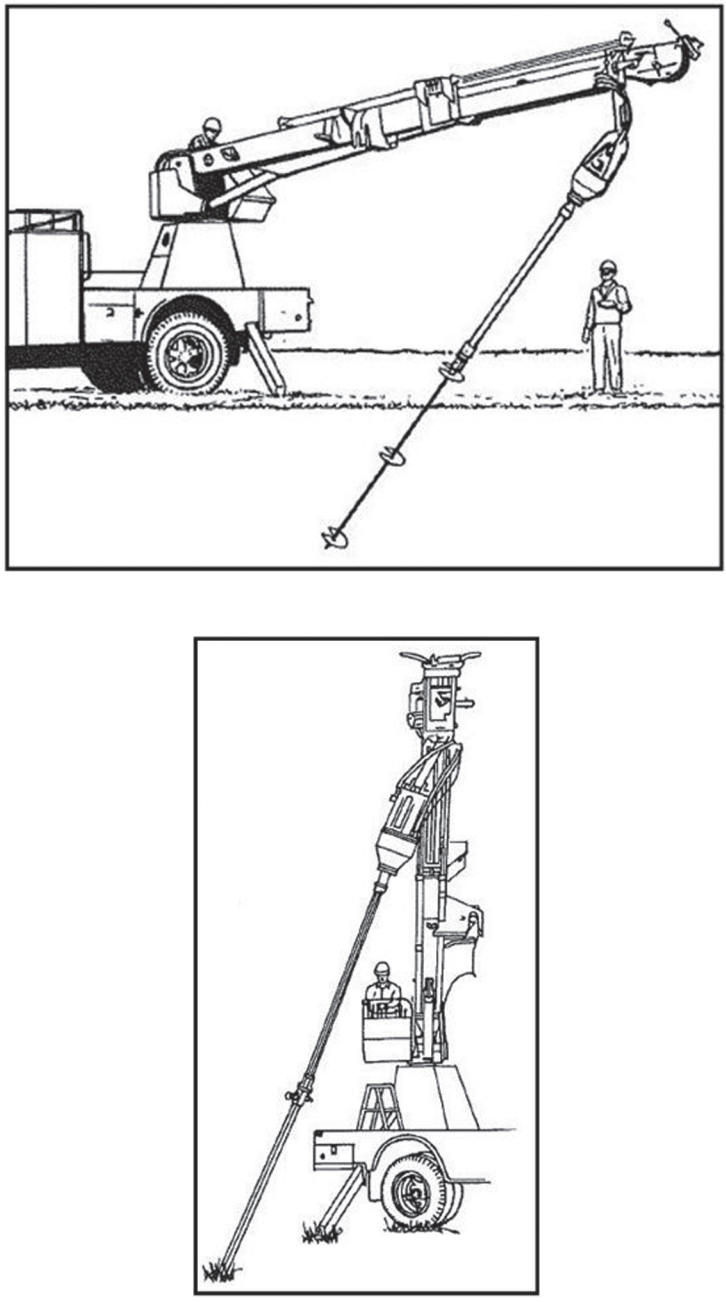

FIGURE 1.10 Installation of helical anchor (Courtesy of A.B. Chance Co., Centralia, Missouri)

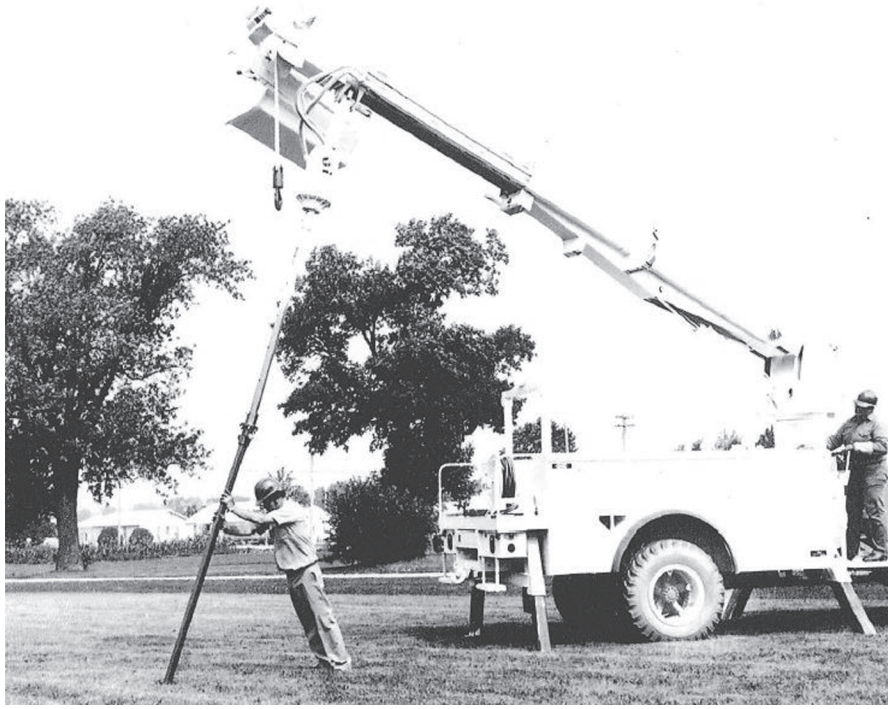

FIGURE 1.11 Installation of helical anchor (Courtesy of A.B. Chance Co., Centralia, Missouri)

1. *Gravity*. For this type of anchor, the grout is poured into the hole from the ground surface without any pressure (Figure 1.12a).
2. *Low pressure*. For this type of anchor, the grout is injected into the hole at pressures up to the overburden pressure (Figure 1.12b). This process ideally increases the effective anchor diameter by penetrating the *in situ* pores or fractures in the ground and/or by compacting the surrounding soil.
3. *High pressure*. For anchors of this type, the grout is injected at high pressure. This pressure increases the effective diameter of the anchor and compacts the loose soil around it. It may also cause hydraulic fracturing in the ground, resulting in a grout-filled system of fissures (Figure 1.12c) and perhaps a larger effective diameter of the system.
4. *Single and multiple bell*. This is primarily a gravity-type anchor; however, single or multiple bells are made in the ground mechanically before grouting (Figures 1.12d and 1.12e).

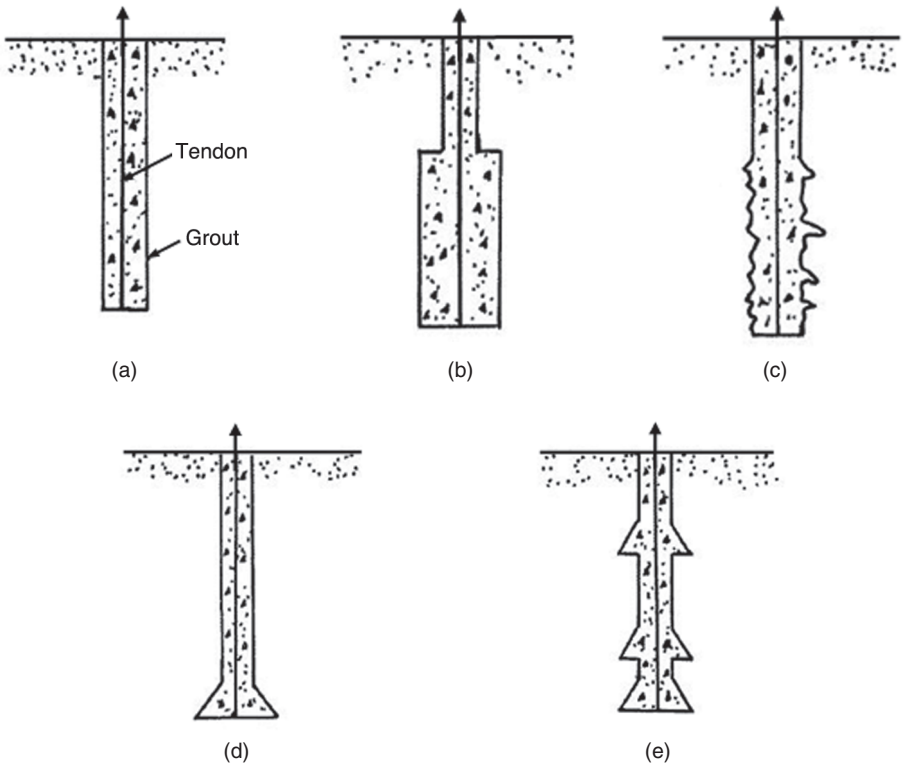

FIGURE 1.12 Grouted anchors: (a) gravity, (b) low pressure, (c) high pressure, (d) single bell, and (e) multiple bell (redrawn after Kulhawy, 1985)

Grouted anchors can be used in many construction projects, such as sheet pile walls (Figure 1.13a), revetment of rock retaining walls (Figure 1.13b), basement floors to resist buoyancy (Figure 1.13c), and foundations of transmission towers to resist overturning.

1.6 ANCHOR PILES AND DRILLED SHAFTS

Piles and drilled shafts (Figure 1.14) can be used in the construction of foundations subjected to uplift where soil conditions are poor or for very heavily loaded foundations. They serve dual purposes; that is, they help support the downward load on the foundation of the structure, and they also resist uplift.

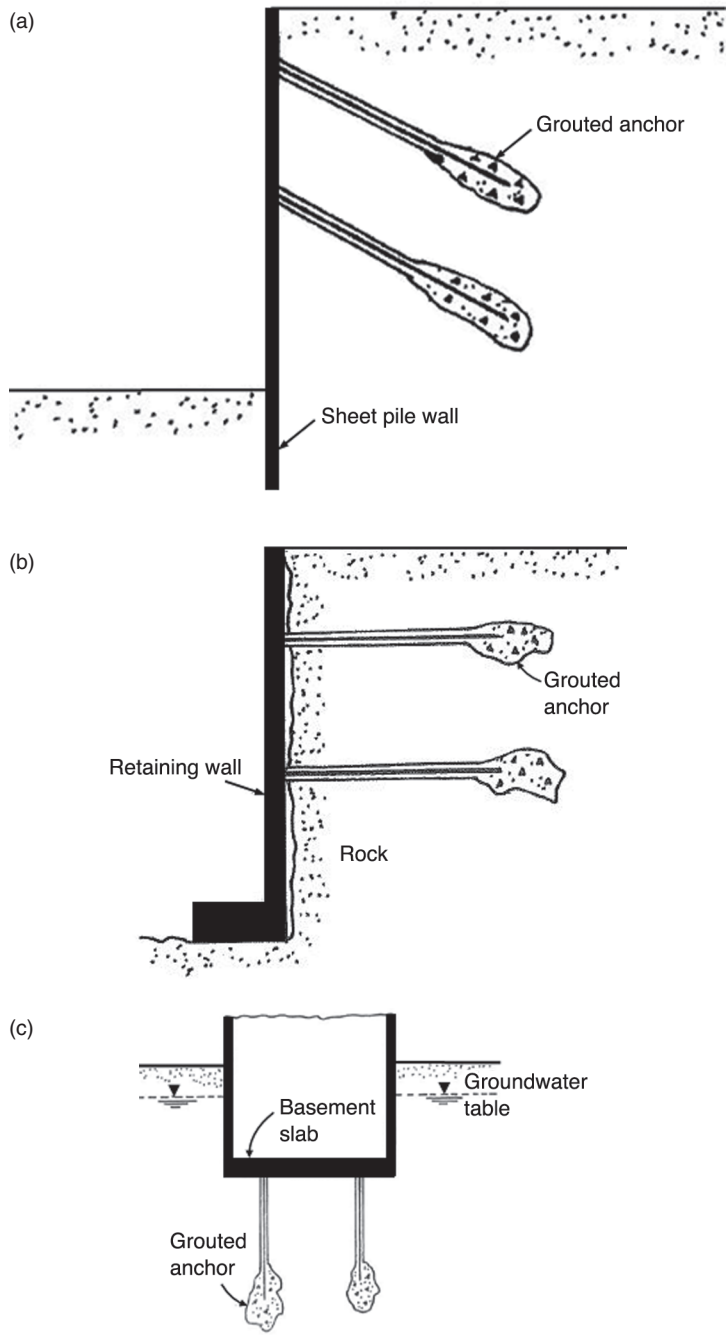

FIGURE 1.13 Use of grouted anchors in (a) sheet pile wall, (b) revetment of rock retaining wall, and (c) floor of basement

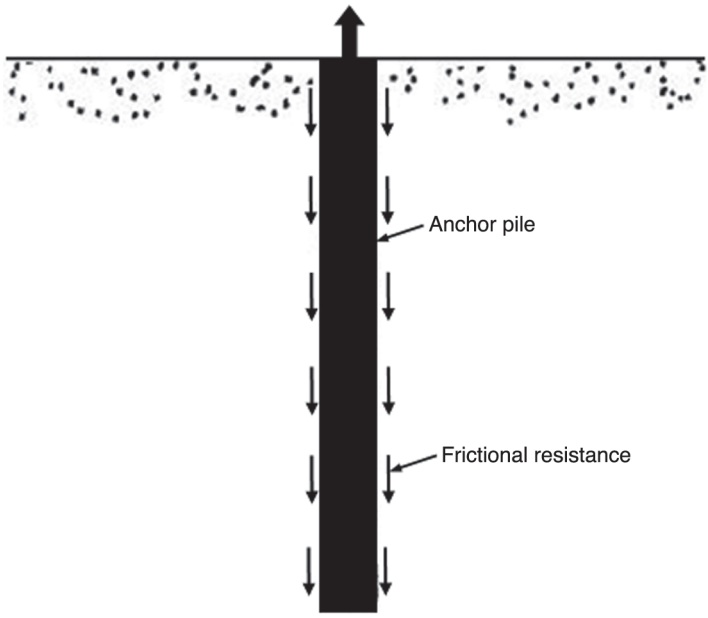

FIGURE 1.14 Anchor pile and drilled shaft subjected to uplifting load

1.7 SUCTION CAISSON AND DRAG ANCHORS

Suction caisson and drag anchors are commonly used to secure mooring systems (steel wire/chain, synthetic rope, steel tendons, etc.) of buoyant platforms to the seabed (Figure 1.15). A suction caisson comprises a large-diameter cylinder, typically in the range of 3 to 8 m, open at the bottom and closed at the top. The length-to-diameter ratio is generally in the range of 3 to 6 (Randolph and Gourvenec, 2011). A traditional drag anchor (also called fixed fluke plate anchor) consists of a broad fluke rigidly connected to a shank. The angle between the shank and the fluke is predetermined, though it may be adjusted prior to anchor placement on the seabed. The traditional drag anchors have a limitation of taking large vertical loads; therefore, vertically loaded anchors (also called drag-in plate anchors) also have been developed.

1.8 GEO-ANCHORS

A geo-anchor consists of a permeable core of coarse sand, gravel, or crushed stone wrapped in one or several layers of high-strength woven geotextile. Geo-

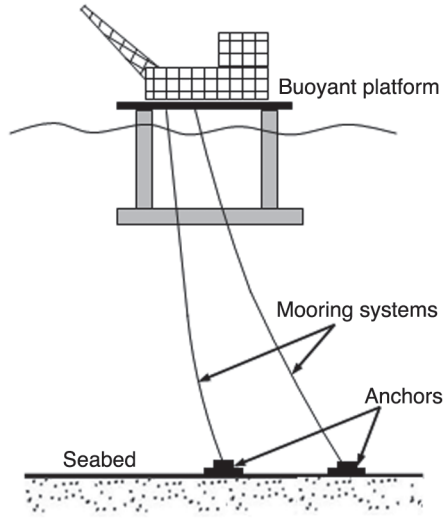

FIGURE 1.15 Buoyant platform anchored to seabed

anchors can be used to increase the stability of steep slopes, to reduce the lateral earth pressures on retaining structures, or to stabilize embankments constructed on soft clay. Figure 1.16 shows the role of geo-anchors in stabilizing a soil slope by their construction in trenches. This type of geo-anchor can be more effective in areas where the annual rainfall is high and the groundwater level is close to the ground level. Another form of geo-anchor is the trench anchor for firmly securing the geosynthetic layer installed as a pond/canal liner or slope surface protection so that geosynthetic movement or pullout does not occur (Shukla and Yin, 2006; Shukla, 2012). Figure 1.17 shows a typical V-trench anchor.

1.9 COVERAGE OF THE TEXT

During the last three to four decades, the pace of experimental and mathematical research works relating to earth anchors has accelerated, and the results of those works have been published in various technical journals and conference proceedings. The purpose of this text is to present in a systematic manner a comprehensive review of some of the past and recent studies. Updated information is provided for evaluation of the holding capacities of *plate anchors oriented in a horizontal, inclined, and vertical manner* in soil; *helical anchors*; *piles subjected to vertical uplift*; *suction caisson* and *drag anchors*; and *geo-anchors.* Limited attempt has been made to provide either the details for the *placement*

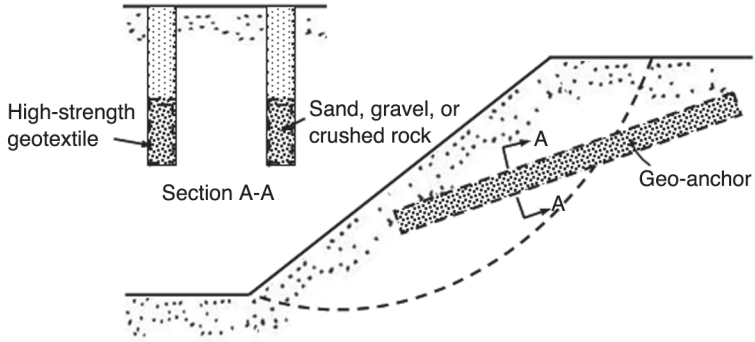

FIGURE 1.16 Geo-anchor in a slope (adapted from Broms, 1993)

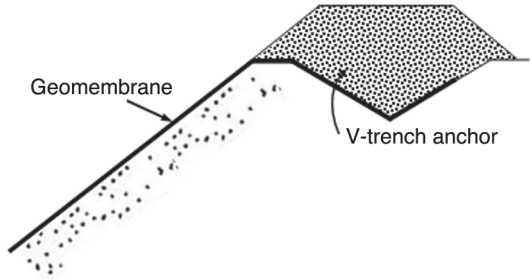

FIGURE 1.17 V-trench anchor (adapted from Shukla and Yin, 2006; Shukla, 2012)

of the anchors in the field or the *construction techniques.* Valuable information in these areas can be obtained from the work of Hanna (1982) and others. No aspects of grouted anchors are covered in this text, since valuable information is available from several other well-organized sources (Hanna, 1982; Littlejohn, 1970). In spite of the accelerated pace of research work on various aspects of anchors at the present time, adequate field verifications are often lacking in several instances. These shortcomings will also be outlined in the text.

1.10 SUMMARY OF MAIN POINTS

1. Earth anchors are primarily designed and constructed to resist outwardly directed loads imposed on structures such as foundations, earth retaining structures, and slopes.

2. The different forms of earth anchors are screw anchors, plate anchors, direct embedment anchors, helical anchors, grouted anchors, anchor piles and drilled shafts, suction caisson and drag anchors, and geo-anchors.
3. Plate anchors are made up of steel plates, precast concrete slab, timber sheets, and so forth; they may be horizontal, vertical, or inclined. They are installed by ground excavation to the required depth and then backfilling or by placing in excavated trenches.
4. Helical anchors consist of a steel shaft with one or more helices attached to it.
5. Grouted anchors primarily consist of placing a steel bar or steel cable into a predrilled hole and then filling the hole with cement grout.
6. Anchor piles and drilled shafts help support the downward load on the foundation of a structure, and they also resist uplift.
7. A suction caisson comprises a large-diameter cylinder, typically in the range of 3 to 8 m, open at the bottom and closed at the top. A traditional drag anchor consists of a broad fluke rigidly connected to a plank.
8. Geotextile-wrapped coarse-grained soil columns and trench anchors are two different forms of geo-anchors.

SELF-ASSESSMENT QUESTIONS

Select the most appropriate answer to each multiple-choice question

1.1. The earliest form of anchor used in soil for resisting vertically directed uplifting load is:
   a. plate anchor
   b. helical anchor
   c. screw anchor
   d. suction caisson anchor

1.2. A vertical plate anchor resists:
   a. horizontally directed pullout load
   b. vertically directed pullout load
   c. axial pullout load
   d. inclined pullout load

1.3. Which of the following anchors is installed by driving into the ground in a rotating manner using truck- or trailer-mounted augering equipment:
   a. plate anchor
   b. helical anchor

c. grouted anchor
d. geo-anchor

1.4. Grouted anchors can be used in:
a. sheet pile walls
b. basement floors
c. foundations of transmission towers
d. all of the above

1.5. Piles and drilled shafts are commonly used in the construction of foundations subjected to uplift:
a. where soil conditions are poor
b. for very heavily loaded foundations
c. both a and b
d. where water is present

1.6. Which of the following anchors is commonly used to secure mooring systems of buoyant platforms to the seabed:
a. suction caisson anchor
b. plate anchor
c. grouted anchor
d. geo-anchor

1.7. The length-to-diameter ratio for suction caisson anchors is generally in the range of
a. 1 to 3
b. 3 to 6
c. 6 to 9
d. 9 to 12

1.8. Geo-anchors in the form of geotextile-wrapped coarse-grained soil columns installed in slopes play the role of:
a. reinforcement
b. drainage
c. both a and b
d. filtration

Answers

1.1: c 1.2: a 1.3: b 1.4: d 1.5: c 1.6: a 1.7: b 1.8: c

REFERENCES

Broms, B.B. (1993). Geo-anchors. *Geotext. Geomembr.,* 12(3):215–234.

Hanna, T.H. (1982). *Foundations in Tension-Ground Anchor,* Trans Tech Publication and McGraw-Hill.

Kulhawy, F.H. (1985). Uplift behavior of shallow soil anchors—an overview. *Proc. Uplift Behavior of Anchor Foundations,* ASCE, 1–25.

Littlejohn, G.S. (1970). Soil anchors. *Proc. Conf. Ground Eng.,* London, 33–44.

Randolph, M. and Gourvenec, S. (2011). *Offshore Geotechnical Engineering,* Spon Press, Taylor and Francis, Abingdon, Oxon.

Shukla, S.K. (2012). *Handbook of Geosynthetic Engineering,* second edition, ICE Publishing, London.

Shukla, S.K. and Yin, J.-H. (2006). *Fundamentals of Geosynthetic Engineering,* Taylor and Francis, London.

2

HORIZONTAL PLATE ANCHORS IN SAND

In the past, several theoretical and semi-empirical methods were developed to predict the ultimate uplifting load of strip, circular, and rectangular anchors embedded in sands. Some of these methods are described in this chapter. Recently some numerical investigations of the behavior of horizontal plate anchors in sands have been reported in the literature; this chapter also summarizes such works briefly.

2.1 INTRODUCTION

As briefly discussed in Chapter 1, horizontal plate anchors are used in the construction of foundations subjected to uplifting load. In the past, a number of increasingly sophisticated theories have been developed to predict the ultimate uplift capacity of horizontal plate anchors embedded in various types of soils. In this chapter, the development of those theories for horizontal plate anchors in sands is discussed.

Figure 2.1 shows a horizontal plate anchor with a width h and a length B ($B \geq h$). The embedment depth of this plate anchor is H measured from the ground surface. The embedment ratio is defined as the ratio of the depth of embedment to the width of the anchor, that is, H/h. If such an anchor is placed at a relatively shallow depth, that is, with a small embedment ratio, the failure surface at ultimate load will extend to the ground surface (Figure 2.2). The angle α at which the failure surface intersects the horizontal ground surface will vary with the type of soil. For loose sand and soft clayey soils, α may be equal to 90°;

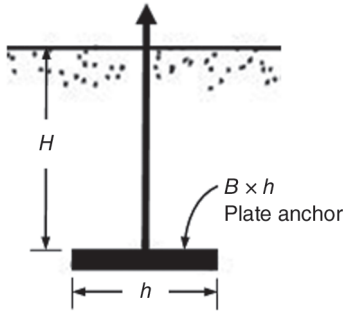

FIGURE 2.1 Geometric parameters of a horizontal plate anchor

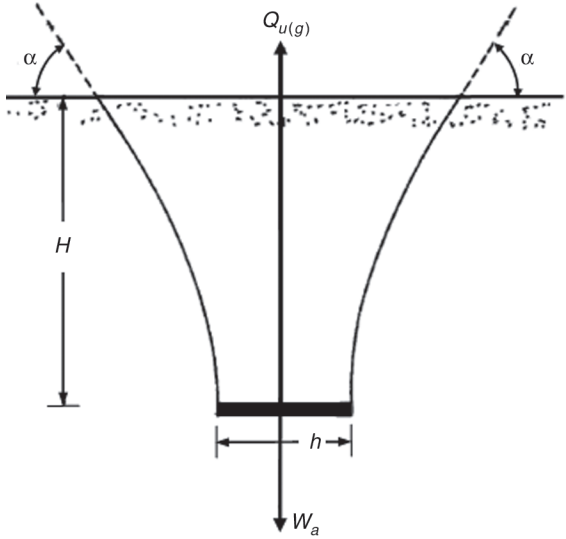

FIGURE 2.2 Shallow horizontal anchor

however, for dense sand and stiff clays, this angle may be close to $45° - \phi/2$ (where ϕ = angle of internal friction of soil). This type of behavior of an anchor is referred to as the *shallow anchor condition.* If the anchor is located at a relatively large embedment ratio, the failure surface in soil at ultimate load does not extend to the ground surface; that is, a local shear failure in soil located around the anchor takes place. This is referred to as the *deep anchor condition.*

For a given anchor, the gross ultimate uplift capacity can be defined as:

$$Q_{u(g)} = Q_u + W_a \tag{2.1}$$

where

$Q_{u(g)}$ = gross ultimate uplift capacity
Q_u = net ultimate uplift capacity
W_a = effective self-weight of the anchor

The net ultimate uplift capacity is the sum of the effective weight of the soil located in the failure zone and the shearing resistance developed along the failure surface.

2.2 EARLY THEORIES

2.2.1 Soil Cone Method

Some of the early theories to determine the net ultimate uplift capacity Q_u were restricted to *shallow circular* plate anchors. Mors (1959) proposed that the failure surface in soil at ultimate load may be approximated as a truncated cone with an apex angle of $\theta = 90° + \phi/2$, as shown in Figure 2.3. The net ultimate

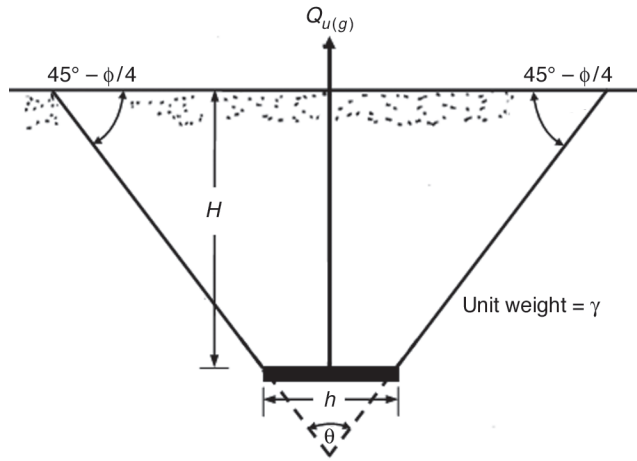

FIGURE 2.3 Mors's theory (1959): soil cone method ($\theta = 90° + \phi/2$, h = diameter of anchor plate)

uplift capacity may be assumed to be equal to the weight of the soil located inside the failure surface. Thus:

$$Q_u = \gamma V \tag{2.2}$$

where

V = volume of soil in the truncated cone
γ = unit weight of soil, and

$$V = \frac{\pi H}{12}\left\{ h^2 + \left[h + 2H \cot\left(45° - \frac{\phi}{4} \right) \right]^2 + h \left[h + 2H \cot\left(45° - \frac{\phi}{4} \right) \right] \right\}$$

or

$$V = \frac{\pi H}{12}\left[3h^2 + 4H^2 \cot^2\left(45° - \frac{\phi}{4} \right) + 6Hh \cot\left(45° - \frac{\phi}{4} \right) \right] \tag{2.3}$$

It needs to be pointed out that the shearing resistance developed along the failure surface has been neglected in Equation 2.2.

A similar theory was also proposed by Downs and Chieurzzi (1966), who suggested that the apex angle θ be taken as being equal to 60°, as shown in Figure 2.4. For this case:

$$\begin{aligned} Q_u &= \gamma V \\ &= \frac{\pi \gamma H^3}{12} \left[h^2 + (h + 2H \cot 60°)^2 + h(h + 2H \cot 60°) \right] \\ &= \frac{\pi \gamma H^3}{12} (3h^2 + 1.333H^2 + 3.464H) \end{aligned} \tag{2.4}$$

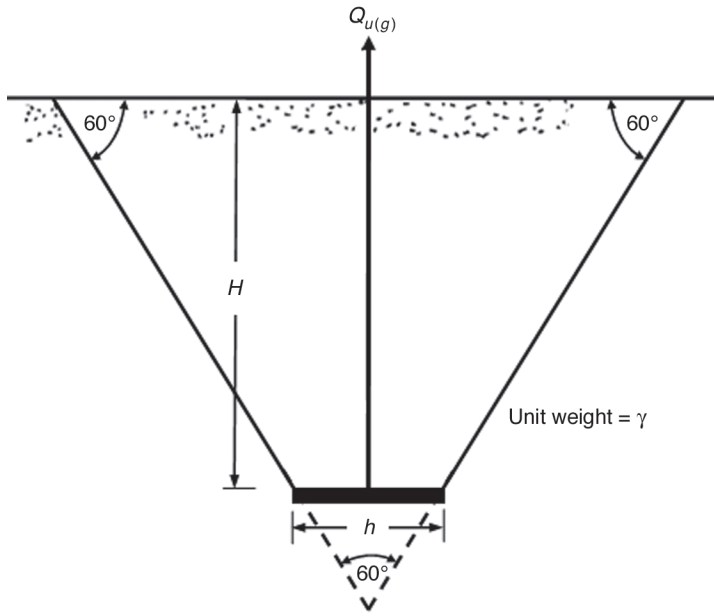

FIGURE 2.4 Downs and Chieurzzi's theory (1966): soil cone method (h = diameter of anchor plate)

2.2.2 Friction Cylinder Method

In many cases in the past, the friction cylinder method was used to estimate the uplift capacity of *shallow circular* anchor plates. In this type of calculation, the friction surface in the soil was assumed to be cylindrical, as shown in Figure 2.5a. For cohesionless soils, the net ultimate load was taken as the sum of the weight of the soil located inside the failure cylinder and the frictional resistance mobilized along the failure surface. Thus:

$$Q_u = \left(\frac{\pi h^2}{4}\right)(H)(\gamma) + \int_0^H (\sigma_0' \tan \phi) dz \tag{2.5a}$$

where

σ_0' = effective overburden pressure at a depth z measured from the ground surface (Figure 2.5b)
ϕ = soil friction angle

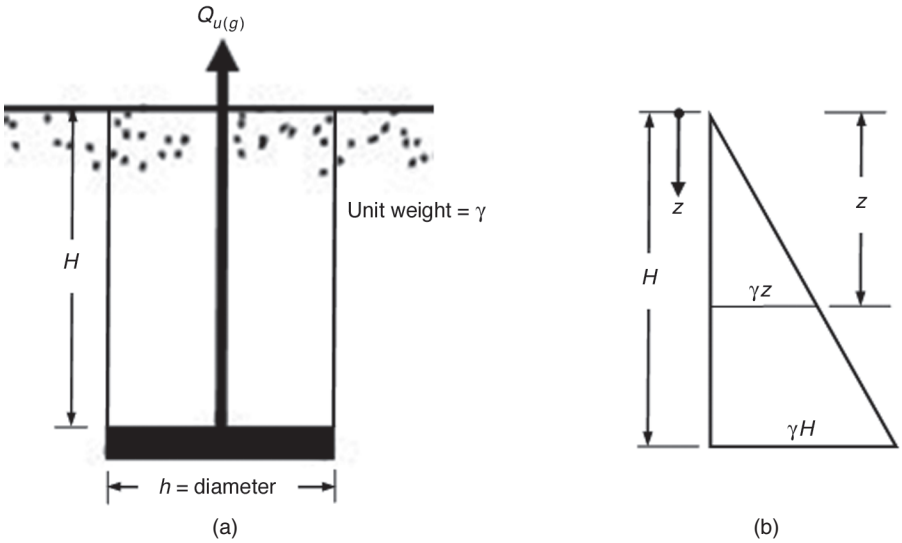

FIGURE 2.5 Friction cylinder method: (a) failure mechanism and (b) variation of effective overburden pressure

With substitution of values, Equation 2.5a becomes:

$$Q_u = \frac{\pi H h^2 \gamma}{4} + \int_0^H (\pi h)(\gamma z \tan \phi) dz$$

$$= \frac{\pi H h^2 \gamma}{4} + \left(\frac{\pi h H^2 \gamma}{4}\right) \tan \phi \qquad (2.5b)$$

In a similar manner, for the saturated cohesive soils:

$$Q_u = \frac{\pi H h^2 \gamma}{4} + (\pi H h) + c_u \qquad (2.6)$$

Surface area of the cylindrical failure surface

where

c_u = undrained cohesion

Ireland (1963) proposed the following relationships for shallow anchors embedded in sands as well as silts and clays:

$$Q_u = \frac{\pi H h^2 \gamma}{4} + \frac{\pi}{2} \gamma h H^2 K_0 \tan \phi \tag{2.7}$$

where

K_0 = coefficient of lateral earth pressure

Ireland (1963) also recommended the following values for K_0 and ϕ:

$$K_0 = \begin{cases} 0.5 \text{ for granular soils} \\ 0.4 \text{ for silts and clays} \end{cases}$$

$$\phi = \begin{cases} 30^\circ \text{ for granular soils} \\ 20^\circ \text{ for silts and clays} \end{cases}$$

2.3 BALLA'S THEORY

Based on several model and field test results in dense soil, Balla (1961) established that for *shallow circular anchors,* the failure surface in soil will be as shown in Figure 2.6. Note from the figure that aa' and bb' are arcs of a circle. The angle α is equal to $45^\circ - \phi/2$. The radius of the circle, of which aa' and bb' are arcs, is expressed as:

$$r = \frac{H}{\sin\left(45^\circ + \frac{\phi}{2}\right)} \tag{2.8}$$

The net ultimate uplift capacity of the anchor is the sum of two components: (a) weight of the soil in the failure zone and (b) the shearing resistance developed along the failure surface. Thus:

$$Q_u = H^3 \gamma \left[F_1\left(\phi, \frac{H}{h}\right) + F_3\left(\phi, \frac{H}{h}\right) \right] \tag{2.9}$$

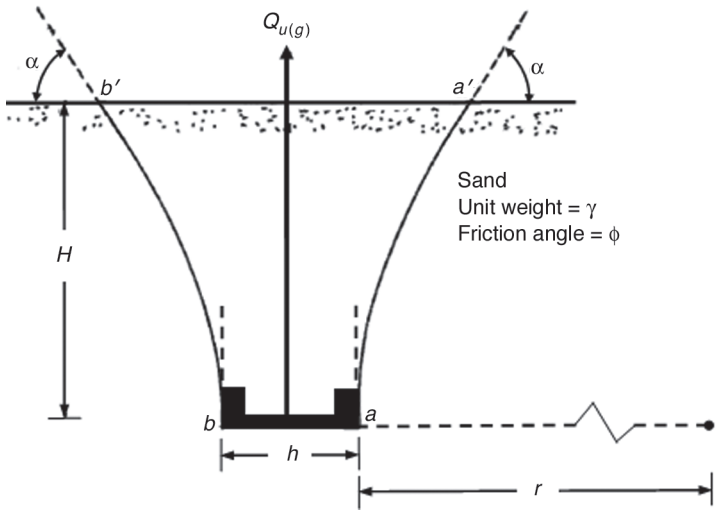

FIGURE 2.6 Balla's theory (1961) for shallow circular anchor plate

The sums of the functions $F_1(\phi, H/h)$ and $F_3(\phi, H/h)$ developed by Balla (1961) are plotted in Figure 2.7 for various values of the soil friction angle ϕ and embedment ratio H/h. The general nature of the plot of Q_u versus H/h will be like that in Figure 2.8.

In general, Balla's theory is in good agreement for the uplift capacity of anchors embedded in dense sand at an embedment ratio of $H/h \leq 5$. However, for anchors located in loose and medium sand, the theory overestimates the net ultimate uplift capacity. The main reason that Balla's theory overestimates the net uplift capacity for $H/h >$ about 5 even in dense sand is because it is essentially a deep anchor condition, and the failure surface does not extend to the ground surface.

The simplest procedure to determine the embedment ratio at which the deep anchor condition is reached may be determined by plotting the nondimensional breakout factor F_q against H/h, as shown in Figure 2.9.

The breakout factor is defined as:

$$F_q = \frac{Q_u}{\gamma AH} \tag{2.10}$$

where

A = area of the anchor plate

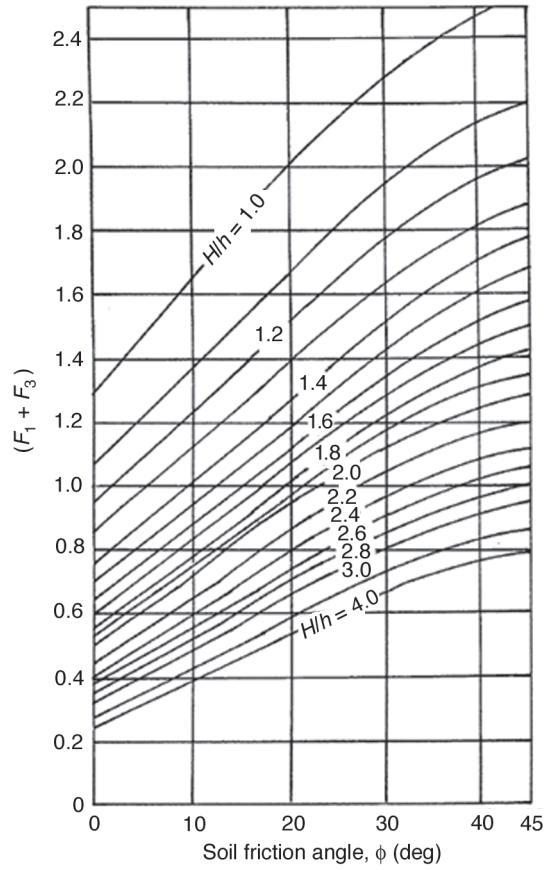

FIGURE 2.7 Variation of $F_1 + F_3$ based on Balla's theory (1961)

The breakout factor increases with H/h up to a maximum value of $F_q = F_q^\star$ at $H/h = (H/h)_{cr}$. For $H/h > (H/h)_{cr}$, the breakout factor remains practically constant, that is, $F_q^\star$. Anchors located at an embedment ratio of $H/h \leq (H/h)_{cr}$ are shallow anchors, and those located at $H/h > (H/h)_{cr}$ are deep anchors.

2.4 BAKER AND KONDNER'S EMPIRICAL RELATIONSHIP

Baker and Kondner (1966) conducted several laboratory model tests, and by using dimensional analysis, they proposed the following relationships:

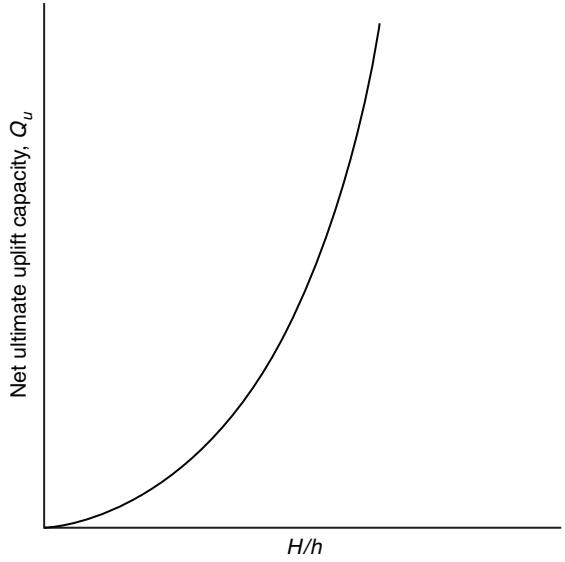

FIGURE 2.8 Nature of variation of Q_u with H/h

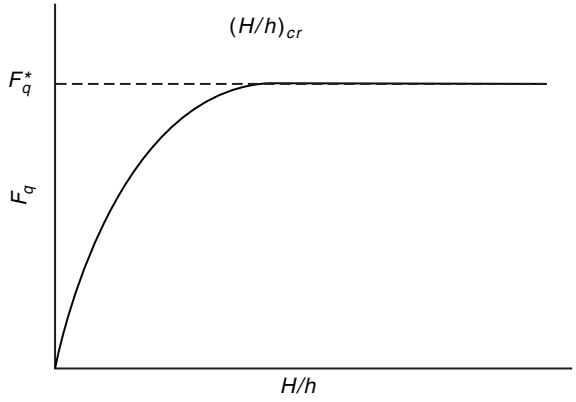

FIGURE 2.9 Nature of variation of F_q with H/h

$$Q_u = c_1 H h^2 \gamma + c_2 H^3 \gamma \quad \text{(for shallow circular anchors)} \tag{2.11}$$

$$Q_u = 170 h^3 \gamma + c_3 h^2 t \gamma + c_4 H h + \gamma \quad \text{(for deep circular anchors)} \tag{2.12}$$

where

t = thickness of the anchor plate
c_1, c_2, c_3, c_4 = constants that are functions of the soil friction angle and the relative density of compaction

For shallow anchors, the model test results of Baker and Kondner agreed well with the theory of Balla (1961). Those tests were conducted in a dense sand with $\phi = 42°$.

2.5 MARIUPOL'SKII'S THEORY

Mariupol'skii (1965) proposed separate mathematical formulations for estimation of the ultimate uplift capacity of shallow and deep circular anchors. According to this theory, for shallow anchors, the progressive failure mechanism commences with compression of the soil located above the anchor plate (Figure 2.10). This compression occurs with a column of soil that has the same diameter as the anchor plate. Hence, the initial force consists of the following components:

1. The effective weight of the anchor
2. The effective weight of the soil column of diameter h and height H
3. The friction and cohesion along the surface of the soil column

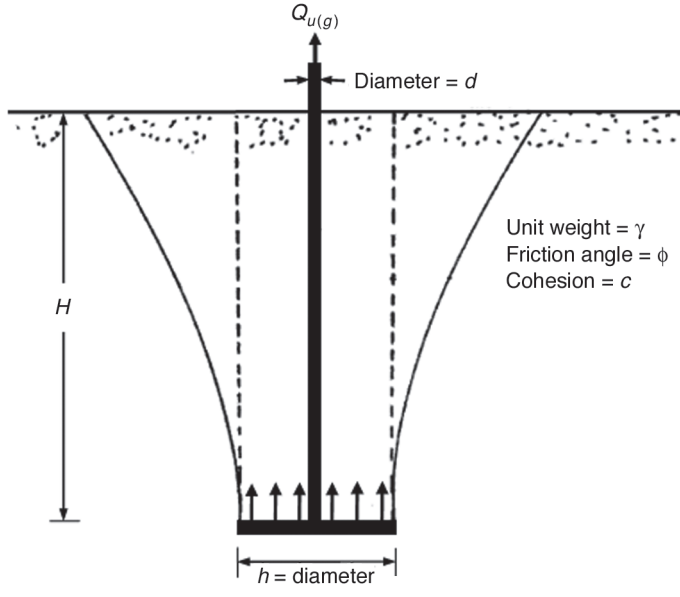

FIGURE 2.10 Mariupol'skii's theory (1965) for shallow circular plate anchor

As pullout progresses, there is continued compaction of soil, and this leads to an increase in the vertical compressive stress. Thus there is a continued increase in the frictional resistance along the surface of the soil column. The increase of the frictional resistance entrains adjacent rings of soil. Ultimately sufficient tensile stress is developed so that failure occurs with the separation of soil in the form of a cone with a curvilinear geneatrix. The net ultimate uplift capacity thus calculated by this theory can be given as:

$$Q_u = \frac{\pi}{4}(h^2 - d^2)\frac{\left\{\begin{array}{l}\gamma H\left[1 - \left(\frac{d}{h}\right)^2 + 2K_0\left(\frac{H}{h}\right)\tan\phi\right] \\ \\ + 4c\left(\frac{H}{h}\right)\end{array}\right\}}{1 - \left(\frac{H}{h}\right)^2 - 2n\left(\frac{H}{h}\right)} \qquad (2.13)$$

where

K_0 = lateral earth pressure coefficient
c = cohesion
n = an empirical coefficient
d = diameter of the anchor shaft

For sand, $c = 0$, so:

$$Q_u = \frac{\pi}{4}(h^2 - d^2)\frac{\left\{\gamma H\left[1 - \left(\frac{d}{h}\right)^2 + 2K_0\left(\frac{H}{h}\right)\tan\phi\right]\right\}}{1 - \left(\frac{H}{h}\right)^2 - 2n\left(\frac{H}{h}\right)} \qquad (2.14)$$

For deep anchors, it was assumed that under the applied load the anchor will reach a limiting condition, after which additional work is required to raise the anchor through a distance L, which is equivalent to the work required to expand a cylindrical cavity of height L and diameter d to a diameter h, as shown in Figure 2.11. Based on this concept, the net ultimate uplift capacity can be expressed as:

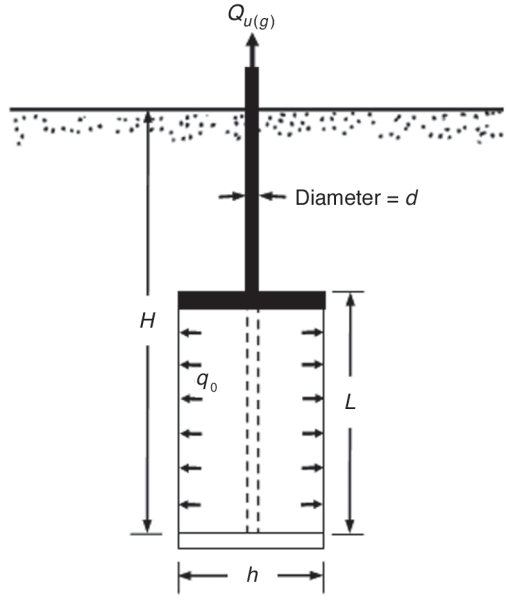

FIGURE 2.11 Mariupol'skii's theory (1965) for deep circular plate anchor

$$Q_u = \left(\frac{\pi q_0}{2}\right)\left(\frac{h^2 - d^2}{2 - \tan\phi}\right) + f(\pi d)\,[H - (h - d)] \qquad (2.15)$$

where

q_0 = radial pressure under which the cavity is expanded
f = unit skin resistance along the stem of the anchor

It was recommended that the lower of the two values (that is, those calculated from either Equation 2.14 or 2.15) be adopted for design. This was primarily because the limit of $H/h = (H/h)_{cr}$ for the deep anchor condition was not clearly established.

2.6 MEYERHOF AND ADAMS'S THEORY

Meyerhof and Adams (1968) proposed a semi-theoretical relationship for estimation of the ultimate uplift capacity of *strip, rectangular,* and *circular* anchors.

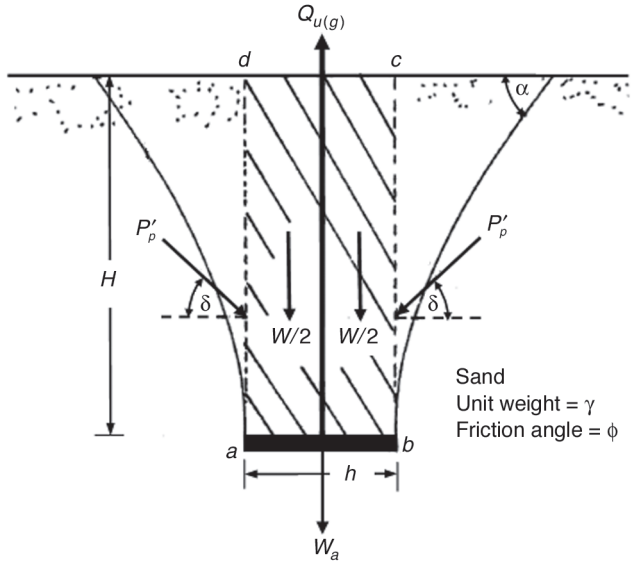

FIGURE 2.12 Failure mechanism from Meyerhof and Adams's theory (1968)

The principles of this theory can be explained by considering a *shallow strip* anchor embedded in sand, as shown in Figure 2.12.

At ultimate load, the failure surface in soil makes an angle α with the horizontal. The magnitude of α depends on several factors, such as the relative density of compaction and the angle of internal friction of the soil, and it varies between $90° - \phi/3$ to $90° - 2\phi/3$, with an average of about $90° - \phi/2$. Let us consider the free body diagram of the soil located in the zone *abcd*. For stability, the following forces per unit length of the anchor need to be considered:

1. The weight of the soil, W
2. The passive force P'_p per unit length along the faces *ad* and *bc*

The force P'_p is inclined at an angle δ to the horizontal. For an average value of $\alpha = 90° - \phi/2$, the magnitude of δ is about $(\frac{2}{3})\phi$.

Note that

$$W = \gamma H h \tag{2.16}$$

$$P'_p = \frac{P'_h}{\cos\delta} = \left(\frac{1}{2}\right)\left(\frac{1}{\cos\delta}\right)(K_{ph}\gamma H^2) \tag{2.17}$$

where

P'_h = horizontal component of the passive force
K_{ph} = horizontal component of the passive earth pressure coefficient

Now, for equilibrium, summing the vertical components of all forces:

$$\sum F_V = 0$$

$$Q_{u(g)} = W + 2P'_p \sin\delta + W_a$$

$$Q_{u(g)} - W_a = W + 2(P'_p \cos\delta)\tan\delta$$

$$Q_u = W + 2P'_h \tan\delta$$

or

$$Q_u = W + 2\left(\frac{1}{2} K_{ph}\gamma H^2\right)\tan\delta = W + K_{ph}\gamma H^2 \tan\delta \qquad (2.18)$$

The passive earth pressure coefficient based on the curved failure surface for $\delta \approx (2/3)\phi$ can be obtained from Caquot and Kerisel (1949). Furthermore, it is convenient to express $K_{ph}\tan\delta$ in the form

$$K_u \tan\phi = K_{ph}\tan\delta \qquad (2.19)$$

where

K_u = nominal uplift coefficient

Combining Equations 2.18 and 2.19, we obtain:

$$Q_u = W + K_u\gamma H^2 \tan\phi \qquad (2.20)$$

The variation of the nominal uplift coefficient K_u with the soil friction angle ϕ is shown in Figure 2.13. It falls within a narrow range and may be taken as equal to 0.95 for all values of ϕ varying from 30° to about 48°.

As discussed in Section 2.3, the nondimensional breakout factor is defined as:

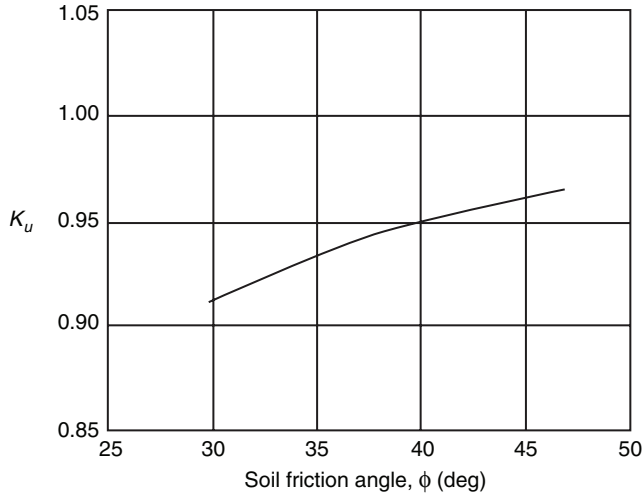

FIGURE 2.13 Variation of K_u with soil friction angle

$$F_q = \frac{Q_u}{\gamma AH}$$

For strip anchors, and area A per unit length is equal to $h \times 1 = h$. Thus, from Das and Seeley (1975a):

$$F_q = \frac{Q_u}{\gamma AH} = \frac{Q_u}{\gamma hH} = W + K_u \gamma H^2 \tan \phi$$

However, $W = \gamma hH$. Therefore:

$$F_q = \frac{\gamma hH + K_u \gamma H^2 \tan \phi}{\gamma hH} = 1 + K_u \left(\frac{H}{h} \tan \phi \right) \tag{2.21}$$

For circular anchors, Equation 2.20 can be modified to the form

$$Q_u = W + \frac{\pi}{2} S_F \gamma hH^2 K_u \tan \phi \tag{2.22}$$

where

W = weight of the soil above the circular anchor = $\left(\frac{\pi}{4} h^2\right) H\gamma$
h = diameter of the anchor
S_F = shape factor

The shape factor can be expressed as:

$$S_F = 1 + m\left(\frac{H}{h}\right) \tag{2.23}$$

where

m = coefficient which is a function of the soil friction angle ϕ

Thus, combining Equations 2.22 and 2.23, we obtain:

$$Q_u = \frac{\pi}{4} h^2 H\gamma + \frac{\pi}{2}\left[1 + m\left(\frac{H}{h}\right)\right]\gamma h H^2 K_u \tan\phi \tag{2.24}$$

The breakout factor F_q can be given as (Das and Seeley, 1975a):

$$F_q = \frac{Q_u}{\gamma A H} = \frac{\frac{\pi}{4} h^2 H\gamma + \frac{\pi}{2}\left[1 + m\left(\frac{H}{h}\right)\right]\gamma h H^2 K_u \tan\phi}{\gamma\left(\frac{\pi}{4} h^2\right) H}$$

$$= 1 + 2\left[1 + m\left(\frac{H}{h}\right)\right]\left(\frac{H}{h}\right) K_u \tan\phi \tag{2.25}$$

For rectangular anchors that have dimensions of $B \times h$, the net ultimate capacity can be expressed as:

$$Q_u = W + \gamma H^2 (2S_F h + B - h) K_u \tan\phi \tag{2.26}$$

The preceding equation was derived with the assumption that the two end portions of length $h/2$ are governed by the shape factor S_F, while the passive

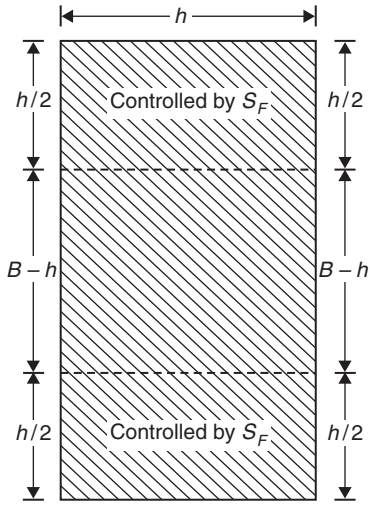

FIGURE 2.14 Assumptions in the derivation of Equation 2.26

pressure along the central portion of length $B - h$ is the same as the strip anchor (Figure 2.14). In Equation 2.26

$$W = \gamma BhH \tag{2.27}$$

and

$$S_F = 1 + m\left(\frac{H}{h}\right) \tag{2.23}$$

Thus:

$$Q_u = \gamma BhH + \gamma H^2 \left\{ 2\left[1 + m\left(\frac{H}{h}\right)\right] h + B - h \right\} K_u \tan\phi \tag{2.28}$$

The breakout factor F_q can be determined as:

$$F_q = \frac{Q_u}{\gamma AH} = \frac{Q_u}{\gamma BhH} \tag{2.29}$$

Combining Equations 2.28 and 2.29, we obtain (Das and Seeley, 1975a):

$$F_q = 1 + \left\{ \left[1 + 2m \left(\frac{H}{h} \right) \right] \left(\frac{h}{B} \right) + 1 \right\} \left(\frac{H}{h} \right) K_u \tan \phi \qquad (2.30)$$

The coefficient m given in Equation 2.23 was determined from experimental observations (Meyerhof and Adams, 1968), and its values are given in Table 2.1. In Figure 2.15, m is also plotted as a function of the soil friction angle ϕ.

Experimental observations of Meyerhof and Adams on circular anchors showed that the magnitude of $S_F K_u = [1 + m(H/h)]K_u$ for a given friction angle

TABLE 2.1 Variation of m (Equation 2.23)

Soil friction angle, ϕ (deg)	m
20	0.05
25	0.1
30	0.15
35	0.25
40	0.35
45	0.5
48	0.6

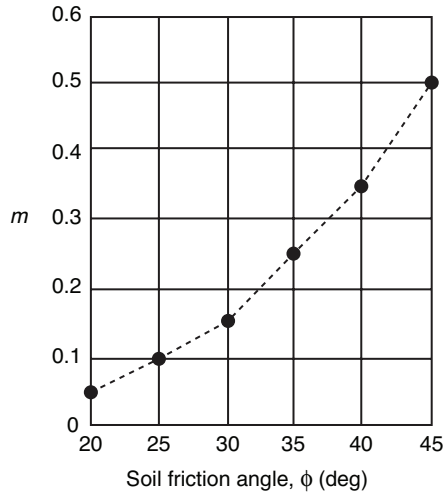

FIGURE 2.15 Variation of m with soil friction angle ϕ

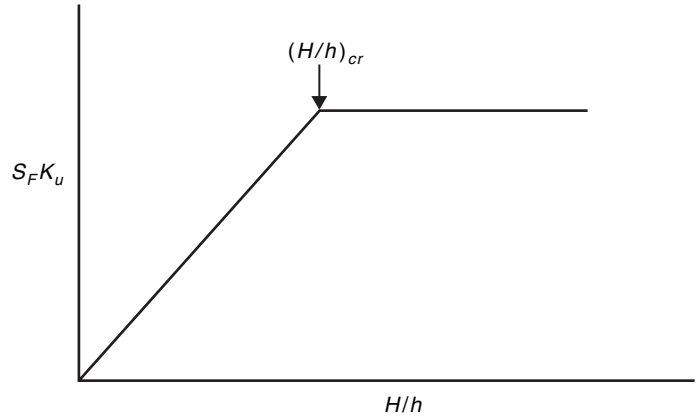

FIGURE 2.16 Nature of variation of $S_F K_u$ with H/h

ϕ increases with H/h to a maximum value at $H/h = (H/h)_{cr}$ and remains constant thereafter, as shown in Figure 2.16. This means that beyond $(H/h)_{cr}$, the anchor behaves as a deep anchor. These $(H/h)_{cr}$ values for square and circular anchors are given in Table 2.2 and also in Figure 2.17.

Thus, for a given value of ϕ for square ($h = B$) and circular (diameter = h) anchors, we can substitute m (Table 2.1) into Equations 2.25 and 2.30 and calculate the breakout factor (F_q) variation with embedment ratio (H/h). The maximum value of $F_q = F_q^\star$ will be attained at $H/h = (H/h)_{cr}$. For $H/h > (H/h)_{cr}$, the breakout factor will remain constant as $F_q^\star$. The variation of F_q with H/h for various values of ϕ made in this manner is shown in Figure 2.18. The variation of the maximum breakout factor $F_q^\star$ for deep square and circular anchors with the soil friction angle ϕ is shown in Figure 2.19.

TABLE 2.2 Critical embedment ratio $(H/h)_{cr}$ for square and circular anchors

Soil friction angle, ϕ (deg)	$(H/h)_{cr}$
20	2.5
25	3
30	4
35	5
40	7
45	9
48	11

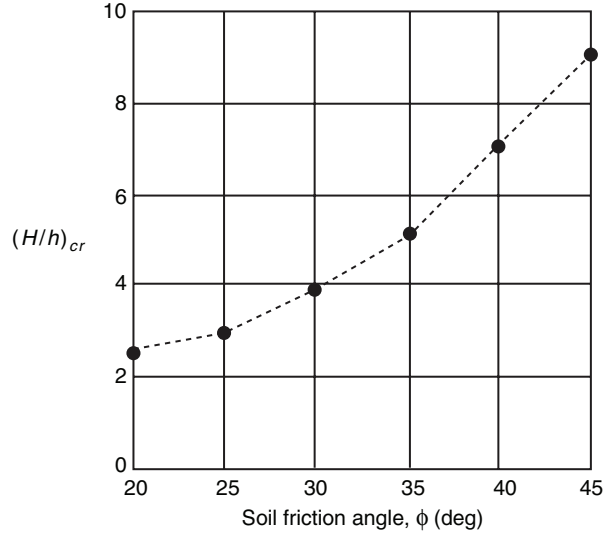

FIGURE 2.17 Variation of $(H/h)_{cr}$ with soil friction angle for square and circular anchors based on the recommendation of Meyerhof and Adams (1968)

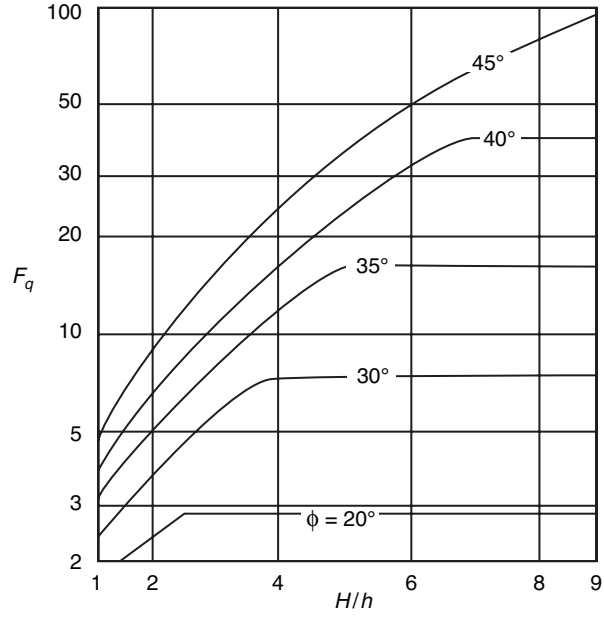

FIGURE 2.18 Plot of F_q (Equations 2.25 and 2.30) for square and circular anchors

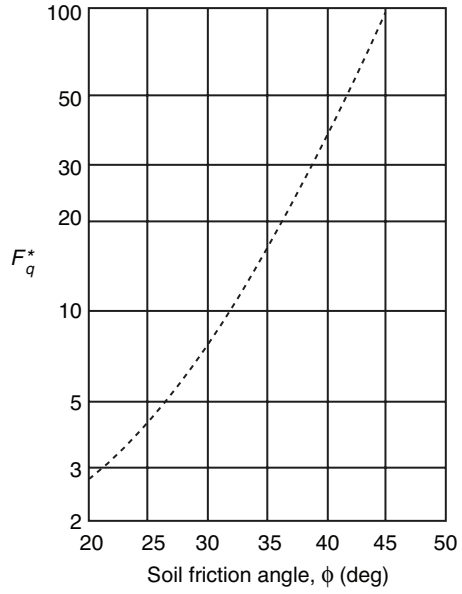

FIGURE 2.19 Plot of F_q^* for deep square and circular anchors

Laboratory experimental observations have shown that the critical embedment ratio for a given soil friction angle ϕ increases with the B/h ratio. Meyerhof (1973) has indicated that for a given value of ϕ:

$$\frac{\left(\frac{H}{h}\right)_{cr\text{-strip}}}{\left(\frac{H}{h}\right)_{cr\text{-square}}} \approx 1.5 \tag{2.31}$$

Based on laboratory model test results, Das and Jones (1982) gave an empirical relationship for the critical embedment ratio of rectangular anchors in the form

$$\left(\frac{H}{h}\right)_{cr\text{-}R} = \left(\frac{H}{h}\right)_{cr\text{-}S} \left[0.133\left(\frac{B}{h}\right) + 0.867\right] \leq 1.4\left(\frac{H}{h}\right)_{cr\text{-}S} \tag{2.32}$$

where

$\left(\frac{H}{h}\right)_{cr\text{-}R}$ = critical embedment ratio of a rectangular anchor with dimensions $B \times h$

$\left(\frac{H}{h}\right)_{cr\text{-}S}$ = critical embedment ratio of a square anchor with dimensions $h \times h$

Using Equation 2.32 and the $(H/h)_{cr\text{-}S}$ values given in Table 2.2, the magnitude of $(H/h)_{cr\text{-}R}$ for rectangular anchors can be estimated. These values of $(H/h)_{cr\text{-}R}$ can be substituted into Equation 2.30 to determine the variation of $F_q = F_q^*$ with the soil friction angle ϕ. Thus, the uplift capacity of shallow and deep anchors can be summarized as follows: For *shallow anchors*:

$$Q_{u(g)} = F_q \gamma A H + W_a \tag{2.33}$$

and for *deep anchors*:

$$Q_{u(g)} = F^* \gamma A H + K_0 p (H - H_{cr}) \overline{\sigma}_0' \tan \phi + W_a \tag{2.34}$$

where

p = perimeter of the anchor shaft
$H - H_{cr}$ = effective length of the anchor shaft (Figure 2.20)
$\overline{\sigma}_0'$ = average effective stress between $z = 0$ to $z = H - H_{cr}$

$$= \frac{1}{2} \gamma (H - H_{cr})$$

K_0 = at-rest earth pressure coefficient ($\approx 1 - \sin \phi$)

The term $K_0 p (H - H_{cr}) \overline{\sigma}_0' \tan \phi$ in Equation 2.34 is the frictional resistance of the shaft. Thus:

$$K_0 p (H - H_{cr}) \overline{\sigma}_0' \tan \phi = \frac{1}{2} \gamma (H - H_{cr})^2 p (1 - \sin \phi) \tan \phi \tag{2.35}$$

Combining Equations 2.34 and 2.35:

$$Q_{u(g)} = F_q^* \gamma A H + \frac{1}{2} \gamma (H - H_{cr})^2 p (1 - \sin \phi) \tan \phi + W_a \tag{2.36}$$

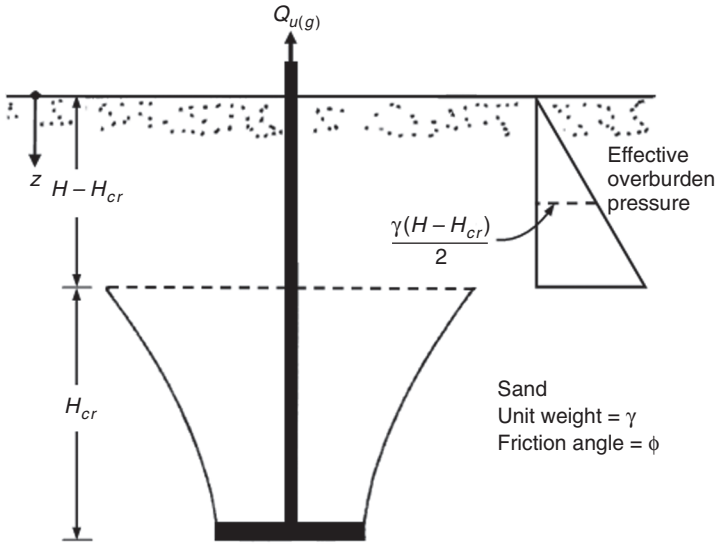

FIGURE 2.20 Deep horizontal plate anchor

2.7 VEESAERT AND CLEMENCE'S THEORY

Based on laboratory model test results, Veesaert and Clemence (1977) suggested that for *shallow circular anchors* the failure surface at ultimate load may be approximated as a truncated cone with an apex angle, as shown in Figure 2.21. With this type of failure surface, the net ultimate uplift capacity can be given as:

$$Q_u = \gamma V + \pi\gamma K(\tan\phi)\left(\cos^2\frac{\phi}{2}\right)\left[\frac{hH^2}{2} + \frac{H^3\tan\left(\frac{\phi}{2}\right)}{3}\right] \quad (2.37)$$

where

V = volume of the truncated cone above the anchor
K = coefficient of lateral earth pressure

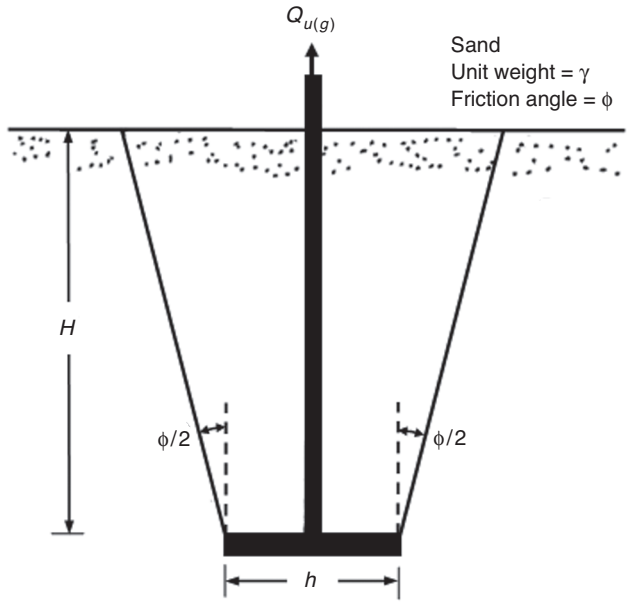

FIGURE 2.21 Assumption of the failure surface in sand for a circular horizontal plate anchor from Veesaert and Clemence's theory (1977)

$$V = \frac{\pi H}{12}\left\{h^2 + \left[h + 2H\tan\left(\frac{\phi}{2}\right)\right]^2 + h\left[h + 2H\tan\left(\frac{\phi}{2}\right)\right]\right\}$$

$$= \frac{\pi H}{12}\left[3h^2 + 4H^2\tan^2\left(\frac{\phi}{2}\right) + 6Hh\tan\left(\frac{\phi}{2}\right)\right] \tag{2.38}$$

Substituting Equation 2.38 into Equation 2.37, we obtain:

$$Q_u = \frac{\pi\gamma H}{3}\left[3h^2 + 4H^2\tan^2\left(\frac{\phi}{2}\right) + 6Hh\tan\left(\frac{\phi}{2}\right)\right]$$

$$+ \pi\gamma K(\tan\phi)\left(\cos^2\frac{\phi}{2}\right)\left[\frac{hH^2}{2} + \frac{H^3\tan\left(\frac{\phi}{2}\right)}{3}\right] \tag{2.39}$$

The breakout factor can now be determined as:

$$F_q = \frac{Q_u}{\gamma AH} = \frac{Q_u}{\gamma\left(\frac{\pi}{4}h^2\right)H} \tag{2.40}$$

Combining Equations 2.39 and 2.40:

$$F_q = \left\{ 4K(\tan\phi)\left[\cos^2\left(\frac{\phi}{2}\right)\right]\left(\frac{H}{h}\right)^2 \times \left[\frac{0.5}{\left(\frac{H}{h}\right)} + \frac{\tan\left(\frac{\phi}{2}\right)}{3}\right]\right\} + \left[1 + 2\left(\frac{H}{h}\right)\tan\left(\frac{\phi}{2}\right) + 1.333\left(\frac{H}{h}\right)^2\tan^2\left(\frac{\phi}{2}\right)\right] \tag{2.41}$$

Veesaert and Clemence (1977) suggested that the magnitude of K_0 may vary between 0.6 to 1.5, with an average value of about 1. Figure 2.22 shows the plot of F_q versus H/h with $K_0 = 1$. In this plot it is assumed that $(H/h)_{cr}$ is the same as that proposed by Meyerhof and Adams (1968) and given in Table 2.2. For $H/h \leq (H/h)_{cr}$, the magnitude of $F_q = F_q^* =$ constant. A comparison of the plots shown in Figures 2.18 and 2.22 reveals the following:

1. For ϕ up to about 35° with $K = 1$, Equation 2.41 yields higher values of F_q compared to those calculated by using Equation 2.30.
2. For $\phi = 40°$ and similar H/h ratios, Equations 2.30 and 2.41 yield practically the same values of F_q.
3. For $\phi > 40°$, the values of F_q calculated by using Equation 2.41 are smaller than those calculated by using Equation 2.30.

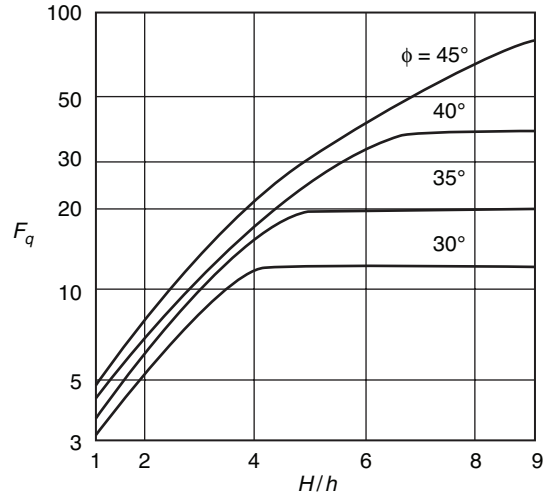

FIGURE 2.22 Variation of F_q for shallow circular anchors (Equation 2.41)

2.8 VESIC'S THEORY

Vesic (1965) studied the problem of an explosive point charge expanding a spherical cavity close to the surface of a semi-infinite, homogeneous, isotropic solid (in this case, the soil). Referring to Figure 2.23, it can be seen that if the distance H is small enough, there will be an ultimate pressure p_0 that will shear away the soil located above the cavity. At that time, the diameter of the spherical

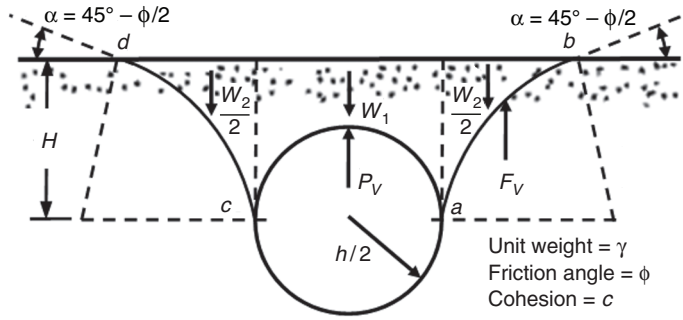

FIGURE 2.23 Vesic's theory (1965) of expansion of cavities

cavity is equal to h. The slip surfaces ab and cd will be tangent to the spherical cavity at a and c. At points b and d, they make an angle $\alpha = 45° - \phi/2$. Now, for equilibrium, summing the components of forces in the vertical direction, we can determine the ultimate pressure p_0 in the cavity. Forces that will be involved are

1. Vertical component of the force inside the cavity, P_V
2. Effective self-weight of the soil, $W = W_1 + W_2$
3. Vertical component of the resultant of internal forces, F_V

For a c-ϕ soil, we can thus determine that

$$p_0 = C\bar{F}_c + \gamma H\bar{F}_q \tag{2.42}$$

where

$$\bar{F}_q = 1.0 - \frac{2}{3}\left[\frac{\left(\frac{h}{2}\right)}{H}\right] + A_1\left[\frac{H}{\left(\frac{h}{2}\right)}\right] + A_2\left[\frac{H}{\left(\frac{h}{2}\right)}\right]^2 \tag{2.43}$$

$$\bar{F}_c = A_3\left[\frac{H}{\left(\frac{h}{2}\right)}\right] + A_4\left[\frac{H}{\left(\frac{h}{2}\right)}\right] \tag{2.44}$$

where

A_1, A_2, A_3, A_4 = functions of the soil friction angle ϕ

For granular soils, $c = 0$. Thus:

$$p_0 = \gamma H\bar{F}_q \tag{2.45}$$

Vesic (1971) applied the preceding concept to determine the ultimate uplift capacity of shallow circular anchors. In Figure 2.23, consider that the circular anchor plate ab, with a diameter h, is located at a depth H below the ground

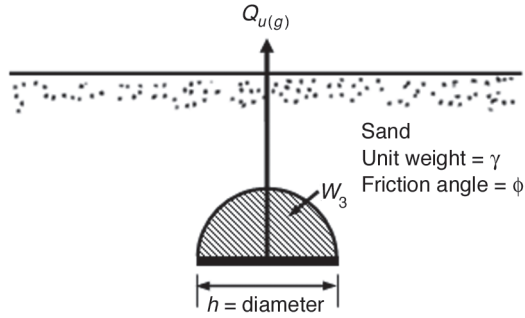

FIGURE 2.24 A hemispherical cavity filled with soil above the anchor plate

surface. If the hemispherical cavity above the anchor plate is filled with soil, it will have a weight of (Figure 2.24):

$$W_3 = \frac{2}{3}\pi\left(\frac{h}{2}\right)^3\gamma \tag{2.46}$$

This weight of soil will increase the pressure by p_1, which can be given as:

$$p_1 = \frac{W_3}{\pi\left(\frac{h}{2}\right)^2} = \frac{\left(\frac{2}{3}\right)\pi\left(\frac{h}{2}\right)^3\gamma}{\pi\left(\frac{h}{2}\right)^2} = \frac{2}{3}\gamma\left(\frac{h}{2}\right)$$

If the anchor is embedded in a cohesionless soil ($c = 0$), then the pressure p_1 should be added to Equation 2.43 to obtain the force per unit area of the anchor, q_u, needed for complete pullout. Thus:

$$q_u = \frac{Q_u}{A} = \frac{Q_u}{\pi\left(\frac{h}{2}\right)^2} = p_0 + p_1 = \gamma H\overline{F}_q + \frac{2}{3}\gamma\left(\frac{h}{2}\right)$$

$$= \gamma H\left[\overline{F}_q + \frac{\frac{2}{3}\left(\frac{h}{2}\right)}{H}\right] \tag{2.47}$$

TABLE 2.3 Vesic's (1971) breakout factor F_q for circular anchors

	H/h				
Soil friction angle, ϕ (deg)	0.5	1.0	1.5	2.5	5.0
0	1.0	1.0	1.0	1.0	1.0
10	1.18	1.37	1.59	2.08	3.67
20	1.36	1.75	2.20	3.25	6.71
30	1.52	2.11	2.79	4.41	9.89
40	1.65	2.41	3.30	5.45	13.0
50	1.73	2.61	3.56	6.27	15.7

or

$$q_u = \frac{Q_u}{A} = \gamma H \left\{ 1 + A_1 \left[\frac{H}{\left(\frac{h}{2}\right)} \right] + A_2 \left[\frac{H}{\left(\frac{h}{2}\right)} \right]^2 \right\} = \gamma H F_q \qquad (2.48)$$

Breakout factor

The variation of the breakout factor F_q for shallow *circular anchor plates* is given in Table 2.3 (and also Figure 2.25). In a similar manner, using the analogy of the expansion of the long cylindrical cavities, Vesic determined the variation of the breakout factor F_q for *shallow strip anchors*. These values are given in Table 2.4 and are also plotted in Figure 2.26.

2.9 SAEEDY'S THEORY

An ultimate holding capacity theory for *circular plate anchors* embedded in sand was proposed by Saeedy (1987) in which the trace of the failure surface was assumed to be an arc of a logarithmic spiral, as shown in Figure 2.27. According to this solution, for shallow anchors the failure surface extends to the ground surface. However, for deep anchors (that is, $H > H_{cr}$), the failure surface extends to a distance of H_{cr} above the anchor plate. Based on this analysis, Saeedy (1987) proposed the net ultimate uplift capacity in a nondimensional form ($Q_u/\gamma H h^2$) for various values of ϕ and the H/h ratio. The authors have converted the solution into a plot of breakout factor $F_q = Q_u/\gamma AH$ (A = area of the anchor

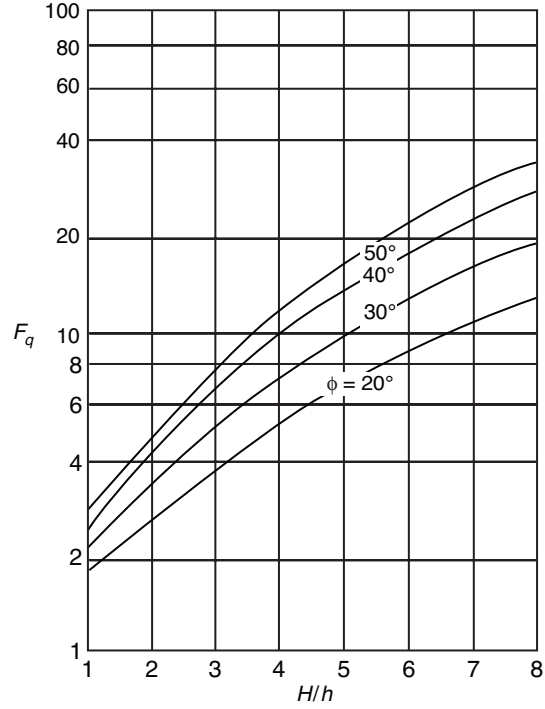

FIGURE 2.25 Vesic's (1971) breakout factor F_q for shallow circular anchors

TABLE 2.4 Vesic's (1971) breakout factor F_q for strip anchors

	H/h				
Soil friction angle, ϕ (deg)	0.5	1.0	1.5	2.5	5.0
0	1.0	1.0	1.0	1.0	1.0
10	1.09	1.16	1.25	1.42	1.83
20	1.17	1.33	1.49	1.83	2.65
30	1.24	1.47	1.71	2.19	3.38
40	1.30	1.58	1.87	2.46	3.91
50	1.32	1.64	2.04	2.6	4.2

plate) versus the soil friction angle ϕ, as shown in Figure 2.28. According to Saeedy (1987), during the anchor pullout, the soil located above the anchor gradually becomes compacted, in turn increasing the shear strength of the soil and, hence, the net ultimate uplift capacity. For that reason, he introduced an empirical *compaction factor,* which is given in the form

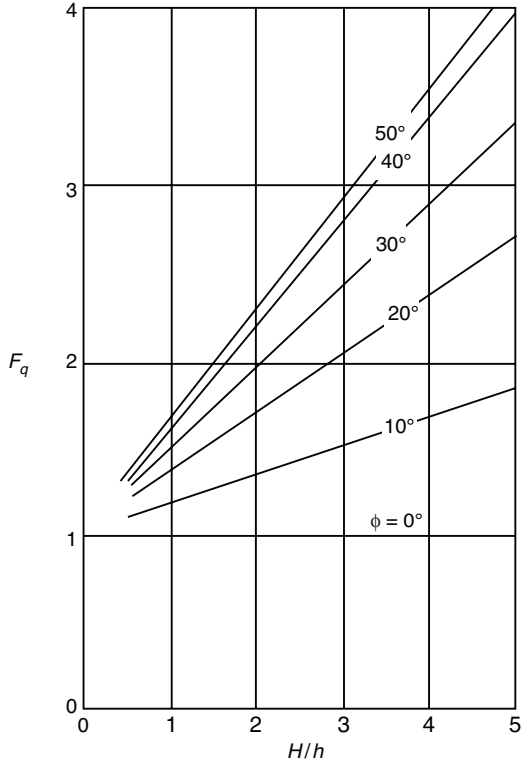

FIGURE 2.26 Vesic's (1971) breakout factor F_q for shallow strip anchors

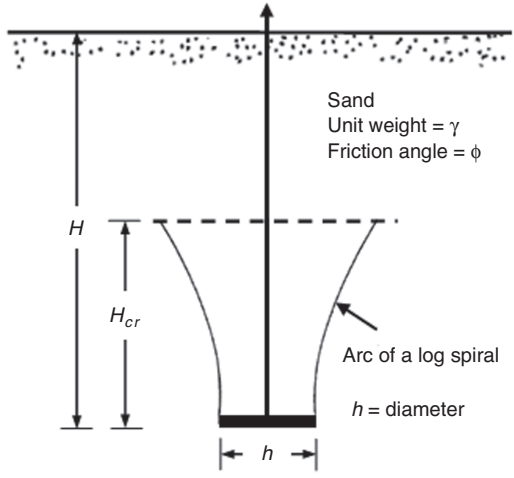

FIGURE 2.27 Saeedy's theory (1987) for circular plate anchors

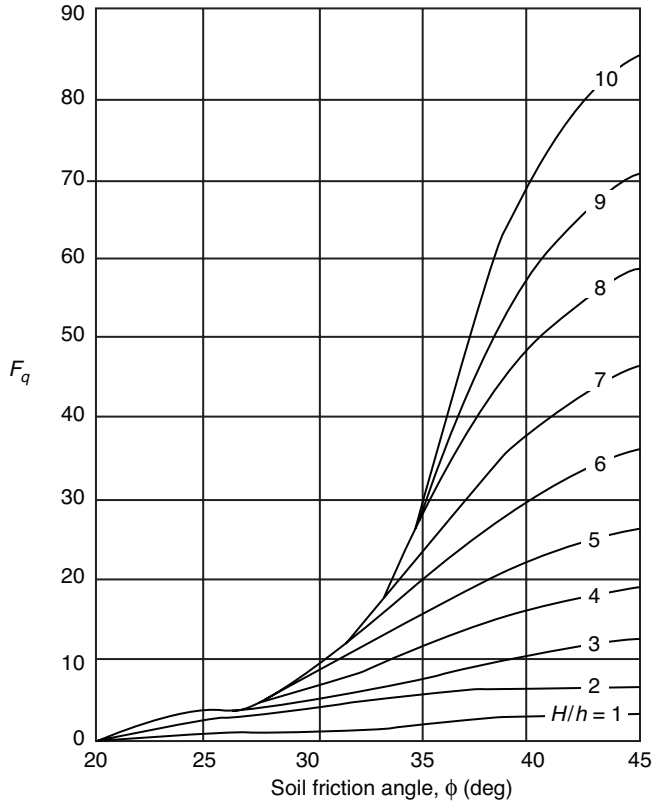

FIGURE 2.28 Plot of F_q based on Saeedy's theory (1987)

$$\mu = 1.044 D_r + 0.44 \tag{2.49}$$

where

μ = compaction factor
D_r = relative density of compaction

Thus, the actual net ultimate capacity can be expressed as:

$$Q_{u(\text{actual})} = \mu F_q \gamma A H \tag{2.50}$$

2.10 DISCUSSION OF VARIOUS THEORIES

Based on various theories presented in the previous sections, we can make some general observations:

1. All of the preceding theories presented, except that of Meyerhof and Adams (1968), are for the axisymmetric case (that is, for use in the case of *circular* anchors). Meyerhof and Adams's theory addresses the case of *rectangular* anchors.
2. Most theories assume that the shallow anchor condition exists for $H/B \leq 5$. Meyerhof and Adams's theory provides a critical embedment ratio $(H/h)_{cr}$ for *square* and *circular* anchors as a function of the soil friction angle.
3. Experimental observations generally tend to show that for shallow anchors embedded in loose sand, Balla's theory (1961) overestimates the net ultimate uplift capacity. However, better agreement is obtained for anchors embedded in dense soil.
4. Vesic's theory (1971) is generally fairly accurate in estimating the net ultimate uplift capacity for shallow anchors in loose sand. However, laboratory experimental observations have shown that for shallow anchors embedded in dense sand, this theory can underestimate the actual capacity by as much as 100% or more.
5. Mariupol'skii's theory (1965) suggests that for calculation of the net ultimate uplift capacity, the lower of the two values obtained from Equations 2.14 and 2.15 should be used. The reason for such recommendation is due to the fact that the critical embedment was not clearly established in the theory.

Figure 2.29 shows a comparison of some published laboratory experimental results for the net ultimate uplift capacity of *circular anchors* with the theories of Balla, Vesic, and Meyerhof and Adams. Table 2.5 gives the references to the laboratory experimental curves shown in Figure 2.29. In developing the theoretical plots for $\phi = 30°$ (loose sand condition) and $\phi = 45°$ (dense sand condition), the following procedures have been used:

1. According to Balla's theory (1961), from Equation 2.9 for circular anchors:

$$Q_u = H^3\gamma(F_1 + F_3)$$

Figure 2.7

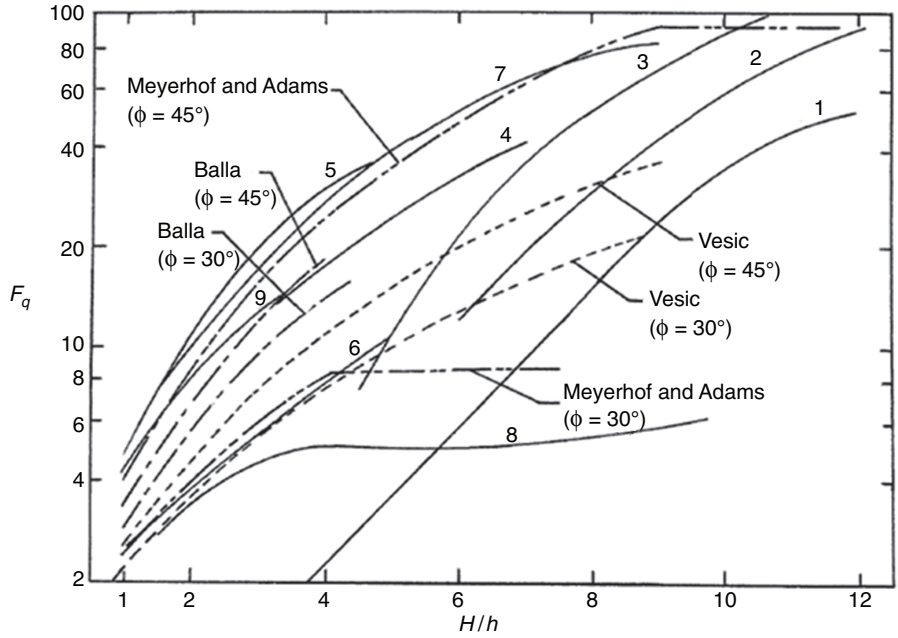

FIGURE 2.29 Comparison of theories with laboratory experimental results for circular anchor plates

TABLE 2.5 References to laboratory experimental curves shown in Figure 2.29

Curve no.	Reference	Circular anchor diameter, h (mm)	Soil properties
1	Baker and Kondner (1966)	25.4	$\phi = 42°$, $\gamma = 17.61$ kN/m^3
2	Baker and Kondner (1966)	38.1	$\phi = 42°$, $\gamma = 17.61$ kN/m^3
3	Baker and Kondner (1966)	50.8	$\phi = 42°$, $\gamma = 17.61$ kN/m^3
4	Baker and Kondner (1966)	76.2	$\phi = 42°$, $\gamma = 17.61$ kN/m^3
5	Sutherland (1965)	38.1–152.4	$\phi = 45°$
6	Sutherland (1965)	38.1–152.4	$\phi = 31°$
7	Esquivel-Diaz (1967)	76.2	$\phi \approx 43°$, $\gamma = 14.81$–15.14 kN/m^3
8	Esquivel-Diaz (1967)	76.2	$\phi \approx 33°$, $\gamma = 12.73$–12.89 kN/m^3
9	Balla (1961)	61–119.4	Dense sand

Thus:

$$F_1 + F_3 = \frac{Q_u}{\gamma H^3} = \frac{\left(\frac{\pi}{4} h^2\right) Q_u}{\gamma H^3 \left(\frac{\pi}{4} h^2\right)} = \frac{\left[\frac{\pi}{4} \left(\frac{h}{H}\right)^2\right] Q_u}{\gamma AH}$$

or

$$F_q = \frac{Q_u}{\gamma AH} = \frac{F_1 + F_3}{\frac{\pi}{4} \left(\frac{h}{H}\right)^2} \tag{2.51}$$

Thus, for a given soil friction angle, the sum of $F_1 + F_3$ has been obtained from Figure 2.7 and the breakout factor has been calculated for various values of H/h, and they have been plotted in Figure 2.29.

2. For Vesic's theory (1971), the variations of F_q versus H/h for circular anchors have been given in Table 2.3. These values of F_q have also been plotted in Figure 2.29.
3. The breakout factor relationship for circular anchors based on Meyerhof and Adams's theory (1968) is given in Equation 2.25. Using $K_u \approx 0.95$, the variations of F_q with H/h have been calculated and are plotted in Figure 2.29.

Based on the comparison between the theories and the laboratory experimental results shown in Figure 2.29, it appears that Meyerhof and Adams's theory (1968) is more applicable to a wide range of anchors and it provides as good an estimate as any for the net ultimate uplift capacity. Therefore, this theory is recommended for use. However, it needs to be kept in mind that the majority of the experimental results presently available in the literature for comparison with the theory are from laboratory model tests. When applying these results to the design of an actual foundation, the *scale effect* needs to be taken into consideration. For that reason, a judicious choice is necessary in selecting the value of the soil friction angle ϕ.

Example 2.1

Consider a circular anchor plate embedded in sand. For the anchor, diameter $h = 0.3$ m and depth of embedment $H = 1.2$ m. For the sand, unit weight $\gamma = 17.4$ kN/m^3 and friction angle $\phi = 35°$. Using Balla's theory, calculate the net ultimate uplift capacity.

Solution

From Equation 2.9:

$$Q_u = H^3\gamma(F_1 + F_3)$$

From Figure 2.7, for $\phi = 35°$ and $H/h = 1.2/0.3 = 4$, the magnitude of $F_1 + F_3 \approx 0.725$. Thus:

$$Q_u = (1.2)^3\,(17.4)\,(0.725) = \mathbf{21.8\ kN}$$

Example 2.2

Redo Example 2.1 using Vesic's theory (1965).

Solution

From Equation 2.48:

$$Q_u = \gamma AHF_q$$

From Figure 2.25, for $\phi = 35°$ and $H/h = 4$, F_q is about 9. Therefore:

$$Q_u = \left[\left(\frac{\pi}{4}\right)(0.3)^2\right](17.4)\,(1.2)\,(9) = \mathbf{13.28\ kN}$$

Example 2.3

Redo Example 2.1 using Meyerhof and Adams's theory (1968).

Solution

From Equation 2.25:

$$F_q = 1 + 2\left[1 + m\left(\frac{H}{h}\right)\right]\left(\frac{H}{h}\right)K_u \tan\phi$$

For $\phi = 35°$, $m = 0.25$ (Table 2.1). Hence:

$$F_q = 1 + 2\,[1 + (0.25)\,(4)]\,(4)\,(0.95)\,(\tan 35°) = 11.64$$

Therefore:

$$Q_u = F_q \gamma AH = (11.64)\,(17.4)\left[\left(\frac{\pi}{4}\right)(0.3)^2\right](1.2) = \mathbf{17.18\ kN}$$

Example 2.4

Redo Example 2.1 using Veesaert and Clemence's theory (1977). Use $K = 1$.

Solution

From Equation 2.41:

$$F_q = \left\{4K(\tan\phi)\left[\cos^2\left(\frac{\phi}{2}\right)\right]\left(\frac{H}{h}\right)^2\left[\frac{0.5}{\left(\frac{H}{h}\right)} + \frac{\tan\left(\frac{\phi}{2}\right)}{3}\right]\right\}$$

$$+ \left[1 + 2\left(\frac{H}{h}\right)\tan\left(\frac{\phi}{2}\right) + 1.333\left(\frac{H}{h}\right)^2 \tan^2\left(\frac{\phi}{2}\right)\right]$$

Using $\phi = 35°$, $H/h = 4$, and $K = 1$:

$$F_q = \left\{ (4)(1)(\tan 35°)[\cos^2(17.5°)](4)^2 \left[\frac{0.5}{4} + \frac{\tan(17.5°)}{3} \right] \right\}$$

$$+ \{1 + (2)(4)[\tan(17.5°)] + (1.333)(4)^2[\tan^2(17.5°)]\}$$

$$= 15$$

Therefore:

$$Q_u = F_q \gamma A H = (15)(17.4)\left[\left(\frac{\pi}{4} \right)(0.3)^2 \right](1.2) = \mathbf{22.14\ kN}$$

2.11 LOAD-DISPLACEMENT RELATIONSHIP

In order to determine the allowable net ultimate uplift capacity of plate anchors, two different procedures can be adopted:

1. Use of a *tentative factor of safety* F_s, based on the uncertainties of determination of the soil shear strength parameters and other associated factors. For this type of analysis:

$$Q_{u(\text{all})} = \frac{Q_u}{F_s} \tag{2.52}$$

2. Use of a *load-displacement relationship*. In this method, the allowable net ultimate uplift capacity is calculated which corresponds to a predetermined allowable vertical displacement of the anchor.

Das and Puri (1989) investigated the load-displacement relationship of *shallow horizontal square and rectangular plate anchors* embedded in medium and dense sands. For these laboratory model tests, the width of the anchor plate (h) was kept at 50.8 mm. The length-to-width ratios of the anchors (B/h) were varied from 1 to 3, and the H/h ratios were varied from 1 to 5. Based on their laboratory observations, the net load Q versus vertical displacement Δ plots can

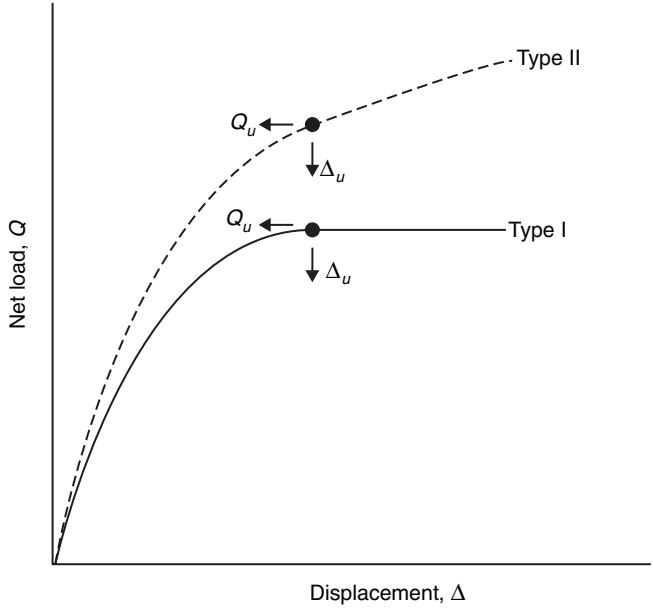

FIGURE 2.30 Nature of load versus displacement plots

be of two types, as shown in Figure 2.30. In Type I, the net load increases with displacement up to a maximum value at which sudden pullout occurs. The maximum load in this case is the net ultimate uplift capacity Q_u. In Type II, the net load increases with the vertical displacement fairly rapidly up to a certain point, beyond which the load-displacement relationship becomes practically linear. For this case, the net ultimate uplift capacity is defined as the point where the slope of the Q versus Δ plot becomes minimum. The vertical displacement which corresponds to load Q_u is defined as Δ_u in Figure 2.30.

Figure 2.31 shows the magnitudes of Δ_u for anchors with various B/h ratios placed at varying embedment ratios (H/h). It needs to be pointed out that for tests conducted in medium sand, the relative density of compaction D_r was about 48%. Similarly, for tests conducted in dense sand, the average value of D_r was about 73%. With their experimental results, Das and Puri (1989) proposed a nondimensional empirical load-displacement relationship for shallow plate anchors which is of the form

$$\overline{Q} = \frac{\overline{\Delta}}{a + b\overline{\Delta}} \tag{2.53}$$

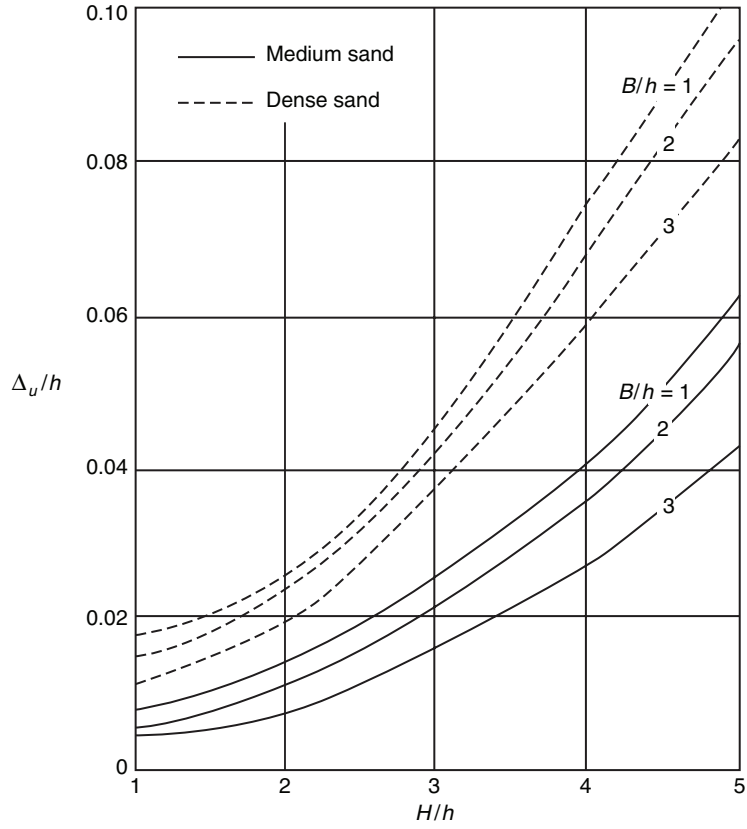

FIGURE 2.31 Variation of Δ_u/h with H/h based on the model tests of Das and Puri (1989) (h = 50.8 mm)

where

$$\overline{Q} = \frac{Q}{Q_u} \tag{2.54}$$

$$\overline{\Delta} = \frac{\Delta}{\Delta_u} \tag{2.55}$$

Δ = anchor displacement at net uplifting load Q
a, b = constants

The constants a and b are approximately equal to 0.175 and 0.825, respectively, and they are not functions of the relative density of compaction. From Equation 2.53, it follows that:

$$\frac{\overline{\Delta}}{Q} = a + b\overline{\Delta} \tag{2.56}$$

The preceding equation implies that a plot of $\overline{\Delta}/\overline{Q}$ versus $\overline{\Delta}$ will be approximately linear.

Example 2.5

Consider a shallow rectangular anchor embedded in sand where $h = 0.3$ m, $B = 0.9$ m, and $H = 1.2$ m. For the sand, $\gamma = 18$ kN/m^3 and $\phi = 35°$. Estimate:

a. The net ultimate uplift capacity using the theory of Meyerhof and Adams (1968)
b. The anchor displacement at ultimate load
c. The net load Q at an anchor displacement of $0.5\Delta_u$

Solution

Part a. For this case:

$$\frac{B}{h} = \frac{0.9}{0.3} = 3; \qquad \frac{H}{h} = \frac{1.2}{0.3} = 4$$

From Table 2.2, $H/h < (H/h)_{cr}$ for $\phi = 35°$. Therefore, it is a shallow anchor. From Equations 2.29 and 2.30:

$$Q_u = F_q \gamma B h H$$

$$F_q = 1 + \left\{ \left[1 + 2m\left(\frac{H}{h}\right) \right] \left(\frac{h}{B}\right) + 1 \right\} \left(\frac{H}{h}\right) K_u \tan\phi$$

For $\phi = 35°$, the value of m is 0.25. Assuming $K_u \approx 0.95$, we can calculate F_q. Hence:

$$F_q = 1 + \left\{ [1 + (2)\,(0.25)\,(4)] \left(\frac{1}{3}\right) + 1 \right\} (4)\,(0.95)\,(\tan 35°) = 6.32$$

Therefore:

$$Q_u = F_q \gamma B h H = (6.32)\,(18)\,(0.9)\,(0.3)\,(1.2) = \mathbf{36.86\ kN}$$

Part b. Consider the sand as loose. From Figure 2.31, for $B/h = 3$ and $H/h = 4$, the value of $\Delta_u/h \approx 0.06$. Therefore:

$$\Delta_u \approx (0.06)\,(0.3) = 0.18\ \text{m} = \mathbf{180\ mm}$$

Part c. From Equation 2.53:

$$\overline{Q} = \frac{\overline{\Delta}}{a + b\overline{\Delta}}; \qquad \overline{\Delta} = \frac{\Delta}{\Delta_u} = 0.5$$

Thus:

$$\overline{Q} = \frac{0.5}{0.175 + (0.825)\,(0.5)} = 0.851; \qquad \overline{Q} = \frac{Q}{Q_u} = 0.851$$

Therefore:

$$Q = (0.851)\,(36.86) = \mathbf{31.37\ kN}$$

Liu et al. (2012) presented a laboratory experimental investigation on soil deformation around plate anchors during uplift in sand by using digital image correlation. This study shows that the soil deformation and the pullout resistance of horizontal plate anchors are substantially influenced by soil density and anchor embedment depth, whereas particle size within the studied range (fine to coarse sand) has limited influence. For the same embedment ratio of 3 in loose sand, the anchor deforms 6.30 mm to reach its peak pullout resistance of

24.8 N compared with the values of 0.76 mm and 61.3 N, respectively, in dense sand. In dense sand, the shape of the failure surface changes from a truncated cone above a shallow anchor to a combined shape of a curved cone and a truncated cone for a deep anchor. In contrast, in loose sand, a cone-shaped failure surface is formed within the soil mass above a shallow anchor; however, no failure surface is observed for a deep anchor, where the compressibility of soil is the dominating factor that influences the behavior of deep plate anchors in loose sand.

2.12 ANCHORS SUBJECTED TO REPEATED LOADING

Horizontal anchors are sometimes used to moor surface vessels or buoys as well as semi-submersible or submersible structures. These anchors may be subjected to a combination of sustained and repeated loads. The application of repeated loads may create a progressive accumulative cyclic strain that will ultimately lead to the uplift of the anchor. Very few studies are available to evaluate the effect of repeated loads on anchors. Andreadis et al. (1978) studied the behavior of model circular anchor plates embedded in saturated dense sand and subjected to cyclic loading. For this study, the embedment ratio H/h was kept as 12 (that is, deep anchor condition). The cyclic load was sinusoidal in nature with 10-second duration cycles (Figure 2.32a). In some tests, the cyclic load Q_c was applied alone, as shown in Figure 2.32b. Also, some tests were conducted with an initial application of a sustained static load Q_s and then a cyclic load of magnitude Q_c, and the results of these tests are shown in Figure 2.33. In Figure 2.33, the relative anchor movement is defined as:

$$\Delta\lambda = \frac{\Delta}{h} \tag{2.57}$$

where

Δ = uplift of anchor
h = anchor diameter

It can be seen from Figure 2.33 that for a given magnitude of Q_c/Q_u, the relative anchor displacement $\Delta\lambda$ increased with the number of cycles.

Based on their model tests, Andreadis et al. (1978) suggested that when the cyclic relative anchor displacement is kept below about half the relative movement to failure in static pullout tests, there is essentially no reduction in strength

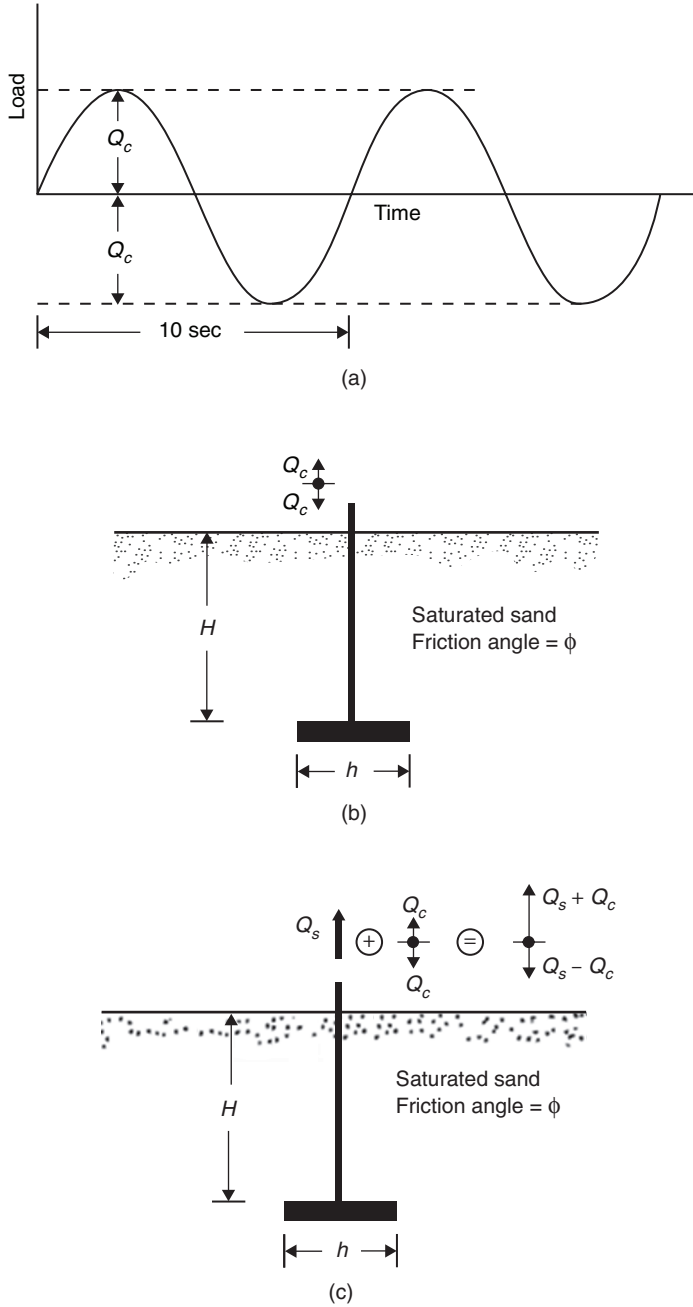

FIGURE 2.32 Details of the model tests of Andreadis et al. (1978) on deep circular anchor plates

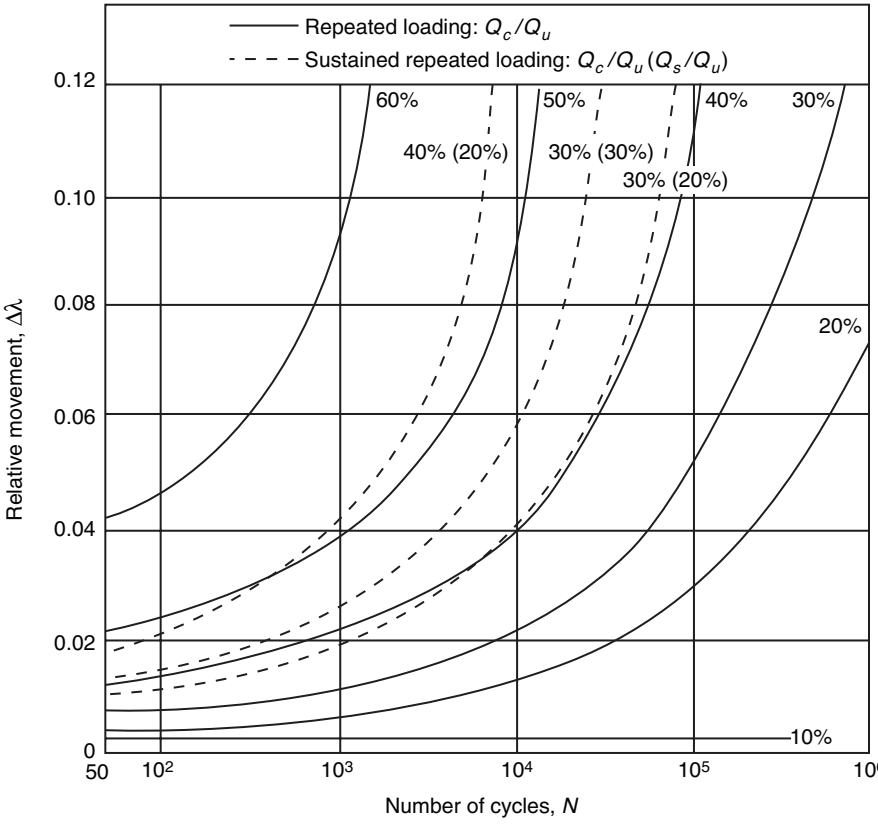

FIGURE 2.33 Relative anchor movement versus number of cycles in dense sand (H/h = 12, circular anchor) (after Andreadis et al., 1978)

due to cyclic loading. For that reason, a plot of Q_c/Q_u versus number of cyclic load applications for various values of $\Delta\lambda$ is shown in Figure 2.34, essentially obtained from the experimental results shown in Figure 2.33. Therefore, if the ultimate displacement Δ_u at ultimate static load Q_u is known, one can calculate the allowable maximum value $\Delta\lambda$ as:

$$\Delta\lambda_{(\text{allowable})} \approx \frac{1}{2}\Delta_u \tag{2.58}$$

Once $\Delta\lambda_{(\text{allowable})}$ is known, the magnitude of Q_c/Q_u and thus Q_c, corresponding to the number of load application cycles during the life span of the anchor, can be estimated.

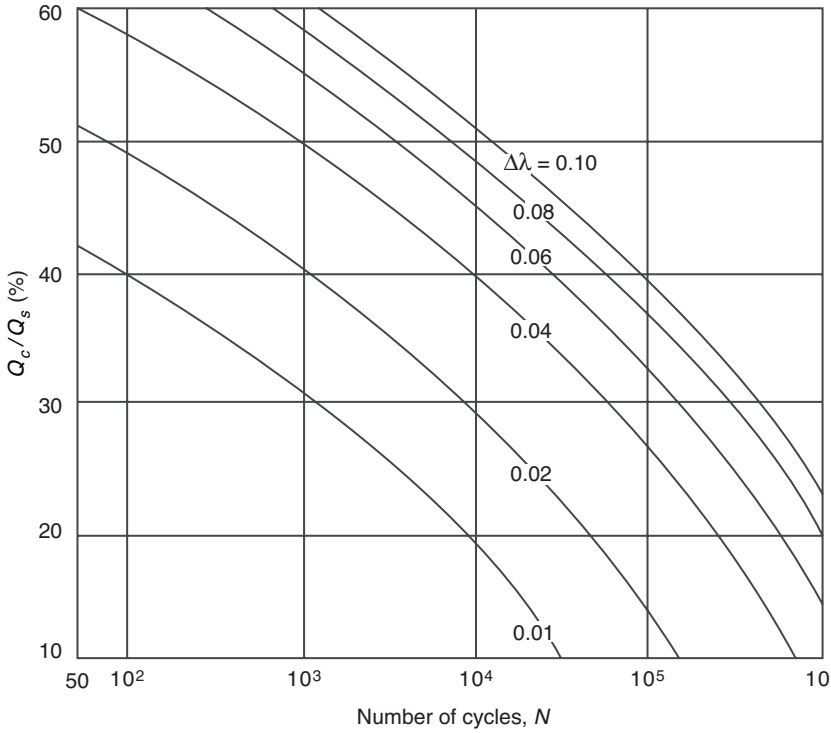

FIGURE 2.34 Relative cyclic load versus number of cycles in dense sand (H/h = 12, circular anchor) (adapted from Andreadis et al., 1978)

2.13 UPLIFT CAPACITY OF SHALLOW GROUP ANCHORS

When anchors placed in a group are subjected to an uplifting load, the net ultimate uplift capacity of the group may possibly be smaller than the net ultimate uplift capacity of a single anchor times the number of anchors in the group. This condition arises when the center-to-center spacing of the anchor is small and when, during the anchor uplift, there is interference of the failure zones in soil. Figure 2.35 shows a group of anchors located at a shallow depth H. All of the anchors are circular in shape, and the center-to-center spacing of the anchors is equal to s. In the plan of the anchor group, there are m number of rows and n columns. The gross ultimate uplift capacity of the anchor group, $Q_{ug(g)}$, can be given as:

$$Q_{ug(g)} = Q_{ug} + W_g \tag{2.59}$$

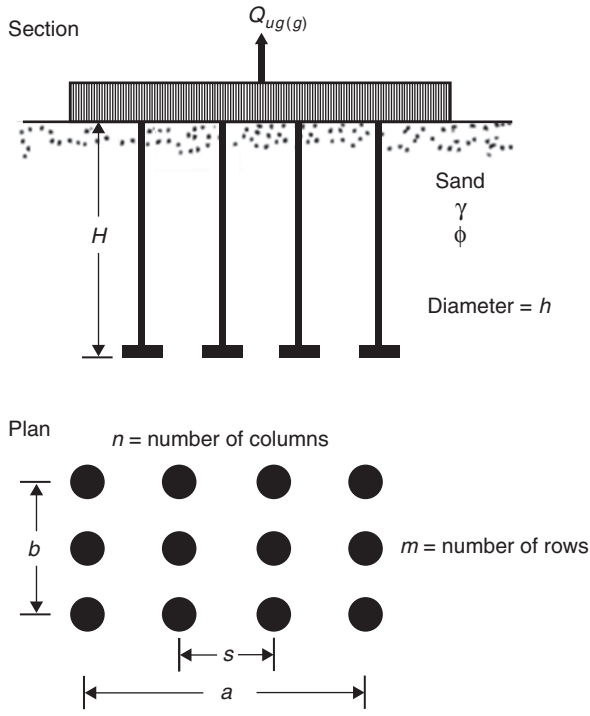

FIGURE 2.35 Group anchors

where

Q_{ug} = net ultimate uplift capacity of the group
W_g = effective self-weight of anchors and the shafts

Meyerhof and Adams (1968) derived a theoretical relationship for the net ultimate capacity of group anchors, according to which

$$Q_{ug} = \gamma H^2 \left[a + b + S_F \left(\frac{\pi}{2} \right) h \right] K_u \tan \phi + W_s \qquad (2.60)$$

where

S_F = shape factor
K_u = nominal uplift coefficient

W_s = effective weight of the sand located above the anchor group
$a = s(n - 1)$ (see Figure 2.35)
$b = s(m - 1)$ (see Figure 2.35)

The shape factor S_F is given by the same relationship as in Equation 2.23, or:

$$S_F = 1 + m\left(\frac{H}{h}\right)$$

Table 2.1

The nominal uplift coefficient K_u is the same as shown in Figure 2.13 and may be taken as approximately 0.95 for all values of the soil friction angle ϕ. In deriving Equation 2.60, it is assumed that the passive pressure along the curved portion of the perimeter of the group is governed by the shape factor S_F, and the passive earth pressure along the straight portions is the same as for strip anchors.

In the conventional manner, the group efficiency η can now be defined as:

$$\eta = \frac{Q_{ug}}{mnQ_u} \tag{2.61}$$

Thus, combining Equations 2.60, 2.61, and 2.22, we obtain:

$$\eta\,(\%) = \left\{ \frac{\gamma H^2 \left[a + b + S_F\left(\frac{\pi}{2}\right)h\right] K_u \tan\phi + W_s}{mn\left[\left(\frac{\pi}{2}\right) S_F \gamma h H^2 K_u \tan\phi + W\right]} \right\} (100) \leq 100\% \tag{2.62}$$

In order to investigate the applicability of the preceding equation, Das and Jin-Kaun (1987) conducted a limited number of laboratory model tests in compacted sand at a relative density of 68% with an angle of friction of 37°. Figures 2.36 and 2.37 show the model test results for group efficiency for the cases of $H/h = 4$ and 6, respectively. The theoretical variations of the group efficiency with the center-to-center spacing of anchors are also shown in Figures 2.36 and 2.37. A comparison of the theoretical and experimental results shows that for a given anchor configuration and H/h, the s/h ratio at which $\eta = 100\%$ is approximately twice that predicted by the theory. However, the general trend

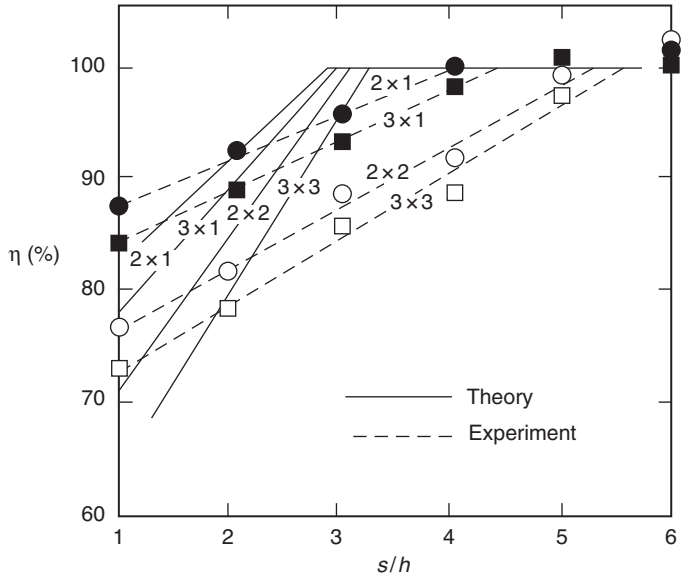

FIGURE 2.36 Variation of η versus s/h for group piles (relative density = 68%, H/h = 4) (adapted from Das and Jin-Kaun, 1987)

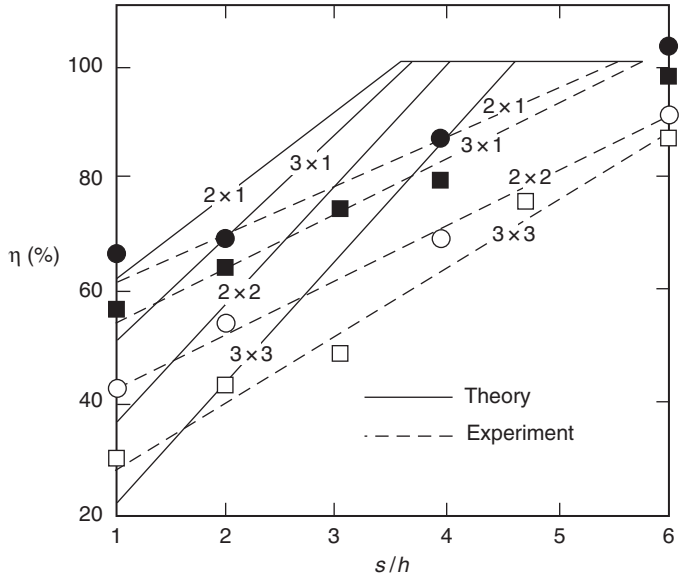

FIGURE 2.37 Variation of η versus s/h for group piles (relative density = 68°, H/h = 6) (adapted from Das and Jin-Kaun, 1987)

of the actual variation of η versus s/h for a given anchor configuration is similar to that predicted by the theory.

Kumar and Kouzer (2008a) analyzed the effect of spacing of a group of two and multiple rough strip anchors, with equal widths and placed horizontally in sand, on the magnitude of the vertical uplift resistance. The analysis was carried out by using an upper bound limit analysis with the employment of a simple rigid wedge mechanism bounded by planar rupture surfaces. It has been reported that when the clear spacing S $(= s - h)$ between the anchors is greater than $2H \tan \phi$, no interference of the anchors occurs. On the other hand, for $S < 2H \tan \phi$, the uplift resistance of the anchors reduces substantially with a decrease in S. The uplift resistance for a group of interfering multiple anchors was found to be smaller than that for a group of two anchors installed at a large spacing.

2.14 SPREAD FOUNDATIONS UNDER UPLIFT

Spread foundations constructed for electric transmission towers are subjected to uplifting force. The uplift capacity of such foundations can be estimated by using the same relationship described in this chapter. During the construction of such foundations, the embedment ratio H/h is usually 3 or less. The native soil is first excavated for foundation construction. Once the foundation construction is finished, the excavation is backfilled and compacted. The degree of compaction of the backfill material plays an important role in the actual net ultimate uplift capacity of the foundation. Kulhawy et al. (1987) conducted several laboratory model tests to observe the effect of the degree of compaction of the backfill compared to the native soil. According to their observations, in most cases, at ultimate load, failure in soil takes place by side shear, as shown in Figure 2.38. However, wedge or combined shear failure occurs for foundations with $H/h <$ about 2 in medium to dense native soil where the backfill is at least 85% as dense as the native soil (Figure 2.39). Figure 2.40 shows the effect of backfill compaction on the breakout factor F_q when the native soil is loose. Similarly, Figure 2.41 shows the effect where the native soil is dense. Based on the observations of Kulhawy et al. (1987), this study shows that the compaction of the backfill has a great influence on the breakout factor of the foundation, and the net ultimate uplift capacity is greatly increased with the degree of backfill compaction.

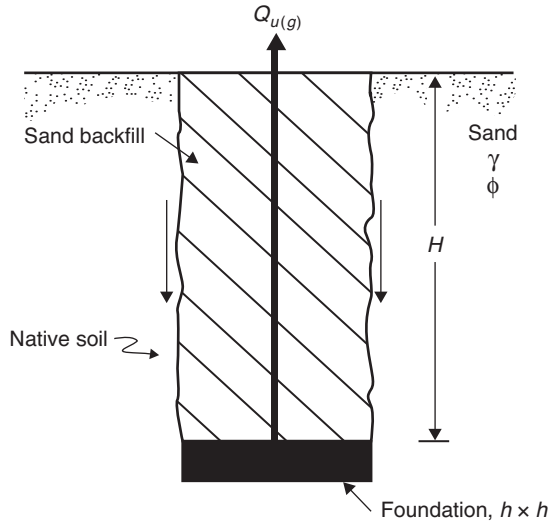

FIGURE 2.38 Failure by side shear

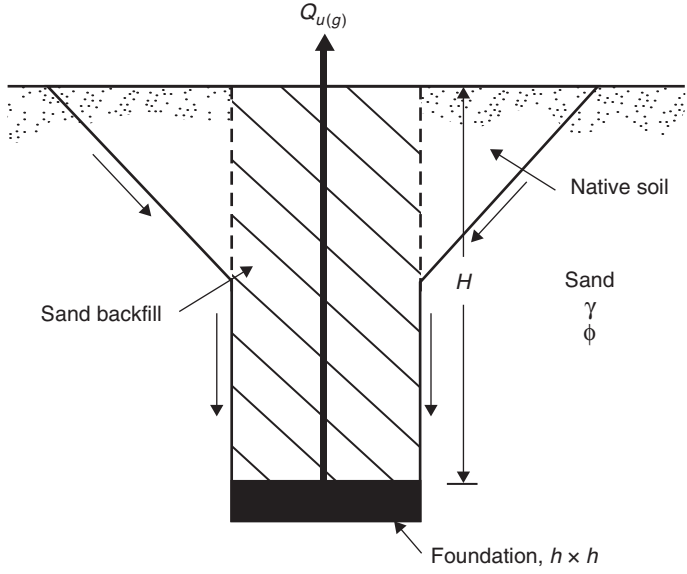

FIGURE 2.39 Wedge or combined shear failure

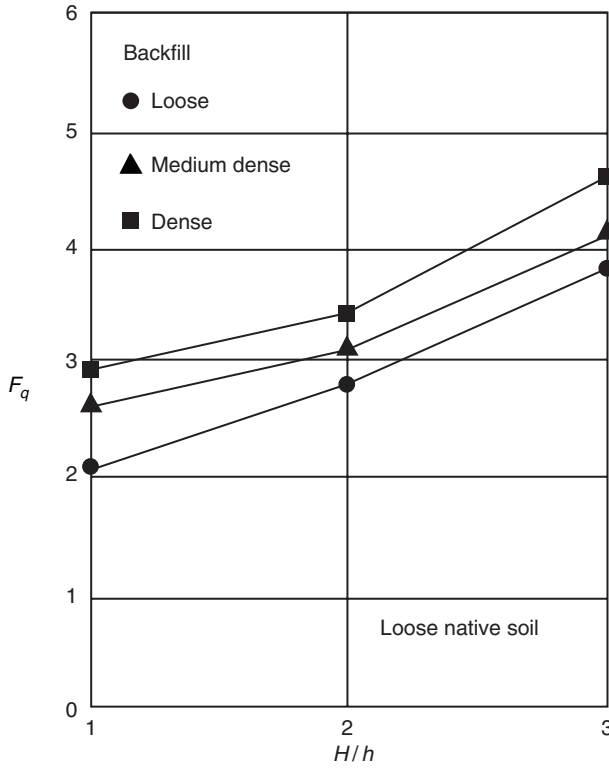

FIGURE 2.40 Effect of backfill on breakout factor for square foundation in loose native soil (adapted from Kulhawy et al., 1987)

2.15 INCLINED LOAD RESISTANCE OF HORIZONTAL PLATE ANCHORS

Das and Seeley (1975b) conducted a limited number of model tests to observe the nature of variation of the ultimate uplifting load of *horizontal square plate anchors* embedded in loose sand and subjected to inclined pull. The plate anchor used for the tests was 61 mm × 61 mm. The friction angle of the sand for the density of compaction at which tests were conducted was 31°. For this study, the pullout load on the anchor was applied by a cable that can allow full rotation of the anchor during pullout. Such conditions may arise to moor surface vessels or buoys and also semi-submersible or submerged structures. Figure 2.42 shows an anchor plate embedded at a depth H and subjected to a gross ultimate uplift

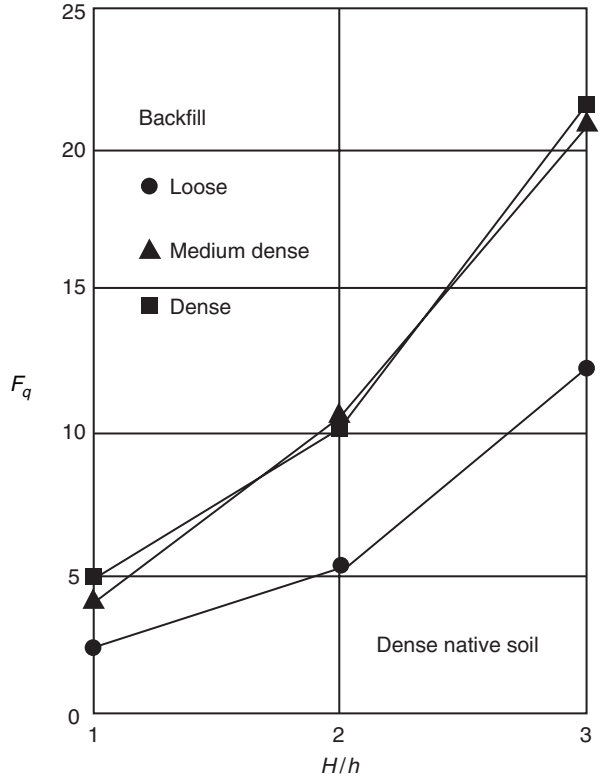

FIGURE 2.41 Effect of backfill on breakout factor for square foundation in dense native soil (adapted from Kulhawy et al., 1987)

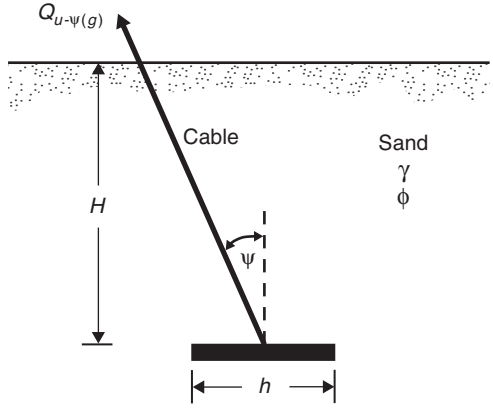

FIGURE 2.42 Inclined uplifting load on horizontal plate anchor

load $Q_{u\text{-}\psi(g)}$, with the load inclined at an angle ψ with respect to the vertical. The net ultimate uplift capacity can thus be given as:

$$Q_{u\text{-}\psi} = Q_{u\text{-}\psi(g)} - W_a \cos\psi \tag{2.63}$$

where

$Q_{u\text{-}\psi}$ = net ultimate uplift capacity measured in the direction of the load application
W_a = effective weight of the anchor

Figure 2.43 shows the variation of $Q_{u\text{-}\psi}$ with the angle of load inclination ψ for $H/h = 1$, 2, 2.5, and 4.5. From this figure it can be seen that for $\psi \leq 45°$,

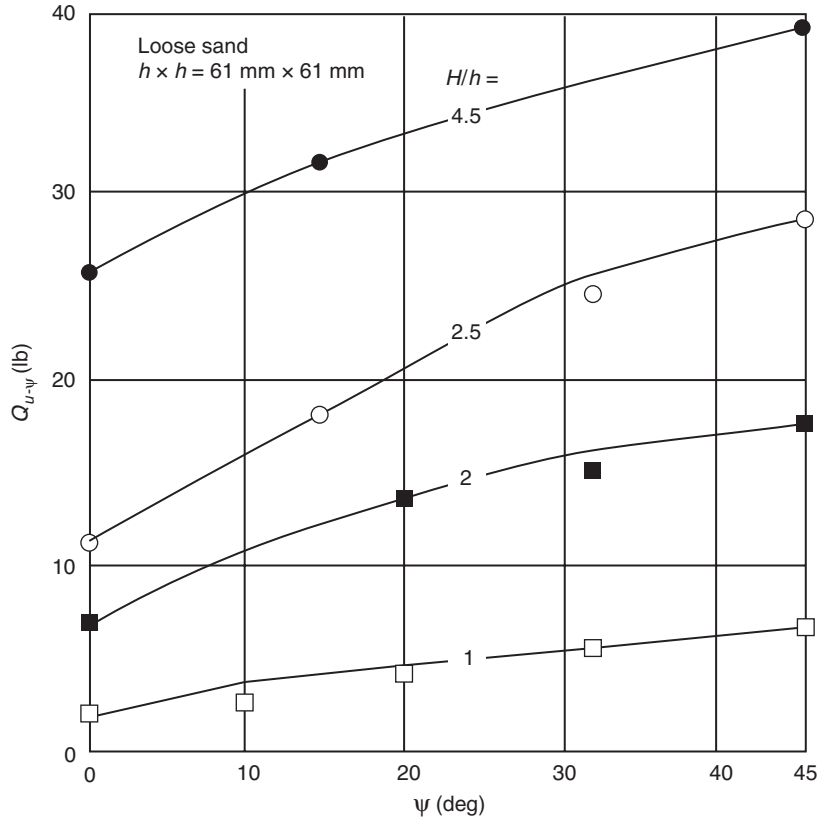

FIGURE 2.43 Effect of load inclination on $Q_{u\text{-}\psi}$ (adapted from Das and Seeley, 1975b)

the magnitude of $Q_{u\text{-}\psi}$ increases with the increase of the load inclination. Also, as the embedment ratio H/h increases, the ratio $Q_{u\text{-}\psi}/Q_{u\text{-}\psi=0}$ decreases (for a given value of ψ).

2.16 OTHER STUDIES

Some more analytical and numerical studies have been carried out by researchers until the recent past to estimate the ultimate pullout load of horizontal plate anchors in sands (Rowe and Davis, 1982; Tagaya et al., 1983, 1988; Smith, 1988, 2012; Merifield and Sloan, 2006; Kumar and Kouzer, 2008b; White et al., 2008; Deshmukh et al., 2011).

Merifield and Sloan (2006) presented rigorous lower and upper bound solutions for the ultimate capacity of horizontal strip anchors in frictional soils. They have reported that the failure mode for horizontal anchors consists of the upward movement of a rigid column of soil immediately above the anchor, accompanied by lateral deformation extending out and upward from the anchor edge. As the anchor is pulled vertically upward, the material above the anchor tends to lock up as it attempts to dilate during deformation. The effect of anchor interface roughness was found to have little or no effect on the calculated pullout capacity for horizontal anchors at all embedment depths and friction angles analyzed.

Merifield et al. (2006) studied the effect of anchor shape upon the ultimate capacity of horizontal anchors by developing lower bound solutions for the ultimate capacity of horizontal square and circular anchors in sand. It has been reported that the breakout factors for circular and square anchors increase nonlinearly with increasing embedment ratio. The rate of increase is greatest for medium to dense cohesionless soils where the effective soil friction angle $\phi' \geq 30°$. The capacity of both square and circular anchors is significantly greater than that of strip anchors at the same embedment ratio.

Kumar and Kouzer (2008b) examined the vertical uplift capacity of strip anchors embedded horizontally at shallow depths in sand by using an upper bound limit analysis in conjunction with finite elements and linear programming. They have reported that the uplift capacity increases substantially with increase in the embedment ratio of the anchor and the friction angle of the soil mass. The influence of friction angle ϕ on the pullout resistance is found to be greater at higher embedment ratios. Even though the analysis considers the development of plastic strains within elements, it has been noticed that the soil mass lying above the anchor remains rigid and a planar rupture surface emanating from the rupture edge and making an angle ϕ with the vertical develops.

White et al. (2008) described a limit equilibrium solution for predicting the uplift resistance of plate and pile anchors buried in sand by assuming that an inverted trapezoidal block is lifted above the pipe. The shear planes on each side of the block are inclined at the angle of dilation. The uplift resistance is equal to the weight of the lifted soil block plus the shear resistance along the two inclined failure surfaces. It is also assumed that the normal stress on the sliding planes is equal to the *in situ* value inferred from at-rest earth pressure conditions. The developed analytical expression requires the friction and dilation angles, which vary with density and stress level. It has been shown that the solution for uplift resistance based on the limit theorems of plasticity is generally very unconservative, which can be attributed to the assumption of normality that is required by the limit theorems. Normality leads to unrealistically high dilation, which imposes an improbable uplift mechanism involving uplift of a far wider zone of soil than is seen in model tests.

Deshmukh et al. (2011) presented the details of the theoretical analysis of net uplift capacity of horizontal strip anchors in cohesionless soils by assuming a plane failure surface inclined at $90° - \phi/2$ to the horizontal. The vertical soil reaction on the failure surface was evaluated using Kotter's equation. It has been reported that this analysis demonstrates a successful application of Kotter's equation and is reliable for embedment ratios less than 8.

The information about the vertical uplift capacity of horizontal plate anchors under seismic loads is limited. Kumar (2001) theoretically examined the influence of horizontal earthquake acceleration on the vertical uplift capacity of shallow strip anchors buried in cohesionless material by using the upper bound theorem of limit analysis and with the assumption of planar rupture surfaces. It has been reported that the pseudo-static horizontal seismic forces induce a progressive reduction in the uplift resistance of shallow anchors. The reduction becomes greater with increase in the magnitude of the earthquake acceleration coefficient and is found to be more significant for smaller values of soil friction angle ϕ and higher values of embedment ratio H/h.

2.17 SUMMARY OF MAIN POINTS

1. Horizontal plate anchors are used in the construction of foundations subjected to uplifting load.
2. The embedment ratio of the anchor is the ratio of the depth of embedment (H) to the width of the anchor (h), that is, H/h, which governs the anchor condition as shallow or deep. For greater values of H/h, the deep condition occurs where the failure surface does not extend to the ground surface.

3. The net ultimate uplift capacity is the sum of the effective weight of the soil located in the failure zone and the shearing resistance developed along the failure surface.
4. The soil cone and friction cylinder methods are the early uplift capacity theories used to determine the net ultimate uplift capacity of shallow circular plate anchors.
5. Balla's theory (1961) is generally in good agreement for the uplift capacity of anchors embedded in dense sand at an embedment ratio of $H/h \leq 5$. However, for anchors located in loose and medium sand, the theory overestimates the net ultimate uplift capacity.
6. The breakout factor, defined by Equation 2.10, increases with H/h up to a maximum value at $H/h = (H/h)_{cr}$. For $H/h > (H/h)_{cr}$, the breakout factor remains practically constant. Anchors located at an embedment ratio of $H/h \leq (H/h)_{cr}$ are shallow anchors, and those located at $H/h > (H/h)_{cr}$ are deep anchors. Most theories assume that the shallow anchor condition exists for $H/B \leq 5$. Meyerhof and Adams's theory (1968) provides a critical embedment ratio $(H/h)_{cr}$ for *square* and *circular* anchors as a function of the soil friction angle.
7. Meyerhof and Adams (1968) proposed a semi-theoretical relationship for estimation of the ultimate uplift capacity of *strip, rectangular,* and *circular* anchors. This is the only theory presently available for estimation of the net ultimate uplift capacity for rectangular anchors.
8. Vesic's theory (1971) is generally fairly accurate in estimating the net ultimate uplift capacity for shallow anchors in loose sand. Meyerhof and Adams's theory (1968) is more applicable to a wide range of anchors and it provides as good an estimate as any for the net ultimate uplift capacity.
9. The model tests suggest that when the cyclic relative anchor displacement is kept below about half the relative movement to failure in static pullout tests, there is essentially no reduction in strength due to cyclic loading.
10. The net ultimate uplift capacity of a group of anchors may possibly be smaller than the net ultimate uplift capacity of a single anchor times the number of anchors in the group when the center-to-center spacing of the anchor is small and when there is interference of the failure zones in the soil during anchor uplift.
11. The compaction of the backfill above the anchor plate has a great influence on the breakout factor of the foundation, and the net ultimate uplift capacity is greatly increased with the degree of backfill compaction.
12. The recent numerical studies with their limitations show that the anchor interface roughness has little or no effect on the calculated pullout capacity for horizontal anchors at all embedment depths and friction angles. The

pseudo-static horizontal seismic forces induce a progressive reduction in the uplift resistance of shallow anchors.

SELF-ASSESSMENT QUESTIONS

Select the most appropriate answer to each multiple-choice question

2.1. The sum of the effective self-weight of the horizontal plate anchor, the effective weight of the soil located in the failure zone, and the shearing resistance developed along the failure surface is called:
   a. ultimate capacity
   b. net ultimate capacity
   c. gross ultimate capacity
   d. none of the above

2.2. The soil cone method of determining the net ultimate uplift capacity of a horizontal plate anchor assumes that the failure surface in soil at ultimate load may be approximated as a truncated cone having an apex angle, where ϕ is the soil friction angle, of:
   a. $45° - \phi/2$
   b. $45° + \phi/2$
   c. $90° - \phi/2$
   d. $90° + \phi/2$

2.3. The breakout factor:
   a. always increases with increase in embedment ratio
   b. increases with increase in embedment ratio up to a maximum value
   c. always decreases with increase in embedment ratio
   d. decreases with increase in embedment ratio up to a minimum value

2.4. Which of the following is not required for the calculation of the net ultimate uplift capacity of a horizontal plate anchor embedded in sand:
   a. area of the anchor plate
   b. depth of the anchor plate below the ground
   c. unit weight of the soil above the anchor plate
   d. unit weight of the soil below the anchor plate

2.5. Estimation of the net ultimate uplift capacity of a horizontal plate anchor embedded in sand for rectangular anchors can be done by:
   a. Balla's theory (1961)
   b. Vesic's theory (1971)
   c. Mariupol'skii's theory (1965)
   d. Meyerhof and Adams's theory (1968)

2.6. Horizontal plate anchors for transmission line towers are usually constructed with an embedment depth ratio of:
   a. 3
   b. 3 or less
   c. greater than 3
   d. 1

2.7. For a given embedment depth ratio, the inclined load resistance of a horizontal plate anchor:
   a. increases with increase in inclination of the load with respect to vertical
   b. decreases with increase in inclination of the load with respect to vertical
   c. increases with increase in inclination of the load with respect to horizontal
   d. remains unaffected with variation of inclination of the load with respect to vertical or horizontal

2.8. The net allowable ultimate uplift capacity of horizontal plate anchors can be determined by using:
   a. a tentative factor of safety
   b. a load displacement relationship
   c. both a and b
   d. none of the above

2.9. With increase in friction angle of the soil backfill above the horizontal plate anchor, the breakout factor of the anchor:
   a. increases linearly
   b. increases nonlinearly
   c. decreases linearly
   d. decreases nonlinearly

2.10. For a circular plate anchor embedded in sand with diameter $h = 1$ m, depth of embedment $H = 1$ m, unit weight of sand above the plate anchor $\gamma = 15$ kN/m^3, and sand friction angle $\phi = 20°$, the net ultimate uplift capacity calculated from Balla's theory (1961) will be:
   a. 7.5 kN
   b. 15 kN
   c. 30 kN
   d. 300 kN

Answers

2.1: c 2.2: d 2.3: b 2.4: d 2.5: d 2.6: b 2.7: a 2.8: c 2.9: b 2.10: c

REFERENCES

Andreadis, A., Harvey, R.C., and Burley, E. (1978). Embedment anchors subjected to repeated loading. *J. Geotech. Eng. Div. ASCE,* 104(7):1033–1036.

Baker, W.H. and Kondner, R.L. (1966). Pullout load capacity of a circular earth anchor buried in sand. *Highw. Res. Rec.,* No. 108, National Academy of Sciences, Washington, D.C., 1–10.

Balla, A. (1961). The resistance to breaking-out of mushroom foundations for pylons. *Proc. 5th Int. Conf. Soil Mech. Found. Eng.,* Paris, 1, 569–576.

Caquot, A. and Kerisel, L. (1949). *Traite de Mecanique des Sols,* Gauthier-Villars, Paris.

Das, B.M. and Jin-Kaun, Y. (1987). Uplift capacity of model group anchors in sand. *Foundations for Transmission Line Towers,* Geotech. Spec. Publ. 8, ASCE, 57–71.

Das, B.M. and Jones, A.D. (1982). Uplift capacity of rectangular foundations in sand. *Transp. Res. Rec.,* No. 884, National Academy of Sciences, Washington, D.C., 54–58.

Das, B.M. and Puri, V.K. (1989). Load displacement relationship for horizontal rectangular anchors in sand. *Proc. 4th Int. Conf. Civil Struct. Eng. Computing,* London, Civil-Comp Press, 2, 207–212.

Das, B.M. and Seeley, G.R. (1975a). Breakout resistance of horizontal anchors. *J. Geotech. Eng. Div. ASCE,* 101(9):999–1003.

Das, B.M. and Seeley, G.R. (1975b). Inclined load resistance of anchors in sand. *J. Geotech. Eng. Div. ASCE,* 101(9):995–998.

Deshmukh, V.B., Dewaikar, D.M., and Choudhary, D. (2011). Uplift capacity of horizontal strip anchors in cohesionless soil. *Geotech. Geol. Eng.,* 29:977–988.

Downs, D.I. and Chieurzzi, R. (1966). Transmission tower foundations. *J. Power Div. ASCE,* 88(2):91–114.

Esquivel-Diaz, R.F. (1967). Pullout Resistance of Deeply Buried Anchors in Sand, M.S. thesis, Duke University, Durham, NC.

Ireland, H.O. (1963). Discussion, uplift resistance of transmission tower footing. *J. Power Div. ASCE,* 89(1):115–118.

Kulhawy, F.H., Trautmann, C.H., and Nicolaides, C.N. (1987). Spread foundations in uplift: experimental study. *Foundations for Transmission Line Towers,* Geotech. Spec. Publ. 8, ASCE, 110–127.

Kumar, J. (2001). Seismic vertical uplift capacity of strip anchors. *Geotechnique,* 51(3):275–279.

Kumar, J. and Kouzer, K.M. (2008a). Vertical uplift capacity of a group of shallow horizontal anchors in sand. *Geotechnique,* 58(10):821–823.

Kumar, J. and Kouzer, K.M. (2008b). Vertical uplift capacity of horizontal anchors using upper bound limit analysis and finite elements. *Can. Geotech. J.,* 45:698–704.

Liu, J., Liu, M., and Zhu, Z. (2012). Sand deformation around an uplift plate anchor. *J. Geotech. Geoenviron. Eng.,* 138(6):728–737.

Mariupol'skii, L.G. (1965). The bearing capacity of anchor foundations (English translation). *Soil Mech. Found. Eng.* (in Russian), 26–37.

Merifield, R.S. and Sloan, S.W. (2006). The ultimate pullout capacity of anchors in frictional soils. *Can. Geotech. J.,* 43:852–868.

Merifield, R.S., Lyamin, A.V., and Sloan, S.W. (2006). Three-dimensional lower-bound solutions for the stability of plate anchors in sand. *Geotechnique,* 56(2): 123–132.

Meyerhof, G.G. (1973). Uplift resistance of inclined anchors and piles. *Proc. 8th Int. Conf. Soil Mech. Found.,* Moscow, 167–172.

Meyerhof, G.G. and Adams, J.I. (1968). The ultimate uplift capacity of foundations. *Can. Geotech. J.,* 5(4):225–244.

Mors, H. (1959). The behavior of mast foundations subjected to tensile forces. *Bautechnik,* 36(10):367–378.

Rowe, R.K. and Davis, H. (1982). The behaviour of anchor plates in sand. *Geotechnique,* 32(1):25–41.

Saeedy, H.S. (1987). Stability of circular vertical earth anchors. *Can. Geotech. J.,* 24(3):452–456.

Smith, C. (1998). Limit loads for an anchor/trapdoor embedded in an associative Coulomb soil. *Int. J. Num. Anal. Meth. Geomech.,* 22(11):855–865.

Smith, C.C. (2012). Limit loads for a shallow anchor/trapdoor embedded in a non-associative Coulomb soil. *Geotechnique,* 62(7):563–571.

Sutherland, H.B. (1965). Model studies for shaft raising through cohesionless soils. *Proc. 6th Int. Conf. Soil Mech. Found. Eng.,* Montreal, 2, 410–413.

Tagaya, K., Tanaka, A., and Aboshi, H. (1983). Application of finite element method to pullout resistance of buried anchor. *Soils Found.,* 23(3):91–104.

Tagaya, K., Scott, R.F., and Aboshi, H. (1988). Pullout resistance of buried anchor in sand. *Soils Found.,* 28(3):114–130.

Veesaert, C.J. and Clemence, S.P. (1977). Dynamic pullout resistance of anchors. *Proc. Int. Symp. Soil-Structure Interaction,* Rourkee, India, Vol. 1, 389–397.

Vesic, A.S. (1965). Cratering by explosives as an earth pressure problem. *Proc. 6th Int. Conf. Soil Mech. Found. Eng.,* Montreal, 427–431.

Vesic, A.S. (1971). Breakout resistance of objects embedded in ocean bottom. *J. Soil Mech. Found. Div. ASCE,* 97(9):1183–1205.

White, D.J., Cheuk, C.Y., and Bolton, M.D. (2008). The uplift resistance of pipes and plate anchors buried in sand. *Geotechnique,* 58(10):771–779.

3

HORIZONTAL PLATE ANCHORS IN CLAY

This chapter describes the theoretical and experimental research results presently available for determination of the net ultimate uplift capacity of horizontal plate anchors embedded in saturated clay. In the recent past, some numerical investigations including three-dimensional lower bound study of the behavior of horizontal plate anchors in clays have been reported in the research literature. This chapter also summarizes such works briefly.

3.1 INTRODUCTION

Figure 3.1 shows a plate anchor embedded in a saturated clay at a depth H below the ground surface. The width of the anchor plate is equal to h, and the undrained cohesion of the clay is c_u. In soft saturated clay, when the anchor is subjected to an uplift force, the soil located above the anchor will be compressed and, at the same time, the soil below the anchor will be relieved of some stress. This will, in turn, result in an increase in the pore water pressure above the anchor accompanied by a decrease in the pore water pressure below the anchor. The difference will result in a suction force. This suction force will increase the short-term uplift capacity of the anchor. Thus, the uplift capacity can be given by the expression

$$Q_{u(g)} = Q_u + W_a + U \tag{3.1}$$

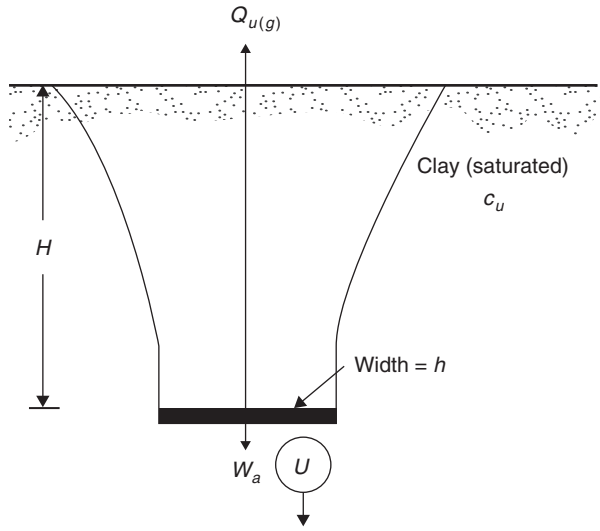

FIGURE 3.1 Horizontal anchor in saturated clay

where

$Q_{u(g)}$ and Q_u = gross and net ultimate uplift capacity, respectively
W_a = effective weight of the anchor
U = suction force below the anchor

Very little is known at the present time about the magnitude of the suction force and its variation with depth and type of clay soil. However, for design purposes, the suction force can be neglected and the net ultimate uplift capacity can be taken as:

$$Q_u = Q_{u(g)} - W_a \tag{3.2}$$

In the following sections, the existing theories for estimation of the net uplift capacity Q_u are summarized.

3.2 VESIC'S THEORY

In Section 2.8, it was shown that for anchors embedded in sand ($c = 0$):

$$Q_u = A\gamma HF_q \tag{3.3}$$

where

A = area of the anchor plate

The preceding relation was derived by Vesic (1971) using the analogy of expansion of cavities. In a similar manner, it can be shown that in a c-ϕ soil

$$Q_u = A(\gamma H F_q + c F_c) \tag{3.4}$$

where

F_q, F_c = breakout factors
c = cohesion of the soil

For the undrained condition, $\phi = 0$ and $c = c_u$. It was shown in Tables 2.3 and 2.4 that for $\phi = 0$, the value of F_q is equal to 1. Thus:

$$Q_u = A(\gamma H + c_u F_c) \tag{3.5}$$

Vesic (1971) presented the theoretical variation of the breakout factor F_c (for $\phi = 0$ condition) with the embedment ratio H/h, and these values are given in Table 3.1. In Table 3.1, B is the dimension of the anchor at right angle to the cross section shown in Figure 3.1. A plot of these same values of F_c against H/h is also shown in Figure 3.2. Based on the laboratory model test results available, it appears that Vesic's theory gives a closer estimate only for shallow anchors embedded in softer clay.

In general, the breakout factor increases with embedment ratio up to a maximum value and remains constant thereafter, as shown in Figure 3.3. The maximum value of $F_c = F_c^*$ is reached at $H/h = (H/h)_{cr}$. Anchors located at $H/h > (H/h)_{cr}$ are referred to as deep anchors. For these anchors, at ultimate uplifting load, local shear failure in soil located around the anchor takes place. Anchors located at $H/h \leq (H/h)_{cr}$ are shallow anchors.

TABLE 3.1 Variation of F_c ($\phi = 0$ condition)

	H/h				
Anchor type	0.5	1.0	1.5	2.5	5.0
Circular (diameter = h)	1.76	3.80	6.12	11.6	30.3
Strip ($h/B \approx 0$)	0.81	1.61	2.42	4.04	8.07

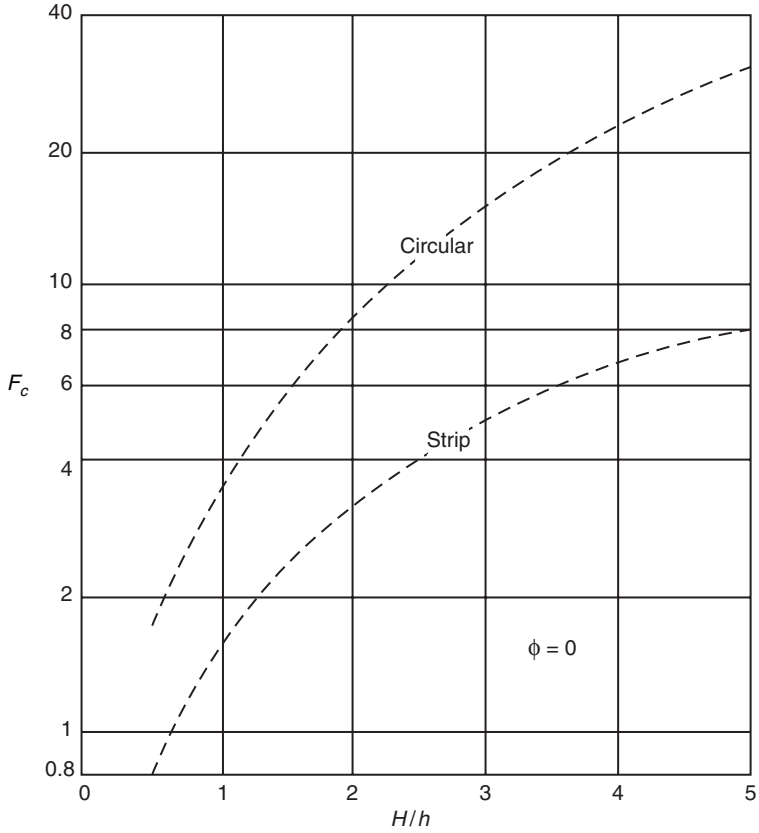

FIGURE 3.2 Variation of Vesic's (1971) breakout factor F_c

3.3 MEYERHOF'S THEORY

Based on experimental results, Meyerhof (1973) proposed a relationship the same as Equation 3.5. For *circular* and *square* anchors:

$$F_c = 1.2\left(\frac{H}{h}\right) \leq 9 \tag{3.6}$$

and for *strip* anchors:

$$F_c = 0.6\left(\frac{H}{h}\right) \leq 8 \tag{3.7}$$

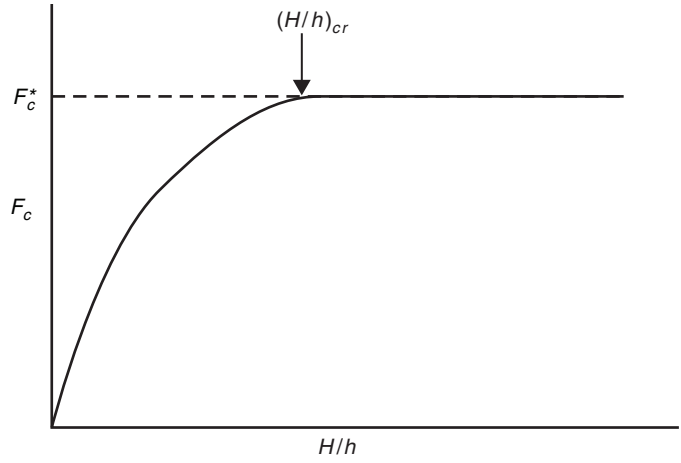

FIGURE 3.3 Nature of variation of F_c with H/h

Equations 3.6 and 3.7 imply that for *circular* and *square* anchors:

$$\left(\frac{H}{h}\right)_{cr} = \frac{9}{1.2} = 7.5 \tag{3.8}$$

and for *strip* anchors:

$$\left(\frac{H}{h}\right)_{cr} = \frac{8}{0.6} \approx 13.5 \tag{3.9}$$

The breakout factor variations with embedment ratio according to Equations 3.6 and 3.7 are shown in Figure 3.4. Based on the experimental results, it appears that Equations 3.6 and 3.7 are reasonable estimates for anchors embedded in stiff clay.

3.4 DAS'S THEORY

Das (1978) compiled a number of laboratory model test results on *circular* anchors embedded in saturated clay with the undrained cohesion c_u varying from 5.18 kN/m^2 to about 172.5 kN/m^2. Figure 3.5 shows the average plots of F_c versus H/h obtained from these studies, along with the critical embedment ratios. The details relating to curves *a, b, c, d,* and *e* shown in Figure 3.5 are given in Table 3.2.

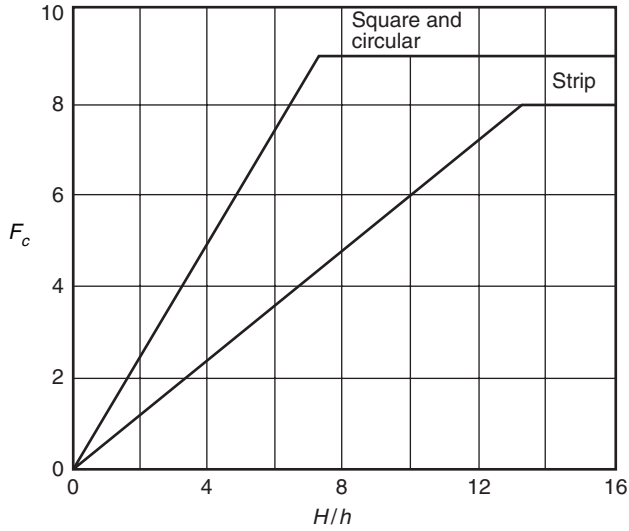

FIGURE 3.4 Variation of F_c with H/h (Equations 3.6 and 3.7)

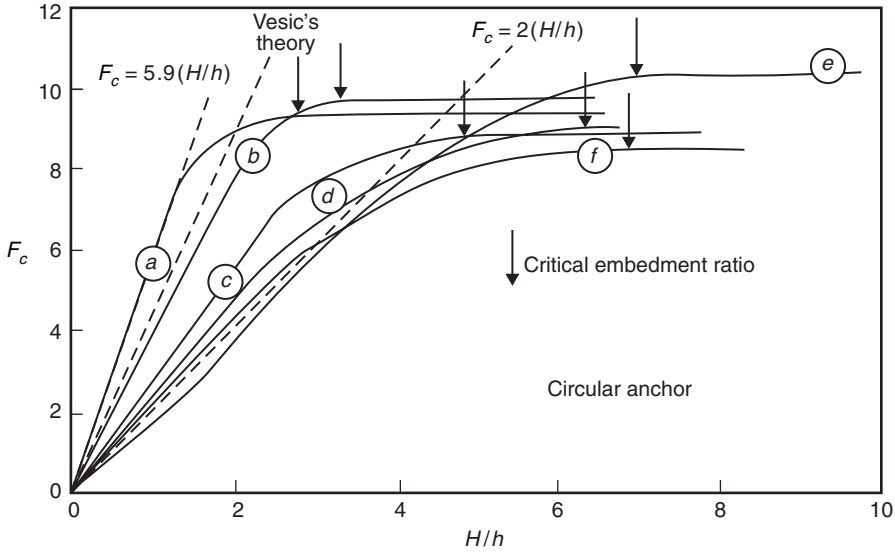

FIGURE 3.5 Variation of breakout factor with H/h for various experimental observations

TABLE 3.2 Details for the curves shown in Figure 3.5

Curve	Reference	Year	c_u (kPa)
a	Ali	1968	5.18
b	Kupferman	1971	6.9
c	Adams and Hayes	1967	10.35–13.8
d	Bhatnagar	1969	53.17
e	Adams and Hayes	1967	96.6–172.5

From Figure 3.5, it can be seen that for shallow anchors:

$$F_c \approx n\left(\frac{H}{h}\right) \leq 8 \text{ to } 9 \tag{3.10}$$

where

n = a constant

The magnitude of n varies between 5.9 to 2.0 and is a function of the undrained cohesion c_u. Since n is a function of c_u and $F_c = F_c^*$ is about 8 to 9 in all cases, it is obvious that the critical embedment ratio $(H/h)_{cr}$ will be a function of c_u.

Das (1978) also reported some model test results conducted with *square* and *rectangular* anchors of width $h = 50.8$ mm. Based on these model test results, the variation of F_c with H/h is shown in Figure 3.6. Using the critical embedment ratios obtained from Figures 3.5 and 3.6, it was proposed that

$$\left(\frac{H}{h}\right)_{cr\text{-}S} = 0.107c_u + 2.5 \leq 7 \tag{3.11}$$

where

$(H/h)_{cr\text{-}S}$ = critical embedment ratio of *square* anchor (or *circular* anchor)
c_u = undrained cohesion in kN/m^2

A plot based on Equation 3.11 is shown in Figure 3.7. It was also observed by Das (1980) that

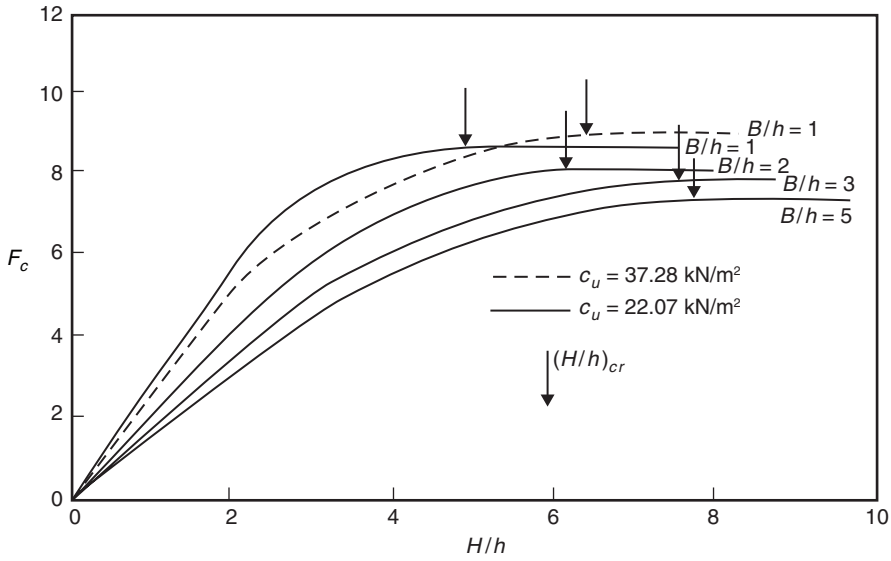

FIGURE 3.6 Model test results of Das (1978) for variation of F_c with H/h

$$\left(\frac{H}{h}\right)_{cr\text{-}R} = \left(\frac{H}{h}\right)_{cr\text{-}S}\left[0.73 + 0.27\left(\frac{B}{h}\right)\right] \leq 1.55\left(\frac{H}{h}\right)_{cr\text{-}S} \tag{3.12}$$

where

$(H/h)_{cr\text{-}R}$ = critical embedment ratio of rectangular anchors (Figure 3.8)

Based on these model test results, Das (1980) proposed an empirical procedure to obtain the breakout factors for shallow and deep anchors. According to this procedure, α' and β' are two nondimensional factors defined as:

$$\alpha' = \frac{\dfrac{H}{h}}{\left(\dfrac{H}{h}\right)_{cr}} \tag{3.13}$$

and

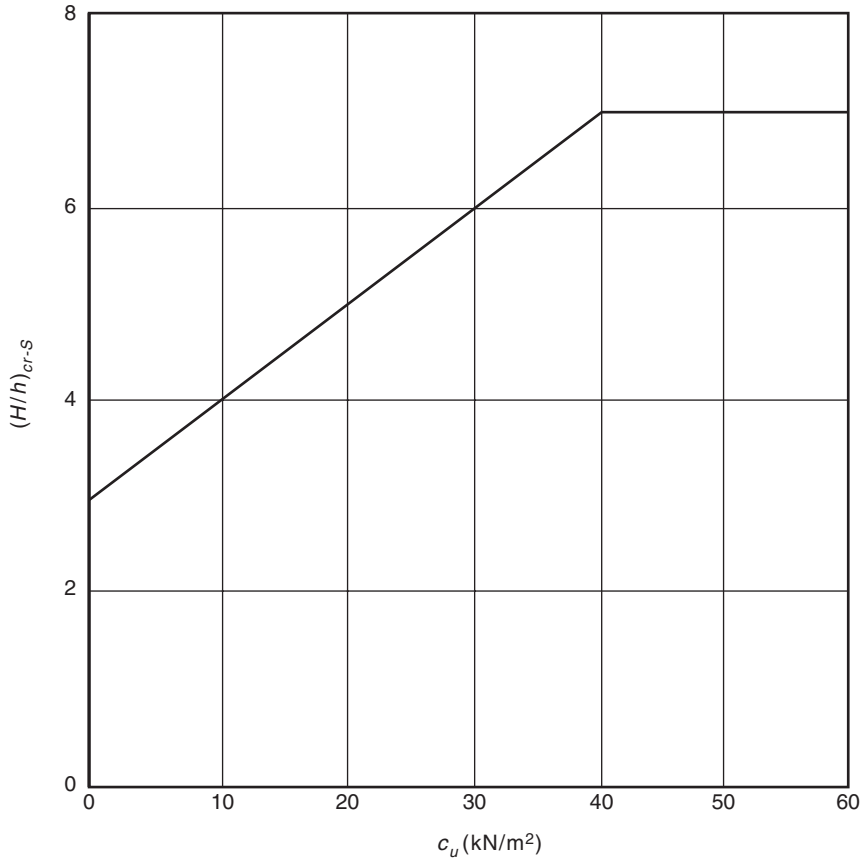

FIGURE 3.7 Plot of $(H/h)_{cr\text{-}S}$ versus c_u (in kN/m^2) from Equation 3.11

$$\beta' = \frac{F_c}{F_c^\star} \tag{3.14}$$

For a given anchor (that is, circular, square, or rectangular), the critical embedment ratio can be calculated by using Equations 3.11 and 3.12. The magnitudes of $F_c^\star$ can be given by the following empirical relationship:

$$F_{c\text{-}R}^\star = 7.56 + 1.44\left(\frac{h}{B}\right) \tag{3.15}$$

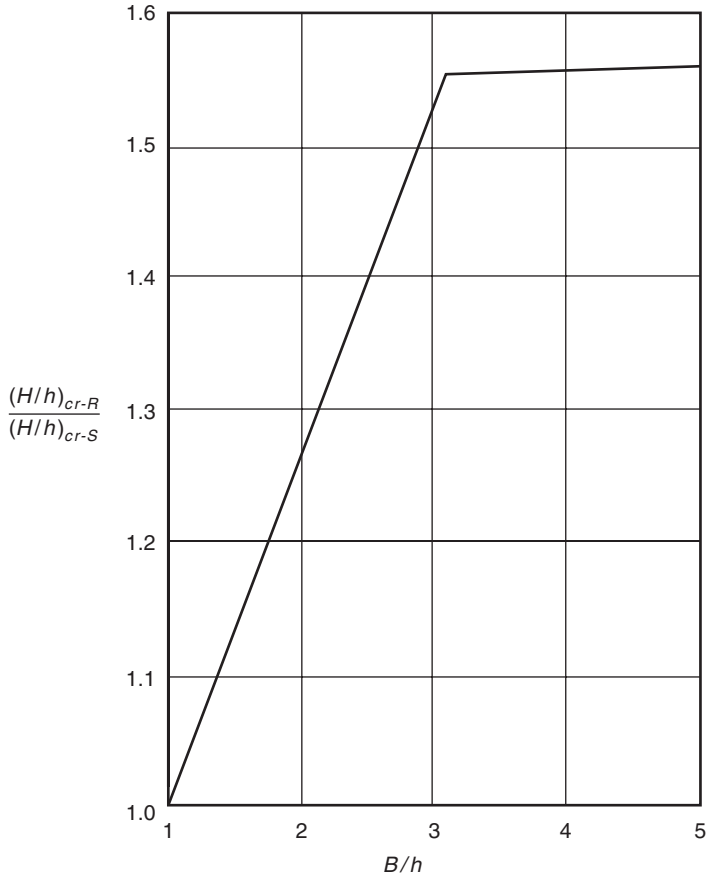

FIGURE 3.8 Plot of $(H/h)_{cr\text{-}R}/(H/h)_{cr\text{-}S}$ against B/h from Equation 3.12

where

$F^{\star}_{c\text{-}R}$ = breakout factor for deep rectangular anchor

It can be seen from Equation 3.15 that for *square* and *circular* anchors $F^{\star}_{c\text{-}R}$ is equal to 9. Using all the experimental curves shown in Figures 3.5 and 3.6, when the nondimensional breakout factor β' is plotted against the nondimensional embedment ratio α', they appear to fall in a rather narrow range, as

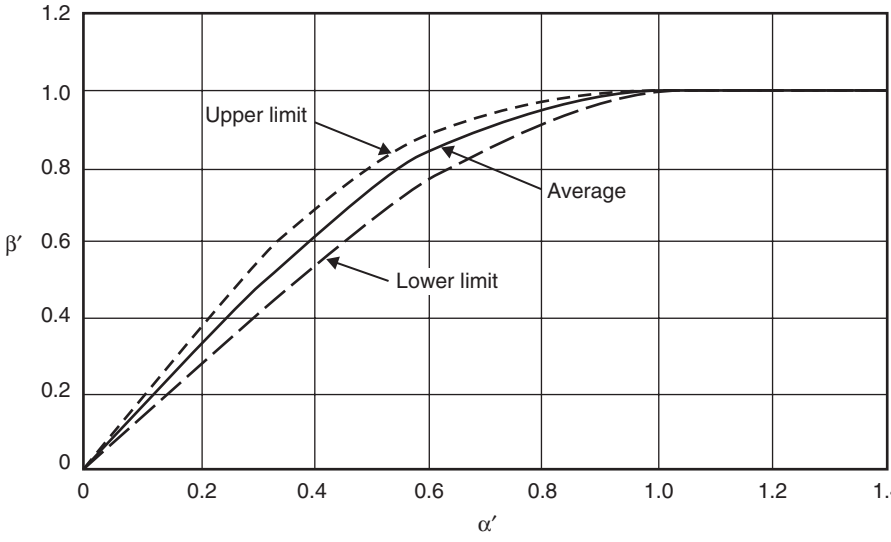

FIGURE 3.9 Plot of β′ versus α′ (adapted from Das, 1980)

shown in Figure 3.9. The average plot of β' versus α' is also shown in Figure 3.9. Hence, the following is a step-by-step procedure for estimation of the net ultimate uplift capacity:

1. Determine the representative value of the undrained cohesion c_u.
2. Determine the critical embedment ratio using Equations 3.11 and 3.12.
3. Determine the H/h ratio for the anchor.
4. If $H/h > (H/h)_{cr}$ as determined by Step 2, it is a deep anchor. However, if $H/h \leq (H/h)_{cr}$, it is a shallow anchor.
5. For $H/h > (H/h)_{cr}$:

$$F_c = F_c^* = 7.56 + 1.44\left(\frac{h}{B}\right)$$

Thus:

$$Q_u = A\left\{\left[7.56 + 1.44\left(\frac{h}{B}\right)\right]c_u + \gamma H\right\} \tag{3.16}$$

where

A = area of the anchor

6. For $H/h \le (H/h)_{cr}$:

$$Q_u = A(\beta' F_c^* c_u + \gamma H)$$

$$= A\left\{\beta'\left[7.56 + 1.44\left(\frac{h}{B}\right)\right]c_u + \gamma H\right\} \tag{3.17}$$

The value of β' can be obtained from the average curve of Figure 3.9. The procedure outlined above gives fairly good results in estimating the net ultimate holding capacity of anchors.

Example 3.1

A plate anchor that measures 0.4 m × 0.6 m is embedded at a depth of 1.8 m. The undrained cohesion of the clay is 42 kN/m^2, and its saturated unit weight γ is 18.9 kN/m^3. Estimate the net ultimate uplift capacity.

Solution

From Equation 3.11:

$$\left(\frac{H}{h}\right)_{cr\text{-}S} = 0.107c_u + 2.5 = (0.107)(42) + 2.5 \approx 7$$

Again, from Equation 3.12:

$$\left(\frac{H}{h}\right)_{cr\text{-}R} = \left(\frac{H}{h}\right)_{cr\text{-}S}\left[0.73 + 0.27\left(\frac{B}{h}\right)\right]$$

$$= (7)\left[0.73 + 0.27\left(\frac{0.6}{0.4}\right)\right] \approx 7.95$$

The actual embedment ratio is $H/h = 1.8/0.4 = 4.5$. Hence this is a shallow anchor.

$$\alpha' = \frac{\dfrac{H}{h}}{\left(\dfrac{H}{h}\right)_{cr}} = \frac{4.5}{7.95} = 0.566$$

Referring to Figure 3.9, for $\alpha' = 0.566$, the magnitude of β' is 0.82. From Equation 3.17:

$$Q_u = A\left\{\beta'\left[7.56 + 1.44\left(\frac{h}{B}\right)\right]c_u + \gamma H\right\}$$

$$= (0.4)(0.6)\left\{(0.82)\left[7.56 + (1.44)\left(\frac{0.4}{0.6}\right)\right](42) + (18.9)(1.8)\right\}$$

$$= \mathbf{78.6\ kN}$$

3.5 THREE-DIMENSIONAL LOWER BOUND SOLUTION

Merifield et al. (2003) presented three-dimensional numerical limit analysis to evaluate the effect of anchor shape on the pullout capacity of horizontal anchors in undrained clay. The anchor was idealized as either square, circular, or rectangular in shape. Estimates of the ultimate pullout load were obtained by using a newly developed three-dimensional numerical procedure based on a finite element formulation of the lower bound theorem of limit analysis. The formulation assumed a perfectly plastic soil model with a Tresca yield criterion. Consideration has been given to the effect of anchor embedment depth, anchor roughness, and overburden pressure. It has been reported that the breakout factors for square, circular, and rectangular anchors in weightless soil are always greater than those obtained for strip anchors at corresponding embedment ratios. Rectangular anchors with aspect ratios (B/h) greater than 10 can be considered to behave essentially as a strip anchor. The ultimate capacity of horizontal square, circular, or rectangular anchors is not likely to be affected noticeably by anchor roughness.

The following list enumerates the suggested procedure for estimating the uplift capacity of circular and square anchors in homogeneous soil profiles:

1. Determine representative values of material parameters, c_u and γ.
2. Knowing the anchor size (h = diameter or width, B = length) and embedment depth H, calculate the embedment ratio H/h.
3. Determine the overburden ratio $\gamma H/c_u$.
4. Adopt a limiting value of the breakout factor $F_c^\star = 12.56$ for circular anchors and $F_c^\star = 11.9$ for square anchors.
5. A. Calculate the breakout factor F_{c0} for a homogeneous soil profile with no unit weight ($\gamma = 0$) as:

$$F_{c0} = S\left\{2.56 \ln\left[2\left(\frac{H}{h}\right)\right]\right\} \tag{3.18}$$

where S is a shape factor illustrated in Figure 3.10 for circular anchors and in Figure 3.11 for square anchors.

B. Calculate the breakout factor $F_c = F_{c\gamma}$ for a homogenous soil profile with unit weight ($\gamma \neq 0$) as:

$$F_c = F_{c\gamma} = F_{c0} + \frac{\gamma H}{c_u} \tag{3.19}$$

C. If $F_c \geq F_c^\star$, then the anchor is a deep anchor. The ultimate pullout load is given by:

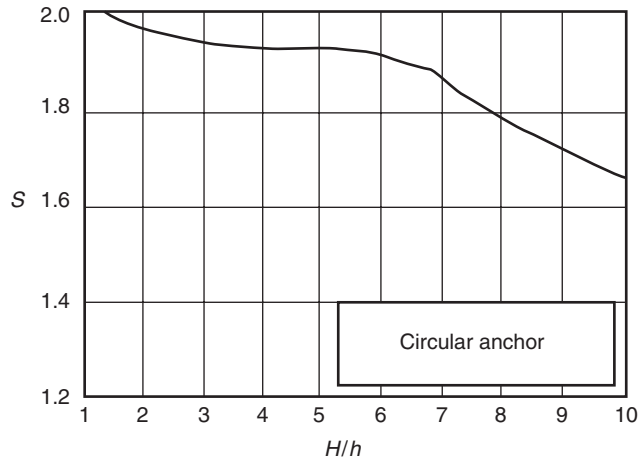

FIGURE 3.10 Shape factor S for circular anchor (adapted from Merifield et al., 2003)

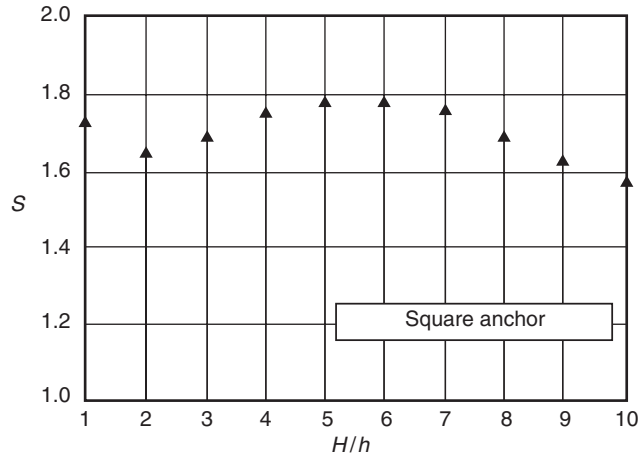

FIGURE 3.11 Shape factor *S* for square anchor (adapted from Merifield et al., 2003)

$$Q_u = c_u A F_c^{\star} \tag{3.20}$$

D. If $F_c \leq F_c^{\star}$, then the anchor is a shallow anchor. The ultimate pullout load is given by:

$$Q_u = c_u A F_{c\gamma} \tag{3.21}$$

Example 3.2

A square horizontal plate anchor 0.25 m wide is to be embedded 1.75 m in a homogeneous clay. Determine the ultimate pullout capacity given that the clay has a shear strength $c_u = 60$ kPa and unit weight $\gamma = 15.3$ kN/m^3.

Solution

The embedment ratio is

$$\frac{H}{h} = \frac{1.75}{0.25} = 7.0$$

The overburden ratio is

$$\frac{\gamma H}{c_u} = \frac{(15.3 \times 1.75)}{60} = 0.45$$

For a square anchor, $F_c^\star = 11.9$. From Figure 3.11, $S \approx 1.75$. Using Equation 3.18:

$$F_{c0} = 1.75\{2.56 \ln[2(7.0)]\} = 11.82$$

Using Equation 3.19:

$$F_c = F_{c\gamma} = 11.82 + 0.45 = 12.27$$

Since $F_c > F_c^\star$, the anchor is deep, and using Equation 3.20:

$$Q_u = (60)(0.25 \times 0.25)(11.9) = \mathbf{44.6\ kN}$$

It is important to note that the study by Wang et al. (2010) shows that for square and circular deep anchors under immediate breakaway conditions, the maximum uplift capacity increases with soil elastic modulus. This fact suggests that the lower bound limit analysis and small-strain finite element analysis may overestimate the pullout capacity of horizontal plate anchors during vertical pullout. Therefore, for design purpose, it becomes important to reduce the estimated value of the ultimate uplift capacity suitably to arrive at the allowable ultimate uplift capacity.

3.6 FACTOR OF SAFETY

In most cases of anchor design, it is recommended that a factor of safety of 2 to 2.5 be used to arrive at the net allowable ultimate uplift capacity.

3.7 UPLIFT CAPACITY OF ANCHORS IN LAYERED SOIL

The uplift capacity of anchors embedded in a saturated clay layer overlain by a compact sand deposit was studied by Stewart (1985) using laboratory model tests. The basic conclusions of this study can qualitatively be summarized by referring to Figure 3.12. In Figure 3.12a, a plate anchor is embedded in a satu-

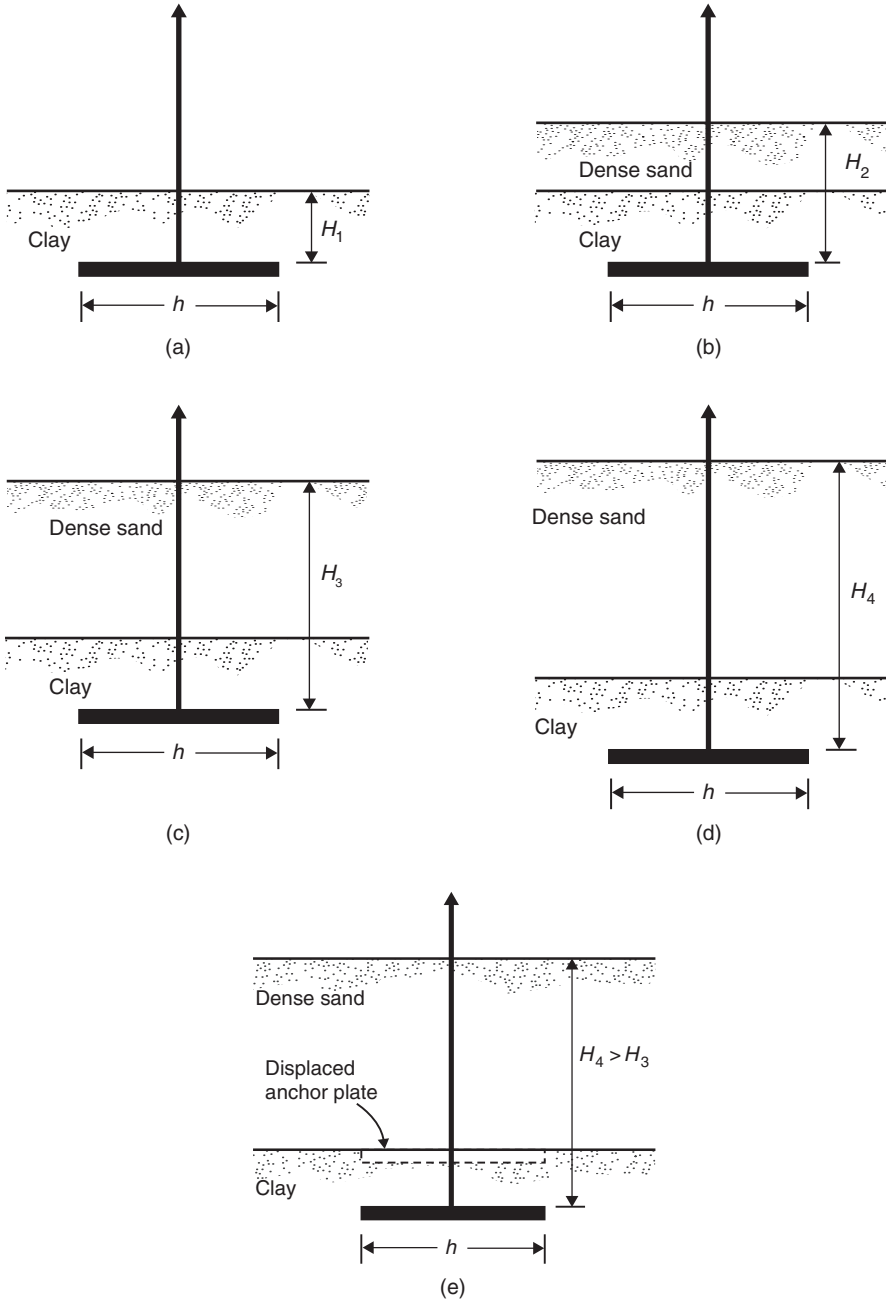

FIGURE 3.12 Plate anchor in saturated clay overlain by dense sand

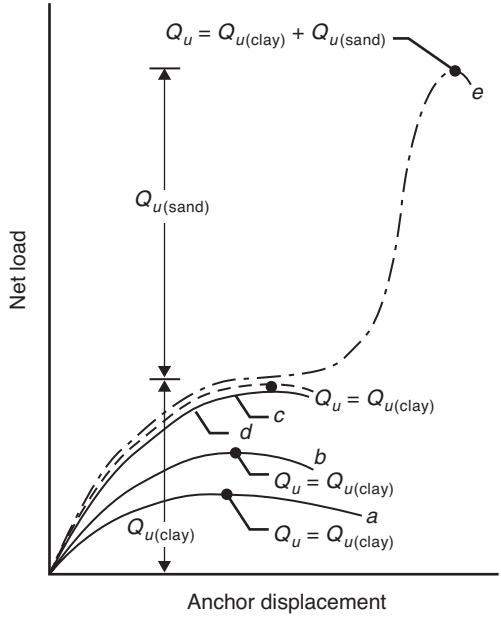

FIGURE 3.13 Nature of net load versus anchor displacement plots for plate anchor in clay overlain by dense sand

rated clay at a depth $H = H_1$. When subjected to an uplifting load, the nature of the plot of the net load Q versus anchor uplift Δ will be of the type shown by curve *a* in Figure 3.13. If H_1 is relatively small, then the failure surface will extend to the top of the clay layer, indicating a shallow anchor condition. If a layer of dense sand is now placed on the clay layer, the total thickness of the soil above the anchor will be equal to H_2 (Figure 3.12b). For this condition, the nature of the Q versus Δ plot will be as shown by curve *b* in Figure 3.13. For this condition, the sand acts as a surcharge on the clay layer and increases the net ultimate uplift capacity. If the thickness of the clay layer is gradually increased, depending on the relative value of c_u, the angle of friction of sand, γ_{clay}, and γ_{sand}, there will be a condition when the anchor will behave like a deep anchor located in clay. For this condition, let the thickness of the sand and clay above the anchor be equal to H_3, as shown in Figure 3.12c. Curve *c* in Figure 3.13 represents the Q versus Δ plot for this condition. If the thickness of the sand layer is further increased (Figure 3.12d) and an uplifting load is applied to the anchor, the load-displacement plot will follow the path shown by curve *d* in Figure 3.13, which is the same path as shown by curve *c* in Figure 3.13. However, if sufficient upward anchor displacement is allowed such that the anchor reaches

the top of the sand (Figure 3.12e), then the load resistance increases again and follows the path shown by curve *e* in Figure 3.13. Based on this, we can draw the following conclusions:

1. The sand overlay can significantly increase the net ultimate uplift capacity.
2. The net ultimate uplift capacity is composed of two parts:

$$Q_u = Q_{u(\text{clay})} + Q_{u(\text{sand})} \tag{3.22}$$

where

$Q_{u(\text{clay})}$ = clay component
$Q_{u(\text{sand})}$ = sand component

The magnitude of $Q_{u(\text{clay})}$ increases with H/h ratio up to a maximum value at $H/h = H_3/h$ (Figure 3.12c). A further increase in H/h has no effect on the magnitude of $Q_{u(\text{clay})}$. The sand component, $Q_{u(\text{sand})}$, is mobilized only when the anchor plate punches through the clay layer and reaches the sand-clay interface.

3.8 OTHER STUDIES

Some more analytical and numerical analyses have been carried out by researchers in the recent past to estimate the ultimate pullout load of horizontal plate anchors in clays.

Rowe and Davis (1982) reported a finite element study of the undrained behavior of horizontal anchor plates in homogeneous, isotropic saturated clay. This study shows that in many cases, ultimate collapse is preceded by significant anchor displacement, and therefore a definition of failure which allows reasonable displacement predictions to be made at working loads should be considered. They defined the failure load as the load which would give rise to a displacement four times that predicted by an elastic analysis. The failure loads defined on this basis are largely insensitive to elastic parameters of the soil and to the depth of soil beneath the anchor. It has been reported that for the limiting conditions of immediate or no breakaway of the soil behind the anchor, an anchor can be considered deep at an embedment ratio of 3 to 4; increasing the embedment beyond this has no effect on anchor capacity. Anchor capacity for the intermediate case in which breakaway occurs during loading is dependent on overburden pressure, which is a function of anchor depth. It was reported

that the anchor roughness was of little importance for shallow horizontal anchor plates. The anchor capacity of circular anchors was found to be up to twice that of a strip for very shallow anchors.

Merifield et al. (2001) applied numerical limit analysis to rigorously evaluate the stability of horizontal strip anchors in both homogeneous and inhomogeneous undrained clays. Rigorous bounds on the ultimate pullout capacity were obtained by using two numerical procedures that were based on finite element formulations of the upper and lower bound theorems of limit analysis. These formulations followed standard procedure by assuming a rigid perfectly plastic clay model with a Tresca yield criterion and generated large linear programming problems. The analysis considered the effect of anchor embedment depth, anchor roughness, material homogeneity, and overburden pressure. In this approach, the true pullout capacity can be bracketed by obtaining both upper and lower bound estimates of the pullout capacity. Results were presented for the case where no suction forces exist between the anchor and the soil, which constitutes what is known as the *immediate breakaway* condition. The study shows that for most cases they considered, the exact anchor capacity can be predicted to within $\pm 5\%$ using numerical finite element formulations of the lower and upper bound limit theorems. The ultimate capacity increases linearly with overburden pressure up to a limiting value, which reflects the transition from shallow to deep anchor behavior where the mode of failure becomes localized around the anchor. At a given embedment depth, an anchor may behave as shallow or deep, depending on the dimensionless overburden ratio $\gamma H/c_u$. The ultimate capacity of horizontal anchors is less affected by anchor roughness.

Song et al. (2008) studied the behavior of strip and circular plate anchors with fully attached and vented rear faces during vertical pullout in uniform and normally consolidated clays by means of small-strain and large-deformation finite element analyses. Suction behind the anchor was ignored for the vented case so that separation occurs when the normal stress reduces to zero. From small-strain analysis of fully attached anchors, the transitional embedment depth from shallow to deep failure mechanisms was found to be $(H/h)_{cr} = 2$ for strip anchors and $(H/h)_{cr} = 1$ for circular anchors. Soil unit weight had no effect on the pullout response of an attached anchor. The ultimate pullout capacity factors for deeply embedded and fully attached anchors were found to be $F_c^\star = 11.6$ and 11.7, respectively, for smooth and rough strip anchors; $F_c^\star = 13.1$ and 13.5 for smooth and rough circular anchors, both for a thickness ratio (thickness t of the anchor plate to its width or diameter h) of 0.05. In large-deformation analysis of plate anchors in uniform soil, the pullout response of an attached anchor formed a unique curve regardless of soil unit weight, soil strength, and

anchor size for any anchor embedded to a depth of at least half of the anchor size initially. However, the transitional embedment depth from shallow to deep embedment was reduced to $(H/h)_{cr} = 1.4$ for strip anchors and $(H/h)_{cr} = 0.75$ for circular anchors due to the soil heave formed during continuous pullout. For a vented anchor in uniform soil, the anchor broke away from the soil below the anchor at a certain embedment depth, called the separation embedment depth (H_s). The separation embedment depth ratio (H_s/h) was found to increase linearly with the undrained shear strength ratio of soil, $c_u/\gamma h$. When the anchor embedment reached H_s, the pullout capacity decreased rapidly and linearly. The increasing pullout capacity factor for an attached anchor during continuous pullout was due to the stronger soil from the initial embedment depth trapped around the anchor and also due to the increasing effect of soil weight above the anchor.

3.9 SUMMARY OF MAIN POINTS

1. Horizontal plate anchors are used in the construction of foundations in clays subjected to uplifting load.
2. In general, the breakout factor F_c increases with embedment depth ratio H/h up to a maximum value and remains constant thereafter. The embedment depth ratio H/h corresponding to the maximum F_c is called the critical embedment depth ratio $(H/h)_{cr}$, the lower and higher values of which categorize the anchors as shallow and deep, respectively.
3. Vesic's theory (1971) gives a closer estimate of the uplift capacity only for shallow horizontal plate anchors embedded in softer clays.
4. The critical embedment ratio $(H/h)_{cr}$ is a function of undrained shear strength c_u of clays.
5. The ultimate capacity of horizontal square, circular, or rectangular anchors is not likely to be affected noticeably by anchor roughness.
6. The breakout factors for square, circular, and rectangular anchors in weightless soil are always greater than those obtained for strip anchors at corresponding embedment ratios.
7. A rectangular anchor with an aspect ratio (length-to-width ratio) greater than 10 can be considered to behave essentially as a strip anchor.
8. The lower bound limit analysis and small-strain finite element analysis may overestimate the pullout capacity of horizontal plate anchors during vertical pullout.
9. The sand overlay on a clay layer can significantly increase the net ultimate uplift capacity of the horizontal plate anchor.

SELF-ASSESSMENT QUESTIONS

Select the most appropriate answer to each multiple-choice question

3.1. A horizontal plate anchor located at an embedment depth ratio greater than the critical embedment depth ratio is called:
   a. a shallow anchor
   b. a deep anchor
   c. an inclined anchor
   d. none of the above

3.2. For undrained clays, the angle of internal friction is equal to:
   a. 0°
   b. 45°
   c. 90°
   d. 180°

3.3. According to Meyerhof's theory (1973), the critical embedment depth ratio for horizontal circular plate anchors in clays is approximately:
   a. 7.5
   b. 8.0
   c. 9.0
   d. 13.5

3.4. For a given embedment depth ratio, a horizontal strip anchor in clay has a breakout factor of 3. Which of the following can be a possible value of the breakout factor for a horizontal circular anchor for the same embedment depth ratio and the same clay:
   a. 1
   b. 2
   c. 3
   d. 4

3.5. Select the correct statement:
   a. The ultimate pullout capacity of horizontal square, circular, or rectangular anchors is likely to be affected noticeably by anchor roughness
   b. The ultimate pullout capacity of only horizontal square anchors is likely to be affected noticeably by anchor roughness
   c. The ultimate pullout capacity of horizontal square, circular, or rectangular anchors is not likely to be affected noticeably by anchor roughness
   d. The ultimate pullout capacity of vertical square, circular, or rectangular anchors is not likely to be affected noticeably by anchor roughness

3.6. In most cases of anchor design, the recommended factor of safety is about:
   a. 1 to 1.5
   b. 2 to 2.5
   c. 3 to 3.5
   d. 4 to 5.5

3.7. Das's theory (1978) is applicable to:
   a. circular anchors only
   b. square anchors only
   c. rectangular anchors only
   d. circular, square, and rectangular anchors

3.8. The breakout factor for a deep rectangular anchor (width = h, length = B) is:
   a. directly proportional to (h/B)
   b. directly proportional to $(h/B)^2$
   c. inversely proportional to (h/B)
   d. inversely proportional to $(h/B)^2$

3.9. According to three-dimensional lower bound solution, the limiting value of the breakout factor for circular anchors is approximately:
   a. 0
   b. 11.9
   c. 12.56
   d. none of the above

3.10. With the presence of a sand overlay on the clay layer, the net ultimate uplift capacity of a horizontal plate anchor:
   a. decreases
   b. increases
   c. becomes extremely small
   d. remains unaffected

Answers

3.1: b 3.2: a 3.3: a 3.4: d 3.5: c 3.6: b 3.7: d 3.8: a 3.9: c 3.10: b

REFERENCES

Adams, J.I. and Hayes, D.C. (1967). The uplift capacity of shallow foundations. *Ont. Hydro Res. Q.,* 19(1):1–13.

Ali, M. (1968). Pullout Resistance of Anchor Plates in Soft Bentonite Clay, M.S. thesis, Duke University, Durham, NC.

Bhatnagar, R.S. (1969). Pullout Resistance of Anchors in Silty Clay, M.S. thesis, Duke University, Durham, NC.

Das, B.M. (1978). Model tests for uplift capacity of foundations in clay. *Soils Found.,* 18(2):17–24.

Das, B.M. (1980). A procedure for estimation of ultimate uplift capacity of foundations in clay. *Soils Found.,* 20(1):77–82.

Kupferman, M. (1971). The Vertical Holding Capacity of Marine Anchors in Clay Subjected to Static and Cyclic Loading, M.S. thesis, University of Massachusetts, Amherst.

Merifield, R.S., Sloan, S.W., and Yu, H.S. (2001). Stability of plate anchors in undrained clay. *Geotechnique,* 51(2):141–153.

Merifield, R.S., Lyamin, A.V., Sloan, S.W., and Yu, H.S. (2003). Three-dimensional lower bound solutions for stability of plate anchors in clay. *J. Geotech. Geoenviron. Eng.,* 129(3):243–253.

Meyerhof, G.G. (1973). Uplift resistance of inclined anchors and piles. *Proc. VIII Int. Conf. Soil Mech. Found.,* Moscow, 167–172.

Rowe, R.K. and Davis, E.H. (1982). The behaviour of anchor plates in clay. *Geotechnique,* 31(1):9–23.

Song, Z., Hu, Y., and Randolph, F. (2008). Numerical simulation of vertical pullout of plate anchors in clay. *J. Geotech. Geoenviron. Eng.,* 134(6):866–875.

Stewart, W. (1985). Uplift capacity of circular plate anchors in sand. *Can. Geotech. J.,* 22(4):589–592.

Vesic, A.S. (1971). Breakout resistance of objects embedded in ocean bottom. *J. Soil Mech. Found. Div. ASCE,* 97(9):1183–1205.

Wang, D., Hu, Y., and Randolph, M.F. (2010). Three-dimensional large deformation finite-element analysis of plate anchors in uniform clay. *J. Geotech. Geoenviron. Eng.,* 136(2):355–365.

4

VERTICAL PLATE ANCHORS

In this chapter, the holding capacity of vertical anchors is analyzed in detail. A number of theoretical and experimental studies conducted to define the actual failure surface in soil around an anchor at ultimate load also are included. The discussion is divided into two major parts: behavior of anchors in sand and behavior of anchors in clay (undrained condition).

4.1 INTRODUCTION

The use of vertical plate anchors to resist horizontal loading in the construction of sheet pile walls was discussed in Chapter 1 (see Figure 1.4). Inadequate design of anchors has been the cause of failure of many sheet pile walls. Sheet pile walls are flexible structures, and due to the outward bulging of these walls, the lateral earth pressure produced is quite different than that calculated for rigid structures using the classical Rankine or Coulomb earth pressure theories. In conducting laboratory measurements, Rowe (1952) showed that the bending moment to which an anchored sheet pile wall is subjected can be substantially reduced when the anchor movement is less than about 0.1% of the height of the wall. The movement of 0.1% of the anchor includes the elongation of the tie-rod connecting the vertical plate anchors and the wall. Hence, it is important to properly estimate the ultimate and allowable holding capacities of plate anchors

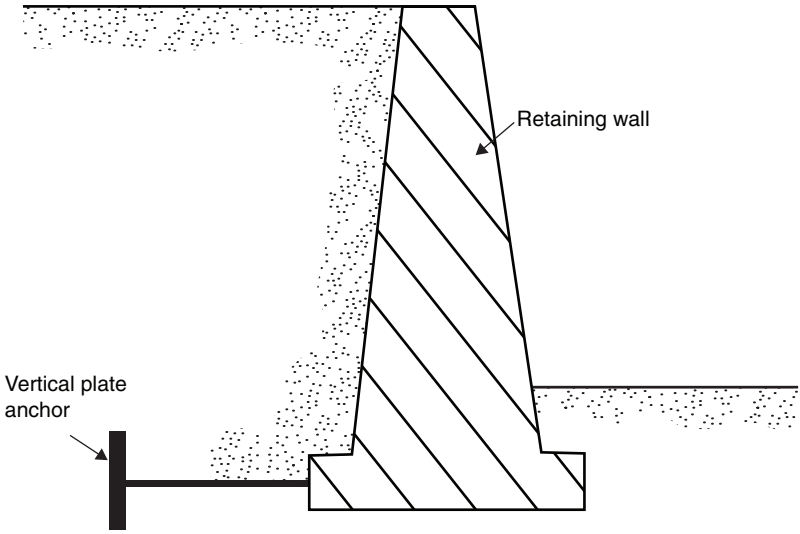

FIGURE 4.1 Vertical plate anchor at the base of a retaining wall to resist sliding

and also the corresponding displacements. Vertical plate anchors can also be used at pressure pipeline bends, at the base of retaining walls to resist sliding (Figure 4.1), and also where it is necessary to control thermal stresses.

Figure 4.2 shows the geometric parameters of a vertical anchor plate. The height and width of the anchor plate are h and B, respectively. The depth of the embedment of the anchor plate (that is, the distance from the ground surface to the bottom of the plate) is H. In most practical cases, the anchor can be considered as a strip anchor (two-dimensional plane strain case) if the B/h ratio is greater than about 6.

The holding capacity of an anchor is primarily derived from the passive force imposed by the soil in front of the anchor slab. If the embedment ratio H/h of the anchor is relatively small, at ultimate pullout load on the anchor the passive failure surface developed in soil in front of the anchor will intersect the ground surface. This is referred to (as in the case of horizontal anchors, discussed in Chapters 2 and 3) as the *shallow anchor condition*. Figure 4.3 shows the failure surface in front of a shallow square plate anchor (that is, $h = B$) embedded in sand as observed by Hueckel (1957). At greater embedment ratios, the *local shear failure* in soil will take place at ultimate load, and these anchors are called *deep anchors*. Thus the ultimate holding capacity Q_u is a function of several parameters:

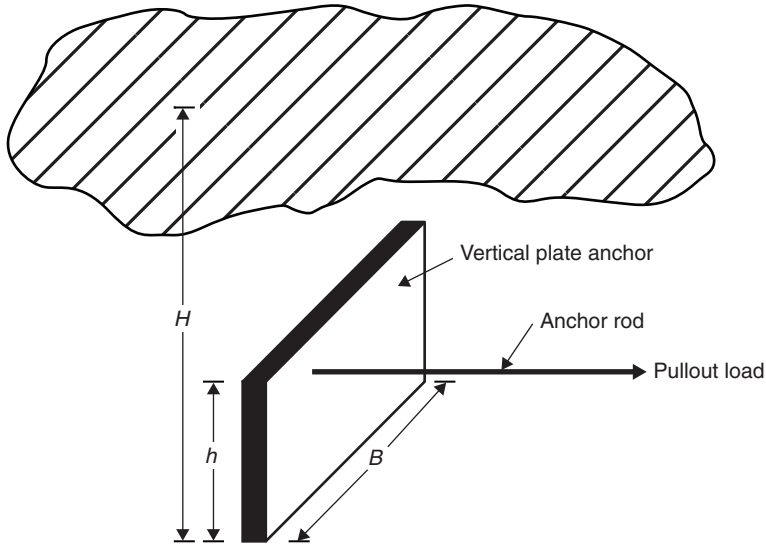

FIGURE 4.2 Geometric parameters of a vertical plate anchor

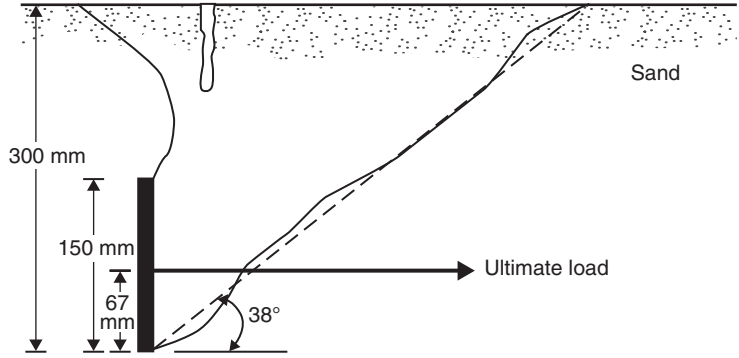

FIGURE 4.3 Failure surface in front of a square anchor slab (150 mm × 150 mm) embedded in sand at $H/h = 2$ (soil friction angle $\phi = 34°$) as observed by Hueckel (1957)

1. H/h ratio
2. Width-to-height ratio, B/h
3. Shear strength parameters of the soil (soil friction angle, ϕ, and cohesion, c)
4. The angle of friction of the anchor-soil interface, δ

It is important to note that for vertical anchors, the gross ultimate holding capacity $Q_{u(g)}$ is equal to the net ultimate holding capacity Q_u.

4.2 ANCHORS IN SAND

4.2.1 Ultimate Holding Capacity from Rankine's Theory

One of the earlier methods for estimation of the holding capacity of vertical anchors used the theory of *Rankine's lateral earth pressure* (Teng, 1962). Figure 4.4a shows a vertical strip anchor embedded in a granular soil, at a relatively shallow depth. The relatively *shallow depth condition* refers to the case where

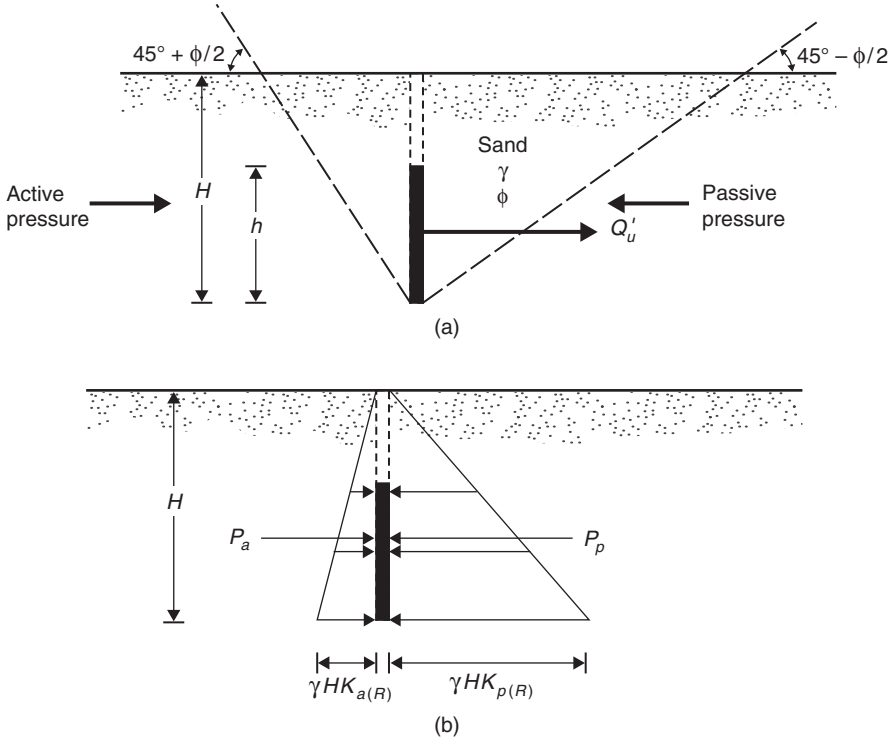

FIGURE 4.4 Ultimate holding capacity of strip vertical anchor as derived by Teng (1962)

$h/H < ⅓$ to ½. Assuming that the Rankine state exists, the failure surface in soil around the anchor at ultimate load also is shown in Figure 4.4a.

According to this procedure, for a strip anchor, the ultimate holding capacity per unit width (that is, at right angles to the cross section shown in Figure 4.4b) can be given as:

$$Q'_u = P_p - P_a \tag{4.1}$$

where

Q'_u = ultimate holding capacity per unit width
P_p = passive force in front of the anchor per unit width (Figure 4.4b)
P_a = active force at the back of the anchor per unit width (Figure 4.4b)

The relationships for P_p and P_a are as follows:

$$P_p = \frac{1}{2}\gamma H^2 \tan^2\left(45° + \frac{\phi}{2}\right) \tag{4.2a}$$

$$P_a = \frac{1}{2}\gamma H^2 \tan^2\left(45° - \frac{\phi}{2}\right) \tag{4.2b}$$

where

γ = unit weight of soil
ϕ = soil friction angle
$\tan^2\left(45° + \frac{\phi}{2}\right) = K_{p(R)}$ = Rankine passive earth pressure coefficient
$\tan^2\left(45° - \frac{\phi}{2}\right) = K_{a(R)}$ = Rankine active earth pressure coefficient

For anchors with a limited width B, the frictional resistance developed along the vertical faces of the failure surface must be taken into account (Figure 4.5). Following the procedure of Teng (1962), the total earth pressure normal to *abc* and *def* is

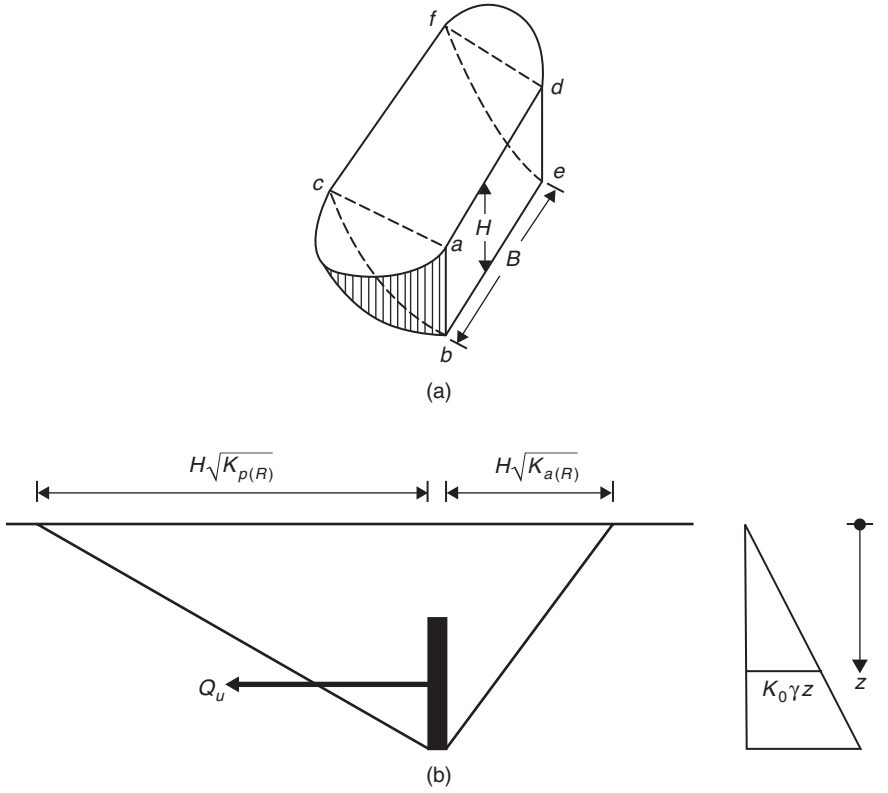

FIGURE 4.5 Frictional resistance developed along the vertical faces of the failure surface: Teng's method (1962)

$$N = 2\int_0^H \left(\frac{H - z}{H}\right)\left[H\sqrt{K_{p(R)}} + H\sqrt{K_{a(R)}}\right](dz)\,(\gamma K_0)$$

$$= \frac{1}{3}K_0\gamma\left[\sqrt{K_{p(R)}} + \sqrt{K_{a(R)}}\right]H^3 \qquad (4.3a)$$

where

K_0 = earth pressure coefficient at rest ≈ 0.4

Hence, the total frictional resistance at the ends is

$$F = N \tan \phi = \frac{1}{3} K_0 \left[\sqrt{K_{p(R)}} + \sqrt{K_{a(R)}} \right] H^3 \tan \phi \qquad (4.3b)$$

Hence, the ultimate holding capacity can be given as:

$$Q_u = Q'_u B + F$$

$$= B(P_p - P_a) + \frac{1}{3} K_0 \left[\sqrt{K_{p(R)}} + \sqrt{K_{a(R)}} \right] H^3 \tan \phi \qquad (4.4)$$

Example 4.1

For a vertical plate anchor, assume the following values: $h = 2$ ft, $B = 5$ ft, $H = 4$ ft, $\gamma = 105$ lb/ft^3, and $\phi = 32°$. Determine the ultimate holding capacity, Q_u.

Solution

$$K_{p(R)} = \tan^2 \left(45° + \frac{\phi}{2} \right) = \tan^2 \left(45° + \frac{32°}{2} \right) = 3.25$$

$$K_{a(R)} = \tan^2 \left(45° - \frac{\phi}{2} \right) = \tan^2 \left(45° - \frac{32°}{2} \right) = 0.307$$

$$P_p = \frac{1}{2} \gamma H^2 K_{p(R)} = \left(\frac{1}{2} \right) (105) (4)^2 (3.25) = 2730 \text{ lb/ft}$$

$$P_a = \frac{1}{2} \gamma H^2 K_{a(R)} = \left(\frac{1}{2} \right) (105) (4)^2 (0.307) = 257.9 \text{ lb/ft}$$

$$F = \frac{1}{3} K_0 \gamma \left[\sqrt{K_{p(R)}} + \sqrt{K_{a(R)}} \right] H^3 \tan \phi$$

$$= \left(\frac{1}{3} \right) (0.4) (105) \left(\sqrt{3.25} + \sqrt{0.307} \right) (4)^3 \tan 32°$$

$$= 699.25 \text{ lb}$$

Therefore:

$$Q_u = B(P_p - P_a) + F = (5)(2730 - 257.9) + 699.25 \approx \mathbf{13{,}060\ lb}$$

4.2.2 Analysis of Ovesen and Stromann

In 1964, Ovesen reported the results of several model tests conducted for shallow anchors in sand at the Danish Geotechnical Institute. The method of analysis developed in this section (Ovesen and Stromann, 1972) is primarily based on those model tests and also on the following concepts:

1. Determination of the holding capacity per unit width of a continuous anchor plate, $Q'_{u(B)}$, of height H, as shown in Figure 4.6a. This is known as the *basic case.*

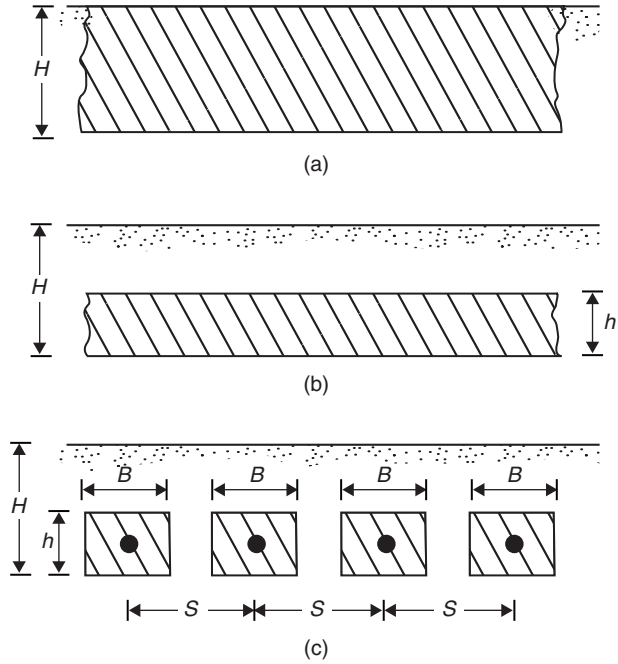

FIGURE 4.6 Ovesen and Stromann's analysis (1972): (a) basic case, (b) strip case, and (c) actual case

2. Estimation of the holding capacity per unit width of an anchor whose height is h (Figure 4.6b) and has an embedment depth of $H (h \leq H)$. This is known as the *strip case*.
3. Estimation of the holding capacity of an anchor with limited width-to-height ratio, B/h (Figure 4.6c). This is known as the *actual case*.

4.2.2.1 Basic Case

Figure 4.7 shows the basic case for a vertical anchor embedded in sand. The assumed failure surface in soil for translation of the anchor at ultimate load $Q'_{u(B)}$ (load per unit width) is also shown in this figure. For a rough anchor surface, P_a is the active force per unit width. The horizontal and vertical components of P_a can be given as:

$$P_{a(H)} = P_a \cos \phi \tag{4.5}$$

$$P_{a(V)} = P_a \sin \phi \tag{4.6}$$

where

$P_{a(H)}$, $P_{a(V)}$ = horizontal and vertical components of P_a, respectively
ϕ = soil friction angle

The passive failure surface in front of the anchor slab consists of (a) straight rupture line *BC*, (b) Prandtl radial shear zone *ACD*, and (c) Rankine passive zone *ADE*. (Note: Angles *EAD* and *AED* are both equal to $45° - \phi/2$).

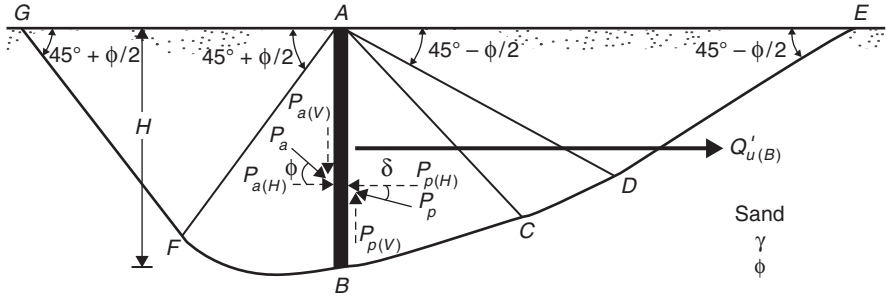

FIGURE 4.7 Basic case for failure surface at ultimate load

The horizontal and vertical components of the passive force P_p are

$$P_{p(H)} = \frac{1}{2}\gamma H^2 K_{pH} \tag{4.7}$$

$$P_{p(V)} = \frac{1}{2}\gamma H^2 K_{pH} \tan\delta \tag{4.8}$$

where

γ = unit weight of the soil
K_{pH} = horizontal component of the passive earth pressure coefficient
δ = anchor-soil friction angle

For vertical equilibrium:

$$P_{a(V)} + W = P_{p(V)} \tag{4.9}$$

where

W = weight of anchor per unit width

From Equations 4.8 and 4.9:

$$K_{pH} \tan\delta = \frac{P_{a(V)} + W}{\frac{1}{2}\gamma H^2} \tag{4.10}$$

Figure 4.8 shows the variation of $K_{pH} \tan\delta$ and ϕ from which K_{pH} can be estimated. Now, for horizontal equilibrium:

$$Q'_{u(B)} = P_{p(H)} - P_{a(H)} = \frac{1}{2}\gamma H^2 K_{pH} - P_{a(H)} \tag{4.11}$$

The magnitudes of $P_{a(V)}$ and $P_{a(H)}$ can be determined using any ordinary active earth pressure theory. Figure 4.9 shows the variation of the active earth pressure coefficient K_a according to Caquot and Kerisel (1949). Note that:

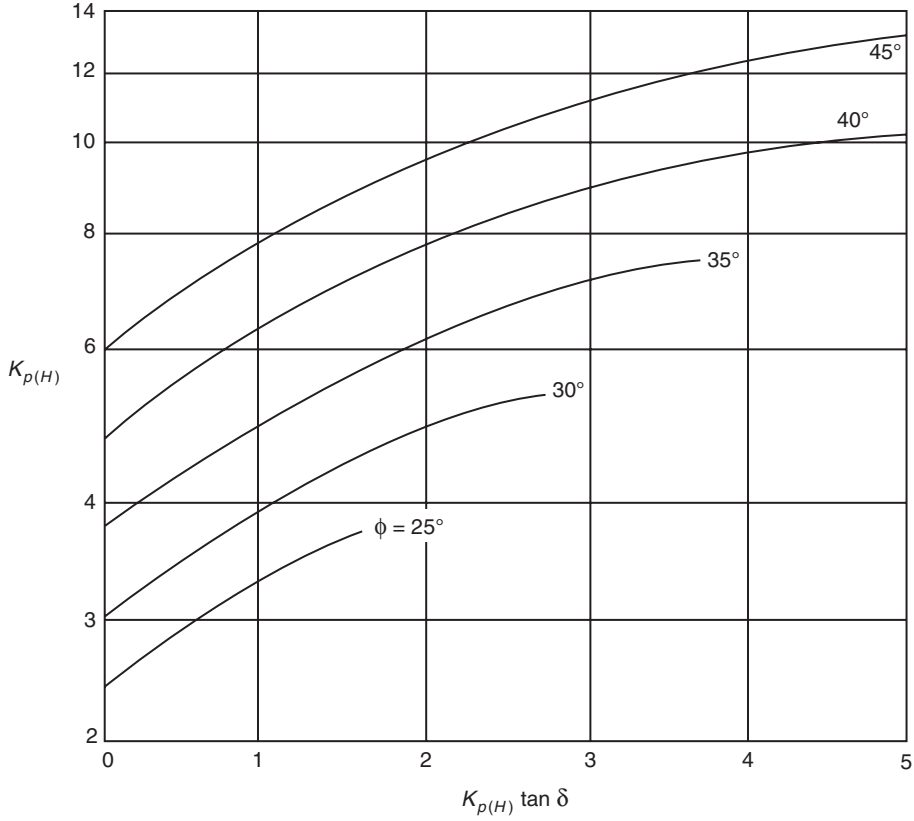

FIGURE 4.8 Variation of $K_{p(H)}$ with $K_{p(H)}$ tan δ and ϕ (after Ovesen and Stromann, 1972)

$$P_a = \frac{1}{2}\gamma H^2 K_a \tag{4.12}$$

4.2.2.2 Strip Case

Based on the experimental evidence of Ovesen (1964), the ultimate holding capacity of a *strip anchor* can be given as:

$$Q'_u = R_{ov} Q'_{u(B)} \tag{4.13}$$

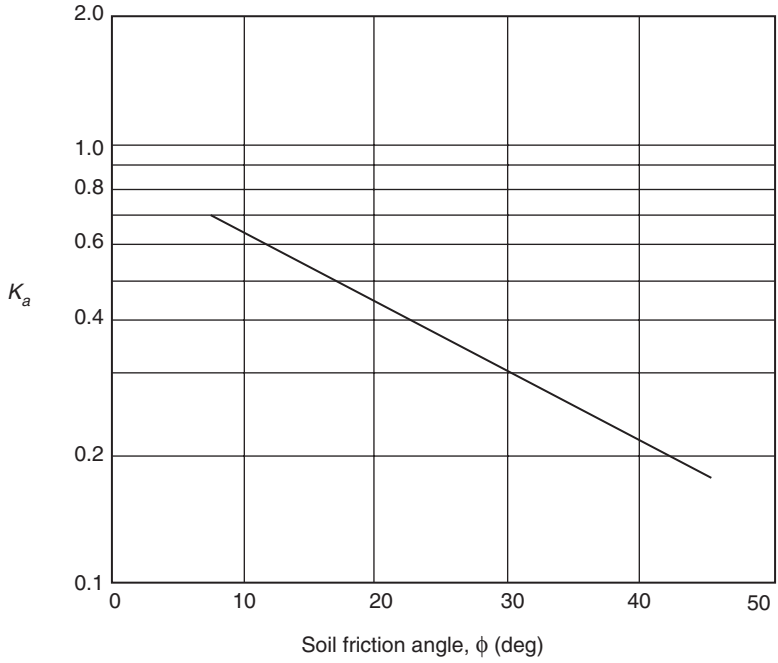

FIGURE 4.9 Variation of K_a with ϕ

where

Q'_u = ultimate holding capacity per unit width for strip anchor

The variation of R_{ov} with the ratio h/H is shown in Figure 4.10. Note that:

$$R_{ov} = \frac{C_{ov} + 1}{C_{ov} + \dfrac{H}{h}} \tag{4.14}$$

where

C_{ov} = 19 for dense sand and 14 for loose sand

Equation 4.14 was developed by Dickin and Leung (1985) from Figure 4.10.

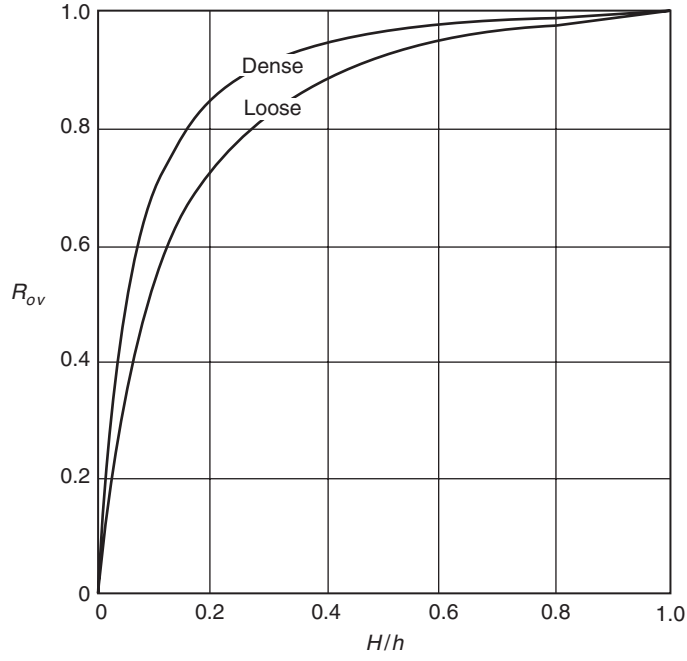

FIGURE 4.10 Variation of R_{ov} with H/h (after Ovesen and Stromann, 1972)

4.2.2.3 Anchor with Limited B/h Ratio (Actual Case)

When an anchor has a limited width-to-height ratio (B/h), the failure surface in soil will be three-dimensional, as shown in Figure 4.5. Hence, the ultimate holding capacity of an anchor, Q_u, can be given by Equation 4.4 as $Q_u = Q'_u + F$. However, if a number of vertical anchors are used in a row, depending on the S/B ratio (S = center-to-center spacing of the anchor, as shown in Figure 4.11), the failure surface may overlap. In that case, $Q_u = Q'_u B + F'$, where F' is the friction resistance $\leq F$.

Hueckel (1957) conducted a number of laboratory model tests on three square anchors (Figure 3.11) to determine the S/B ratio at which $F = F'$, and these results are shown in Figure 4.12. Note that Q_{ug} is the notation for the holding capacity of the anchor group. In this case, the group consists of three anchors, each measuring 100 mm × 100 mm. From this figure, it can be seen that at $S/B \approx 3$ to 4, the effect of interference practically disappears.

Ovesen and Stromann (1972) expressed Q_u as:

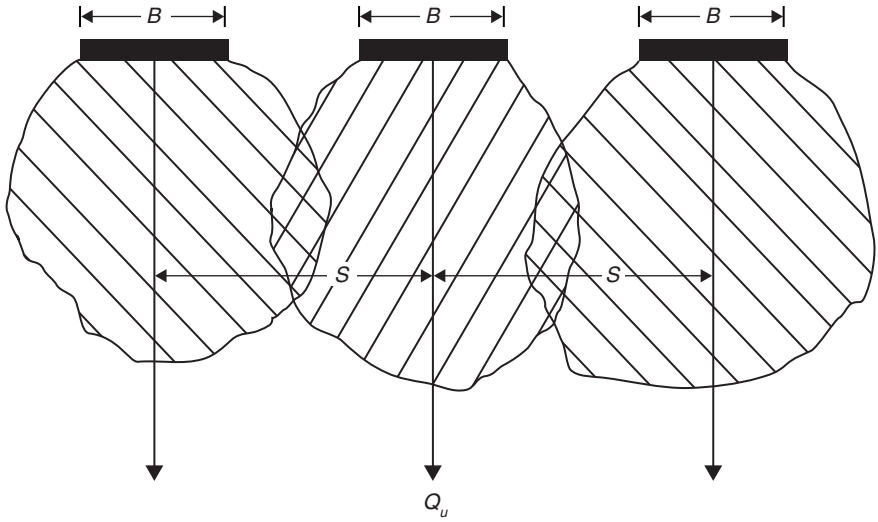

FIGURE 4.11 Overlapping of failure surface in soil in front of a row of vertical anchors

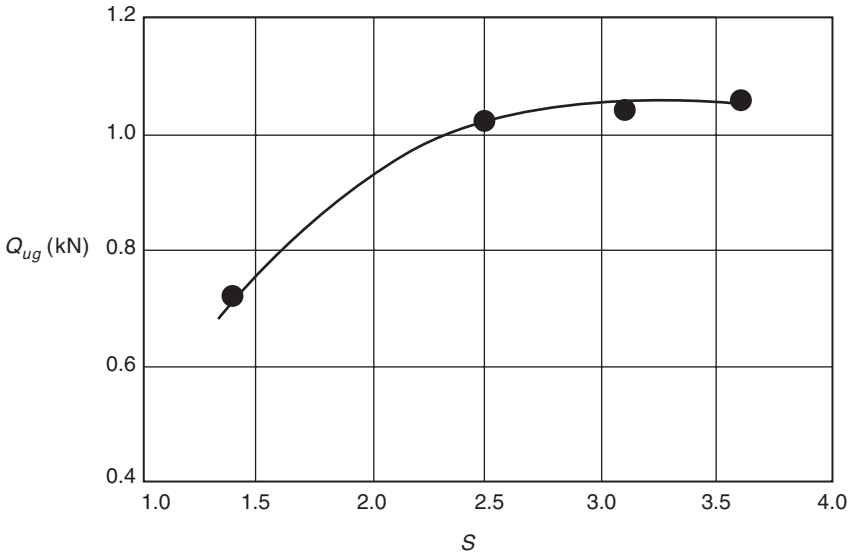

FIGURE 4.12 Variation of the ultimate group capacity with center-to-center spacing of anchor as observed by Hueckel (1957) ($B = h = 100$ mm, $H/h = 2$, number of anchors = 3, $\phi = 36°$)

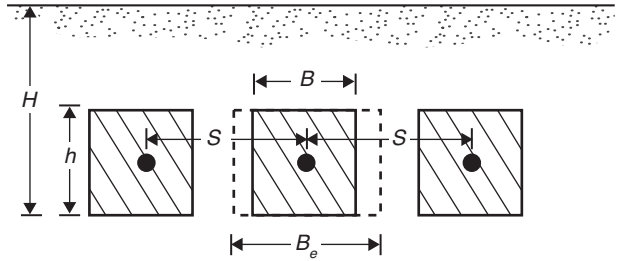

FIGURE 4.13 Definition of equivalent width

$$Q_u = Q'_u B_e \tag{4.15}$$

where

B_e = equivalent width $\leq B$ (Figure 4.13)

The variation of B_e can be obtained from Figure 4.14.

In the case of a single anchor (that is, $S = \infty$), we can also write that:

$$Q_u = Q'_u B S_f \tag{4.16}$$

where

$S_f = B_e/B$ = shape factor

From Figure 4.14, it can be shown that with $S = \infty$ (also see Dickin and Leung, 1983):

$$S_f = 0.42 \left(\frac{\frac{H}{h} + 1}{\frac{B}{h}} \right) + 1 \qquad \text{(for dense sand)} \tag{4.17}$$

and

$$S_f = 0.26 \left(\frac{\frac{H}{h} + 1}{\frac{B}{h}} \right) + 1 \qquad \text{(for loose sand)} \tag{4.18}$$

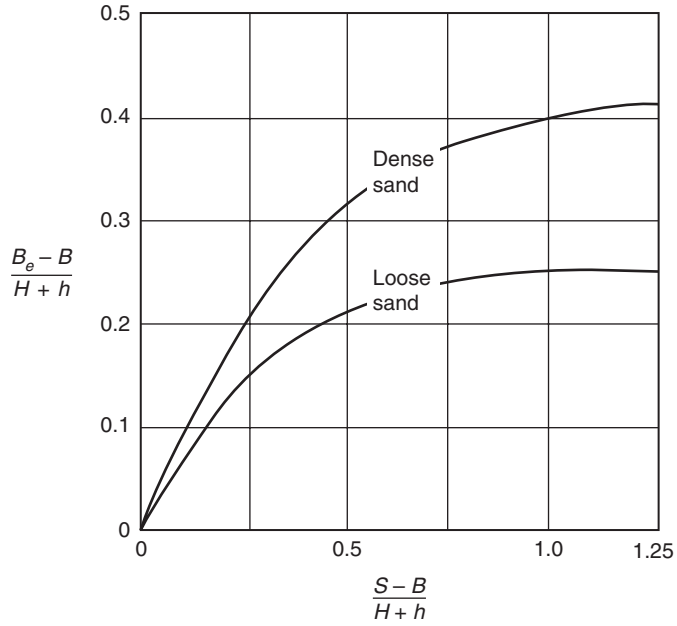

FIGURE 4.14 Variation of $(B_e - B)/(H + h)$ with $(S - B)/(H + h)$ (after Ovesen and Stromann, 1972)

Hence, for single anchors with limited width-to-height ratio, combining Equations 4.11, 4.14, 4.17, and 4.18, we obtain:

$$Q_u = B\left[\frac{1}{2}\gamma H^2 K_{pH} - P_{a(H)}\right]\left(\frac{C_{ov} + 1}{C_{ov} + \frac{H}{h}}\right) \times \left[F\left(\frac{\frac{H}{h} + 1}{\frac{B}{h}}\right) + 1\right] \tag{4.19}$$

where for dense sand $C_{ov} = 19$ and $F = 0.42$, and for loose sand $C_{ov} = 14$ and $F = 0.26$.

Example 4.2

Redo Example 4.1 using the theory of Ovesen and Stromann (1972) (Section 4.2.2). Assume $W = 0$.

Solution

Calculation of $P_{a(H)}$ and $P_{a(V)}$. From Equations 4.5, 4.6, and 4.12:

$$P_{a(H)} = \frac{1}{2}\gamma H^2 K_a \cos\phi$$

$$P_{a(V)} = \frac{1}{2}\gamma H^2 K_a \sin\phi$$

For $\phi = 32°$, $K_a \approx 0.28$ (Figure 4.9):

$$P_{a(H)} = \frac{1}{2}(105)(4)^2(0.28)(\cos 32°) = 199.46 \text{ lb/ft}$$

$$P_{a(V)} = \frac{1}{2}(105)(4)^2(0.28)(\sin 32°) = 111.28 \text{ lb/ft}$$

Calculation of K_{pH}. From Equation 4.10:

$$K_{pH}\tan\delta = \frac{P_{a(V)} + W}{\frac{1}{2}\gamma H^2}$$

Assume $W \approx 0$:

$$K_{pH}\tan\delta = \frac{111.28}{(0.5)(105)(4)^2} = 0.132$$

Using Figure 4.8, for $\phi = 32°$ and $K_{pH}\tan\delta = 0.132$, the value of $K_{pH} \approx 3.4$.

Calculation of Q_u. Using Equation 4.19:

$$Q_u = B\left[\frac{1}{2}\gamma H^2 K_{pH} - P_{a(H)}\right]\left(\frac{C_{ov}+1}{C_{ov}+\frac{H}{h}}\right) \times \left[F\left(\frac{\frac{H}{h}+1}{\frac{B}{h}}\right)+1\right]$$

Assume loose sand condition; hence, $C_{ov} = 14$ and $F = 0.26$. Thus:

$$Q_u = (5)\left[\left(\frac{1}{2}\right)(105)(4)^2(3.4) - 199.46\right]\left(\frac{14+1}{14+2}\right)\left[0.26\left(\frac{2+1}{2.5}\right)+1\right]$$

$$= (5)(2656.54)(0.9375)(1.312)$$

$$= \mathbf{16{,}338\ lb}$$

4.2.3 Analysis of Meyerhof

Meyerhof (1973) took the passive and active earth pressure coefficients proposed by Caquot and Kerisel (1949) and Sokolovskii (1965) into consideration and proposed the following simple relationship for the ultimate holding capacity per unit width (Q'_u) of a continuous (strip) anchor (see Figure 4.6b for notations):

$$Q'_u = \frac{1}{2}\gamma H^2 K_b \tag{4.20}$$

where

K_b = pullout coefficient

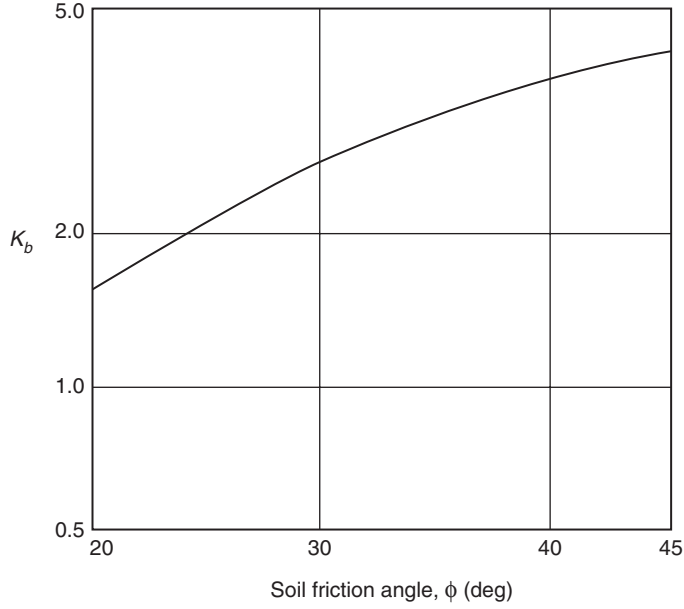

FIGURE 4.15 Meyerhof's (1973) pullout coefficient

The variation of K_b is shown in Figure 4.15. It is the opinion of the authors that for a single anchor with a limited width-to-height ratio (B/h), Equations 4.14, 4.17, and 4.18 can be incorporated into Equation 4.20 to determine the ultimate holding capacity as:

$$Q'_u = B\left(\frac{1}{2}\gamma H^2 K_b\right)\left(\frac{C_{ov} + 1}{C_{ov} + \dfrac{H}{h}}\right)\left[F\left(\frac{\dfrac{H}{h} + 1}{\dfrac{B}{h}}\right) + 1\right] \quad (4.21)$$

The values of C_{ov} and F are given after Equation 4.19.

Example 4.3

Redo Example 4.1 using Meyerhof's procedure (1973) described in Section 4.2.3.

Solution

From Equation 4.21:

$$Q_u = B\left(\frac{1}{2}\gamma H^2 K_b\right)\left(\frac{C_{ov}+1}{C_{ov}+\frac{H}{h}}\right)\left[F\left(\frac{\frac{H}{h}+1}{\frac{B}{h}}\right)+1\right]$$

From Figure 4.15, $K_b \approx 2.95$:

$$Q_u = (5)\left[\left(\frac{1}{2}\right)(105)\,(4)^2\,(2.95)\right]\left(\frac{14+1}{14+2}\right)\left[0.26\left(\frac{2+1}{2.5}\right)+1\right]$$

$$= (5)\,(2478)\,(0.9375)\,(1.312)$$

$$= \mathbf{15{,}239.7\ lb}$$

4.2.4 Analysis of Biarez et al.

Biarez et al. (1965) presented calculation methods for limiting equilibrium of vertical anchor piles subjected to translation and rotation. This analysis showed that at an embedment ratio of $H/h < 4$, the ultimate holding capacity is a function of the weight and roughness, that is, $Q_u = f(W_a, \delta)$ where W_a = weight of the anchor and δ = anchor-soil friction angle.

Dickin and Leung (1985) indicated that the analysis of Biarez et al. gave satisfactory results at embedment ratios of $4 < H/h < 7$. With the assumption that $\delta = 0$, the original equation of Biarez et al. (1965) can be conservatively expressed in a simplified form (Dickin and Leung, 1985) for a strip anchor as:

$$Q'_u = \gamma h^2 \left\{ \begin{array}{l} \left[K_{p(R)} - K_{a(R)}\right]\left(\frac{H}{h} - \frac{1}{2}\right) \\ + \left[\frac{K_{p(R)} \sin 2\phi}{2\tan\left(45° + \frac{\phi}{h}\right)}\right]\left(\frac{H}{h} - 1\right)^2 \end{array} \right\} \qquad (4.22)$$

The preceding relationship can be expressed in a nondimensional form as:

$$F_q = \frac{Q_u'}{\gamma h H} = \frac{h}{H}\left\{\begin{array}{l}\left[K_{p(R)} - K_{a(R)}\right]\left(\dfrac{H}{h} - \dfrac{1}{2}\right) \\ + \left[\dfrac{K_{p(R)} \sin 2\phi}{2 \tan\left(45° + \dfrac{\phi}{2}\right)}\right]\left(\dfrac{H}{h} - 1\right)^2\end{array}\right\} \quad (4.23)$$

where

F_q = breakout factor (similar to those given in Chapters 2 and 3)

In the preceding two equations, $K_{a(R)}$ and $K_{p(R)}$ are Rankine active and passive earth pressure coefficients, respectively.

In a similar manner, the ultimate resistance of a shallow single anchor with dimensions $B \times h$ can be expressed in a simplified nondimensional form as (Dickin and Leung, 1985):

$$\begin{aligned} F_q &= \frac{Q_u}{\gamma(hB)H} \\ &= F_{q(\text{strip})} + \phi\left(\frac{h}{B}\right)\left(\frac{h}{H}\right)\left[\sqrt{K_{p(R)}} - \sqrt{K_{a(R)}}\right]\left(\frac{H}{h} - \frac{2}{3}\right) \\ &\quad + \frac{1}{2}(1 + \phi)\left(\frac{h}{B}\right)\left(\frac{h}{H}\right)K_{p(R)} \sin 2\phi\left(\frac{H}{h} - 1\right) \end{aligned} \quad (4.24)$$

It should be noted that $F_{q(\text{strip})}$ in Equation 4.24 comes from Equation 4.23.

4.2.5 Analysis of Neely et al.

Neely et al. (1973) predicted the holding capacity of vertical strip anchors using the *stress characteristics analysis* (Sokolovskii, 1965). The theoretical study consisted of developing the so-called force coefficient $M_{\gamma q}$ by two methods:

1. *Surcharge method.* According to this method, it is assumed that the soil located above the top of the anchor can be taken as a simple surcharge

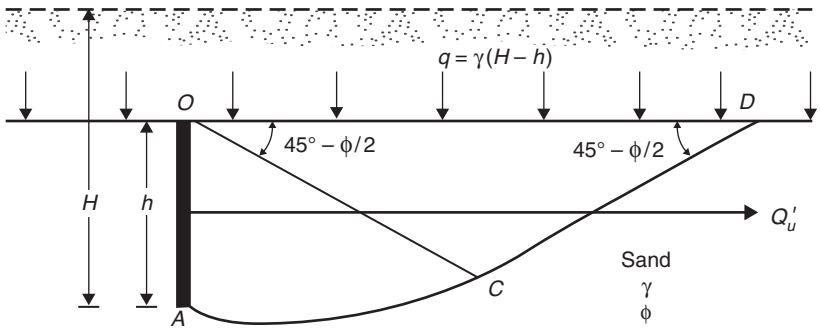

FIGURE 4.16 Surcharge method of analysis

of $q = \gamma(H - h)$. As shown in Figure 4.16, the failure surface in soil consists of an arc of a logarithmic spiral, *AC*, and a straight line, *CD*. Note that the zone *OCD* is a Rankine passive zone.

2. *Equivalent free surface method.* The assumed failure surface in soil, *ACD* (Figure 4.17), is an arc of a logarithmic spiral with the center at *O*. *OD* is a straight line which is the equivalent free surface. The concept of the equivalent free surface is based on that developed by Meyerhof (1951) in the process of predicting the ultimate bearing capacity of foundations. Note that along the equivalent free surface *OD*, the shear stress τ can be expressed as:

$$\tau = m\sigma \tan \phi \tag{4.25}$$

where

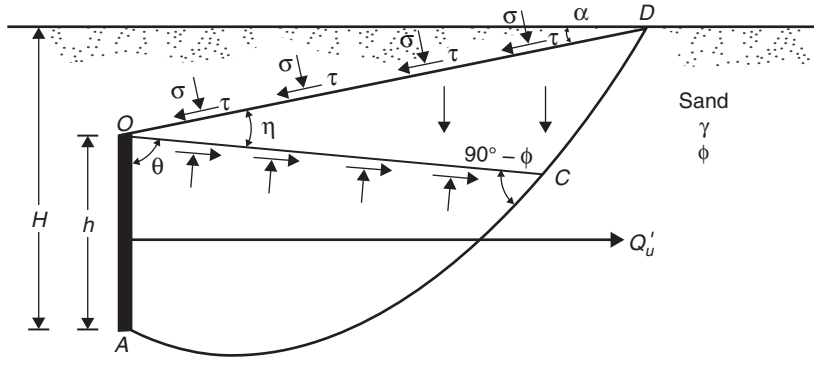

FIGURE 4.17 Failure mechanism assumed by Neely et al. (1973) for analysis by the equivalent free surface method

σ = effective normal stress
ϕ = soil friction angle
m = shear mobilization factor

The magnitude of m may vary between zero and one. When the value of m is less than one, the failure mechanism includes a mixed shear zone OCD in which the full shearing resistance of the soil becomes mobilized.

In the assumed failure mechanism shown in Figure 4.17, note that:

$$\frac{H}{h} = 1 + \frac{\sin\alpha \cos\phi e^{\theta \tan\phi}}{\cos(\phi + \eta)} \tag{4.26}$$

A nondimensional term $M_{\gamma q}$ (force coefficient) mentioned earlier in this section may now be defined as:

$$M_{\gamma q} = \frac{Q_u'}{\gamma h^2} \tag{4.27}$$

where

Q_u' = ultimate holding capacity per unit width of a strip anchor

The relationship between the nondimensional force coefficient (Equation 4.27) and the breakout factor (Equation 4.23) can be given as:

$$F_q = M_{\gamma q}\left(\frac{h}{H}\right) \tag{4.28}$$

Figures 4.18 and 4.19 show the variation of $M_{\gamma q}$ for strip anchors determined by the surcharge method and the equivalent free surface method, respectively. Note that, among other factors, the magnitude of $M_{\gamma q}$ based on the surcharge method is a function of δ/ϕ (δ = soil-anchor friction angle). Similarly, the force coefficient based on the equivalent free surface method is a function of the mobilization factor, m. Neely et al. (1973) recommended the use of the analysis based on the equivalent free surface method.

As shown in Equation 4.16, the force coefficient (or the ultimate load) for a single anchor with a limited B/h ratio can be obtained by incorporating a nondimensional shape factor (S_f). In a similar manner:

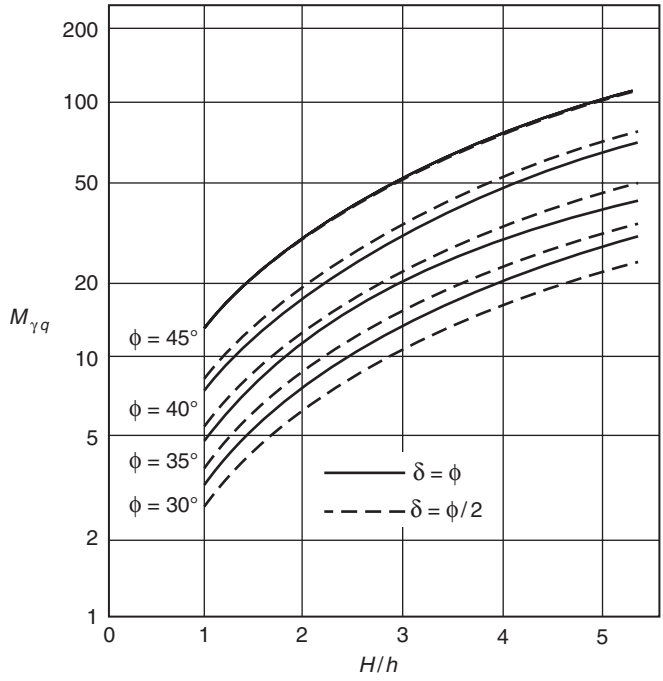

FIGURE 4.18 Variation of $M_{\gamma q}$ with H/h based on the surcharge method of analysis (after Neely et al., 1973)

$$M_{\gamma q} = \frac{Q_u}{\gamma B h^2} = M_{\gamma q(\text{strip})} S_f \tag{4.29}$$

or

$$Q_u = (\gamma B h^2) M_{\gamma q(\text{strip})} S_f \tag{4.30}$$

The shape factor S_f given in Equations 4.29 and 4.30 was determined by Neely et al. (1973) from laboratory tests as:

$$S_f = \frac{\left(\frac{Q_u}{B}\right)_{\text{rectangular}}}{Q'_{u(\text{strip})}} \tag{4.31}$$

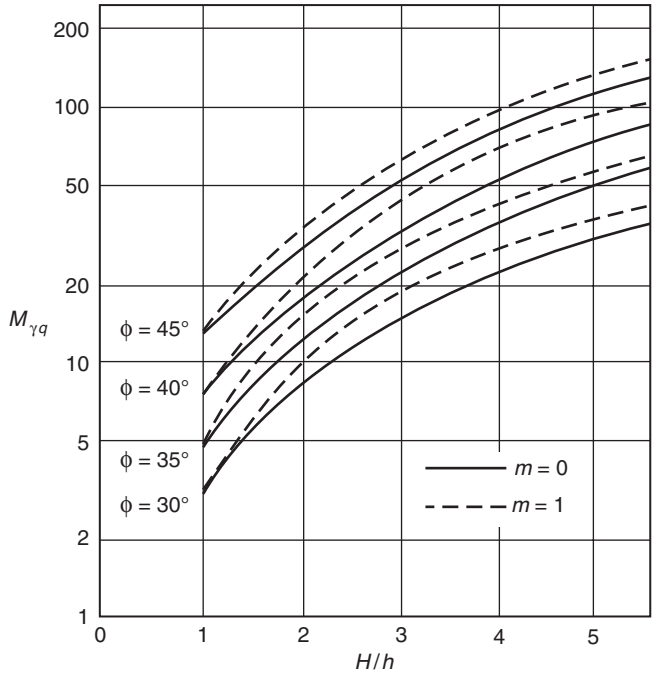

FIGURE 4.19 Variation of $M_{\gamma q}$ with H/h based on the equivalent free surface method of analysis (after Neely et al., 1973)

The variation of S_f, which is a function of H/h and B/h, as defined by Equation 4.31 is shown in Figure 4.20. One important thing that needs to be pointed out here is that Neely et al. (1973) assumed that an anchor with $B/h \geq 5$ should be treated as a strip anchor, or:

$$Q'_{u(\text{strip})} \approx Q'_{u(B/h=5)}$$

Das (1975) used the results of Neely et al. (1973) to express the ultimate holding capacity of square anchors ($B = h$) as:

$$Q_u = C\gamma \left(\frac{H}{h}\right)^n h^3 \tag{4.32}$$

where

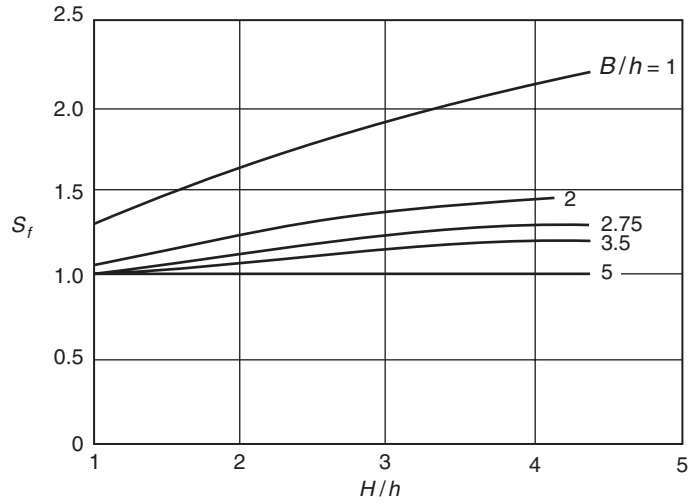

FIGURE 4.20 Variation of S_f (Equation 4.31) (adapted from Neely et al., 1973)

$$C = f(\phi)$$
$$n = f(m)$$

The variation of C with the soil friction angle ϕ is shown in Figure 4.21. The magnitude of n is equal to 1.7 for mobilization factor $m = 0$ and $n = 1.9$ for $m = 1$. Thus, based on a number of experimental results on small-scale laboratory model tests (Figure 4.22), Das (1975) suggested that the average value of n be taken as 1.8, or:

$$Q_{u(\text{square})} = C\gamma \left(\frac{H}{h} \right)^{1.8} h^3 \tag{4.33}$$

Other laboratory model test results such as those conducted by Hueckel (1957) and Kostyukov (1967) compared reasonably well with the equivalent free surface method of analysis.

Example 4.4

Redo Example 4.2 using the procedure of Neely et al. (1973) outlined in Section 4.2.5. Use:

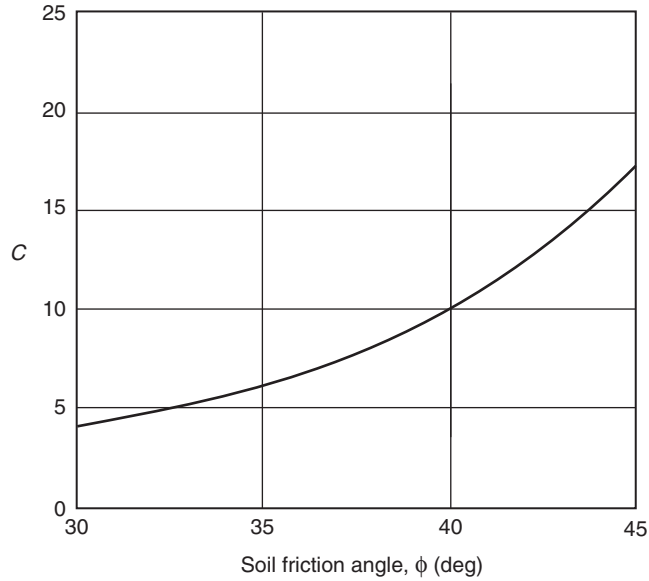

FIGURE 4.21 Variation of C with ϕ (Equation 4.32)

a. The equivalent free surface solution
b. The surcharge method

Assume $\delta/\phi = 0.5$.

Solution

Part a. From Equation 4.30:

$$Q_u = (\gamma B h^2) M_{\gamma q(\text{strip})} S_f$$

Use $m = 0$. From Figure 4.19, for $\phi = 32°$ and $H/h = 2$, $M_{\gamma q} \approx 9.9$. Also, for $B/h = 2.5$, $H/h = 2$, and $S_f \approx 1.1$ (from Figure 4.20). Therefore:

$$Q_u = [(105)(5)(2)^2](9.9)(1.1) = \mathbf{22{,}869\ lb}$$

Part b. With $\delta = \phi/2$, Figure 4.18 gives $M_{\gamma q} \approx 7.2$. Therefore:

$$Q_u = [(105)(5)(2)^2](7.2)(1.1) = \mathbf{16{,}632\ lb}$$

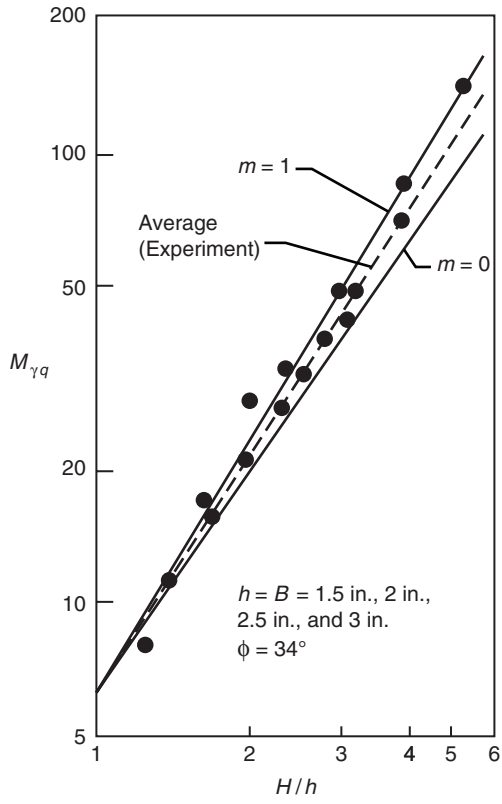

FIGURE 4.22 Force coefficient for shallow square anchors (after Das, 1975)

From the solutions given in Examples 4.1 to 4.4, it can be seen that Teng's method (1962) yields the smallest value of $Q_u \approx 13{,}060$ lb. The methods of Ovesen and Stromann (1972), Meyerhof (1973), and Neely et al. (1973) (surcharge method) give an average value of $Q_u \approx 16{,}000$ lb. However, the equivalent free surface method of Neely et al. (1973) results in the highest value of $Q_u \approx 23{,}000$ lb.

4.2.6 Nature of Passive Pressure Distribution in Front of a Shallow Vertical Anchor

It is now clear that the passive pressure developed in front of a vertical anchor when it is subjected to a horizontal force is the primary contributing factor to

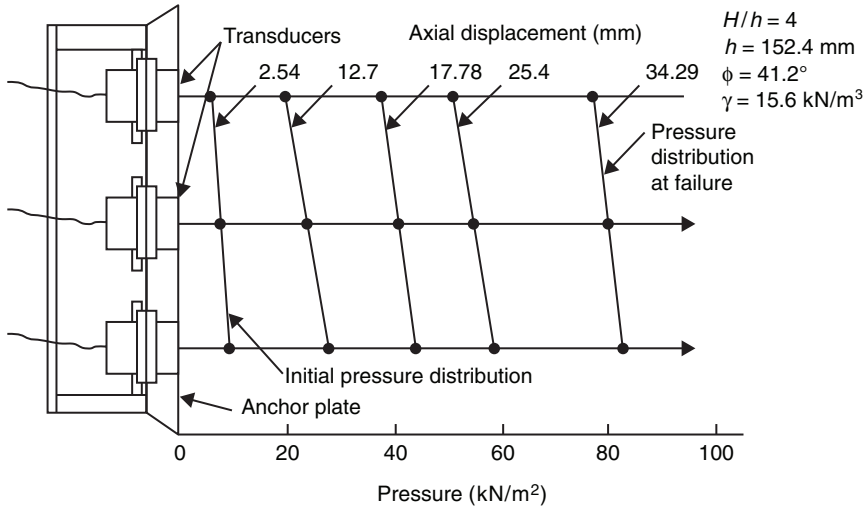

FIGURE 4.23 Nature of passive pressure distribution in front of a shallow vertical anchor (adapted from Hanna et al., 1988)

its holding capacity. It is thus of interest to know the nature of actual distribution of the passive pressure on the face of an anchor plate. Hanna et al. (1988) measured the passive pressure distribution on the face of a vertical strip anchor along with the horizontal displacement, and these results are shown in Figure 4.23. The passive pressure was measured by attaching several transducers to the anchor. For these laboratory tests, the following parameters apply: $\gamma = 15.6$ kN/m^3, $H/h = 4$, $\phi = 41.2°$, and $h = 152.4$ mm.

Hueckel et al. (1965) also presented results of similar pressure distribution on a square anchor plate embedded in sand. Figure 4.24 shows one of their laboratory test results. The parameters for this test were as follows: $\gamma = 16.38$ kN/m^3, $H/h = 2.5$, $\phi = 34.2°$, $B = h = 300$ mm, and horizontal displacement = 70 mm.

From the above laboratory observations, the following conclusions can be drawn:

1. The exact passive pressure distribution on the face of an anchor plate does not follow the classical pattern.
2. The nature of the pressure distribution diagram will be approximately the same irrespective of the horizontal displacement.

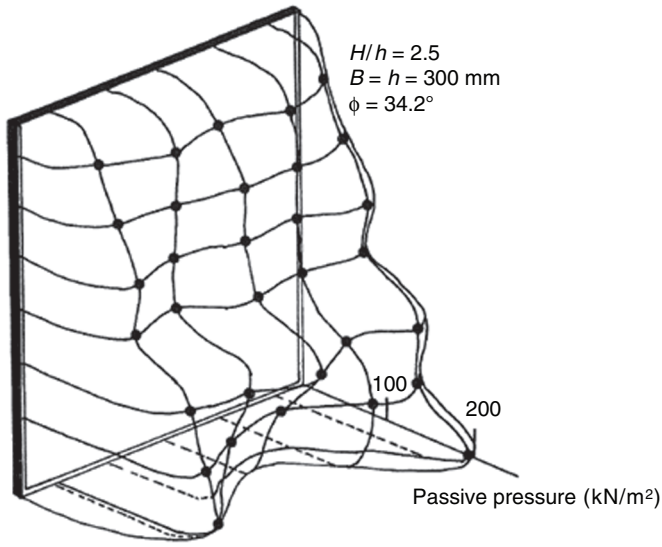

FIGURE 4.24 Nature of passive pressure distribution in front of a shallow vertical anchor as observed by Hueckel et al. (1965)

4.2.7 Deep Vertical Anchor

For a vertical anchor located at a shallow depth, the failure surface at ultimate load extends to the ground surface (Section 4.1). Under such condition, the breakout factor F_q introduced in Section 4.2.4 increases with embedment ratio H/h (Figure 4.25). However, at a given embedment ratio, $H/h = (H/h)_{\text{critical}}$,

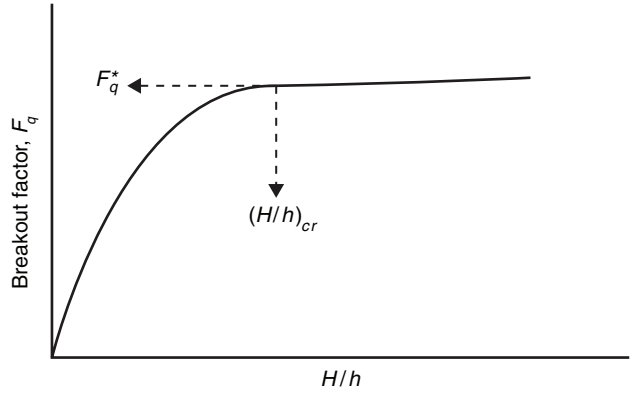

FIGURE 4.25 Nature of variation of F_q with H/h

the magnitude of F_q remains practically constant. The maximum value of F_q may be denoted by $F_q^\star$. The critical embedment ratio $(H/h)_{\text{critical}}$ and the maximum breakout factor $F_q^\star$ are functions of ϕ and B/h. Anchors located at $H/h < (H/h)_{\text{critical}}$ are called *deep anchors*, and for this condition, at ultimate load local shear failure in soil around the anchor takes place.

Ovesen (1964) derived a relationship for the breakout factor of rectangular anchors as:

$$F_q^\star = \frac{Q_u}{\gamma(Bh)H} = S_f K_0 e^{\pi \tan\phi} \tan^2\left(45^\circ + \frac{\phi}{2}\right) d_c \tag{4.34}$$

where

K_0 = earth pressure coefficient at rest (which may be taken as $1 - \sin\phi$)

$$d_c = 1.6 + 4.1\tan^4\phi \tag{4.35}$$

$$S_f = \text{shape factor} \approx 1 + 0.2\frac{h}{B} \tag{4.36}$$

Ovesen (1964), however, suggested that for deep anchors, the shape factor S_f may be assumed to be one for all anchors, irrespective of the B/h ratio. Figure 4.26 shows the plot of $F_q^\star$ obtained from Equation 4.34 assuming $S_f = 1$.

Meyerhof (1973) extended his theory on shallow anchors (Section 4.2.3) to the deep anchor condition and expressed the variation of $Q_u/\gamma(Bh)(H - h/2)$ as a function of the soil friction angle ϕ. However, for $H/h = 5$, the ratio of $Q_u/\gamma(Bh)(H - h/2)$ to $Q_u/\gamma(Bh)H$ is about 1.11 (Das et al., 1977). Thus, for all practical purposes:

$$F_q^\star = \frac{Q_u}{\gamma(Bh)\left(H - \frac{h}{2}\right)} \approx \frac{Q_u}{\gamma(Bh)H}$$

Based on this concept, Figure 4.27 shows the variation of Meyerhof's (1973) $F_q^\star$ (for square and strip anchors with the soil friction angle ϕ).

Biarez et al. (1965) analyzed the characteristic rotational mechanism for *deep strip anchors* $(H/h > 7)$ as shown in Figure 4.28 by considering the couple necessary for the rotation of a soil cylinder. According to this solution (also see Dickin and Leung, 1985):

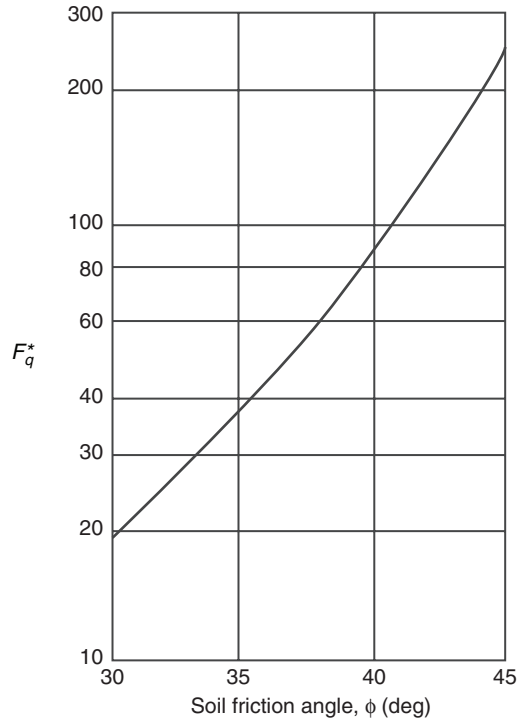

FIGURE 4.26 Variation of F_q^* with soil friction angle (Equation 4.34)

$$F_{q(\text{strip})}^{\star} = 4\pi \left(\frac{h}{H}\right)\left(\frac{H}{h} - 1\right)\tan\phi \tag{4.37}$$

It appears that a shape factor similar to the type given by Equation 4.36 may be added to Equation 4.37 to obtain the breakout factor for rectangular anchors, or:

$$F_{q(\text{rectangular})}^{\star} = 4\pi \left(\frac{h}{H}\right)\left(\frac{H}{h} - 1\right)\tan\phi \left(1 + 0.2\,\frac{h}{B}\right) \tag{4.38}$$

A comparison of the breakout factors shown in Figures 4.26 and 4.27 shows that for a given value of ϕ, $F_{q(\text{strip})\text{-Ovesen}}^{\star} > F_{q(\text{strip})\text{-Meyerhof}}^{\star}$. Das (1983) compiled the limited results of the $F_q^{\star}$ given by Das et al. (1977) and Akinmusuru (1978), and this correlation is shown in Figure 4.29. Note that these results are for

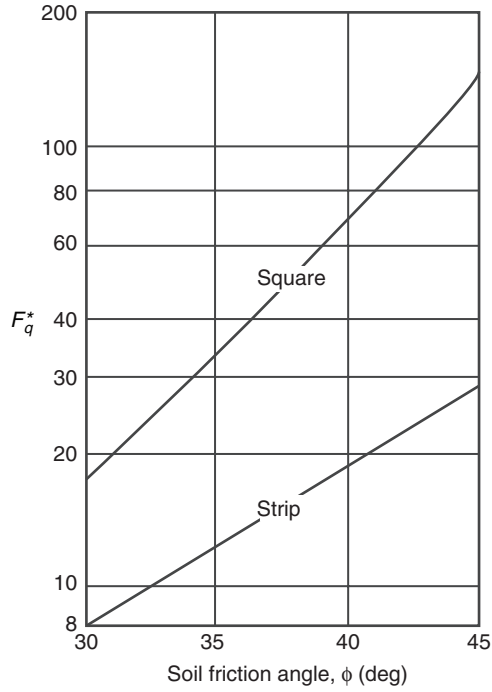

FIGURE 4.27 Meyerhof's values of F_q^* (1973)

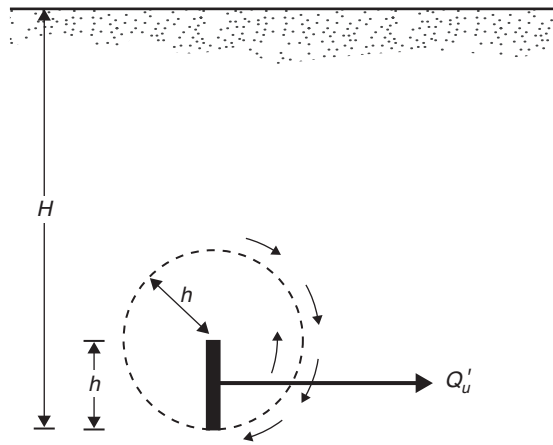

FIGURE 4.28 Failure mechanism around deep anchor as assumed by Biarez et al. (1965)

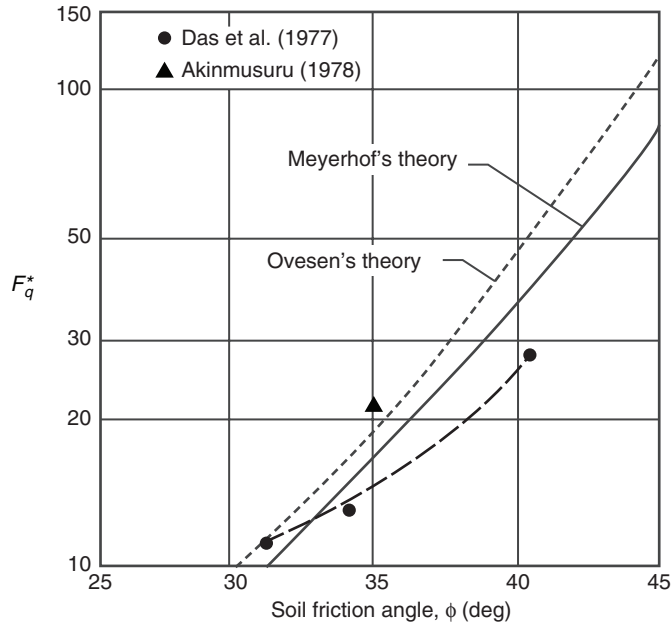

FIGURE 4.29 Comparison of Ovesen's (1964) and Meyerhof's (1973) theories with laboratory model test results for the variation of F_q^*

square anchors only ($B/h = 1$) and are based on small-scale laboratory model tests. These experimental results show that both of the theories predict a higher value of F_q^* than those obtained theoretically.

Das (1983) also gave a correlation for the critical embedment ratio of square anchors (based on model test results) in the form

$$\left(\frac{H}{h}\right)_{cr\text{-square}} = 5.5 + 0.166(\phi - 30^\circ) \qquad (\text{for } \phi = 30 \text{ to } 45^\circ) \qquad (4.39)$$

where ϕ is in degrees. Based on the experiences of the authors, it can be said that the critical embedment ratio of strip anchors is about 20 to 30% higher than that of square anchors under similar condition.

4.2.8 Load-Displacement Relationship

In many instances, design restrictions allow limited horizontal movement of the anchors. Neely et al. (1973) showed the typical nature of variation of the load versus horizontal displacement diagrams from their laboratory model tests (Figure

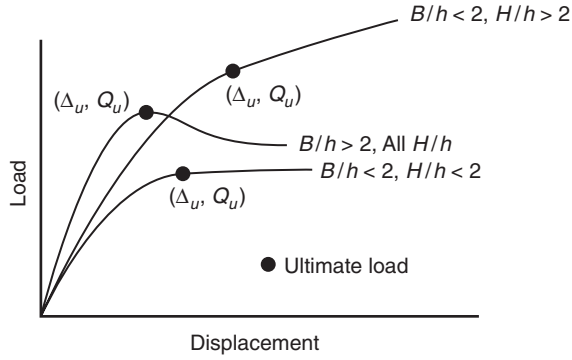

FIGURE 4.30 Typical nature of load versus displacement diagram for shallow anchors based on the observations of Neely et al. (1973)

4.30). According to their results, three types of load-displacement diagrams may be observed for vertical anchors in sand:

1. For anchors with $B/h < 2$ and $H/h < 2$, the load increases with displacement up to a maximum value (Q_u) and remains constant thereafter.
2. For anchors with $B/h < 2$ and $H/h > 2$, the load increases with displacement up to a maximum value (Q_u), after which the load-displacement diagram becomes practically linear.
3. For anchors with $B/h > 2$ at all values of H/h, the load increases with displacement to reach a peak value (Q_u) and decreases thereafter with displacement.

The displacement of the anchor corresponding to the Q_u load may be referred to as Δ_u. The magnitudes of Δ_u obtained from the laboratory tests of Neely et al. (1973) are shown in a nondimensional form in Figure 4.31.

Based on their model test results, Das and Seeley (1975) recommended that for $1 \leq B/h \leq 5$ and $1 \leq H/h \leq 5$, the load-displacement relationship can be expressed in the form

$$\frac{Q}{Q_u} = \frac{\dfrac{\Delta}{\Delta_u}}{0.15 + 0.85\left(\dfrac{\Delta}{\Delta_u}\right)} \tag{4.40}$$

where

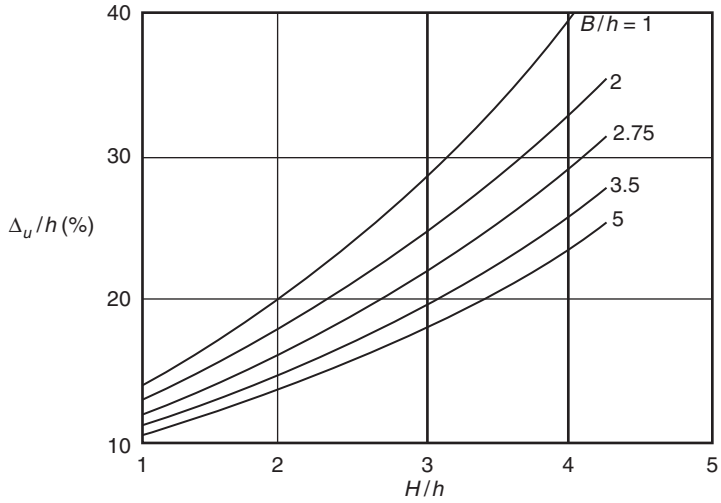

FIGURE 4.31 Nondimensional plot of Δ_u/h versus H/h for various values of B/h (adapted from Neely et al., 1973)

Δ = displacement at load Q

Figure 4.32 shows a plot of Q/Q_u versus Δ/Δ_u based on Equation 4.40. It is important to realize that in obtaining the preceding empirical relationship, some scattering of test results was observed and caution should be exercised in using the equation.

Example 4.5

Refer to Example 4.2.

a. Determine the anchor displacement at ultimate load Q_u.
b. Determine the allowable load Q for an anchor displacement of 1 in.

Solution

Part a. Referring to Figure 4.31, for $B/h = 2.5$ and $H/h = 2$, $\Delta_u/\Delta = 15\% = 0.15$. Hence:

$$\Delta_u \approx (0.15)(2 \times 12) = \mathbf{3.6\ in.}$$

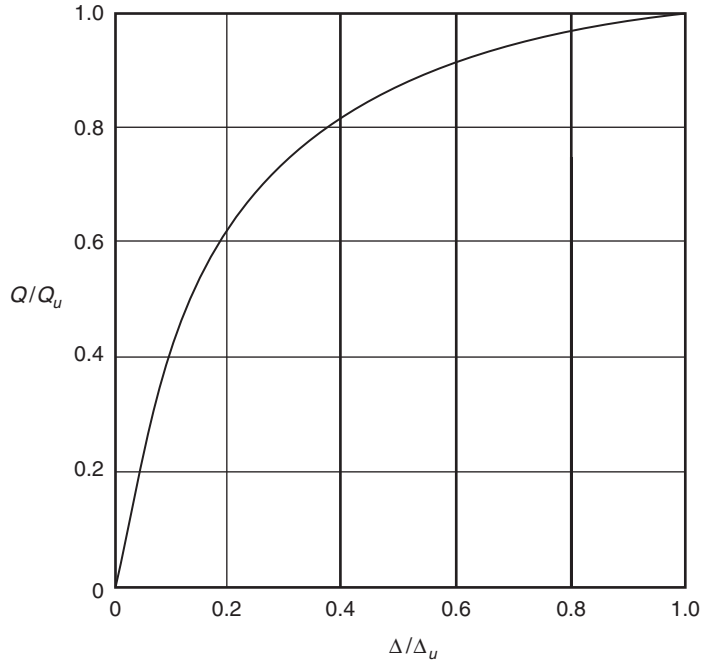

FIGURE 4.32 Plot of Q/Q_u versus Δ/Δ_u (Equation 4.40)

Part b. $\Delta = 1$ in. $\Delta/\Delta_u = 1/3.6 = 0.278$:

$$\frac{Q}{Q_u} = \frac{\dfrac{\Delta}{\Delta_u}}{0.15 + 0.85\left(\dfrac{\Delta}{\Delta_u}\right)} = \frac{0.278}{0.15 + (0.85)(0.278)} = 0.72$$

$$Q = (0.72)(Q_u) = (0.72)(16{,}338) \approx \mathbf{11{,}763\ lb}$$

4.2.9 Design Considerations

4.2.9.1 Angle of Friction

Prediction of the holding capacity of anchors for design requires careful consideration of the soil friction angle ϕ. Model test results generally overpredict

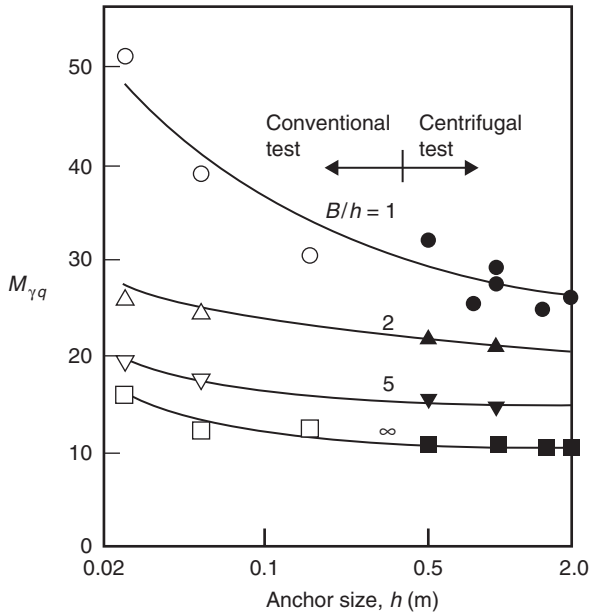

FIGURE 4.33 Variation of $M_{\gamma q}$ with anchor size ($H/h = 2$) (adapted from Dickin and Leung, 1983)

the holding capacity when compared to the prototype. This is due primarily to the *scale effect*. Dickin and Leung (1983) conducted centrifuge model tests on vertical anchor plates, the results of which are shown in Figures 4.33 and 4.34. It is obvious that as the anchor size (h) increases, the holding capacity decreases. This is true for all H/h and B/h ratios. The reason for this type of behavior is that in the case of prototypes, the failure in the soil mass is progressive, and the applicable value of ϕ is not the peak value (that is, ϕ_{peak}). Furthermore, model tests are conducted at low stress levels. In reality for soils, Mohr's failure envelope is actually curved, as shown in Figure 4.35. This means that the peak friction angle, $\phi = \phi_{peak}$, obtained at a lower stress level is higher than that obtained at a higher stress level. From Figure 4.35, note that since ($\sigma_2 > \sigma_1$):

$$\phi_{peak} = \phi_2 = \tan^{-1}\left(\frac{\tau_2}{\sigma_2}\right) < \phi_{peak} = \phi_1 = \tan^{-1}\left(\frac{\tau_1}{\sigma_1}\right)$$

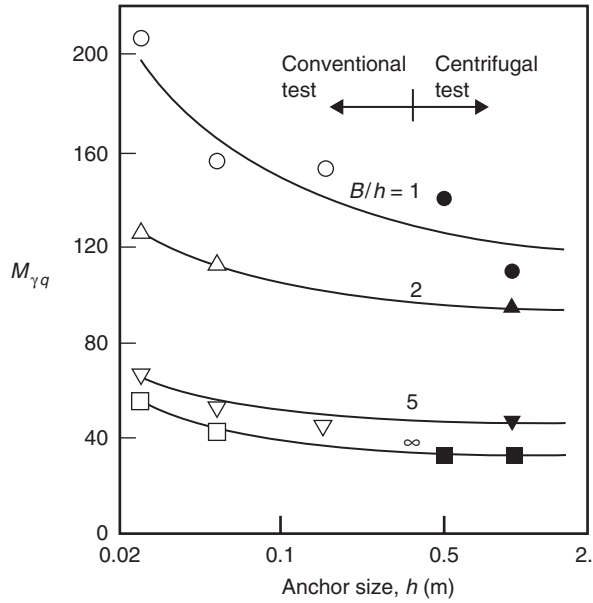

FIGURE 4.34 Variation of $M_{\gamma q}$ with anchor size ($H/h = 4$) (adapted from Dickin and Leung, 1983)

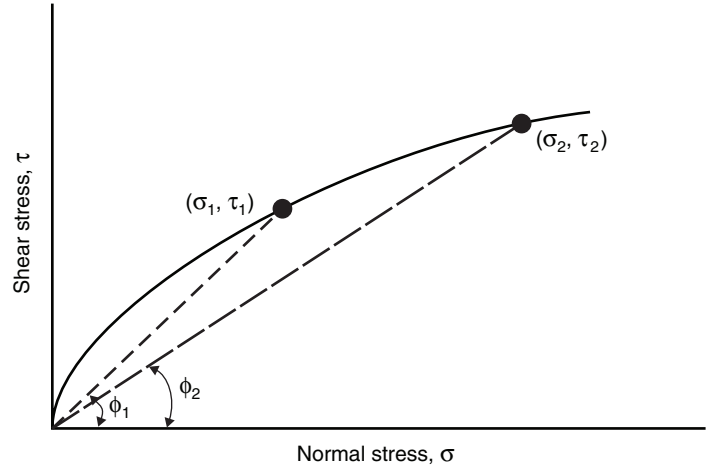

FIGURE 4.35 Curvilinear Mohr's failure envelope

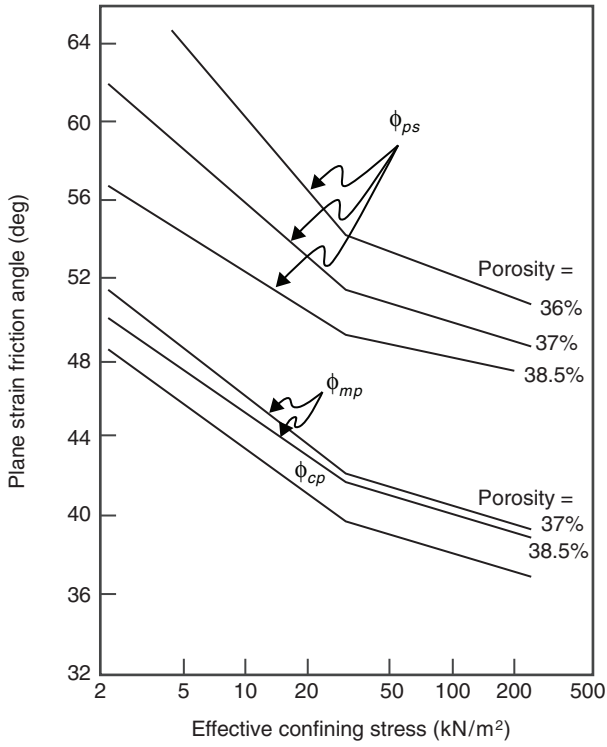

FIGURE 4.36 Variation of plane strain friction angle with effective confining pressure for Erith sand (adapted from Dickin and Leung, 1985)

Hence, for similar soil conditions, a lower peak value of ϕ may be expected in the case of a prototype when compared to that of a model. As an example, the variation of the plane strain peak friction angle for dense Erith sand (in which the test results shown in Figures 4.34 and 4.35 were conducted) with confining pressure is shown in Figure 4.36. Keeping the above considerations in mind, for continuous anchors Dickin and Leung (1985) suggested that the most appropriate friction angle to use for predicting the prototype anchor capacity is the mobilized plane strain friction angle, ϕ_{mp}, or:

$$\phi_{mp} = \phi_{ps}(1 - P_r) + P_r\phi_{cp}$$

where

ϕ_{ps} = plane strain peak friction angle
ϕ_{cp} = critical state friction angle
P_r = progressivity index ≈ 0.8 (Rowe, 1969)

Figure 4.36 also shows the variation of ϕ_{cp} and ϕ_{mp} for Erith sand (based on Equation 4.40).

Based on the study of Dickin and Leung (1985), the following general conclusions can be drawn:

1. For prototype strip anchors, all the theories (except for Biarez et al. [1965]) predict higher values of $M_{\gamma q}$ when the peak plane strain friction angle is used for calculation.
2. Neely et al.'s surcharge method (1973) (with $\delta = \phi/2$), Ovesen and Stromann's method (1972), and Meyerhof's method (1973) give fairly good agreement with the experimental results when $\phi = \phi_{mp}$ is used for calculation. However, the theory of Neely et al. (1973) (based on the equivalent free surface method with $m = 1$) highly overestimates the experimental results.

4.2.9.2 Shape Factor

In most cases of construction, the soil will be compacted after placement of the anchor. In such cases, according to Ovesen and Stromann (1972), for single anchors (Equation 4.17):

$$S_f = 0.42 \left(\frac{\frac{H}{h} + 1}{\frac{B}{h}} \right) + 1$$

Using the preceding equation, the variations of S_f with H/h and B/h for shallow anchors were calculated and are shown in Figure 4.37. For comparison purposes, the shape factors proposed by Neely et al. (1973) are also plotted in the figure. It appears that for a given H/h and B/h, the shape factor given by Ovesen and Stromann (1972) is higher than that given by Neely et al. (1973). This is primarily due to the fact that Neely et al. assumed that the behavior of anchors with $B/h = 5$ is essentially the same as that of a strip anchor.

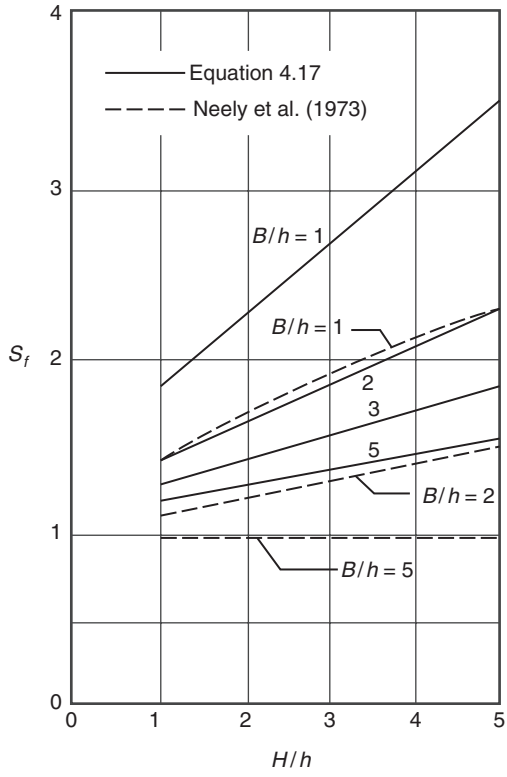

FIGURE 4.37 Comparison of shape factor relationships

4.2.9.3 General Recommendations

Although many factors that affect the ultimate holding capacity of anchors have yet to be evaluated and determined by further research, the following tentative design recommendations may be made based on the available information:

1. For routine works, plane strain tests on sand are rarely conducted in the laboratory to determine the friction angle. For that reason, it is recommended that the triaxial peak friction angle at a confining pressure of about 10 psi (100 kN/m^2) be determined. The $\phi_{\text{peak (triaxial)}}$ will be about 10% less than the magnitude of $\phi_{\text{peak (plane strain)}}$.
2. The peak friction angle determined from triaxial tests may be used to determine the ultimate holding capacity for single anchors by using Ovesen and Stromann's procedure (1972) (Equation 4.19). For strip anchors, from Equation 4.19 note that

$$Q_u' = \frac{1}{2}\gamma H^2 \left(K_{pH} - K_a \cos\phi\right) \left(\frac{C_{ov} + 1}{C_{ov} + \frac{H}{h}}\right)$$

or

$$F_q = \frac{Q_u'}{\gamma h H} = 0.5\left(\frac{H}{h}\right)\left(K_{pH} - K_a \cos\phi\right) \left(\frac{C_{ov} + 1}{C_{ov} + \frac{H}{h}}\right)$$

The maximum value of F_q should be equal to $F^*_{q(\text{strip})}$ given by Meyerhof (1973) and shown in Figure 4.27, or:

$$F^*_{q(\text{strip})} = 0.5\left(\frac{H}{h}\right)\left(K_{pH} - K_a \cos\phi\right) \left(\frac{C_{ov} + 1}{C_{ov} + \frac{H}{h}}\right)$$

$$\leq F^*_{q(\text{strip})\text{-Meyerhof}}$$

In a similar manner:

$$F_{q(\text{square})} = \frac{Q_u}{\gamma h^2 H}$$

$$= 0.5\left(\frac{H}{h}\right)\left(K_{pH} - K_a \cos\phi\right) \left(\frac{C_{ov} + 1}{C_{ov} + \frac{H}{h}}\right)$$

$$\times \left[F\left(\frac{H}{h} + 1\right) + 1\right]$$

$$\leq F^*_{q(\text{square})\text{-Meyerhof}}$$

For rectangular anchors, Meyerhof's values (1973) of F_q^* should be interpolated and used as the upper limit, or:

$$F_{q(\text{rectangular})} = \frac{Q_u}{\gamma h B H}$$

$$= 0.5\left(\frac{H}{h}\right)\left(K_{pH} - K_a \cos\phi\right)\left(\frac{C_{ov} + 1}{C_{ov} + \dfrac{H}{h}}\right)$$

$$\times \left[F\left(\frac{\dfrac{H}{h} + 1}{\dfrac{B}{h}}\right) + 1\right]$$

$$\leq F^*_{q(\text{rectangular})\text{-Meyerhof}}$$

The surcharge method with $\delta = \phi/2$ or the equivalent free surface method with $m = 0$ as provided by Neely et al. (1973) along with the recommended shape factors may also be used for obtaining the ultimate holding capacity of anchors for $H/h \leq 3$, or:

$$Q_u = \gamma B h^2 M_{\gamma q(\text{strip})} S_f$$

3. The ultimate holding capacity for single anchors determined from Step 2 needs to be reduced to account for scale effects. Neely et al. (1973) suggested that a 31% reduction of Q_u for a tenfold increase in size should be considered as a probable upper limit of the magnitude of the scale effects. Dickin and Leung (1985) suggested that the reduction due to scale effects could be larger still. It appears that a reduction of about 30% in Q_u in conjunction with the triaxial peak friction angle may be appropriate. Therefore:

$$Q_{u(\text{field})} \approx 0.3 Q_{u(\text{Step 2})}$$

4. For allowable load, a factor of safety (F_s) of about 2 may be used, or:

$$Q_{\text{all(field)}} \approx \frac{0.3 Q_{u(\text{Step 2})}}{2} = 0.15 Q_{u(\text{Step 2})}$$

According to Equation 4.40:

$$\frac{Q}{Q_u} = \frac{\dfrac{\Delta}{\Delta_u}}{0.15 + 0.85\left(\dfrac{\Delta}{\Delta_u}\right)}$$

With $Q/Q_u = 1/2$:

$$\frac{\Delta}{\Delta_u} = 0.075 + 0.425\left(\frac{\Delta}{\Delta_u}\right)$$

or

$$\frac{\Delta}{\Delta_u} = \frac{0.075}{0.575} = 0.13$$

or

$$\Delta = 0.13\Delta_u$$

A deflection of $\Delta = 0.13\Delta_u$ will roughly correspond to a value of $\Delta \leq 0.065h$ for square anchors and $\Delta \leq 0.03h$ for strip anchors.

5. When shallow anchors are used in groups, the procedure of Ovesen and Stromann (1972) outlined in Section 4.2.2 should be used to obtain Q_u by using the triaxial peak friction angle (Step 1). A reduction factor of about 30% for scale effects (Step 3) and a factor of safety of about 2 (Step 4) should be used to obtain Q_{all} in the field.

4.2.10 Effect of Anchor Inclination

Limited studies are available relating to the holding capacity of inclined plate anchors subjected to horizontal pull. Hueckel (1957) conducted laboratory tests using model anchor plates that have dimensions of 150 mm × 150 mm ($B/h = 1$). The average embedment depth H' (= depth of the anchor rod from the top of the sand layer) was $1.5h$. The pullout tests were conducted with anchor inclination $\theta = 0°$, $\pm 30°$, and $\pm 45°$. Figure 4.38 shows the positive and negative orientations of the anchor inclination with respect to the vertical. Figure 4.39a shows the nature of variation of $Q_{u(\theta)}/Q_{u(\theta=0°)}$ with θ. Das and Seeley (1975)

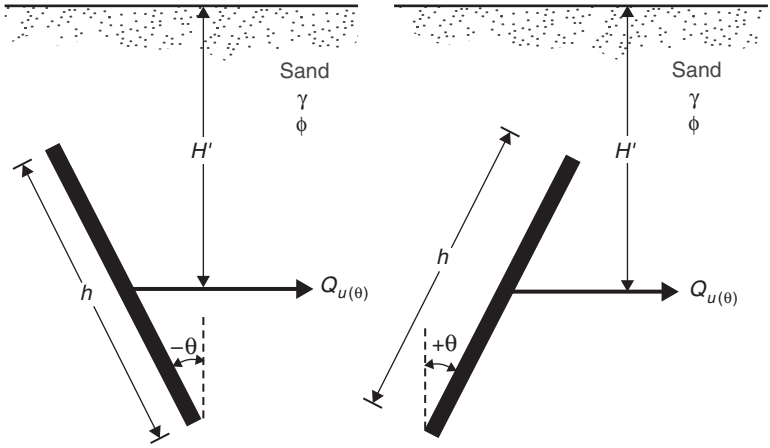

FIGURE 4.38 Positively and negatively oriented anchors

also conducted similar tests with model anchor plates measuring 51 mm × 51 mm ($B/h = 1$), 51 mm × 153 mm ($B/h = 3$), and 51 mm × 255 mm ($B/h = 5$) with $\theta = 0°$, $\pm 15°$, and $\pm 30°$, and $H'/h = 0.5$, 1.5, 2.5, and 3.5. The variations of $Q_{u(\theta)}/Q_{u(\theta=0°)}$ from these test are shown in Figures 4.39b, 4.39c, and 4.39d. Although theoretical developments to quantify these results are not yet available, the following general conclusions can be drawn (based on Figure 4.39):

1. For a given anchor plate H'/h and soil compaction, negatively inclined anchors offer more resistance to horizontal pull than positively inclined anchors.
2. For given values of θ and B/h, the ratio of $Q_{u(\theta)}/Q_{u(\theta=0°)}$ increases with the increase in H'/h.
3. For given values of θ and H'/h, the value of $Q_{u(\theta)}/Q_{u(\theta=0°)}$ increases with the decrease in the width-to-height ratio of the anchor plate.

4.3 ANCHORS IN CLAY (UNDRAINED COHESION, $\phi = 0$)

4.3.1 Ultimate Holding Capacity

Figure 4.40 shows the geometric parameters of a vertical plate anchor embedded in saturated clay. The undrained shear strength of the clay is c_u ($\phi = 0$ condition).

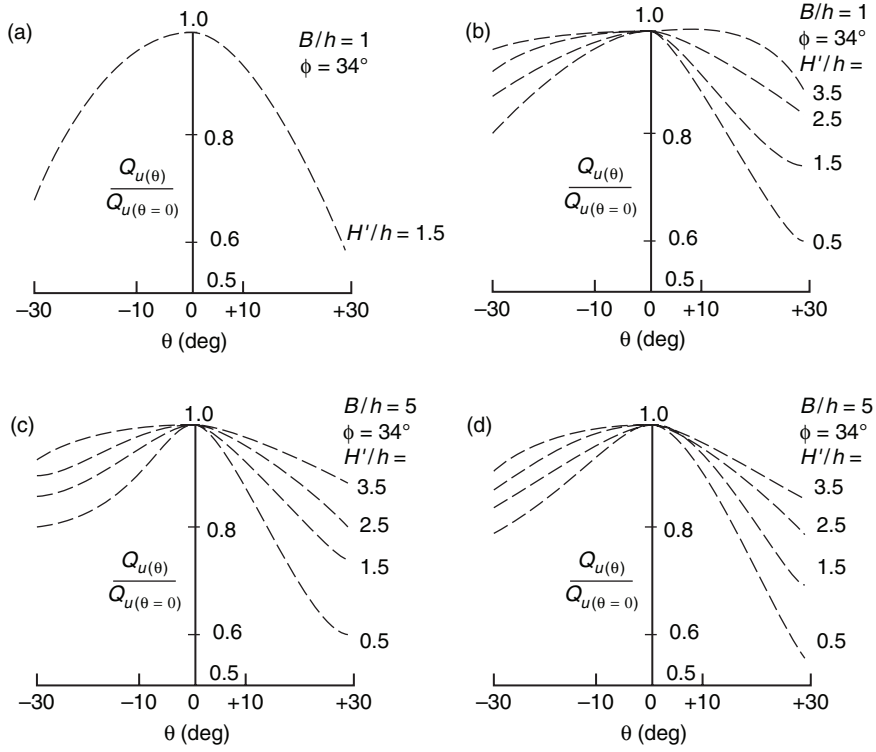

FIGURE 4.39 Nondimensionalized form of ultimate pullout resistance for inclined anchors (part a adapted from Hueckel, 1957; parts b, c, and d adapted from Das and Seeley, 1975)

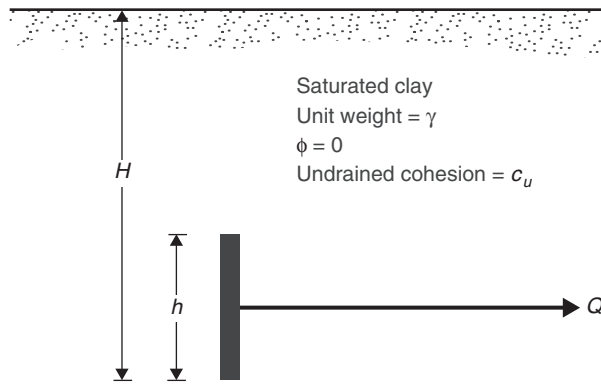

FIGURE 4.40 Geometric parameters of vertical anchor embedded in saturated clay

The height, width, and depth of embedment of the plate anchor are *h*, *B*, and *H*, respectively. If the ultimate holding capacity of the anchor plate is equal to Q_u, then:

$$Q'_u = \frac{Q_u}{B} \tag{4.41}$$

where

Q'_u = ultimate holding capacity per unit width at right angles to the cross section shown in Figure 4.40

The ultimate holding capacity for an anchor embedded in clay can be expressed in a nondimensional form (Tschebotarioff, 1973) as:

$$F_c = \frac{Q'_u}{c_u h} \tag{4.42}$$

where

F_c = breakout factor

Large-scale field test results to determine the ultimate holding capacity of plate anchors in undrained clay are scarce. Some of the initial laboratory model test results on this subject were reported by Mackenzie (1955). The tests were conducted on strip anchors (plane strain condition) in two different clayey soils. The average plot of these laboratory model test results is given in Figure 4.41. From this plot it can be seen that the breakout factor F_c increases with the embedment ratio (H/h) up to a maximum limit ($F_c = F_c^*$) and remains constant thereafter. Thus, as in the case of vertical anchors in sand, the failure mode in soil can be divided into two categories: (1) shallow anchor condition and (2) deep anchor condition. The dividing line between the two modes of failure is the critical embedment ratio, $(H/h)_{cr}$. For $H/h \leq (H/h)_{cr}$, the anchor behaves as a shallow anchor, and the failure surface in soil at ultimate load extends to the ground surface. These failure modes are shown in Figure 4.42. For Mackenzie's model tests (1955), the magnitudes of F_c^* and $(H/h)_{cr}$ were approximately 9 and 12, respectively.

Based on a limited number of laboratory model tests, Meyerhof (1973) proposed the following conservative estimate of the breakout factor and critical embedment ratio for square and strip anchors. For *square anchors*:

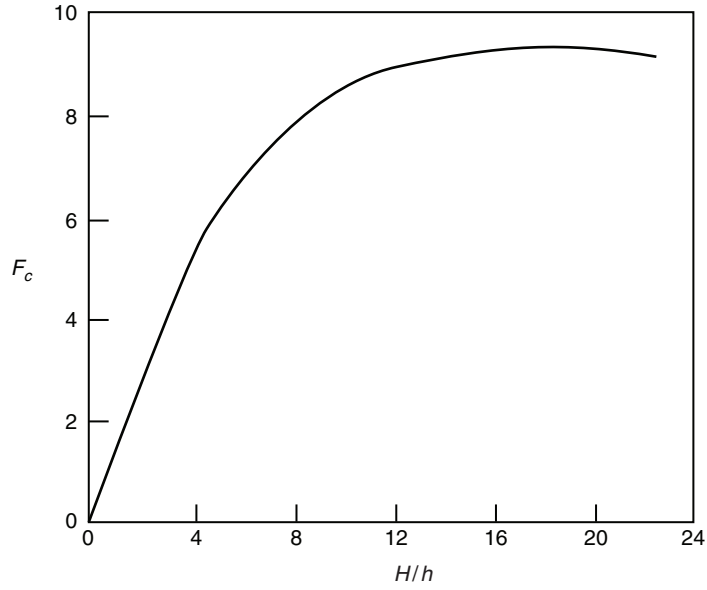

FIGURE 4.41 Average plot of F_c versus H/h for strip anchors in clay ($\phi = 0$) based on Mackenzie (1955) and Tschebotarioff (1973)

$$F_c = 1.2\left(\frac{H}{h}\right) \leq 9 \tag{4.43a}$$

$$\left(\frac{H}{h}\right)_{cr} = 7.5 \tag{4.43b}$$

and for *strip anchors*:

$$F_c = 1.0\left(\frac{H}{h}\right) \leq 8 \tag{4.44a}$$

$$\left(\frac{H}{h}\right)_{cr} = 8 \tag{4.44b}$$

The findings on the holding capacity of anchors discussed in the preceding paragraphs leave some unanswered questions:

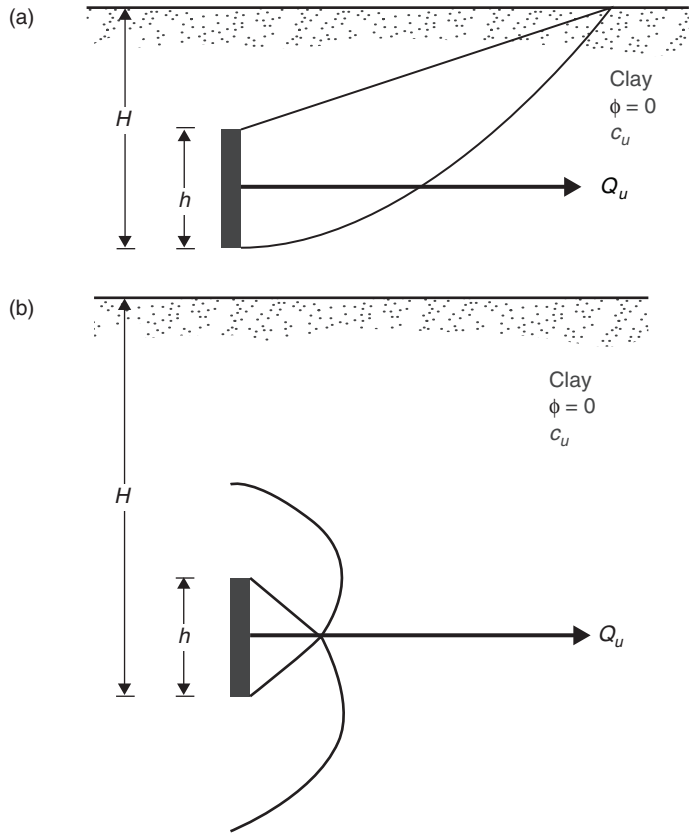

FIGURE 4.42 Failure modes: (a) shallow anchor and (b) deep anchor

1. What is the dependence of $(H/h)_{cr}$ on the undrained shear strength of clay and also the width-to-height ratio of the plate?
2. What is the nature of variation of F_c for rectangular anchors?

For that reason, Das et al. (1985) conducted a number of small-scale laboratory model tests, the results of which provide considerable insight into the problem. Figure 4.43 shows the variation of the breakout factor F_c for square anchors with the undrained shear strength of the clay. From this figure it can be seen that the critical embedment ratio in soft and medium clays increases with c_u up to a maximum limit and remains constant thereafter. This general behavior can be expressed as:

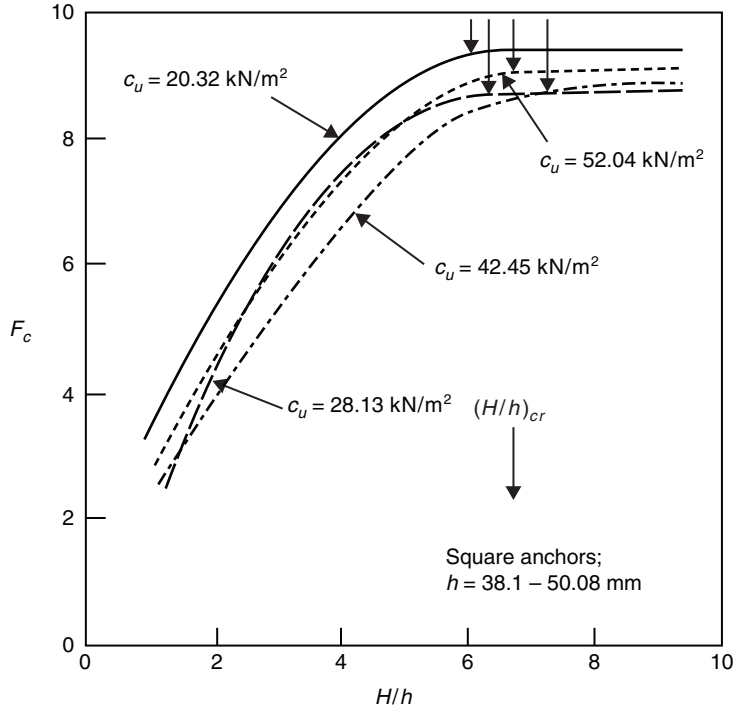

FIGURE 4.43 Model test results of Das et al. (1985) for variation of F_c versus H/h for square anchor

$$\left(\frac{H}{h}\right)_{cr\text{-}S} = 4.7 + 2.9 \times 10^{-3} c_u \leq 7 \tag{4.45}$$

where

$(H/h)_{cr\text{-}S}$ = critical embedment ratio of square anchors (that is, $h = B$)

c_u is in lb/ft^2. In SI units, the preceding expression can be stated as:

$$\left(\frac{H}{h}\right)_{cr\text{-}S} = 4.7 + 0.0606 c_u \leq 7 \tag{4.46}$$

where c_u is in kN/m^2.

The upper limit of $(H/h)_{cr\text{-}S}$ is generally consistent with the recommendations of Meyerhof (1973) as given by Equation 4.43. Based on limited model test results, Das et al. (1985) also showed that for similar undrained shear strength of clay, the critical embedment ratio of rectangular anchors and that of square anchors can be approximated as:

$$\frac{\left(\frac{H}{h}\right)_{cr\text{-}R}}{\left(\frac{H}{h}\right)_{cr\text{-}S}} = \left[0.9 + 0.1\left(\frac{B}{h}\right)\right] \leq 1.31 \tag{4.47}$$

From Equations 4.46 and 4.47 it is obvious that for strip anchors with $B/h = \infty$, $(H/h)_{cr\text{-strip}} = 1.31(H/h)_{cr\text{-}S}$. In medium stiff to stiff clays, $(H/h)_{cr\text{-}S}$ is about 7, so $(H/h)_{cr\text{-strip}} \approx 9.17$. This value of 9.17 falls between Meyerhof's (1973) recommended value of 8 (Equation 4.44) and the value of 12 obtained from Mackenzie's tests (1955).

Das et al. (1985) recommended that the breakout factor for deep rectangular anchors can be given by the relationship

$$F^{\star}_{c(R)} = F^{\star}_{c(S)}\left[0.825 + 0.175\left(\frac{h}{H}\right)\right] \tag{4.48}$$

where

$F^{\star}_{c(R)}$ = breakout factor for deep rectangular anchor
$F^{\star}_{c(S)}$ = breakout factor for deep square anchor = 9

For shallow square and rectangular anchors, the breakout factor can be expressed by two nondimensional parameters:

$$\beta = \frac{F_c}{F^{\star}_c} \tag{4.49}$$

and

$$\alpha = \frac{\left(\frac{H}{h}\right)}{\left(\frac{H}{h}\right)_{cr}} \tag{4.50}$$

The relationships between α and β can be expressed as (Das et al., 1985):

$$\beta = \frac{\alpha}{0.41 + 0.59\alpha} \tag{4.51}$$

or

$$F_c = \frac{F_c^{\star}\left(\frac{H}{h}\right)}{0.41\left(\frac{H}{h}\right)_{cr} + 0.59\left(\frac{H}{h}\right)} \tag{4.52}$$

4.3.2 Step-by-Step Procedure for Estimation of Ultimate Load

With limited experimental results available at the present time, the following step-by-step procedure may be used for estimation of the ultimate holding capacity of single rectangular anchors in clay ($\phi = 0$ condition):

1. Estimate the embedment ratio (H/h) and the width-to-height ratio (B/h).
2. Estimate the undrained shear strength of clay (c_u).
3. Using Equation 4.45 (or Equation 4.46 and c_u in Step 2), determine the critical embedment ratio of a square anchor.
4. With known values of B/h (Step 1) and Equation 4.47, obtain the ratio of $(H/h)_{cr\text{-}R}/(H/h)_{cr\text{-}S}$.
5. With known values of $(H/h)_{cr\text{-}S}$ from Step 3 and the ratio of $(H/h)_{cr\text{-}R}/(H/h)_{cr\text{-}S}$ from Step 4, calculate $(H/h)_{cr\text{-}R}$.
6. If the actual embedment ratio of H/h (Step 1) is equal to or greater than the $(H/h)_{cr\text{-}R}$ calculated in Step 5, it is a deep anchor condition. Hence:

$$F^{\star}_{c(R)} = 9\left[0.825 + 0.175\left(\frac{h}{H}\right)\right]$$

or

$$Q_u = 9c_uBh\left[0.825 + 0.175\left(\frac{h}{H}\right)\right]$$

7. If the actual H/h is less than the critical embedment ratio calculated in Step 5, it is a shallow anchor. Equation 4.52 can be used to estimate Q_u, or:

$$Q_u = c_uBh\left[\frac{F^{\star}_{c(R)}\left(\frac{H}{h}\right)}{0.41\left(\frac{H}{h}\right)_{cr\text{-}R} + 0.59\left(\frac{H}{h}\right)}\right]$$

where

$$F^{\star}_{c(R)} = 9\left[0.825 + 0.175\left(\frac{h}{H}\right)\right]$$

Example 4.6

Estimate the ultimate breakout load of a rectangular anchor plate with the following parameters: $H = 1.2$ m, $h = 0.3$ m, $B = 0.6$ m, and $c_u = 48$ kN/m^2.

Solution

$$\frac{H}{h} = \frac{1.2\text{ m}}{0.3\text{ m}} = 4$$

$$\frac{B}{h} = \frac{0.6\text{ m}}{0.3\text{ m}} = 2$$

From Equation 4.46:

$$\left(\frac{H}{h}\right)_{cr\text{-}S} = 4.7 + 0.0606c_u = 4.7 + 0.0606\,(48) = 7.609 > 7$$

Therefore, use:

$$\left(\frac{H}{h}\right)_{cr\text{-}S} = 7$$

From Equation 4.47:

$$\frac{\left(\frac{H}{h}\right)_{cr\text{-}R}}{\left(\frac{H}{h}\right)_{cr\text{-}S}} = \left[0.9 + 0.1\left(\frac{B}{h}\right)\right] = 0.9 + (0.1)\,(2) = 1.1$$

Hence:

$$\left(\frac{H}{h}\right)_{cr\text{-}R} = (1.1)\,(7) = 7.7$$

The actual H/h is 2, so this is a shallow anchor.

$$Q_u = c_u B h \left[\frac{F^{\star}_{c(R)}\left(\frac{H}{h}\right)}{0.41\left(\frac{H}{h}\right)_{cr\text{-}R} + 0.59\left(\frac{H}{h}\right)}\right]$$

$$F^{\star}_{c(R)} = 9\left[0.825 + 0.175\left(\frac{h}{H}\right)\right] = 9\left[0.825 + 0.175\left(\frac{0.3}{0.6}\right)\right] = 8.21$$

Thus:

$$Q_u = [(48)(0.6)(0.3)]\left[\frac{(8.21)\,(4)}{(0.41)\,(7.7) + (0.59)\,(4)}\right] = \mathbf{51.43\ kN}$$

4.3.3 Limitations of the Existing Study

There are certain limitations and uncertainties in applying the existing results in the literature to the estimation of the allowable holding capacity of a plate anchor embedded in a clay (under undrained conditions):

1. Since most of the relationships cited in Section 4.3.2 are based on small-scale model test results, the scale effect has not yet been investigated. However, such effects in clay soils are expected to be minimal.
2. All the model test results thus far reported are based on tests on single anchors. However, vertical plate anchors may be, and are, used in groups. Figure 4.11 shows the plan view of a group of vertical anchor plates subjected to horizontal pull. The failure surfaces in soil around the anchor at ultimate load may overlap each other. In effect, this will reduce the magnitude of Q_u. Thus:

$$Q_{u(\text{actual})} = \eta Q_{u(\text{isolated})} \tag{4.53}$$

where

$$\eta = \text{efficiency factor} = f\left(\frac{S}{B}, \frac{H}{h}\right)$$

The efficiency factor η in Equation 4.53 has not as yet been investigated. For that reason, a conservative estimate of $F_{c(R)}$ would be to assume $h/B = 0$ (strip case), and thus, from Equation 4.48:

$$F^{\star}_{c(R)} \approx 7.43$$

3. A factor of safety of at least 3 should be used to determine the allowable holding capacity.

4.4 OTHER STUDIES

Rowe and Davis (1982) examined the undrained behavior of vertical anchor plates resting in homogeneous, isotropic saturated clay using a finite element study. Theoretical consideration was given to the effect of anchor embedment and layer depth, overburden pressure, and breakaway condition, as well as anchor roughness, thickness, and shape. Their work shows that the anchor roughness increases the capacity of shallow vertical anchor plates. The anchor thick-

ness does not alter the capacity of deep rough anchors for practical ranges of thickness. However, it is reported that the capacity of deep, perfectly smooth anchors decreases with increasing thickness.

Ghaly (1997) incorporated the data reported in 128 published field and laboratory investigations in a generalized form to predict the ultimate horizontal pullout resistance of vertical anchor plates embedded in different types of sands in terms of the influencing parameters. Using the data reported by Das and Seeley (1975), the following relationship was established:

$$\left(\frac{Q}{Q_u}\right) = 2.2\left(\frac{u}{H}\right)^{0.3} \tag{4.54}$$

where

Q = pullout force
Q_u = ultimate pullout resistance
u = horizontal displacement
H = depth of embedment

Equation 4.54 can be used to calculate the horizontal displacement of the vertical anchor plate for a given load level. Also, the displacement at failure can be calculated by substituting $Q/Q_u = 1.0$. Furthermore, for a constrained displacement, the corresponding load level can be determined.

Merifield et al. (2001) carried out numerical limit analysis, based on finite element formulations, of vertical plate anchors in undrained clay. In their study, anchor roughness was found to increase the ultimate capacity of vertical anchors with embedment ratios less than 2 by as much as 22%. The ultimate anchor capacity increases linearly with overburden pressure up to a limiting value that reflects the transition from shallow to deep anchor behavior.

4.5 SUMMARY OF MAIN POINTS

1. Vertical anchor plates are commonly used to resist horizontal loading in the construction of sheet pile walls, at pressure pipeline bends, and at the base of retaining walls to resist sliding.
2. If the embedment of the anchor is relatively small, at ultimate pullout load on the anchor, the passive failure surface developed in soil in front of the

anchor will intersect the ground surface. At greater embedment ratios, the local shear failure in soil will take place at ultimate load.
3. For vertical anchors, the gross ultimate holding capacity is equal to the net ultimate holding capacity.
4. Model test results in sand generally overpredict the holding capacity when compared to the prototype. This is due primarily to the scale effect.
5. The critical embedment ratio in soft and medium clays increases with undrained shear strength up to a maximum limit and remains constant thereafter.
6. A step-by-step procedure for estimation of ultimate load of a single vertical rectangular plate anchor in undrained clay is explained in Section 4.3.2.
7. As the depth of the vertical plate anchor increases, the displacement measured at failure increases.
8. The anchor roughness increases the capacity of shallow vertical anchor plates in undrained clay. The anchor thickness does not alter the capacity of deep rough anchors for practical ranges of thickness. However, the capacity of deep, perfectly smooth anchors decreases with increasing thickness.
9. Most relationships presented are based on small-scale model test results, and the scale effect has not yet been investigated. However, such effects in clay soils are expected to be minimal.

SELF-ASSESSMENT QUESTIONS

Select the most appropriate answer to each multiple-choice question

4.1. Vertical plate anchors are used to resist horizontal loading:
   a. in the construction of sheet pile walls
   b. at pressure pipeline bends
   c. at the base of retaining walls to resist sliding
   d. all of the above

4.2. The holding capacity of an anchor is primarily derived from:
   a. passive force imposed by the soil in front of the anchor plate
   b. active force imposed by the soil in front of the anchor plate
   c. earth pressure imposed by the soil in front of the anchor plate
   d. tie-rod connected to the anchor plate

4.3. The ultimate holding capacity of a vertical anchor does not depend on:
   a. embedment ratio and width-to-height ratio
   b. shear strength parameters of soil and angle of friction at the anchor-soil interface

c. both b and c
d. none of the above

4.4. The dividing line between the shallow and deep modes of failure is the:
a. critical embedment ratio
b. width of the anchor and height of the anchor plate
c. depth of the anchor plate
d. soil type

4.5. The capacity of shallow vertical anchor plates in undrained clay:
a. remains unaffected with change in anchor plate roughness
b. decreases with increase in anchor plate roughness
c. increases with increase in anchor plate roughness
d. may increase or decrease depending on clay plasticity

4.6. If H is the depth of embedment, then the displacement of a vertical anchor plate at failure is approximately:
a. $0.072H$
b. $0.45H$
c. $0.72H$
d. H

4.7. The minimum factor of safety used to determine the allowable holding capacity of vertical plate anchors is:
a. 1
b. 2
c. 3
d. 5

4.8. The breakout factor for deep square anchors is:
a. 1
b. 3
c. 5
d. 9

4.9. With increase in center-to-center spacing of anchors in their group, the ultimate group capacity of vertical anchors:
a. increases linearly
b. increases nonlinearly
c. decreases nonlinearly
d. decreases linearly

4.10. The pullout capacity in Meyerhof's analysis (1973) of vertical plate anchors in sand is a function of:
a. soil friction angle
b. soil unit weight

c. geometrical dimensions of the plate anchor
d. all of the above

Answers

4.1: d 4.2: a 4.3: c 4.4: a 4.5: c 4.6: a 4.7: c 4.8: d 4.9: b 4.10: a

REFERENCES

Akinmusuru, J.O. (1978). Horizontally loaded vertical plate anchors in sand. *J. Geotech. Eng. Div. ASCE,* 104(2):283–286.

Biarez, I., Boucraut, L.M., and Negre, R. (1965). Limiting equilibrium of vertical barriers subjected to translation and rotation forces. *Proc. VI Int. Conf. Soil Mech. Found. Eng.,* Montreal, 368–372.

Caquot, A. and Kerisel, L. (1949). *Traite de Macanique des Sols,* Gauthier-Villars, Paris.

Das, B.M. (1975). Pullout resistance of vertical anchors. *J. Geotech. Eng.,* 101(1):87–91.

Das, B.M. (1983). Holding capacity of vertical anchor slabs in granular soil. *Proc. Coastal Structures '83,* ASCE, 379–392.

Das, B.M. and Seeley, G.R. (1975). Load-displacement relationship for vertical anchor plates. *J. Geotech. Eng. Div. ASCE,* 101(7):711–715.

Das, B.M., Seeley, G.R., and Das, S.C. (1977). Ultimate resistance of deep vertical anchor in sand. *Soils Found.,* 17(2):52–56.

Das, B.M., Tarquin, A.J., and Moreno, R. (1985). Model tests for pullout resistance of vertical anchors in clay. *Civ. Eng. Pract. Design Eng.,* 4(2):191–209.

Dickin, E. and Leung, C.F. (1983). Centrifugal model tests on vertical anchor plates. *J. Geotech. Eng.,* 109(12):1503–1525.

Dickin, E. and Leung, C.F. (1985). Evaluation of design methods for vertical anchor plates. *J. Geotech. Eng.,* 111(4):500–520.

Ghaly, A.M. (1997). Load-displacement prediction for horizontally loaded vertical plates. *J. Geotech. Geoenviron. Eng.,* 123(1):74–76.

Hanna, A.M., Das, B.M., and Foriero, A. (1988). *Behavior of Shallow Inclined Plate Anchors in Sand,* Geotech. Spec. Tech. Publ. No. 16, ASCE, 54–72.

Hueckel, S. (1957). Model tests on anchoring capacity of vertical and inclined plates. *Proc. IV Int. Conf. Soil Mech. Found. Eng.,* London, 2, 203–206.

Hueckel, S., Kwasniewski, J., and Baran, L. (1965). Distribution of passive earth pressure on the surface of a square vertical plate embedded in soil. *Proc. VI Int. Conf. Soil Mech. Found. Eng.,* Montreal, 2, 381–385.

Kostyukov, V.D. (1967). Distribution of the density of sand in the sliding wedge in front of anchor plates. *Soil Mech. Found. Eng.* (in Russian), 1:12–13.

Mackenzie, T.R. (1955). Strength of Deadman Anchors in Clay, M.S. thesis, Princeton University, Princeton, NJ.

Merifield, R.S., Sloan, S.W., and Yu, H.S. (2001). Stability of plate anchors in undrained clay. *Geotechnique,* 51(2):141–153.

Meyerhof, G.G. (1951). The ultimate bearing capacity of foundations. *Geotechnique,* 2(4):301–332.

Meyerhof, G.G. (1973). Uplift resistance of inclined anchors and piles. *Proc. VIII Int. Conf. Soil Mech. Found. Eng.,* Moscow, 2(1), 167–172.

Neely, W.J., Stuart, J.G., and Graham, J. (1973). Failure loads of vertical anchor plates in sand. *J. Soil Mech. Found. Div. ASCE,* 99(9):669–685.

Ovesen, N.K. (1964). *Anchor Slabs, Calculation Methods and Model Tests,* Bull. 16, Danish Geotechnical Institute, Copenhagen.

Ovesen, N.K. and Stromann, H. (1972). Design methods for vertical anchor slabs in sand. *Proc. Specialty Conf. Performance of Earth and Earth-Supported Structures,* ASCE, 2(1), 1481–1500.

Rowe, P.W. (1952). Anchored sheet pile walls. *Proc. Inst. Civ. Eng. London,* 1(1): 27–70.

Rowe, P.W. (1969). The relationship between the shear strength of sands in triaxial compression, plane strain and direct shear. *Geotechnique,* 19(1):75–86.

Rowe, R.K. and Davis, E.H. (1982). The behaviour of anchor plates in clay. *Geotechnique,* 31(1):9–23.

Sokolovskii, V.V. (1965). *Statics of Granular Media,* Pergamon Press, New York.

Teng, W.C. (1962). *Foundation Design,* Prentice-Hall, Englewood Cliffs, NJ.

Tschebotarioff, G.P. (1973). *Foundations, Retaining Structures and Earth Structures,* McGraw-Hill, New York.

5

INCLINED PLATE ANCHORS

This chapter is devoted primarily to a review and compilation of existing theoretical and experimental results relating to the ultimate holding capacity of inclined plate anchors subjected to axial pull. The discussion is divided into two major parts: behavior of anchors in sand and behavior of anchors in clay (undrained condition).

5.1 INTRODUCTION

As pointed out in Chapter 1, in the construction of various types of foundations, plate anchors are sometimes placed at an inclination to the horizontal. These anchors may be subjected to inclined or axial pull, as shown in Figures 5.1a and 5.1b. However, in many cases, foundations most likely to be subjected to uplifting forces are constructed with horizontal and/or inclined anchors with the assumption that the pullout force will be transmitted axially to the anchors. For an inclined anchor subjected to axial pull, the gross ultimate holding capacity can be expressed as (Figure 5.1b):

$$Q_{u(g)} = Q_u + W_a \cos \psi$$

where

$Q_{u(g)}$ = gross ultimate holding capacity
Q_u = net ultimate holding capacity
W_a = self-weight of the anchor

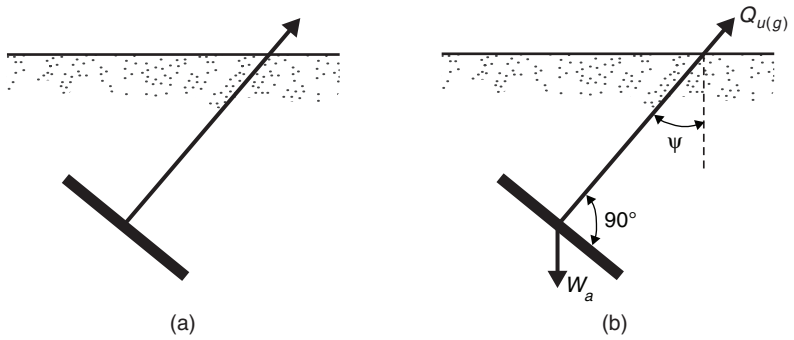

FIGURE 5.1 Inclined plate anchor subjected to (a) inclined pull and (b) axial pull

5.2 INCLINED PLATE ANCHORS IN SAND

5.2.1 Inclined Anchors: Axisymmetric Case (Analysis of Harvey and Burley)

Harvey and Burley (1973) made an analysis of the holding capacity of shallow inclined circular anchor plates, the details of which are presented in this section. Figure 5.2 shows a vertical section through the assumed failure zone corresponding to the major axis of the ground surface failure ellipse. The diameter of the circular anchor is equal to h. The anchor is inclined at an angle ψ with respect to the horizontal, and the average depth of embedment is equal to H'. AC and BD are assumed failure surfaces, which are arcs of circles. The arcs AC and BD make an angle of 90° at A and B and intersect the ground surface at an angle of $45° - \phi/2$ (Rankine's passive state assumption). This assumption is similar to that of Balla's (1961) for horizontal anchors presented in Chapter 2. The assumption of the failure surface in soil can be further simplified by replacing the curvilinear surface by a single curved surface defined by the angle θ. Hence the trace of the simplified failure surface in Figure 5.2 can be given by the straight lines AC and BD.

In the analysis presented below, the following notations are used:

ξ = horizontal angle locating a typical sector of the failure zone measured from the major axis of the surface failure ellipse
ω = angle of inclination of a typical sector of the failure zone relative to the vertical axis

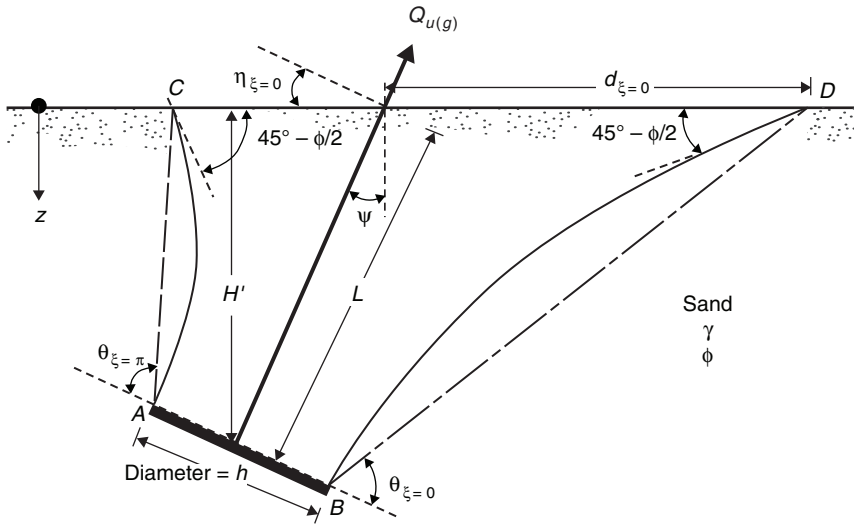

FIGURE 5.2 Inclined shallow circular plate anchor

η = angle of inclination of the pullout axis to the plane perpendicular to the failure zone axis

α = angle between the curvilinear surface of sliding and the horizontal surface in the plane failure sector

Now, considering a typical sector of the failure zone located at an angle ξ from the vertical section:

$$\tan \omega = \tan \psi \sin \xi \tag{5.1}$$

$$\sin \eta = \sin \psi \cos \xi \tag{5.2}$$

$$\tan \alpha = \tan\left(45° - \frac{\phi}{2}\right) \sqrt{(1 + \tan^2 \psi \sin^2 \xi)} \tag{5.3}$$

and

$$\theta = \frac{\pi}{4} + \frac{\alpha}{2} + \frac{\eta}{2} \tag{5.4}$$

The volume of a typical sector of the failure zone subtending at angle $d\xi$ can be given as:

$$\delta V = \left[\frac{d^2}{6} \left(L + \frac{h}{2} \tan\theta \right) \cos\eta - \frac{h^3}{48} \tan\theta \sin\eta \right] \delta\xi \qquad (5.5)$$

where

$$d = \frac{L + \frac{h}{2} \tan\theta}{\cos\eta \tan\theta - \sin\eta} \qquad (5.6)$$

Similarly, the area of the simplified curved surface of a sector of the failure zone is

$$\delta A = \frac{1}{2} \left(d + \frac{h}{2} \sec\eta \right) \left(\frac{d \cos\eta - \frac{h}{2}}{\cos\theta} \right) d\xi \qquad (5.7)$$

Similarly, the area of the sector of the anchor plate is

$$\delta A_a = \frac{1}{8} h^2 \delta\xi \qquad (5.8)$$

The lateral at-rest earth pressure at depth z is

$$p_z = K_0 \gamma z \qquad (5.9)$$

where

K_0 = coefficient of at-rest earth pressure ($\approx 1 - \sin\phi$)
γ = unit weight of soil

Thus, the circumferential force on the sector due to earth pressure forces is equal to:

$$\left[\frac{K_0\gamma d}{\left(L + \frac{h}{2}\tan\theta\right)}\right] \times \int_{z=0}^{z=L\cos\psi} \left(z\frac{h}{2}\tan\theta + zL - \frac{z^2}{\cos\psi}\right) dz$$

From the preceding relationship, the radial force on the section can be determined as:

$$\left[\frac{K_0\gamma d L^2\cos^2\psi}{2\left(L + \frac{h}{2}\tan\theta\right)}\right]\left[\left(\frac{h}{2}\tan\theta\right) + \frac{L}{3}\right] d\xi$$

Now, the radial force that includes the effect of the weight component is

$$\begin{aligned} F_R = & \left[\frac{K_0\gamma d L^2\cos^2\psi}{2\left(L + \frac{h}{2}\tan\theta\right)}\right]\left[\left(\frac{h}{2}\right)\tan\theta + \frac{L}{3}\right] \\ & + \frac{1}{2}(\gamma)(\delta V)\sin\omega\cos\omega \\ & + \frac{1}{8}\gamma d\sin^2\omega\cos\omega\cos^2\psi\left[L + \left(\frac{h}{2}\right)\tan\theta\right]^2 \\ & - \frac{1}{8}\left[\frac{\gamma h^2 d\sin^2\omega\cos\omega\cos^2\psi\tan^2\theta}{\left(L + \frac{h}{8}\tan\theta\right)}\right]\left[\left(\frac{h}{2}\right)\tan\theta + L\right] \end{aligned} \tag{5.10}$$

If the anchor plate reaction on the adjacent soil is Q acting at an angle ϕ, then:

$$Q \sin \theta = \gamma(\delta V) \cos \omega \sin(\phi + \theta - \eta) - F_R \cos(\theta + \phi - \eta)$$

The net ultimate holding capacity can now be given as:

$$Q_u = \sum_{\xi=0}^{\xi=2\pi} Q \cos \phi \tag{5.11}$$

Equation 5.11 can be solved by using a computer program. The size of each sector can be defined by assigning a certain value to ξ. Note that L is equal to $H/\cos \psi$.

Harvey and Burley (1973) compared the analysis proposed above with the experimental results of Kanayan (1966) as well as those of Baker and Kondner (1966). However, this procedure for determining the ultimate holding capacity of circular inclined anchor plates is rarely used in practice now.

5.2.2 Meyerhof's Procedure

Figure 5.3 shows an inclined shallow strip anchor with a height h embedded in a c-ϕ soil. The bottom of the anchor plate is at a depth H measured from the ground surface. The average depth of embedment of the anchor is H'. The anchor is inclined at an angle ψ with respect to the horizontal and is subjected to an axial pullout force. For the shallow anchor condition, the net ultimate holding capacity per unit width Q_u' at right angles to the cross section shown is (Meyerhof, 1973)

$$Q_u' = P_p - P_a = cK_cH + \frac{1}{2} K_b \gamma H^2 + W \cos \psi \tag{5.12}$$

where

c = cohesion
γ = unit weight of soil
K_c, K_b = net earth pressure coefficients
W = weight of soil located directly above the anchor = $\gamma hH \cos \psi$

Thus:

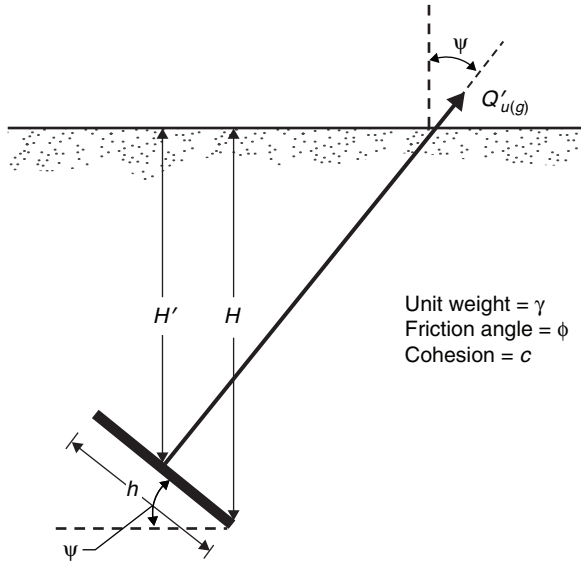

FIGURE 5.3 Inclined shallow strip anchor plate

$$Q'_u = cK_cH + \frac{1}{2}K_b\gamma H^2 + \gamma hH\cos^2\psi \tag{5.13}$$

For granular soils, $c = 0$, so:

$$Q'_u = \frac{1}{2}K_b\gamma H^2 + \gamma hH\cos^2\psi \tag{5.14}$$

The variations of K_b for shallow strip anchors can be obtained from the earth pressure coefficients for an inclined wall (Caquot and Kerisel, 1949; Sokolovskii, 1965). These values are shown in Figure 5.4 for $\psi = 20°$, 45°, 75°, and 90°. Note that the variation of K_b for $\psi = 90°$ given in Figure 5.4 is the same as shown in Figure 4.15.

Equation 5.14 can be rewritten in the form

$$Q'_u = \frac{1}{2}K_b\gamma\left(H' + \frac{h\sin\psi}{2}\right)^2 + \gamma h\left(H' + \frac{h\sin\psi}{2}\right)\cos^2\psi \tag{5.15}$$

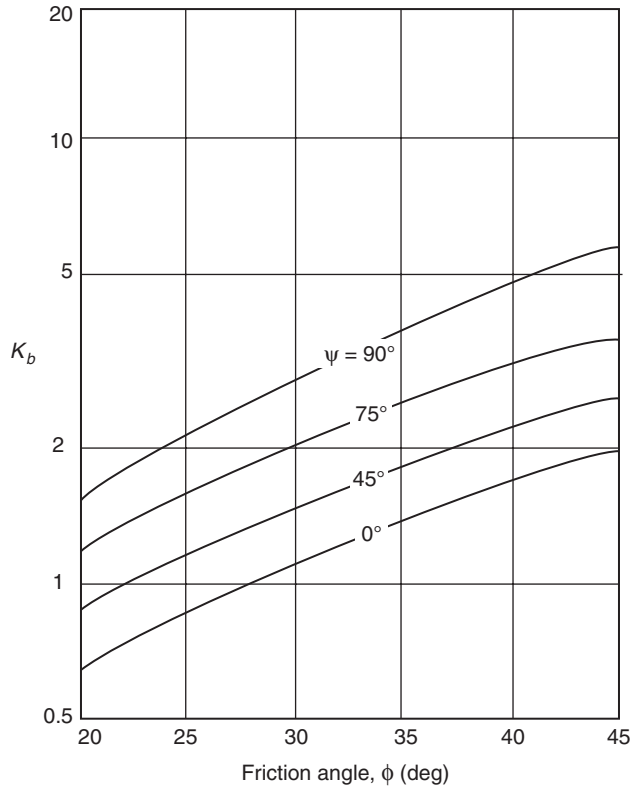

FIGURE 5.4 Variation of Meyerhof's (1973) earth pressure coefficient K_b

The average breakout factor is

$$F_q' = \frac{Q_u'}{\gamma h H'} = \frac{1}{2} K_b \left(\frac{H'}{h} \right) \left(1 + \frac{h}{2H'} \sin \psi \right)^2 + \left(1 + \frac{h}{2H'} \sin \psi \right) \cos^2 \psi \tag{5.16}$$

Note that with $\psi = 0$, $H = H'$. Hence:

$$F_q' = F_q \qquad \text{(see Chapter 2)} \tag{5.17}$$

Again, with $\psi = 90°$, $H' = H - h/2$. Therefore:

$$F_q' = \frac{Q_u'}{\gamma h\left(H - \frac{h}{2}\right)} = \frac{Q_u'}{\gamma hH\left(1 - \frac{h}{2H}\right)} = \frac{F_q}{1 - \frac{h}{2H}} \tag{5.18}$$

where

F_q = breakout factor as defined in Chapter 4

For $H/h \geq 5$:

$$\frac{F_q'}{F_q} \leq 1.1$$

Hence, for shallow anchors, the average breakout factor can be calculated knowing the values of K_b, H'/h, and ψ (for a given soil friction angle). As in the case of horizontal and vertical anchors (Chapters 2 to 4), for a given anchor orientation (that is, ψ) there exists a critical average embedment ratio $H'/h = (H'/h)_{cr}$ beyond which the average breakout factor will remain practically constant, signifying *deep anchor behavior,* by which local shear failure in soil takes place (Figure 5.5). For $H'/h \geq (H'/h)_{cr}$ and given values of ψ, the average breakout factor will remain practically constant ($F_q' = F_q'^*$). Thus, if the critical embedment ratio $(H'/h)_{cr}$ can be substituted into Equation 5.16, the average breakout factor for deep anchors can be estimated.

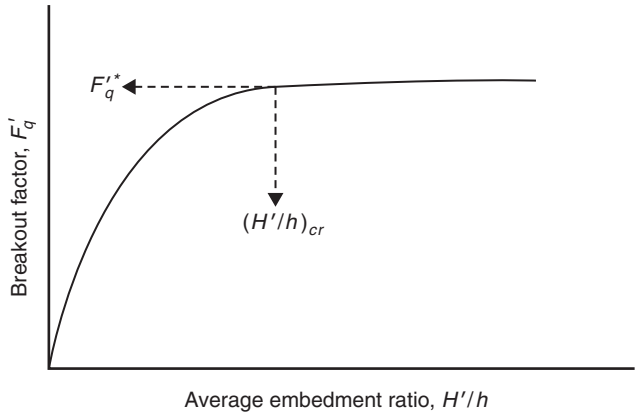

FIGURE 5.5 Nature of variation of F_q' with H'/h

Based on the experimental observations of Meyerhof and Adams (1968), with $\psi = 0$, the critical embedment ratio $[(H'/h)_{cr} = (H/h)_{cr}]$ for square anchors in loose sand is about 4 and increases to about 8 in dense sand (as discussed in Chapter 2). However, for strip anchors (for $\psi = 0$):

$$\left(\frac{H'}{h}\right)_{cr\text{-strip}} \approx 1.5\left(\frac{H'}{h}\right)_{cr\text{-square}}$$

For anchor inclination $\psi > 0$, the magnitude of $(H'/h)_{cr}$ gradually decreases. Using the preceding conditions, the variations of the magnitude of $F_q'^*$ for $\psi = 0°$, 45°, and 90° for *deep strip anchors* have been determined and are shown in Figure 5.6.

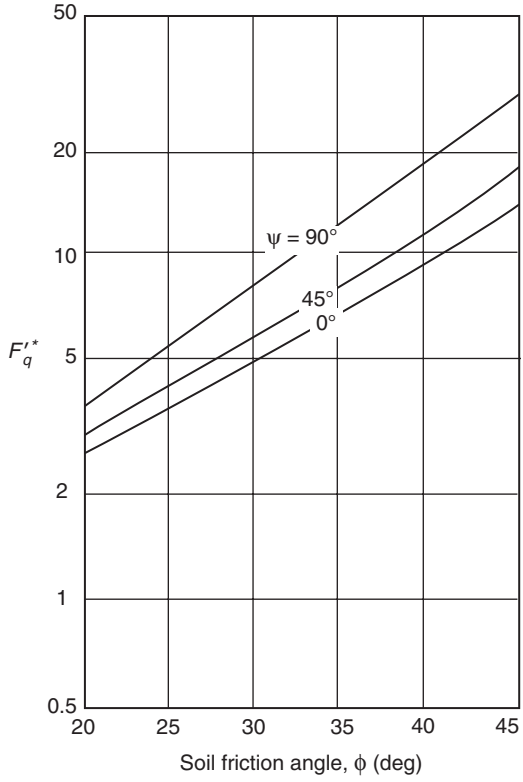

FIGURE 5.6 Variation of Meyerhof's (1973) $F_q'^*$ with soil friction angle ϕ for strip anchor

Again, for a given value of ψ:

$$F'^{*}_{q(\text{square})} = \frac{Q_u}{\gamma A H'} = F'^{*}_{q(\text{strip})} S_f \tag{5.19}$$

where

A = area of the anchor plate
S_f = shape factor

For horizontal anchors ($\psi = 0°$), the shape factor increases roughly with H'/h (Meyerhof and Adams, 1968) up to the above-mentioned critical depths. A similar relationship which is applicable for establishing the shape factors of square vertical anchors ($\psi = 90°$) can be developed from the work of Brinch Hansen (1961) on horizontally loaded rigid piles. Using the above-stated shape factors and the critical embedment ratios (H'/h) in Equation 5.16, the variations of F'^{*}_q for *deep square anchors* with $\psi = 0°$ and 90° have been calculated and are shown in Figure 5.7. The magnitude of F'^{*}_q for a rectangular anchor slab of width B and height h can be interpolated between the values of strips and squares in proportion to the B/h ratio.

Example 5.1

For the strip anchor shown in Figure 5.8, $\phi = 35°$, $\gamma = 17$ kN/m^3, $h = 0.4$ m, and $H' = 1$ m. Determine the variation of the net ultimate load Q'_u for $\psi = 20°$, 45°, 75°, and 90°.

Solution

From Equation 5.15:

$$Q'_u = \frac{1}{2} K_b \gamma \left(H' + \frac{h \sin \psi}{2} \right)^2 + \gamma h \left(H' + \frac{h \sin \psi}{2} \right) \cos^2 \psi$$

Referring to Figure 5.4, the variation of K_b with the anchor inclination ψ can be determined. Thus:

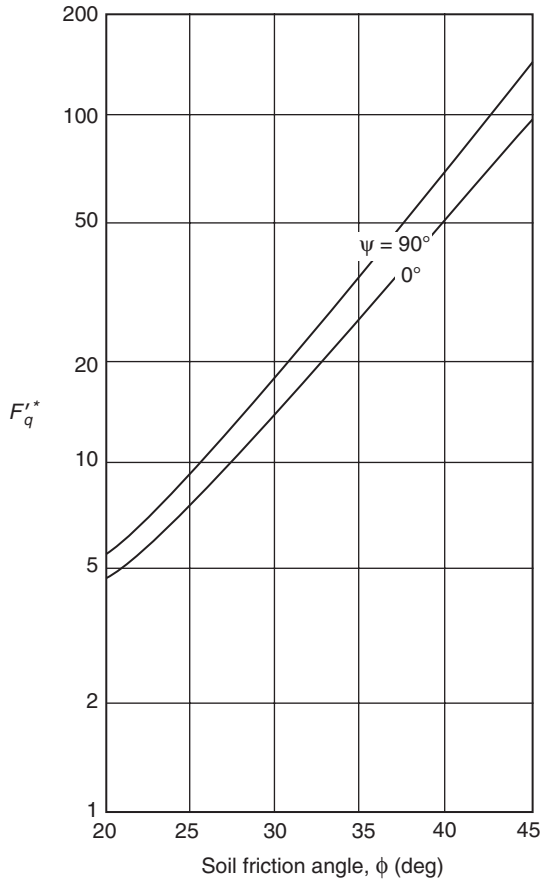

FIGURE 5.7 Variation of Meyerhof's (1973) F'^{*}_{q} with soil friction angle ϕ for square anchor

ϕ (deg)	Anchor inclination, ψ (deg)	K_b
35	20	≈1.4
35	45	≈1.8
35	75	≈2.7
35	90	≈3.9

Using the above values of K_b, the magnitude of Q'_u can be determined.

For $\psi = 20°$:

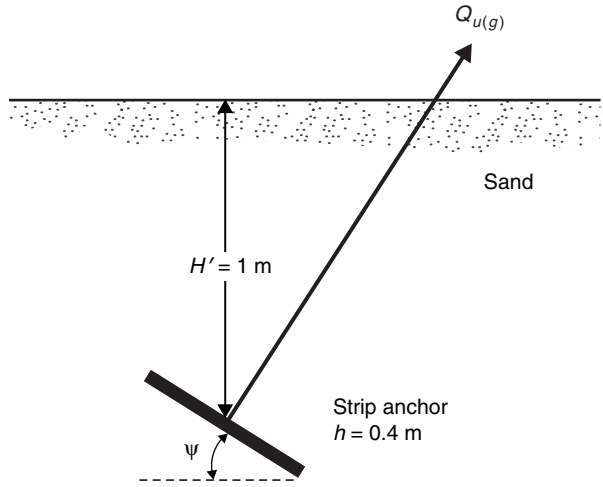

FIGURE 5.8 Example 5.1

$$Q'_u = \left(\frac{1}{2}\right)(1.4)(17)\left[1 + \frac{(0.4)(\sin 20°)}{2}\right]^2 + (17)(0.4)\left[1 + \frac{(0.4)(\sin 20°)}{2}\right]\cos^2 20°$$

$$= 13.58 + 6.41$$

$$= \mathbf{19.99\ kN/m}$$

For $\psi = 45°$:

$$Q'_u = \left(\frac{1}{2}\right)(1.8)(17)\left[1 + \frac{(0.4)(\sin 45°)}{2}\right]^2 + (17)(0.4)\left[1 + \frac{(0.4)(\sin 45°)}{2}\right]\cos^2 45°$$

$$= 19.93 + 3.88$$

$$= \mathbf{23.81\ kN/m}$$

For $\psi = 75°$:

$$Q'_u = \left(\frac{1}{2}\right)(2.7)(17)\left[1 + \frac{(0.4)(\sin 75°)}{2}\right]^2 + (17)(0.4)\left[1 + \frac{(0.4)(\sin 75°)}{2}\right]\cos^2 75°$$

$$= 32.67 + 0.54$$

$$= \mathbf{33.21\ kN/m}$$

For $\psi = 90°$:

$$Q'_u = \left(\frac{1}{2}\right)(3.9)(17)\left[1 + \frac{(0.4)(\sin 90°)}{2}\right]^2 + (17)(0.4)\left[1 + \frac{(0.4)(\sin 90°)}{2}\right]\cos^2 90°$$

$$= 47.74 + 0$$

$$= \mathbf{47.74\ kN/m}$$

5.2.3 Analysis of Hanna et al.

Hanna et al. (1988) developed an analytical method for estimation of the ultimate holding capacity of shallow inclined strip anchors with ψ varying from 0 to 60°. In order to explain this method of analysis, let us consider a shallow strip anchor (Figure 5.9). At ultimate load, the actual failure surface in soil will be somewhat similar to ab' and cd' (Figure 5.9a). However, along planes ab and cd, the passive forces per unit width of the anchor will be P_1 and P_2, respectively (Figure 5.9b). These resultant forces will be inclined at an angle δ to the normal drawn to ab and cd. Therefore, it can be written that

$$Q'_u = P_1 \sin\delta + P_2 \sin\delta + W\cos\psi \tag{5.20}$$

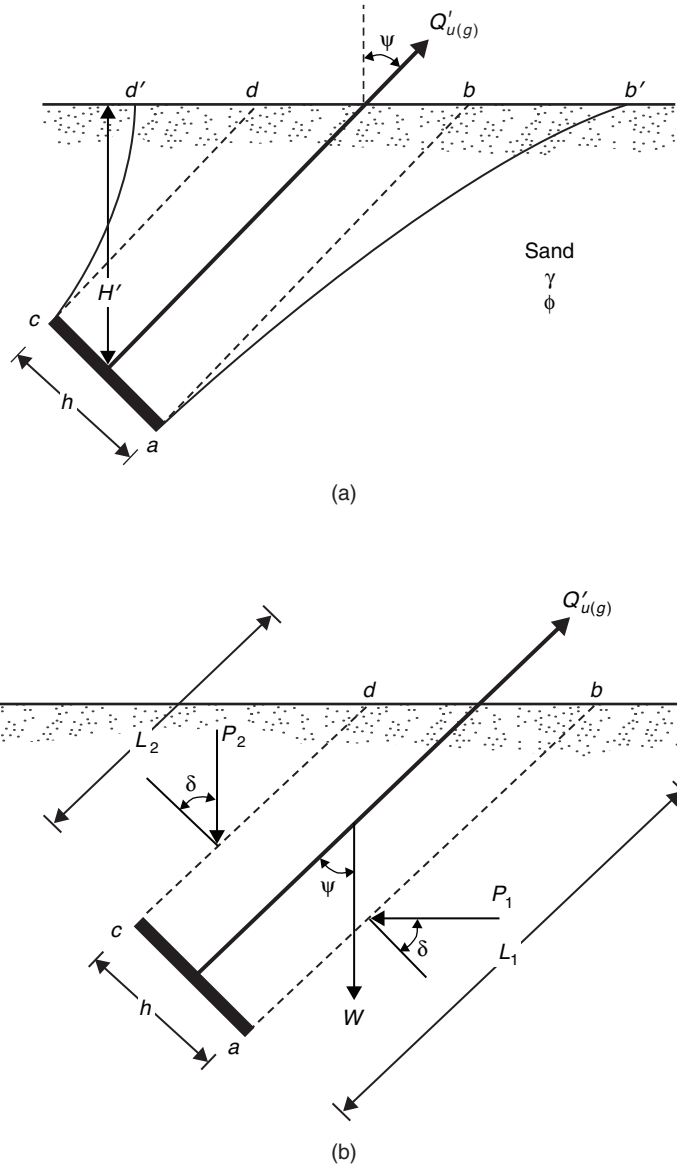

FIGURE 5.9 Shallow inclined strip anchor

where

Q_u' = net ultimate holding capacity per unit width
W = weight of the soil in zone *abcd* per unit width of the anchor at right angles to the cross section shown

Note that:

$$W = \frac{1}{2}(L_1 + L_2)h\gamma\cos\psi \tag{5.21}$$

$$P_1 = \frac{1}{2}R_\gamma K_p \gamma L_1^2 \tag{5.22}$$

$$P_2 = \frac{1}{2}R_\gamma K_p \gamma L_2^2 \tag{5.23}$$

where

K_p = passive earth pressure coefficient with $\delta = \phi$ = soil friction angle
R_γ = reduction factor for K_p, which is a function of δ/ϕ

The magnitudes of K_p and R_γ can be determined from the earth pressure tables of Caquot and Kerisel (1949). It must be pointed out that if the earth pressure analysis is conducted based on the actual failure surfaces *ab′* and *cd′* (Figure 5.9), then the mobilized friction angle δ would be equal to ϕ. On the other hand, if the analysis is made on the assumed failure surfaces *ab* and *cd*, then the mobilized angle of friction δ cited in Equation 5.20 is the average value. The locally mobilized friction angle δ_Z would be similar to the type shown in Figure 5.10. At points *b* and *d*, $\delta_Z = \lambda\phi$ (where λ is a function that depends on ψ), and at points *a* and *c*, $\delta = \phi$ (since points *a* and *c* are located on the actual failure surface).

In the study of Hanna et al. (1988), the average value of δ was determined by combining some laboratory model test results in conjunction with Equations 5.20, 5.22, and 5.23, or:

$$R_\gamma K_p \sin\delta = \frac{Q_u' - 0.5(L_1 + L_2)h\gamma\cos\psi}{0.5\gamma(L_1^2 + L_2^2)} \tag{5.24}$$

The right-hand side of Equation 5.24 was obtained from the laboratory model test results, and the left-hand side was determined by assuming several δ/ϕ

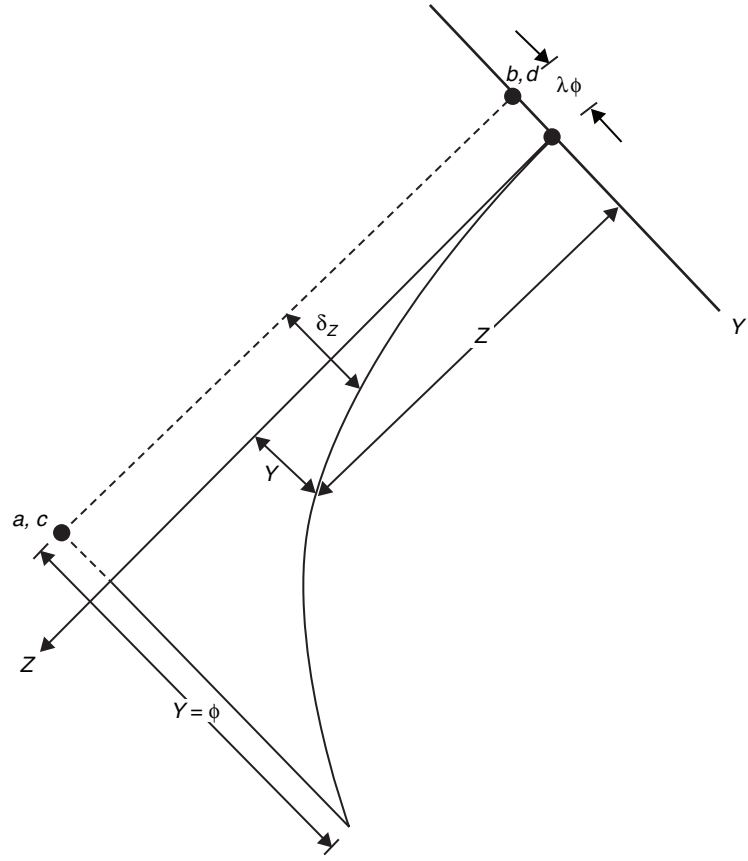

FIGURE 5.10 Nature of distribution of δ_Z

values and the passive earth pressure coefficient tables of Caquot and Kerisel (1949). The solution proceeded by trial and error until both sides of Equation 5.24 were equal. Once the average value of δ was determined from Equation 5.24, the variations of the locally mobilized angle of shearing resistance δ_Z were determined in the following manner:

$$P_1 + P_2 = \frac{1}{2} R_\gamma K_p \gamma (L_1^2 + L_2^2)$$

$$= \gamma \left[\int_0^{L_1} K_{p(Z)} Z dZ + \int_0^{L_2} K_{p(Z)} Z d \right] \tag{5.25}$$

The magnitude of the term $\frac{1}{2}R_\gamma K_p \gamma (L_1^2 + L_2^2)$ shown in Equation 5.25 was obtained by knowing the average value of δ. Use of laboratory experimental results and several trials and errors showed that the solution to Equation 5.25 can be found if

$$\lambda = \left(\frac{\psi^\circ}{90} \right)^3 + e^{-5 \tan \phi} \tag{5.26}$$

and

$$Y = \left(\frac{A'Z}{1 - B'Z} \right) \tag{5.27}$$

where

$$A' = \frac{\lambda \phi}{\beta} \tag{5.28}$$

and

$$B' = \frac{1}{\beta} \tag{5.29}$$

The term β is a constant that is determined by boundary conditions, or along *ab* (Figure 5.9):

$$\beta = \frac{L_1}{1 - \lambda} \tag{5.30}$$

and along *cd* (Figure 5.9):

$$\beta = \frac{L_2}{1 - \lambda} \tag{5.31}$$

The purpose of the above exercise was to predict δ, and hence K_p and R_γ, for soil friction angles other than those used in the model tests of Hanna et al. (1988). The following is a step-by-step procedure for determining these values:

1. Assume a value of ϕ.
2. From Equation 5.26, calculate λ.
3. Calculate the variation of Y from Equations 5.27 to 5.31.
4. Calculate δ_Z as:

$$\delta_Z = \lambda\phi + Y \tag{5.32}$$

5. With the value of δ_Z obtained from Equation 5.32, obtain the magnitude of $K_{p(Z)}$ from the tables of Caquot and Kerisel (1949).
6. Using a computer program, calculate $R_\gamma K_p$ from Equation 5.25, or:

$$R_\gamma K_p = \frac{\int_0^{L_1} K_{p(Z)} Z dZ + \int_0^{L_2} K_{p(Z)} Z dZ}{0.5(L_1^2 + L_2^2)} \tag{5.33}$$

7. Once the right-hand side of Equation 5.33 is known, determine the average δ using the passive earth pressure tables of Caquot and Kerisel (1949).

The results of this type of analysis, if conducted, will be as shown in Figure 5.11, which is a plot of δ/ϕ versus ψ for various soil friction angles ϕ. The analysis can be further simplified if we assume that

$$K_s \sin\phi = R_\gamma K_p \sin\delta \tag{5.34}$$

or

$$K_s = \frac{R_\gamma K_p \sin\delta}{\sin\phi} \tag{5.35}$$

where

K_s = punching uplift coefficient

The variations of K_s thus obtained for various values of ψ and ϕ are shown in Figure 5.12. Now, combining Equations 5.20 to 5.23 and 5.34, we obtain:

$$Q_u' = \frac{1}{2}\gamma K_s \sin\phi\,(L_1^2 + L_2^2) + \frac{1}{2}\gamma(L_1 + L_2)h\cos\psi \tag{5.36}$$

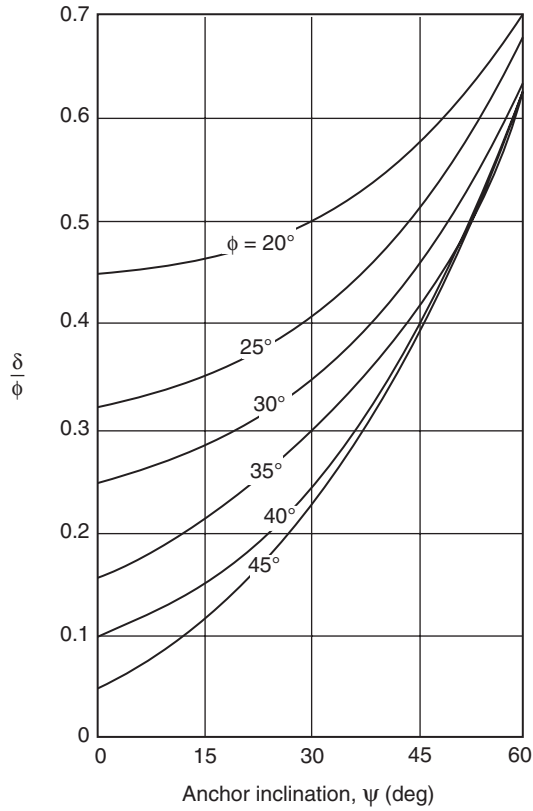

FIGURE 5.11 Variation of δ/ϕ with anchor inclination ψ (after Hanna et al., 1988)

In Equation 5.36, note that (Figure 5.13)

$$L_1 = \frac{H' + \frac{h}{2}\sin\psi}{\cos\psi} \tag{5.37}$$

$$L_2 = \frac{H' - \frac{h}{2}\sin\psi}{\cos\psi} \tag{5.38}$$

Therefore:

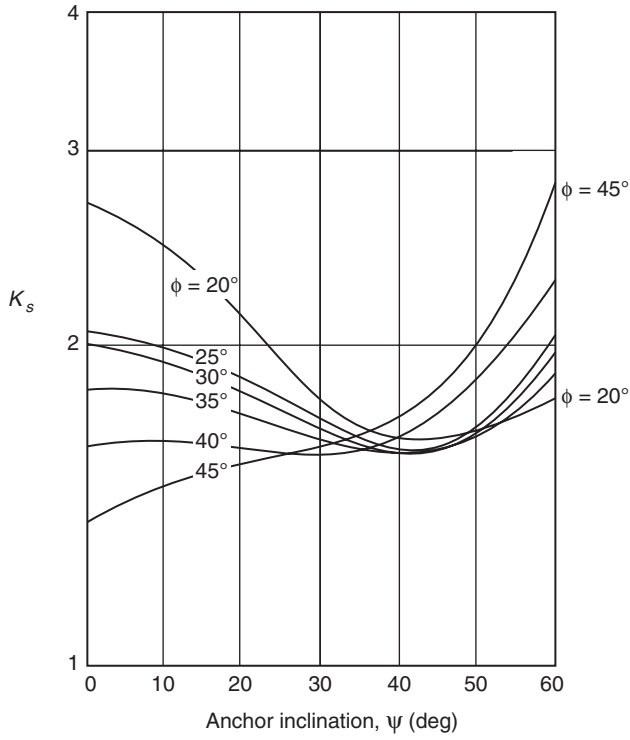

FIGURE 5.12 Variation of punching uplift coefficient (after Hanna et al., 1988)

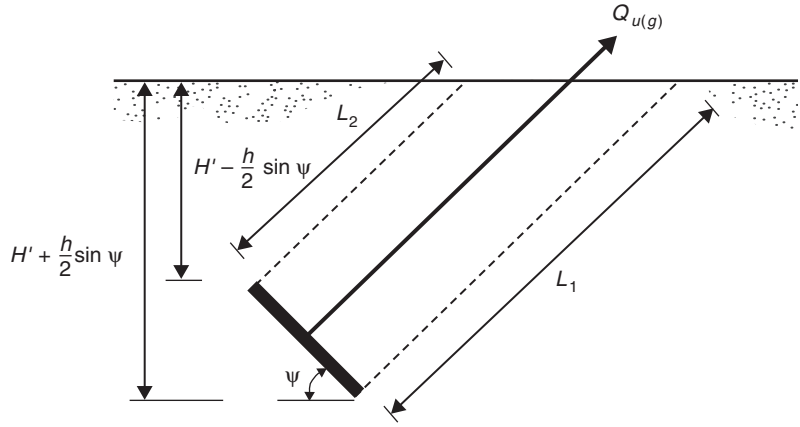

FIGURE 5.13 Definition of L_1 and L_2 (Equations 5.37 and 5.38)

$$Q_u' = \frac{1}{2}\gamma K_s \sin\phi \left[\left(\frac{H' + \frac{h}{2}\sin\psi}{\cos\psi} \right)^2 + \left(\frac{H' - \frac{h}{2}\sin\psi}{\cos\psi} \right)^2 \right]$$

$$+ \frac{1}{2}\gamma \left[\left(\frac{H' + \frac{h}{2}\sin\psi}{\cos\psi} \right) + \left(\frac{H' - \frac{h}{2}\sin\psi}{\cos\psi} \right) \right] h\cos\psi$$

or

$$Q_u' = \gamma K_s \frac{\sin\phi}{\cos^2\psi} \left(H'^2 + \frac{h^2}{4}\sin^2\psi \right) + \gamma H' h \tag{5.39}$$

Example 5.2

With the parameters for sand and anchor given in Example 5.1, determine Q_u' for $\psi = 0°$, 45°, and 60° using the theory of Hanna et al. (1988).

Solution

$H' = 1$ m, $h = 0.4$ m, $\gamma = 17$ kN/m^3, and $\phi = 35°$. From Figure 5.12 for $\phi = 35°$, the variations of K_s are as follows:

Anchor inclination, ψ (deg)	K_s
0	≈1.8
45	≈1.6
60	≈2.0

Now, From Equation 5.39:

$$Q_u' = \gamma K_s \frac{\sin\phi}{\cos^2\psi} \left(H'^2 + \frac{h^2}{4}\sin^2\psi \right) + \gamma H' h$$

For $\psi = 0°$:

$$Q'_u = (17)(1.8)\left(\frac{\sin 35°}{\cos^2 0°}\right)\left[(1)^2 + \frac{(0.4)^2}{4}\sin^2 0°\right] + (17)(1)(0.4)$$

$$= 17.55 + 6.8$$

$$= \mathbf{24.35\ kN/m}$$

For $\psi = 45°$:

$$Q'_u = (17)(1.6)\left(\frac{\sin 35°}{\cos^2 45°}\right)\left[(1)^2 + \frac{(0.4)^2}{4}\sin^2 45°\right] + (17)(1)(0.4)$$

$$= 31.83 + 6.8$$

$$= \mathbf{38.63\ kN/m}$$

For $\psi = 60°$:

$$Q'_u = (17)(1.6)\left(\frac{\sin 35°}{\cos^2 60°}\right)\left[(1)^2 + \frac{(0.4)^2}{4}\sin^2 60°\right] + (17)(1)(0.4)$$

$$= 64.28 + 6.8$$

$$= \mathbf{71.08\ kN/m}$$

5.2.4 Other Empirical Relationships

A simple empirical relationship for estimating the ultimate holding capacity of shallow inclined anchors embedded in sand was proposed by Maiah et al. (1986), which is of the form

$$Q_{u\text{-}\psi} = Q_{u\text{-}\psi=0°} + (Q_{u\text{-}\psi=90°} - Q_{u\text{-}\psi=0°})\left(\frac{\psi°}{90}\right)^2 \qquad (5.40)$$

(for a given value of H'/h)

where

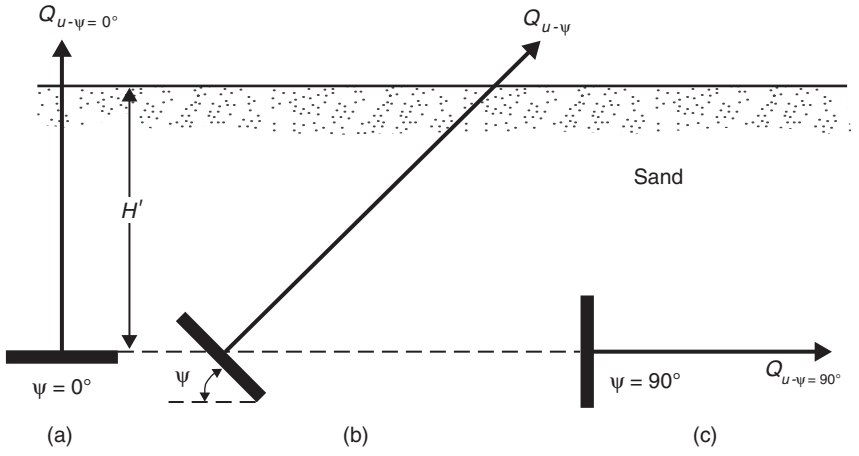

FIGURE 5.14 Definition of $Q_{u\text{-}\psi=0^\circ}$, $Q_{u\text{-}\psi}$, and $Q_{u\text{-}\psi=90^\circ}$

$Q_{u\text{-}\psi}$ = net ultimate holding capacity of anchor inclination of ψ with respect to the horizontal (Figure 5.14b)
$Q_{u\text{-}\psi=0^\circ}$ = net ultimate uplift capacity of horizontal anchor (that is, $\psi = 0^\circ$; see Figure 5.14a)
$Q_{u\text{-}\psi=90^\circ}$ = net ultimate holding capacity of vertical anchor (that is, $\psi = 90^\circ$; see Figure 5.14c)

The above relationship was originally developed for shallow strip anchors; however, the authors feel that it can also be applied to rectangular anchors.

In order to predict $Q_{u\text{-}\psi=0^\circ}$, the relationship presented by Meyerhof and Adams (1968) given in Chapter 2 can be used, or:

$$Q_{u\text{-}\psi=0^\circ} = \gamma H'^2 \left[2\left(1 + m\frac{H'}{h}\right)h + B - h \right] K_u \tan\phi + hBH'\gamma \quad (5.41)$$

(for rectangular anchors)

$$Q'_{u\text{-}\psi=0^\circ} = \gamma H'^2 K_u \tan\phi + hH'\gamma \quad \text{(for strip anchors)} \quad (5.42)$$

where

TABLE 5.1 Variation of m with soil friction angle

Soil friction angle, ϕ (deg)	m
20	0.05
25	0.1
30	0.15
35	0.25
40	0.35
45	0.50
48	0.6

B = length of anchor plate (dimension at right angle to the cross section shown in Figure 5.14)
h = width of anchor plate
m = a coefficient for obtaining the shape factor (see Table 5.1)
K_u = uplift coefficient (see Figure 5.15)

In order to calculate the magnitude of $Q_{u\text{-}\psi=90^\circ}$ for rectangular anchors, the theory of Neely et al. (1973) can be used. This theory is based on the surcharge method with $\delta = \phi$ as discussed in Chapter 4, or:

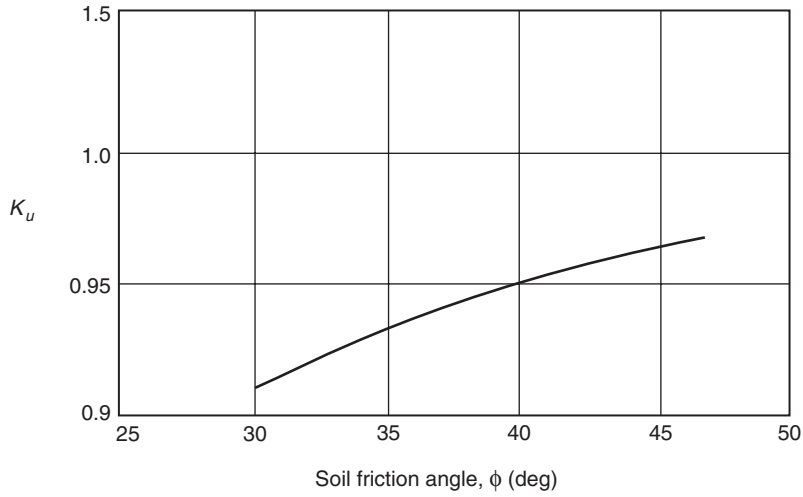

FIGURE 5.15 Meyerhof's (1973) uplift coefficient K_u for horizontal ($\psi = 0^\circ$) plate anchor

$$Q_{u\text{-}\psi=90^\circ} = \gamma h^2 B M_{\gamma q} S_f \tag{5.43}$$

where

$M_{\gamma q}$ = force coefficient (Figure 5.16)
S_f = shape factor (Figure 5.17)

Example 5.3

Refer to Example 5.1. Using Equations 5.40, 5.42, and 5.43, determine $Q'_{u\text{-}\psi}$ (kN/m) for $\psi = 0°$, 45°, 60°, 75°, and 90°.

Solution

From Equation 5.42:

$$Q'_{u\text{-}\psi=0^\circ} = \gamma H'^2 K_u \tan\phi + hH'\gamma$$

For $\phi = 35°$, $K_u = 0.93$ (Figure 5.15). $h = 0.4$ m, $H' = 1$ m, and $\gamma = 17$ kN/m^3:

$$Q'_{u\text{-}\psi=0^\circ} = (17)(1)^2(0.93)(\tan 35°) + (0.4)(1)(17)$$

$$= 11.07 + 6.8 = 17.68 \text{ kN/m}$$

Again, from Figure 5.17, for $H'/h = 2.5$, $M_{\gamma q} \approx 20$. $S_f = 1$ (strip anchor). Thus, from Equation 5.43:

$$Q'_{u\text{-}\psi=90^\circ} = \gamma h^2 B M_{\gamma q} S_f = (17)(0.4)^2(1)(20)(1) = 54.4 \text{ kN/m}$$

Now we can use Equation 5.40 to estimate the variation of $Q'_{u\text{-}\psi}$:

ψ (deg)	$Q'_{u\text{-}\psi}$ (kN/m)
0	17.68
45	26.86
60	34.00
75	43.13
90	54.4

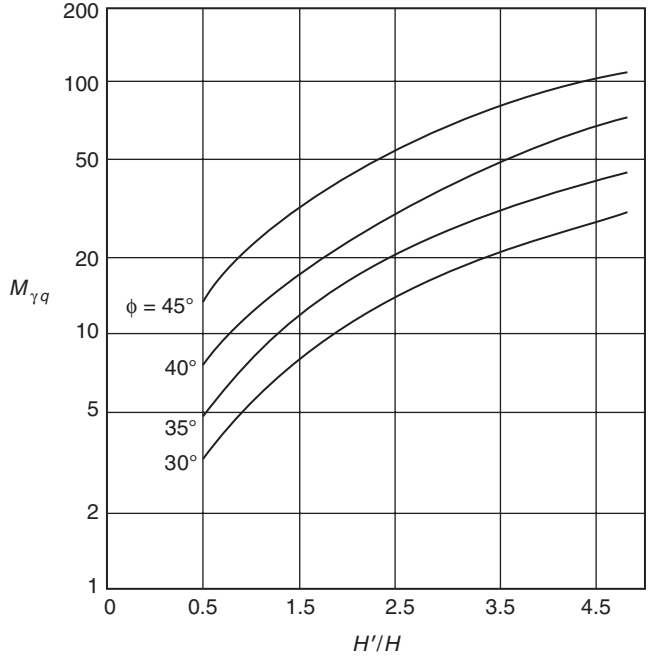

FIGURE 5.16 Variation of force coefficient with H'/h ($\delta = \phi$) (adapted from Neely et al., 1973)

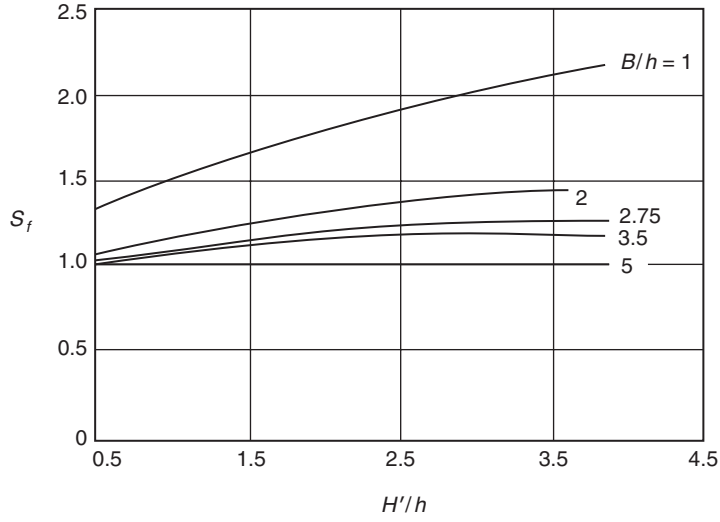

FIGURE 5.17 Variation of S_f with H'/h and B/h (after Neely et al., 1973)

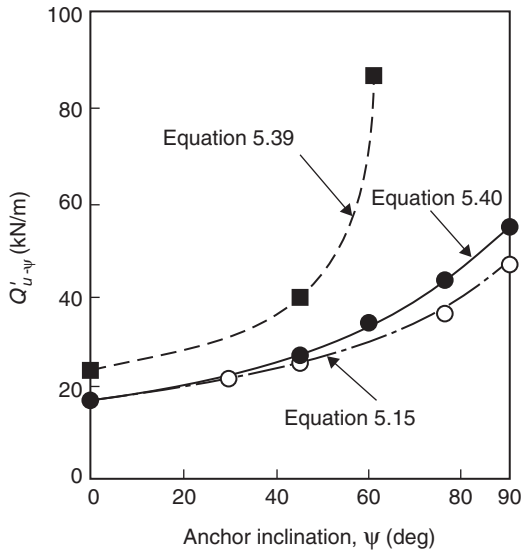

FIGURE 5.18 Example 5.4

Example 5.4

Compare the results of Examples 5.1 to 5.3.

Solution

The variation of $Q'_{u\text{-}\psi}$ with anchor inclination is shown in Figure 5.18. From the plot, the following conclusions can be drawn:

1. Meyerhof's theory (1973) for shallow inclined anchors (Equation 5.15) and the theory of Maiah et al. (1986) (Equation 5.40), in conjunction with Equations 5.42 and 5.43, yield fairly close results.
2. The theory of Hanna et al. (1988) (Equation 5.39) provides excessively high values of $Q'_{u\text{-}\psi}$.

5.2.5 General Remarks

As per the discussions provided in Sections 5.2.1 through 5.2.4, the following general observations may be made:

1. The appropriate average critical embedment ratio $(H'/h)_{cr}$ for square and circular anchors with $\psi = 0°$ and 90° are as follows:

$\psi = 0°$:	Loose sand	4
	Dense sand	8
$\psi = 90°$:	Loose sand	4
	Dense sand	6

2. In a similar manner, the appropriate values of $(H'/h)_{cr}$ for strip anchors are as follows:

$\psi = 0°$:	Loose sand	6
	Dense sand	11 to 12
$\psi = 90°$:	Loose sand	4
	Dense sand	8

3. For shallow strip anchors, the magnitude of $Q'_{u\text{-}\psi}$ can be estimated by using Equation 5.15 (Meyerhof's theory [1973]) or Equation 5.40 in conjunction with Equations 5.42 and 5.43.
4. For shallow rectangular anchors, the magnitude of $Q'_{u\text{-}\psi}$ can be estimated by using Equations 5.40, 5.41, and 5.43.
5. For deep anchors, a similar relationship as in Equation 5.40 can be used, or:

$$F'^{*}_{q\text{-}\psi} = F'^{*}_{q\text{-}\psi=0°} + (F'^{*}_{q\text{-}\psi=90°} - F'^{*}_{q\text{-}\psi=0°}) \left(\frac{\psi°}{90}\right)^2 \tag{5.44}$$

where

$F'^{*}_{q\text{-}\psi}$, $F'^{*}_{q\text{-}\psi=0°}$, $F'^{*}_{q\text{-}\psi=90°}$ = breakout factors for deep anchors defined in Section 5.2.2 with inclinations of $\psi = 0°$ and 90° with respect to the horizontal

The preceding relation should be applicable for strip, square, and rectangular anchors. For strip anchors, $F'_{q\text{-}\psi=0°} = Q'_{u\text{-}\psi=0°}/\gamma hH'$ and $F'^{*}_{q\text{-}\psi=90°} = Q'_{u\text{-}\psi=90°}/\gamma hH'$ can be obtained from Figure 5.6. Similarly, for square anchors, the magnitudes of $F'^{*}_{q\text{-}\psi=0°}$ and $F'^{*}_{q\text{-}\psi=90°}$ can be obtained from Figure 5.7. For rectangular anchors, interpolations need to be made to estimate the breakout factors for $\psi = 0°$ and 90°. Once $F'^{*}_{q\text{-}\psi}$ is determined, the magnitudes of the ultimate load can be obtained. For *strip anchors*:

$$Q'_{u\text{-}\psi}\ (\text{kN/m}) = F'^{*}_{q\text{-}\psi}\gamma hH' \tag{5.45}$$

For *square anchors*:

$$Q_{u\text{-}\psi}\,(\text{kN}) = F'^{*}_{q\text{-}\psi}\gamma h^2 H' \tag{5.46}$$

For *rectangular anchors*:

$$Q_{u\text{-}\psi}\,(\text{kN}) = F'^{*}_{q\text{-}\psi}\gamma hBH' \tag{5.47}$$

6. The anchor displacement Δ_u along the direction of the pull at ultimate load gradually increases with the anchor inclination ψ. Approximate values of Δ_u/h for the shallow anchor condition are as follows:

Anchor type	Δ_u/h at $\psi = 0°$	Δ_u/h at $\psi = 90°$
Strip	6 to 8%	10 to 25%
Square	8 to 10%	15 to 30%

   The preceding approximate values of Δ_u/h are based on laboratory model tests conducted by the first author. The magnitude of Δ_u/h increases with the increase in H'/h.
7. The present theories on inclined anchors are primarily based on observations made during model tests in the laboratory. Further full-scale tests are essential to verify the assumptions and results.
8. Due to the uncertainties involved, a factor of safety of at least 3 may be used to obtain the allowable holding capacity.
9. At the present time, experimental results are not available to consider the effects of center-to-center spacing of inclined anchors when they are placed in a row or a group.

5.3 INCLINED PLATE ANCHORS IN CLAY (ϕ = 0 CONDITION)

5.3.1 Ultimate Holding Capacity

Unlike cases where horizontal plate anchors are subjected to vertical uplift (Chapters 2 and 3) and vertical plate anchors are subjected to horizontal pull (Chapter 4), the existing studies relating to the holding capacity of inclined anchors embedded in clay and subjected to axial pull are fairly limited. Among them, the study by Das (1985) is fairly comprehensive and will be presented in this section. The results were based primarily on laboratory observations on square anchors embedded in saturated and near-saturated clay soils. According

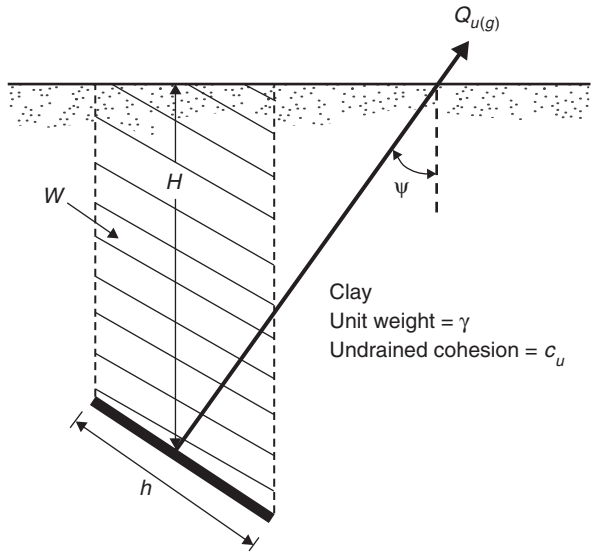

FIGURE 5.19 Inclined plate anchor in clay

to the suggested procedure of Das (1985), the net ultimate holding capacity of an inclined rectangular anchor plate can be given as (Figure 5.19):

$$Q_u = Ac_uF_c' + W\cos\psi \tag{5.48}$$

where

A = area of the anchor plate = Bh
B = width of the anchor plate
c_u = undrained cohesion of the clay soil ($\phi = 0$ condition)
F_c' = average breakout factor
W = weight of soil located immediately above the anchor
ψ = anchor inclination with respect to the horizontal

However:

$$W = A'\gamma H'\cos\psi \tag{5.49}$$

where

H' = average depth of embedment

Substituting Equation 5.49 into Equation 5.48, we obtain:

$$F_c' = \frac{\frac{Q_u}{A} - \gamma H' \cos^2 \psi}{c_u}$$

For square anchors:

$$F_c' = \frac{\frac{Q_u}{h^2} - \gamma H' \cos^2 \psi}{c_u} \tag{5.50}$$

For rectangular anchors:

$$F_c' = \frac{\frac{Q_u}{Bh} - \gamma H' \cos^2 \psi}{c_u} \tag{5.51}$$

Similarly, for strip anchors:

$$F_c' = \frac{\frac{Q_u'}{h} - \gamma H' \cos^2 \psi}{c_u} \tag{5.52}$$

The variation of the average breakout factor can be given as:

$$F'_{c\text{-}\psi} = F'_{c\text{-}\psi=0^\circ} + (F'_{c\text{-}\psi=90^\circ} - F'_{c\text{-}\psi=0^\circ}) \left(\frac{\psi^\circ}{90} \right)^2 \tag{5.53}$$

The breakout factor $F'_{c\text{-}\psi}$ increases with the increase in the average embedment ratio H'/h to a maximum value $F'^{*}_{c\text{-}\psi}$ at $(H'/h)_{cr}$ and remains constant thereafter (Figure 5.20).

The empirical procedures for estimating $F'_{c\text{-}\psi=0^\circ}$ and $F'_{c\text{-}\psi=90^\circ}$ were given in Chapters 3 and 4 (based on the studies of Das [1980] and Das et al. [1985]) and are summarized below.

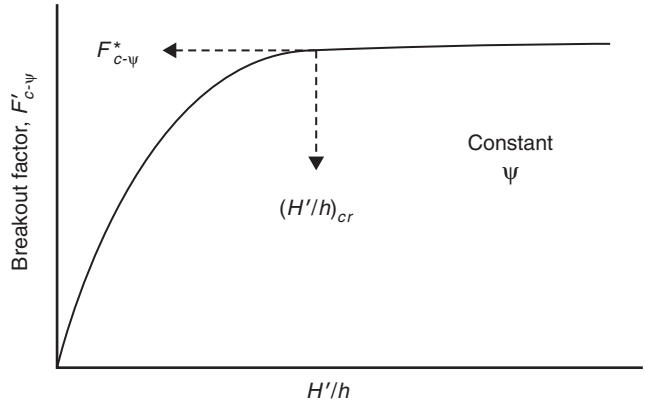

FIGURE 5.20 Variation of $F'_{c\text{-}\psi}$ with H'/h

5.3.1.1 Estimation of $F'_{c\text{-}\psi=0^\circ}$

1. Calculate the critical average embedment ratio $(H'/h)_{cr\text{-}R}$ for a rectangular anchor $(h \times B)$:

$$\left(\frac{H'}{h}\right)_{cr\text{-}R} = \left(\frac{H'}{h}\right)_{cr\text{-}S} \left[0.73 + 0.27\left(\frac{B}{h}\right)\right] \leq 1.55\left(\frac{H'}{h}\right)_{cr\text{-}S} \tag{5.54}$$

where

$$\left(\frac{H'}{h}\right)_{cr\text{-}S} = 0.107c_u + 2.5 \leq 7 \tag{5.55}$$

where c_u is in kN/m^2.

2. If the actual (H'/h) is greater than $(H'/h)_{cr}$, then it is a deep anchor and

$$F'_{c\text{-}\psi=0^\circ} = F'^*_{c\text{-}\psi=0^\circ} = 7.56 + 1.44\left(\frac{h}{B}\right) \tag{5.56}$$

If the actual (H'/h) is less than or equal to $(H'/h)_{cr}$, then it is a shallow anchor and

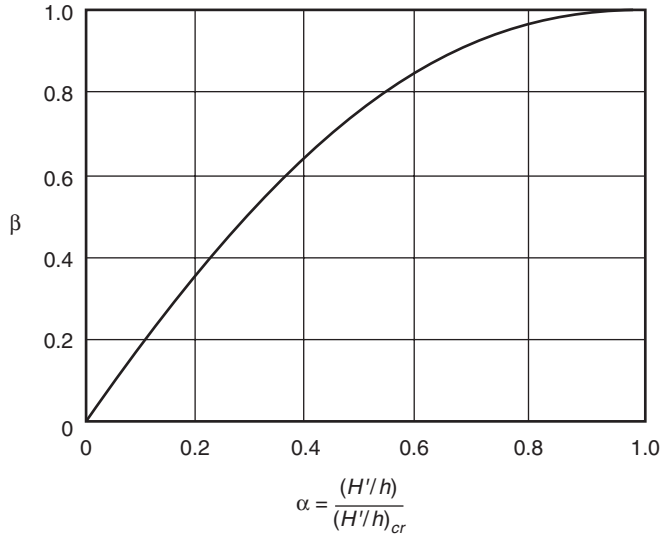

FIGURE 5.21 Variation of β with $(H'/h)/(H'/h)_{cr}$ for $\psi = 0°$

$$F'_{c\text{-}\psi=0°} = \left[7.56 + 1.44\left(\frac{h}{B}\right) \right] \beta \tag{5.57}$$

where

$$\beta = f\left[\frac{\frac{H'}{h}}{\left(\frac{H'}{h}\right)_{cr}} \right] \quad \text{(see Figure 5.21)}$$

5.3.1.2 Estimation of $F'_{c\text{-}\psi=90°}$

1. Calculate $(H'/h)_{cr\text{-}R}$ as:

$$\left[\frac{\left(\frac{H'}{h}\right)_{cr\text{-}R} + 0.5}{\left(\frac{H'}{h}\right)_{cr\text{-}S} + 0.5} \right] = \left[0.9 + 0.1\left(\frac{B}{h}\right) \right] \leq 1.31 \tag{5.58}$$

where

$(H'/h)_{cr\text{-}S}$ = critical embedment ratio of a square anchor measuring $h \times h$

$$\left(\frac{H'}{h}\right)_{cr\text{-}S} = 4.2 + 0.0606c_u \leq 6.5 \tag{5.59}$$

where c_u is in kN/m^2.

2. If the actual (H'/h) is greater than $(H'/h)_{cr}$, then it is a deep anchor:

$$F'_{c\text{-}\psi=90^\circ} = F'^{*}_{c\text{-}\psi=90^\circ} = 9\left[0.825 + 0.175\left(\frac{h}{B}\right)\right] \tag{5.60}$$

If the actual (H'/h) is less than or equal to $(H'/h)_{cr}$, then it is a shallow anchor. In that case:

$$\frac{F'_{c\text{-}\psi=90^\circ}}{F'^{*}_{c\text{-}\psi=90^\circ}} = \frac{n'}{0.41 + 0.59n'} \tag{5.61}$$

where

$$n' = \frac{\dfrac{H'}{h} + 0.5}{\left(\dfrac{H'}{h}\right)_{cr} + 0.5} \tag{5.62}$$

Once $F'_{c\text{-}\psi}$ is determined by using Equation 5.53, the magnitude of the ultimate holding capacity can be determined from Equations 5.50 to 5.52.

Example 5.5

Consider an anchor embedded in a saturated clay. For the anchor, $h = 0.4$ m, $H' = 1.2$ m, $B = 0.8$ m, and $\psi = 30^\circ$. For the clay, $c_u = 28$ kN/m^2 and $\gamma = 18.4$ kN/m^3. Calculate the net ultimate holding capacity.

Solution

Calculation of $F'_{c\text{-}\psi=0^\circ}$. From Equation 5.55:

$$\left(\frac{H'}{h}\right)_{cr\text{-}S} = 0.107c_u + 2.5 = (0.107)(28) + 2.5 \approx 5.5$$

Since $(H'/h)_{cr}$ is less than 7, we use the actual value, or $(H'/h)_{cr\text{-}S} = 5.5$. From Equation 5.54:

$$\left(\frac{H'}{h}\right)_{cr\text{-}R} = \left(\frac{H'}{h}\right)_{cr\text{-}S}\left[0.73 + 0.27\left(\frac{B}{h}\right)\right]$$

$$= (5.5)\left[0.73 + 0.27\left(\frac{0.8}{0.4}\right)\right] \approx 6.99$$

This value of 6.99 is less than $(1.55)(5.5) = 8.525$; therefore, use $(H'/h)_{cr\text{-}R} = 6.99$. However, the actual $H'/h = 1.2/0.4 = 3$, so it is a shallow anchor. From Equation 5.57:

$$F'_{c\text{-}\psi=0^\circ} = \left[7.56 + 1.44\left(\frac{h}{B}\right)\right]\beta$$

Referring to Figure 5.21, for $(H'/h)/(H'/h)_{cr} = 3/6.99 = 0.429$, $\beta = 0.69$. Therefore:

$$F'_{c\text{-}\psi=0^\circ} = \left[7.56 + (1.44)\left(\frac{0.4}{0.8}\right)\right](0.69) = 5.71$$

Calculation of $F'_{c\text{-}\psi=90^\circ}$. From Equation 5.59:

$$\left(\frac{H'}{h}\right)_{cr\text{-}S} = 4.2 + 0.0606c_u = 4.2 + (0.0606)(28) = 5.9$$

Therefore, use $(H'/h)_{cr\text{-}S}$ as 5.9 since it is less than 6.5. From Equation 5.58:

$$\left[\frac{\left(\frac{H'}{h}\right)_{cr\text{-}R} + 0.5}{\left(\frac{H'}{h}\right)_{cr\text{-}S} + 0.5}\right] = \left[0.9 + 0.1\left(\frac{B}{h}\right)\right] = 0.9 + (0.1)(2) = 1.1$$

or

$$\left(\frac{H'}{h}\right)_{cr\text{-}R} + 0.5 = 1.1\left[\left(\frac{H'}{h}\right)_{cr\text{-}S} + 0.5\right] = (1.1)(5.9 + 0.5) = 7.04$$

Therefore:

$$\left(\frac{H'}{h}\right)_{cr\text{-}R} = 6.54$$

For this case, since $(H'/h)_{cr\text{-}R} = 6.54 > H'/h = 1.2/0.4 = 3.0$, the anchor is shallow. Referring to Equation 5.62:

$$n' = \frac{\frac{H'}{h} + 0.5}{\left(\frac{H'}{h}\right)_{cr} + 0.5} = \frac{3 + 0.5}{6.54 + 0.5} = 0.497$$

$$F'^{*}_{c\text{-}\psi=90^\circ} = 9\left[0.825 + 0.175\left(\frac{h}{B}\right)\right]$$

$$= 9\left[0.825 + 0.175\left(\frac{0.4}{0.8}\right)\right] = 8.21$$

Thus, from Equation 5.61:

$$F'_{c\text{-}\psi=90^\circ} = \frac{(8.21)\,(0.497)}{0.41 + (0.59)\,(0.497)} = 5.8$$

However, from Equation 5.53:

$$F'_{c\text{-}\psi} = F'_{c\text{-}\psi=0^\circ} + (F'_{c\text{-}\psi=90^\circ} - F'_{c\text{-}\psi=0^\circ})\left(\frac{\psi^\circ}{90}\right)^2$$

$$= 5.71\,(5.8 - 5.71)\left(\frac{30}{90}\right)^2 = 5.72$$

Therefore, from Equation 5.51:

$$Q_u = Bh(F'_{c\text{-}\psi}\, c_u + \gamma H' \cos^2 \psi)$$

$$= (0.8)\,(0.4)\,[\,(5.72)\,(28) + (18.4)\,(1.2)\,(\cos^2 30^\circ)\,]$$

$$= \mathbf{56.55\ kN}$$

5.4 OTHER STUDIES

As presented in Chapters 2 to 4, most numerical studies have been concerned with either horizontal or vertical anchors.

Merifield et al. (2005) applied the numerical limit analysis and displacement finite element analysis to evaluate the stability of inclined strip anchors in undrained clay. Consideration was given to the effect of embedment depth and anchor inclination. This study shows that using the lower and upper bound limit theorems, error bounds of less than ±7% are achieved on the true value of the breakout factor for anchors inclined at 22.5°, 45°, and 67.5° to the vertical in weightless soil. A simple empirical equation has been proposed which, on average, provides collapse load estimates within ±5% of the actual values. It has been reported that the ultimate anchor capacity increases linearly with overburden pressure up to a limiting value that reflects the transition from a nonlocalized (shallow) to localized (or deep) failure mechanism.

5.5 SUMMARY OF MAIN POINTS

1. Harvey and Burley's theory (1973) provides an analysis of the holding capacity of shallow inclined circular anchor plates, but this procedure is rarely used in practice now.
2. Meyerhof's theory (1973) for shallow inclined anchors and the theory of Maiah et al. (1986) yield fairly close results.
3. The theory of Hanna et al. (1988) provides excessively high values of the ultimate anchor capacity.
4. The average critical embedment ratio for anchors in loose sand is smaller than that for anchors in dense sand.
5. The anchor displacement along the direction of pull at ultimate load gradually increases with the anchor inclination.
6. The ultimate anchor capacity increases linearly with overburden pressure up to a limiting value that reflects the transition from a shallow to deep failure mechanism.

SELF-ASSESSMENT QUESTIONS

Select the most appropriate answer to each multiple-choice question

5.1. The present theories on inclined anchors are primarily based on observations made during:
   a. small-scale tests in the laboratory
   b. large-scale tests in the laboratory
   c. large-scale tests in the field
   d. field constructions

5.2. The minimum factor of safety used to obtain the allowable holding capacity is:
   a. 2
   b. 3
   c. 4
   d. 5

5.3. If the undrained cohesion is negligible, then the net ultimate holding capacity of an inclined anchor is proportional to:
   a. the weight of soil located immediately above the anchor
   b. the cosine of the anchor inclination with respect to horizontal
   c. both a and b
   d. the sine of the anchor inclination with respect to horizontal

5.4. For a soil friction angle equal to 40°, the uplift coefficient is:
   a. 0.9
   b. 0.95
   c. 1.0
   d. 1.5

5.5. For a shallow inclined anchor, with increase in overburden pressure, the ultimate anchor capacity:
   a. does not vary
   b. varies nonlinearly
   c. decreases linearly
   d. increases linearly

Answers

5.1: a 5.2: b 5.3: c 5.4: b 5.5: d

REFERENCES

Baker, W.H. and Kondner, R.L. (1966). Pullout load capacity of a circular earth anchor buried in sand. *Highw. Res. Rec.,* No. 108, National Academy of Sciences, Washington, D.C., 1–10.

Balla, A. (1961). The resistance to breaking-out of mushroom foundations for pylons. *Proc. V Int. Conf. Soil Mech. Found. Eng.,* Paris, 1, 569–576.

Brinch Hansen, J. (1961). *The Ultimate Resistance of Rigid Piles against Transverse Forces,* Bull. No. 12, Danish Geotechnical Institute, Copenhagen.

Caquot, A. and Kerisel, L. (1949). *Traite de Macanique des Sols,* Gauthier-Villars, Paris.

Das, B.M. (1980). A procedure for estimation of ultimate uplift capacity of foundations in clay. *Soils Found.,* 20(1):72–82.

Das, B.M. (1985). Resistance of shallow inclined anchors in clay. *Uplift Behavior of Anchor Found. in Soils,* S.P. Clemence, Ed., ASCE, 86–101.

Das, B.M., Tarquin, A.J., and Moreno, R. (1985). Model tests for pullout resistance of vertical anchors in clay. *Civ. Eng. Pract. Design Eng.,* 4(2):191–209.

Hanna, A.M., Das, B.M., and Foriero, A. (1988). *Behavior of Shallow Inclined Plate Anchors in Sand,* Geotech. Spec. Tech. Publ. No. 16, ASCE, 54–72.

Harvey, R.C. and Burley, E. (1973). Behavior of shallow inclined anchorages in cohesionless sand. *Ground Eng.,* 6(5):48–55.

Kanayan, A.S. (1966). Experimental investigation of the stability of bases of anchor foundations. *Soil Mech. Found. Eng. Moscow,* 3(6):9.

Maiah, A.A., Das, B.M., and Picornell, M. (1986). Ultimate resistance of shallow inclined strip anchor plate in sand. *Proc. Conf. Theor. and Appl. Mech.,* SECTAM XIII, Columbia, SC, 2, 503–509.

Merifield, R.S., Lyamin, A.V., and Sloan, S.W. (2005). Stability of inclined strip anchors in purely cohesive soil. *Geotech. Geoenviron. Eng.,* 131(6):792–799.

Meyerhof, G.G. (1973). Uplift resistance of inclined anchors and piles. *Proc. VIII Int. Conf. Soil Mech. Found. Eng.,* Moscow, 2.1, 167–172.

Meyerhof, G.G. and Adams, J.I. (1968). The ultimate uplift capacity of foundations. *Can. Geotech. J.,* 5(4):225–244.

Neely, W.J. Stuart, J.G., and Graham, J. (1973). Failure load of vertical anchor plates in sand. *J. Soil Mech. Found. Div. ASCE,* 99(9):669–685.

Sokolovskii, V.V. (1965). *Statics of Granular Media,* Pergamon Press, New York.

6

HELICAL ANCHORS IN SAND

At the present time, limited studies on helical anchors are available, the results of which can be used to estimate their ultimate uplift capacity. In many instances, the ultimate load estimate is based on rule of thumb. This chapter summarizes the existing theories relating to the prediction of the net ultimate uplift capacity of single-helix (screw) anchors and tapered multi-helix anchors embedded in sandy soils.

6.1 INTRODUCTION

Basic descriptions of helical anchors and their two main types, *single-helix (screw) anchors* and *multi-helix anchors,* are presented in Section 1.4. Figures 1.8 and 1.9 are photographs of helical anchors with single and dual helices, which are generally used for light to medium loads. However, at the present time, tapered multi-helix anchors (three to four helices) are commonly used to carry uplift loads up to about 550 to 600 kN. Figure 6.1 shows the typical dimensions of a multi-helix anchor used in the United States for construction of foundations of electrical transmission towers. These anchors are fairly easy to install and, hence, are cost effective.

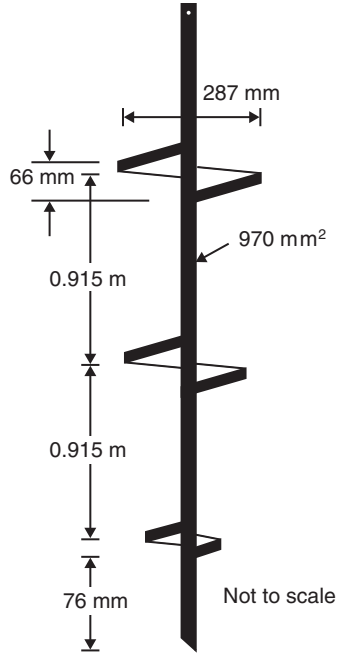

FIGURE 6.1 Typical multi-helix anchor used in the United States

6.2 SINGLE-HELIX (SCREW) ANCHORS

6.2.1 Ultimate Holding Capacity of Single-Helix (Screw) Anchors

Ghaly et al. (1991) presented experimental and theoretical investigations on the behavior of single-helix (screw) anchors in sand. Their laboratory testing program included 56 tests conducted on five model anchors installed in dense, medium, and loose dry sands. The screw elements were fabricated from high-quality mild steel as one unit, with no welded joints. The geometrical dimensions of one of the anchors used for testing dense sand are shown in Figure 6.2. The experimental setup was instrumented to allow the measurement of the pullout load and the upward displacement of the anchor and the deflection of the sand surface.

The experimental results show that the shape of the screw anchor has little effect or no influence on the uplift capacity of the anchor. For a given type of sand, the diameter of the first blade ($D = 2B_1$) of the screw element and the

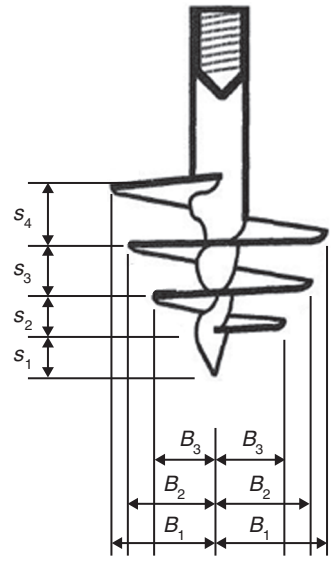

FIGURE 6.2 Dimensions of screw anchors used by Ghaly et al. (1991) (B_1 = 25 mm, B_2 = 20 mm, B_3 = 15 mm, s_1 = 7.5 mm, s_2 = 9 mm, s_3 = 12 mm, and s_4 = 15 mm)

anchor installation depth are the main factors that affect the pullout behavior. Typical pullout load versus upward displacement (u) curves for screw anchors installed in dense sand are shown in Figure 6.3. In this figure, H is the depth of the first blade from the ground surface. It has been observed that for a given installation depth, the pullout capacity increased with the increase in the value of the angle of shearing resistance; this effect is more at greater depths.

Figure 6.4 shows three modes of failure at ultimate load, on the basis of which the screw anchors were classified as (a) shallow screw anchor, (b) deep screw anchor, and (c) transit screw anchor. Shallow screw anchors fail in general shear failure and deep screw anchors in local shear failure. In the case of transit screw anchors, there is no clear distinction between shallow and deep anchors; thus a transit screw anchor in pullout fails under a combined failure mechanism. Figure 6.5 shows the variation of H/D with soil friction angle (ϕ) for shallow, transit, and deep anchors.

Assuming planar surfaces as shown in Figure 6.4, Ghaly et al. (1991) presented the expressions for the ultimate pullout capacity of shallow, transit, and deep screw anchors. They also assumed the following:

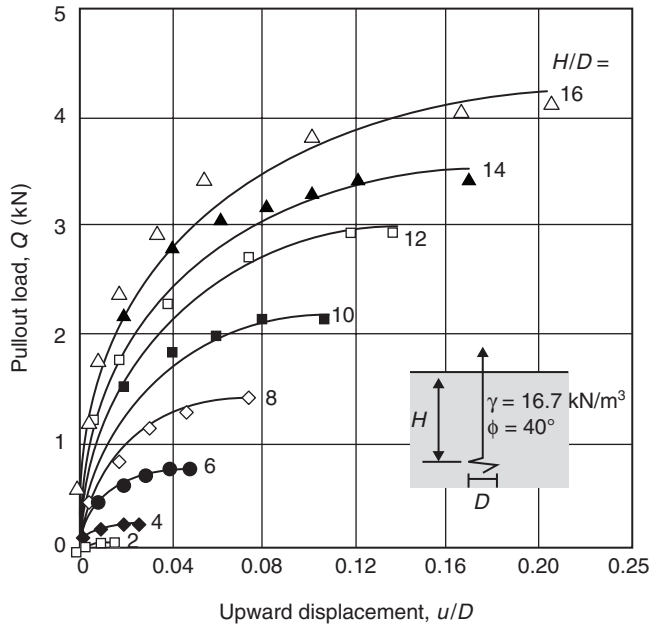

FIGURE 6.3 Typical pullout load versus upward displacement relationship for tests in dense sand ($D = 2B_1 = 50$ mm) (adapted from Ghaly et al., 1991)

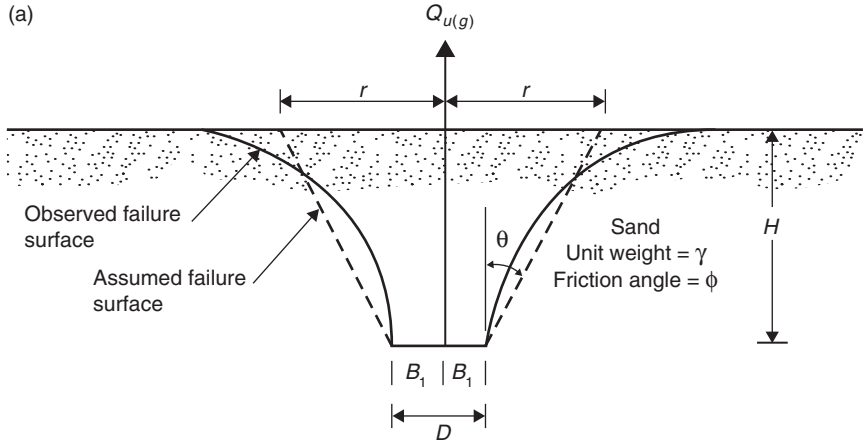

FIGURE 6.4 Assumed and observed failure surfaces in sand based on the study by Ghaly et al. (1991): (a) shallow screw anchor, (b) deep screw anchor, and (c) transit screw anchor

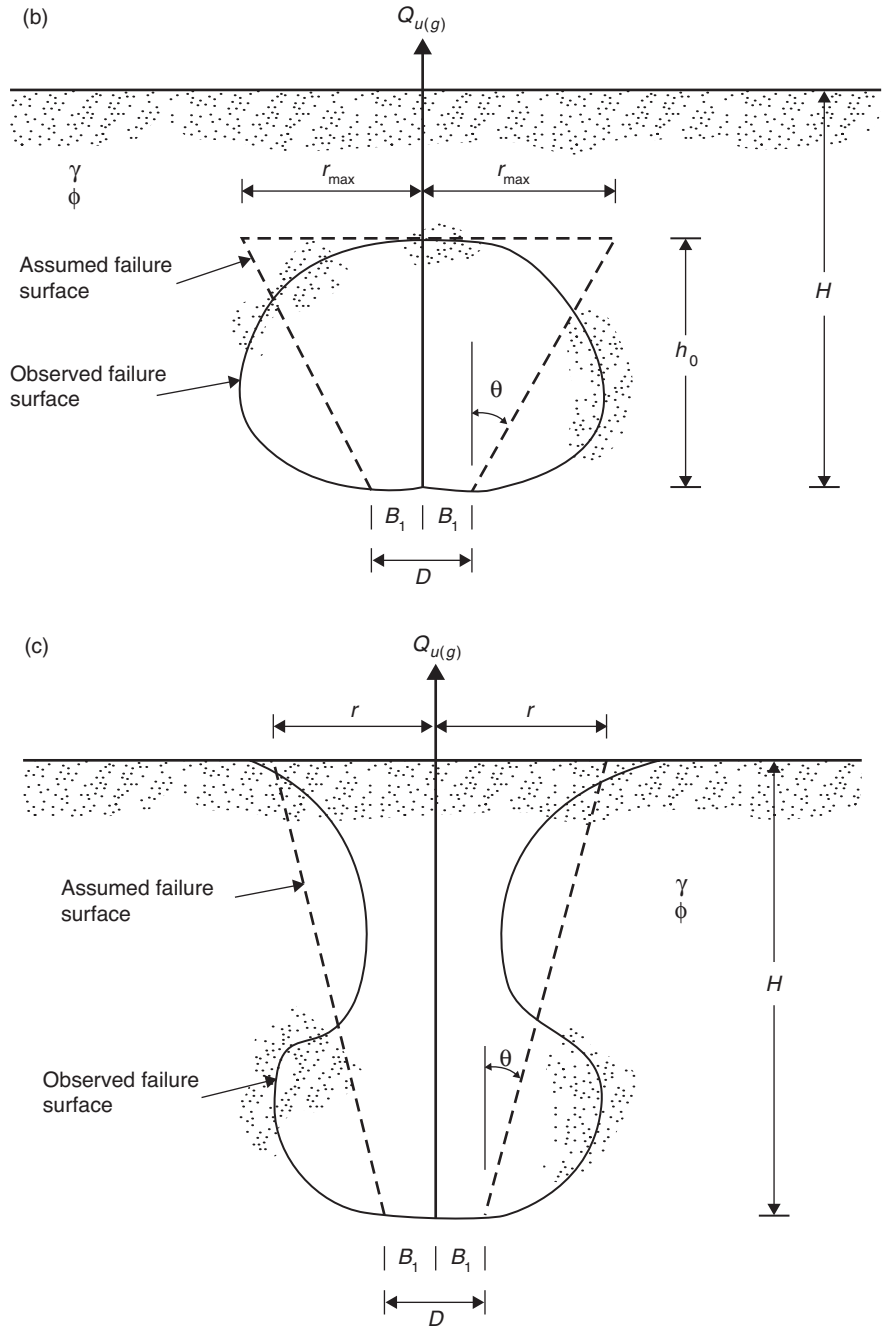

FIGURE 6.4 (continued)

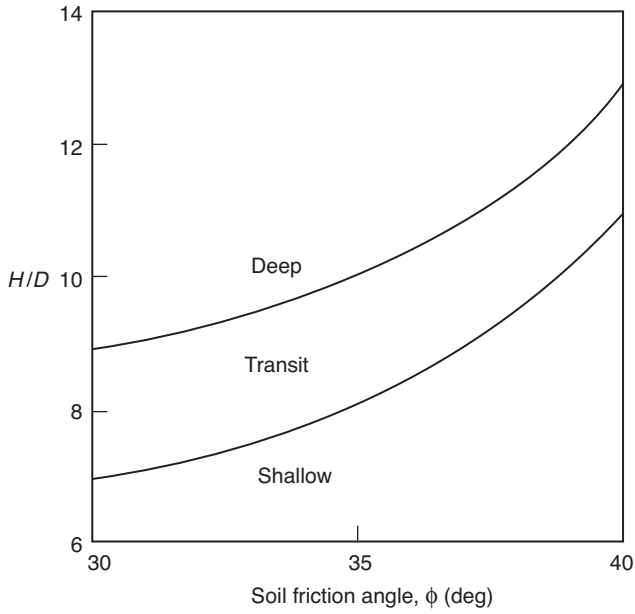

FIGURE 6.5 Variation of H/D with soil friction angle ϕ for shallow, transit, and deep anchors

1. The sand is homogeneous and isotropic, and it behaves in a nonlinear stress-strain relationship.
2. The disk of the screw anchor is thin and rigid, so that its deformation is negligible.
3. The screw anchor is in full contact with the surrounding sand medium.
4. There is no significant friction to be considered either on the tie-rod or on the surface of the screw blade.

For shallow or transit screw anchors:

$$Q_u = Q_{u(g)} - W_a$$

$$= \frac{\pi}{2}\gamma H^2 K_p' \left(\frac{D + H\tan\theta}{\cos\theta} \right) \tan\delta + \frac{\pi}{3}\gamma H (B_1^2 + r^2 + B_1 r) \qquad (6.1)$$

W

where

$Q_{u(g)}$ = gross ultimate pullout load
Q_u = net ultimate pullout load
ϕ = friction angle of sand
δ = average mobilized friction angle on the assumed plane of failure (see Figure 6.6)
D = diameter of the first blade of the screw anchor ($=2B_1$)
B_1 = radius of screw anchor
r = radius of influence failure circle on the sand surface
θ = surface inclination angle of inverted failure cone with respect to the vertical ($\approx \frac{2}{3}\phi$)
K'_p = modified coefficient of passive earth pressure (see Figure 6.7)
W = weight of sand within the failure wedge
W_a = effective self-weight of the anchor

In Equation 6.1:

$$r = B_1 + H \tan\left(\frac{2}{3}\phi\right) \leq r_{\max} \tag{6.2}$$

The variation of $r_{\max}$ is shown in Figure 6.8.

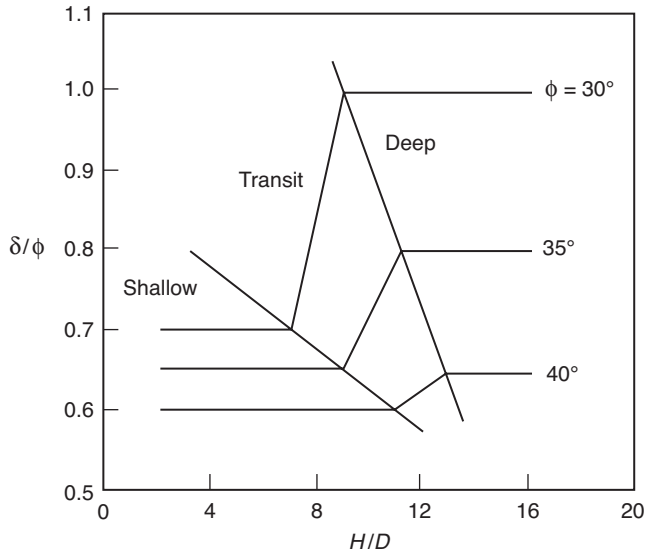

FIGURE 6.6 Variation of δ/ϕ with H/D and ϕ (based on Ghaly et al., 1991)

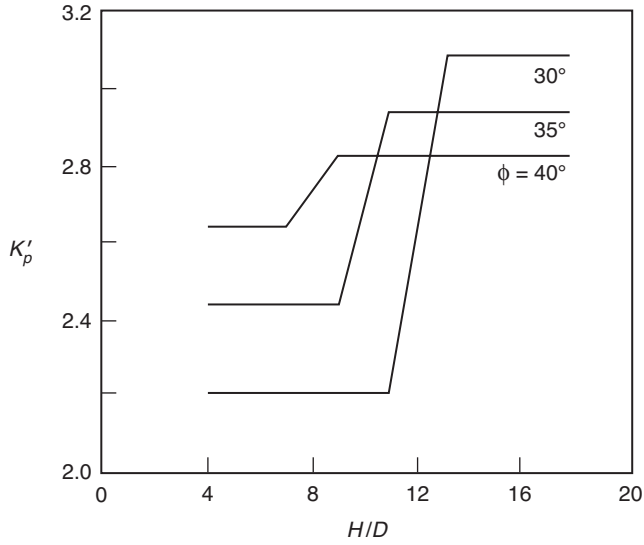

FIGURE 6.7 Variation of K'_p with H/D and ϕ (adapted from Ghaly et al., 1991)

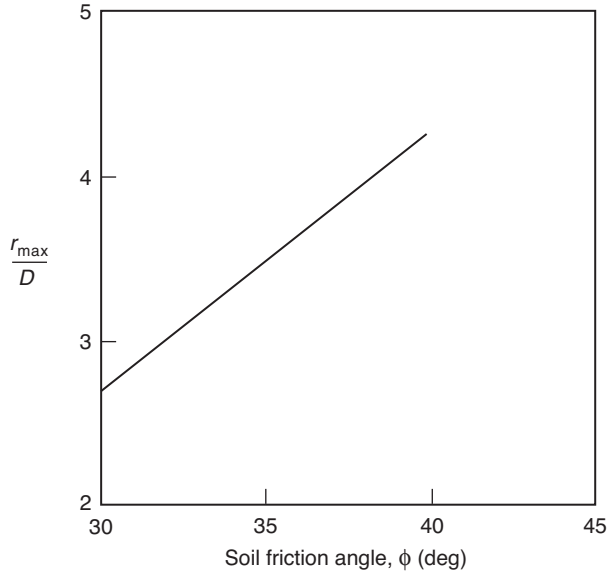

FIGURE 6.8 Variation of r_{max}/D with soil friction angle ϕ

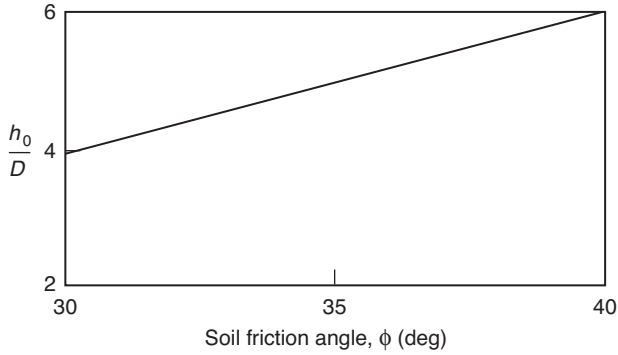

FIGURE 6.9 Variation of h_0/D with soil friction angle ϕ

For deep screw anchors:

$$Q_u = \frac{\pi}{2}\gamma K_p' h_0(2H - h_0)\left(\frac{D + h_0 \tan\theta}{\cos\theta}\right)\tan\delta + \frac{\pi}{3}\gamma h_0(B_1^2 + r_{\max}^2 + B_1 r_{\max}) + \gamma(H - h_0)\pi r_{\max}^2 \quad (6.3)$$

where

h_0 = height of the assumed inverted cone (Figure 6.4)

The variation of h_0/D with soil friction angle is shown in Figure 6.9.

Example 6.1

Consider a screw anchor in sand similar to the one shown in Figure 6.2, where $B_1 = 0.14$ m, $H = 2.24$ m, $\phi = 38°$, and unit weight of sand $\gamma = 16.5$ kN/m^3. Estimate the net ultimate pullout load Q_u.

Solution

$H = 2.24$ m and $D = (2)(0.14\text{ m}) = 0.28$ m.

$$\frac{H}{D} = \frac{2.24}{0.28} = 8$$

With $\phi = 38°$ and $H/D = 8$, Figure 6.5 shows that it is a shallow anchor. From Equation 6.1:

$$Q_u = \frac{\pi}{2}\gamma H^2 K_p' \left(\frac{D + H\tan\theta}{\cos\theta} \right) \tan\delta + \frac{\pi}{3}\gamma H(B_1^2 + r^2 + B_1 r)$$

From Figure 6.7 for $H/D = 8$ and $\phi = 38°$, $K_p' \approx 2.32$. From Figure 6.6 for $H/D = 8$ and $\phi = 38°$, $\delta/\phi \approx 0.62$, or:

$$\delta = (0.62)(38) = 23.56°$$

$$\theta = \left(\frac{2}{3}\right)\phi = \left(\frac{2}{3}\right)(38°) = 25.33°$$

$$r = B_1 + H\tan\theta = 0.14 + 2.24\tan 25.33° = 1.2 \text{ m}$$

From Figure 6.8 for $\phi = 38°$:

$$\frac{r_{max}}{D} \approx 3.9$$

or

$$r_{max} = (3.9)(0.29) = 1.09 \text{ m}$$

Since $r_{max} = 1.09 < r = 1.2$ m, use $r = 1.09$ m. Thus:

$$Q_u = \left(\frac{\pi}{2}\right)(16.8)(2.24)^2(2.32)\left[\frac{0.28 + (2.24)(\tan 25.33°)}{\cos 25.33°}\right]\tan 23.56°$$

$$+ \left(\frac{\pi}{3}\right)(16.8)(2.24)[(0.14)^2 + (1.09)^2 + (0.14)(1.09)]$$

$$= \mathbf{252.2\ kN}$$

Example 6.2

Refer to Example 6.1. Other parameters remaining the same, if H is changed to 3.64 m, calculate Q_u.

Solution

$$\frac{H}{D} = \frac{3.64}{0.28} = 13$$

With $\phi = 38°$ and $H/D = 13$, Figure 6.5 shows that it is a shallow anchor. From Equation 6.3:

$$Q_u = \frac{\pi}{2}\gamma K_p' h_0(2H - h_0)\left(\frac{D + h_0 \tan\theta}{\cos\theta}\right)\tan\delta$$

$$+ \frac{\pi}{3}\gamma h_0(B_1^2 + r_{\max}^2 + B_1 r_{\max}) + \gamma(H - h_0)\pi r_{\max}^2$$

From Figure 6.9 for $\phi = 38°$, $h_0/B \approx 5.7$:

$$h_0 = (5.7)(0.28) = 1.596 \text{ m}$$

From Figure 6.6 for $H/D = 13$, $\delta/\phi \approx 0.71$, or:

$$\delta = (0.71)(38) = 26.98°$$

For $\phi = 38°$ and $H/D = 13$, the value of K_p' is about 2.6 (Figure 6.7). Thus:

$$Q_u = \left(\frac{\pi}{2}\right)(16.8)(2.6)(1.596)[(2)(3.65) - (1.596)]$$

$$\left[\frac{0.28 + (1.596)(\tan 25.33°)}{\cos 25.33°}\right]\tan 26.98°$$

$$+ \left(\frac{\pi}{3}\right)(16.8)(1.596)[(0.14)^2 + (1.09)^2 + (0.14)(1.09)]$$

$$+ (16.8)(3.64 - 1.596)(\pi)(1.09)^2$$

$$= \mathbf{529.22\ kN}$$

6.2.2 Holding Capacity of Group of Single-Helix (Screw) Anchors

Ghaly and Hanna (1994) conducted model tests of groups of three, four, six, and nine screw anchors installed in sands. The effects of installation depth, spacing between anchors, and sand characteristics on the ultimate pullout load of the group were examined. This experimental investigation produced the following major findings:

1. The order of installation of the anchors has little influence on the uplift capacity of a group of screw anchors at failure, whereas it has some effect on the upward displacement of the individual anchors at a low level of applied uplifting load.
2. The central anchor or the central core of the anchors resists a portion of uplift load, which is greater than that resisted by the exterior ones. This is true at a low level of uplifting load, whereas the amount of contribution of resistance to uplifting load is almost the same for all anchors at ultimate load.
3. The upward displacement at a given point of a group cap is a function of the load portion resisted by the particular anchor located at that point. In comparison with the average uplift load and average upward displacement of the group, greater uplifting resistance is associated with smaller displacement.
4. The upward displacement of an anchor representing the average of a group is generally greater than that of a single anchor under the same loading conditions.
5. For medium and loose sands, the group efficiency increases with anchor spacing and decreases with the increase in group size. The group efficiency is not affected too much by the spacing between anchors for groups installed at greater depth in dense sand compared to those placed at relatively shallow depths. Efficiency is greater than 100% for groups installed at relatively greater depths, and it decreases with increased spacing.
6. Installation of a group of screw anchors in sand deposits results in an increase in the lateral confining stress around it and in the near vicinity of the anchors. This results in an increase in the strength properties of the sand. This effect is significant, especially in the case of dense sand.

6.3 MULTI-HELIX ANCHORS

6.3.1 Geometric Parameters and Failure Mode

Figure 6.10 shows a tapered multi-helix anchor embedded in soil subjected to a vertical uplifting force. The diameter of the top helix is D_1 and that of the bottom helix is D_n. The distance between the ground surface and the top helix is H_1, and, similarly, the distance between the bottom helix and the ground surface is H_n. The gross and net ultimate uplift capacities of the anchor can be expressed as:

$$Q_{u(g)} = Q_u + W_a \tag{6.4}$$

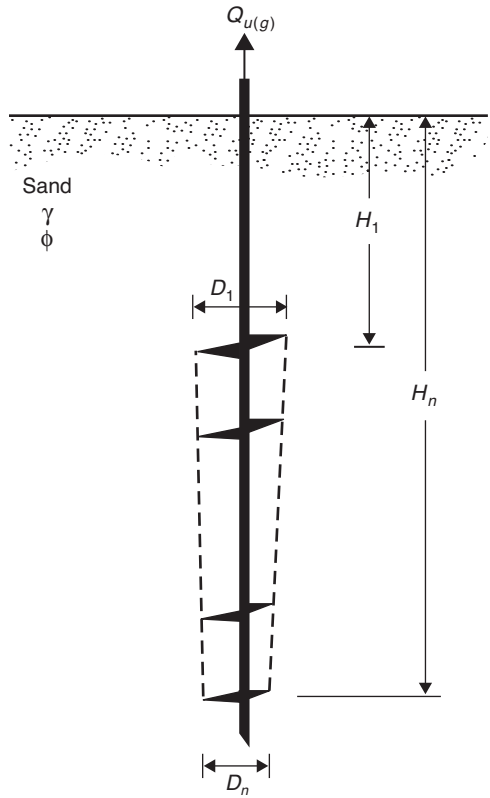

FIGURE 6.10 Tapered multi-helix anchor embedded in sand and subjected to uplift

where

$Q_{u(g)}$ = gross ultimate uplift capacity
Q_u = net ultimate uplift capacity
W_a = effective self-weight of the anchor

Using laboratory model tests, Mitsch and Clemence (1985) studied the failure surface in soil around a helical anchor at ultimate load. Figure 6.11 shows a schematic diagram of the failure pattern for the condition where the embedment ratio H_1/D_1 is relatively small. For this case, it can be seen that:

1. The failure surface above the top helix is a truncated cone extending to the ground surface. The central angle of the truncated cone is approximately equal to the soil friction angle ϕ.
2. Below the top helix, the failure surface in soil is approximately cylindrical. This means that the interhelical soil below the top helix acts similar

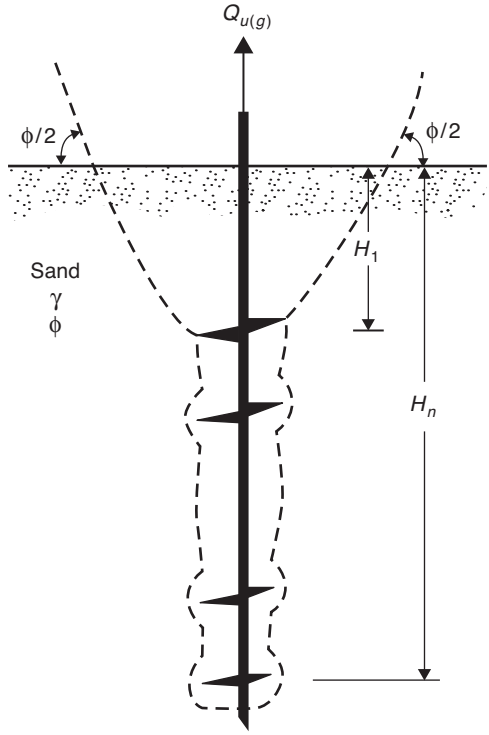

FIGURE 6.11 Typical failure pattern in sand around a multi-helix anchor for shallow anchor condition

to a pile foundation, with shear failure occurring along the interface boundary.

When the conical failure surface of soil located above the top helix extends to the ground surface, it is referred to as the shallow anchor condition. However, if the anchor is located in such a way that H_1/D_1 is fairly large, the failure surface in soil does not extend to the ground surface, as shown in Figure 6.12. This is referred to as the deep anchor condition.

In granular soils, the limiting value of $H_1/D_1 = (H_1/D_1)_{cr}$ at which the anchor condition changes from shallow to deep is similar to that suggested by Meyerhof and Adams (1968). The following are values of $(H_1/D_1)_{cr}$ for various soil friction angles. These variations are also shown in Figure 6.13.

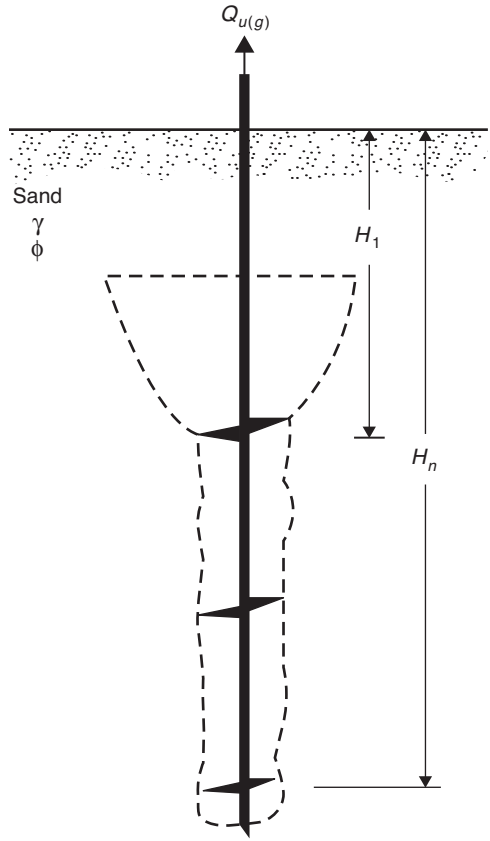

FIGURE 6.12 Typical failure pattern in sand around a multi-helix anchor for deep anchor condition

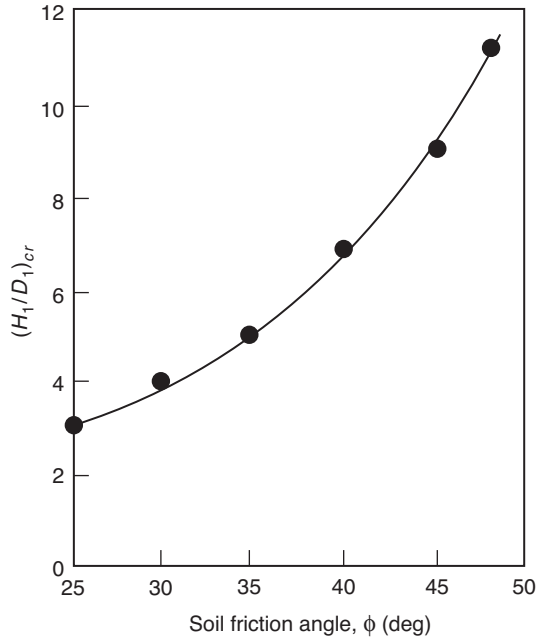

FIGURE 6.13 Variation of $(H_1/D_1)_{cr}$ with soil friction angle ϕ

Soil friction angle, ϕ (deg)	$(H_1/D_1)_{cr}$
25	3
30	4
35	5
40	7
45	9
48	11

6.3.2 Net Ultimate Uplift Capacity for Shallow Anchor Condition

Figure 6.14 shows an idealized failure surface in soil around a helical anchor at ultimate load. The net ultimate load can be approximately estimated according to the procedure outlined by Mitsch and Clemence (1985), or:

$$Q_u = Q_p + Q_f \tag{6.5}$$

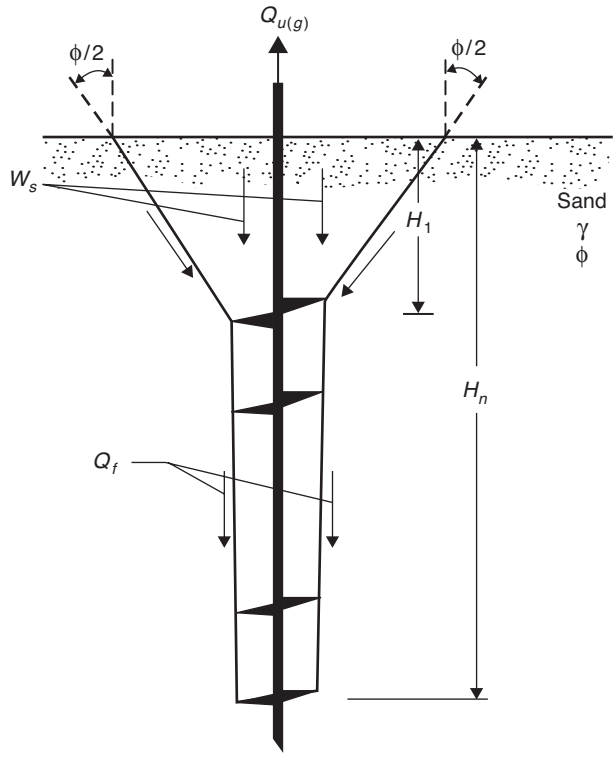

FIGURE 6.14 Idealized failure surface in sand for shallow anchor condition where $(H_1/D_1) \leq (H_1/D_1)_{cr}$

where

Q_p = bearing resistance for the top helix
Q_f = frictional resistance derived at the interface of the interhelical soil, which is cylindrical in shape

The magnitude of Q_p can be given as:

$$Q_p = \pi\gamma K_u \tan\phi \left[\cos^2\left(\frac{\phi}{2}\right)\right]\left[\frac{D_1 H_1^2}{2} + \frac{H_1^3 \tan\left(\frac{\phi}{2}\right)}{3}\right] + W_s \quad (6.6)$$

where

γ = unit weight of soil
ϕ = soil friction angle
K_u = coefficient of lateral earth pressure at uplift
W_s = weight of the soil in the failure zone

The weight of the soil W_s can be expressed as:

$$W_s = \gamma \left\{ \frac{\pi}{12} H_1 \left[D_1^2 + \left(D_1 + 2H_1 \tan \frac{\phi}{2} \right)^2 + D_1 \left(D_1 + 2H_1 \tan \frac{\phi}{2} \right) \right] \right\} \tag{6.7}$$

The magnitude of Q_p can be expressed in a nondimensional form as:

$$F_q = \frac{Q_p}{\gamma A H_1} \tag{6.8}$$

where

$$A = \frac{\pi}{4} D_1^2$$

Now,

$$\frac{\pi \gamma K_u \tan \phi \left[\cos^2 \left(\frac{\phi}{2} \right) \right] \left[\frac{D_1 H_1^2}{2} + \frac{H_1^3 \tan \left(\frac{\phi}{2} \right)}{3} \right]}{\gamma A H_1}$$

$$= \frac{\pi\gamma K_u \tan\phi \left[\cos^2\left(\frac{\phi}{2}\right)\right] H_1^3 \left[\frac{D_1}{2H_1} + \frac{\tan\left(\frac{\phi}{2}\right)}{3}\right]}{\gamma\left(\frac{\pi}{4} D_1^2\right) H_1}$$

$$= 4K_u \tan\phi \left[\cos^2\left(\frac{\phi}{2}\right)\right] \left(\frac{H_1}{D_1}\right)^2 \left[\frac{0.5}{\left(\frac{H_1}{D_1}\right)} + 0.333 \tan\left(\frac{\phi}{2}\right)\right] \quad (6.9)$$

Similarly:

$$\frac{W_s}{\gamma A H_1} = \frac{\frac{\pi\gamma H_1}{12}\left\{D_1^2 + \left[D_1^2 + 4H_1^2 \tan^2\left(\frac{\phi}{2}\right) + 4D_1 H_1 \tan\left(\frac{\phi}{2}\right)\right] + \left[D_1^2 + 2H_1 D_1 \tan\left(\frac{\phi}{2}\right)\right]\right\}}{\gamma\left(\frac{\pi}{4} D_1^2\right) H_1}$$

$$= 1 + 1.33\left(\frac{H_1}{D_1}\right)^2 \tan^2\frac{\phi}{2} + 2\left(\frac{H_1}{D_1}\right)\tan\left(\frac{\phi}{2}\right) \quad (6.10)$$

Let

$$\frac{H_1}{D_1} = G \quad (6.11)$$

Now, combining, Equations 6.6, 6.8, 6.9, 6.10, and 6.11, we obtain:

$$F_q = \frac{Q_p}{\gamma A H_1} = 4G^2 K_u \tan\phi \left[\cos^2\left(\frac{\phi}{2}\right)\right]\left[\frac{0.5}{G} + 0.333\tan\left(\frac{\phi}{2}\right)\right] + 1 + 1.33G^2\tan^2\left(\frac{\phi}{2}\right) + 2G^2\tan\left(\frac{\phi}{2}\right) \tag{6.12}$$

In order to determine the breakout factor F_q, we need to determine the magnitude of the coefficient of lateral earth pressure in uplift, K_u. The variation of K_u with soil friction angle ϕ suggested by Mitsch and Clemence (1985) can be expressed in the form

$$K_u = 0.6 + m\left(\frac{H_1}{D_1}\right) \tag{6.13}$$

where

m = a coefficient that is a function of the soil friction angle ϕ

The variation of m is given in Table 6.1 and also in Figure 6.15.

The magnitude of K_u increases with H_1/D_1 up to a maximum value and remains constant thereafter. This maximum value is attained at $(H_1/D_1)_{cr} = G_{cr}$. Based on this concept, the variations of K_u with H_1/D_1 and ϕ have been calculated and are shown in Figure 6.16. Substituting proper values of K_u and G into Equation 6.12, the variations of the breakout factor were calculated and are shown in Figure 6.17. Note that these plots are for $H_1/D_1 \leq (H_1/D_1)_{cr}$. Hence:

$$Q_p = \frac{\pi}{4} F_q \gamma D_1^2 H_1 \tag{6.14}$$

Again, referring to Equation 6.5, the frictional resistance derived at the interface of the interhelical soil can be given as:

$$Q_f = \frac{\pi}{2} D_a \gamma (H_n^2 - H_1^2) K_u \tan\phi \tag{6.15}$$

where

TABLE 6.1 Variation of *m*

Soil friction angle, ϕ (deg)	*m*
25	0.033
30	0.075
35	0.18
40	0.25
45	0.289

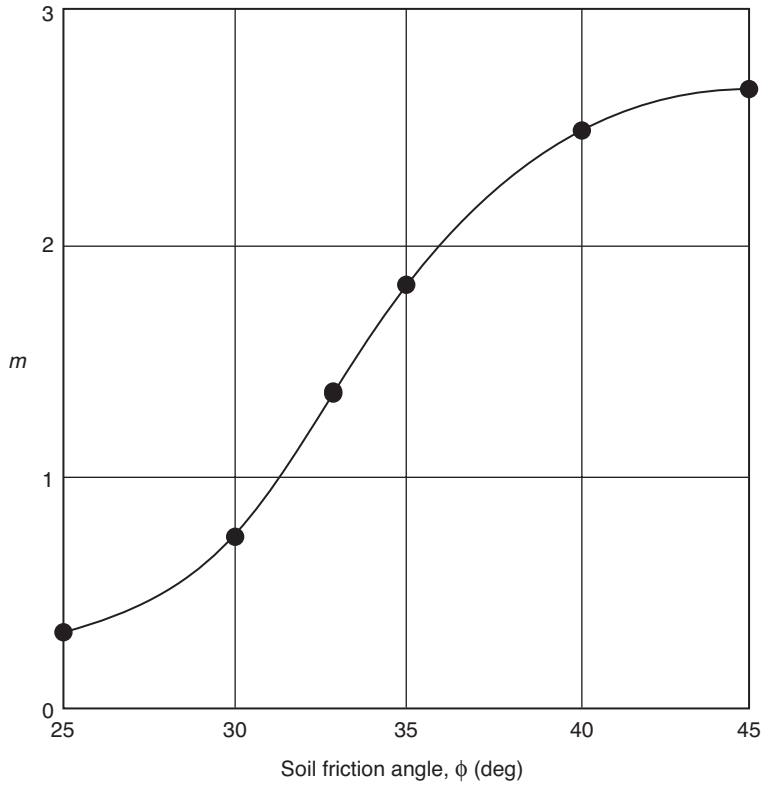

FIGURE 6.15 Variation of *m* with soil friction angle ϕ from Equation 6.10

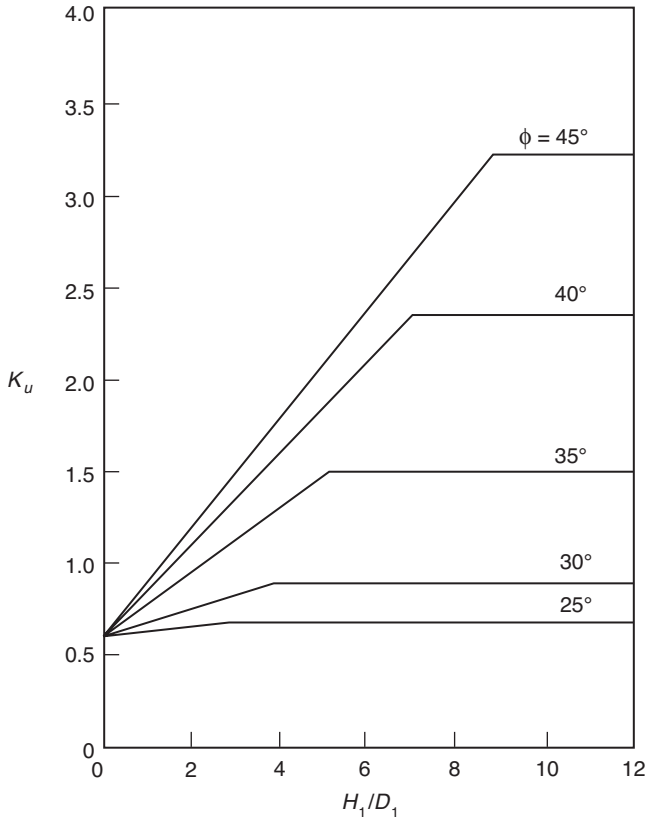

FIGURE 6.16 Variation of K_u with H_1/D_1

D_a = average helix diameter = $(D_1 + D_n)/2$

Thus, the net ultimate uplift capacity can be given as (Equations 6.5, 6.6, and 6.15):

$$Q_u = \pi\gamma K_u \tan\phi \left[\cos^2\left(\frac{\phi}{2}\right)\right] \left[\frac{D_1 H_1^2}{2} + \frac{H_1^3 \tan\left(\frac{\phi}{2}\right)}{3}\right] + W_s + \left(\frac{\pi}{2}\right)\left(\frac{D_1 + D_n}{2}\right)(\gamma)\,(H_n^2 - H_1^2)\,K_u \tan\phi \tag{6.16}$$

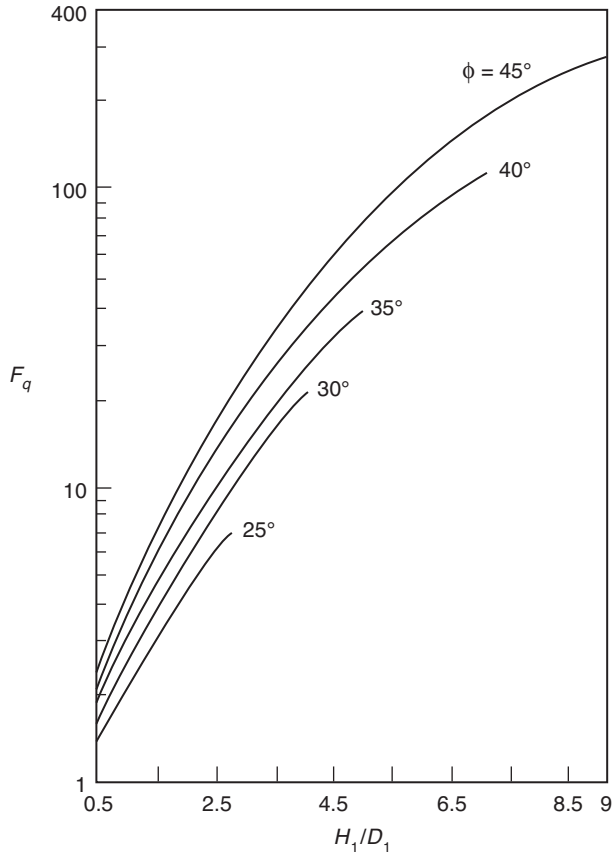

FIGURE 6.17 Variation of breakout factor with H_1/D_1 for shallow condition

or

$$Q_u = \frac{\pi}{4} F_q \gamma D_1^2 H_1 + \left(\frac{\pi}{2}\right)\left(\frac{D_1 + D_n}{2}\right)(\gamma)\,(H_n^2 - H_1^2)\,K_u \tan\phi \qquad (6.17)$$

Equation 6.14 Equation 6.15

When using Equation 6.17, the following facts need to be kept in mind:

1. The breakout factors F_q shown in Figure 6.17 have been calculated using the values of K_u (as shown in Figure 6.16) for given H_1/D_1 ratios. De-

pending on the H_1/D_1 ratio of a given anchor, the magnitude of F_q can be selected from Figure 6.17 and used in Equation 6.17.

2. It is recommended that the K_u value to be used in Equation 6.15 (which is the second term on the right-hand side of Equation 6.17) should be the maximum value (for the given friction angle). This means that:

$$K_u = 0.6 + m\left(\frac{H_1}{D_1}\right)_{cr}$$

The following are the maximum values of K_u for various soil friction angles ϕ:

Soil friction angle, ϕ (deg)	Maximum value of K_u
25	0.7
30	0.9
35	1.5
40	2.35
45	3.2

Example 6.3

Figure 6.18 shows a tapered multi-helix anchor. For the sand, $\gamma = 102$ lb/ft^3 and $\phi = 35°$. For the anchor, $D_1 = 12$ in., $D_n = 7.5$ in., $H_1 = 3$ ft, and $H_n = 10$ ft. Determine the net ultimate uplift capacity.

Solution

From Equation 6.17:

$$Q_u = \frac{\pi}{4} F_q \gamma D_1^2 H_1 + \left(\frac{\pi}{2}\right)\left(\frac{D_1 + D_n}{2}\right)(\gamma)(H_n^2 - H_1^2) K_u \tan\phi$$

From Figure 6.17, for $\phi = 35°$ and $H_1/D_1 = 3/1 = 3$, the magnitude of F_q is 11.19. Also for $\phi = 35°$, the maximum value of K_u is 1.5. Therefore:

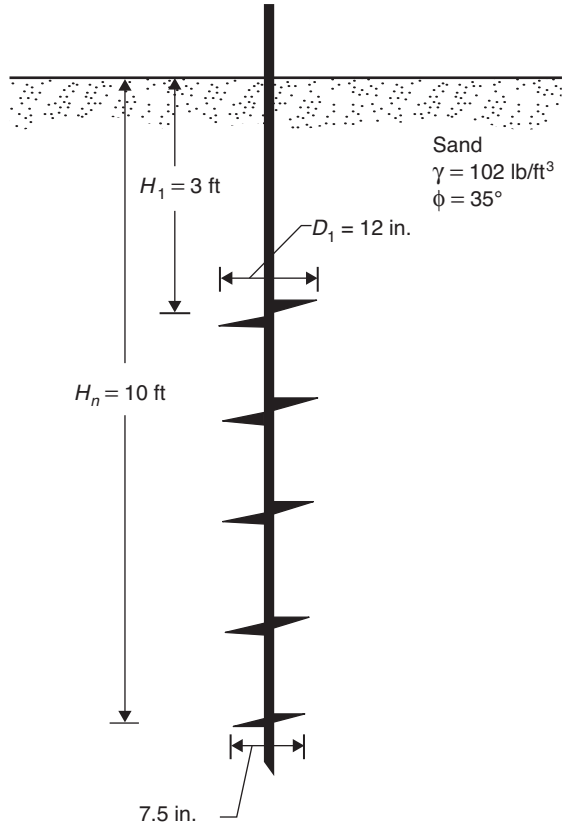

FIGURE 6.18 Example 6.3

$$Q_u = \left(\frac{\pi}{4}\right)(11.19)\,(102)\left(\frac{12}{12}\right)^2(3)$$

$$+ \left(\frac{\pi}{2}\right)\left[\frac{12 + 7.5}{(2)\,(12)}\right](102)\,(10^2 - 3^2)\,(15)\,(\tan 35°)$$

$$= 2689.4 + 12{,}442.4$$

$$\approx \mathbf{15{,}132\ lb}$$

6.3.3 Net Ultimate Uplift Capacity for Deep Anchor Condition

Figure 6.19 shows the idealized failure surface in soil around a deep helical anchor embedded in sand. For this condition (Mitsch and Clemence, 1985):

$$Q_u = Q_p + Q_f + Q_s \tag{6.18}$$

In the preceding equation, Q_p and Q_f are, respectively, the bearing resistance of the top helix and the frictional resistance at the interface of the interhelical

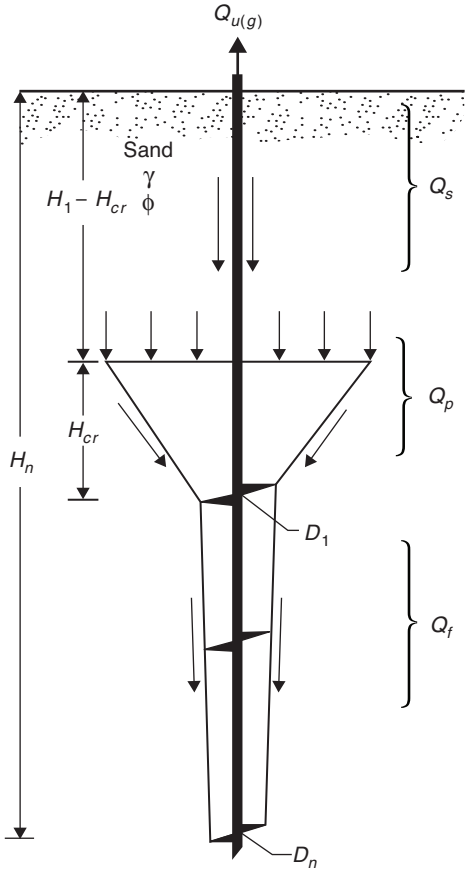

FIGURE 6.19 Idealized failure surface in sand for deep anchor condition

soil. The term Q_s is the frictional resistance derived from friction at the soil-anchor shaft interface above the top helix. It is recommended by the authors that, due to various uncertainties involved in the determination of the soil parameters, the anchor resistance Q_s may be neglected. Hence:

$$Q_u \approx Q_p + Q_f \tag{6.19}$$

6.3.3.1 Bearing Resistance, Q_p

The bearing resistance Q_p of the top helix can easily be determined in terms of the breakout factor (as in Equation 6.14), or:

$$Q_p = \frac{\pi}{4} F_q^{\star} \gamma D_1^2 H_1 \tag{6.20}$$

where

$F_q^{\star}$ = deep anchor breakout factor

The magnitude of $F_q = F_q^{\star}$ can be determined easily by substituting G and G_{cr} and $K_u = K_{u(\max)}$ in Equation 6.12. The variation of $F_q^{\star}$ has been calculated in this manner and is plotted against the soil friction angle ϕ in Figure 6.20.

6.3.3.2 Frictional Resistance, Q_f

The frictional resistance Q_f can be estimated by using Equation 6.15, or:

$$Q_f = \frac{\pi}{2} D_a \gamma (H_n^2 - H_1^2) K_{u(\max)} \tan \phi \tag{6.21}$$

where

$$D_a = \frac{D_1 + D_n}{2} \tag{6.22}$$

6.3.3.3 Net Ultimate Uplift Capacity

Equations 6.20 to 6.22 can now be substituted in Equation 6.17 to obtain the net ultimate uplift capacity. Thus:

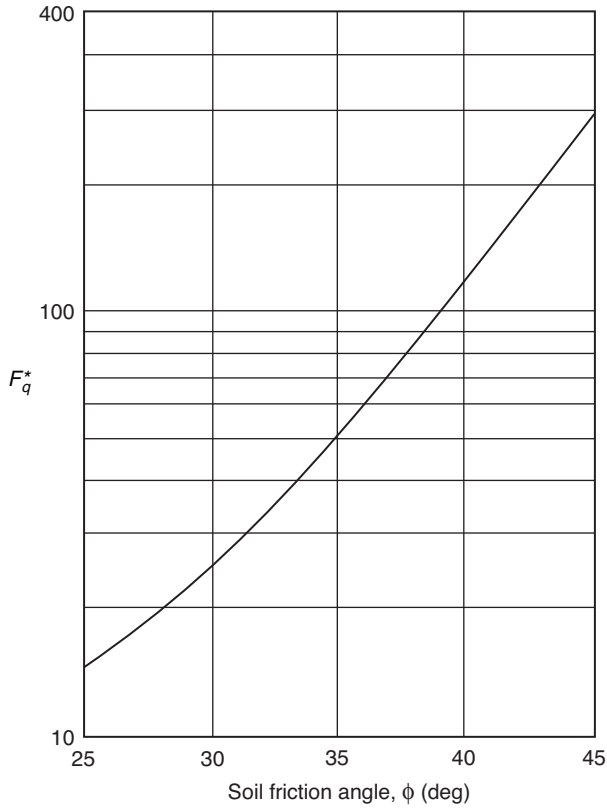

FIGURE 6.20 Variation of F_q^* with soil friction angle ϕ

$$Q_u = \frac{\pi}{4} F_q^* \gamma D_1^2 H_1 + \left(\frac{\pi}{2}\right)\left(\frac{D_1 + D_n}{2}\right)(\gamma)(H_n^2 - H_1^2) K_{u(\max)} \tan \phi \tag{6.23}$$

6.4 INTERFERENCE OF CLOSELY SPACED ANCHORS

If helical anchors are placed too close to each other, the average net ultimate uplift capacity of each anchor may decrease due to the interference of the failure zones in soil located around the anchors. Laboratory model test results have shown that for the noninterference of the anchor failure zones, the optimum

center-to-center spacing in loose and dense sands should be $6D_1$ and $10D_1$, respectively. In any case, it is recommended that the minimum center-to-center spacing of the anchors should be about $5D_1$. A factor of safety of at least 2.5 should be used for estimation of the net allowable uplift capacity.

6.5 OTHER STUDIES

Although both vertical and inclined anchors can be used to resist pullout forces and overturning moments, inclined anchors are more adaptable for resisting overturning moments. Electric power transmission towers and retaining walls supporting deep excavation are typical examples of structures in which inclined anchors are used. Ghaly and Clemence (1998) presented results of experimental and theoretical investigations on the performance of axially loaded, inclined single-helix (screw) anchors installed in sand. Anchors were oriented at 15°, 30°, and 45° with respect to the vertical, and the results were compared with the behavior of vertical anchors under similar conditions. The rupture surface of inclined anchors is complex and difficult to represent geometrically. The boundaries of the rupture surface are segments of logarithmic spiral curves, and their poles differ from one location to another along the perimeter. The rupture surface propagates to the ground surface in the case of shallow anchors in sand, whereas the rupture surface is of a local nature in the case of deep anchors. The results show that the critical depth ratios for inclined anchors are slightly less than those of vertical anchors installed to the same vertical depth in identical sand conditions.

Ghaly and Hanna (2003) carried out experimental investigation on the effect of variations in displacement-based loading on the pullout capacity of single-helix (screw) anchors in sand. Anchors were installed to, and tested at, shallow and deep depths. The results show that variation of displacement-based loading has some effect on the pullout capacity of shallow anchors but has only a slight effect on deep anchors. For a given depth of installation and a given sand state, the ultimate pullout load of an anchor decreases with increasing loading rate. This effect is more pronounced in anchors installed to shallow depths.

6.6 SUMMARY OF MAIN POINTS

1. The shape of the single-helix (screw) anchor has practically no influence on the uplift capacity of the anchor.

2. The group efficiency is not greatly affected by the spacing between anchors for groups installed in dense sand at relatively shallow depths. Efficiency is more than 100% for groups installed at relatively greater depths, and it decreases with increased spacing.
3. The failure surface above the top helix of a multi-helix anchor is a truncated cone that extends to the ground surface. Below the top helix, the failure surface in soil is approximately cylindrical.
4. Due to various uncertainties involved in the determination of the soil parameters, the anchor shaft resistance for the deep anchor condition may be neglected.
5. If helical anchors are placed too close to each other, the average net ultimate uplift capacity of each anchor may decrease due to the interference of the failure zones in soil located around the anchors.
6. The critical depth ratios for inclined anchors are slightly less than those of vertical anchors installed to the same vertical depth in identical sand.

SELF-ASSESSMENT QUESTIONS

Select the most appropriate answer to each multiple-choice question

6.1. Which of the following is the main factor that affects the pullout behavior of a single-helix (screw) anchor:
   a. shape of the single-helix anchor
   b. diameter of the first blade of the screw anchor
   c. anchor installation depth
   d. both b and c

6.2. Which of the following single-helix (screw) anchors fails in local shear failure:
   a. shallow anchor
   b. deep anchor
   c. transit anchor
   d. none of the above

6.3. For medium and loose sands, the anchor group efficiency:
   a. increases with anchor spacing
   b. decreases with group size
   c. both a and b
   d. decreases with anchor spacing

6.4. The central angle of the truncated cone failure surface in the case of a multi-helix anchor is approximately equal to:

a. the soil friction angle
b. half of the soil friction angle
c. one-third of the soil friction angle
d. two times the soil friction angle

6.5. If D is the diameter of the top helix, then for the noninterference of the anchor failure zones, the optimum center-to-center spacing of multi-helix anchors in dense sand should be:
a. $4D$
b. $6D$
c. $8D$
d. $10D$

Answers

6.1: d 6.2: b 6.3: c 6.4: a 6.5: d

REFERENCES

Ghaly, A.M. and Clemence, S.P. (1998). Pullout performance of inclined helical screw anchors in sand. *J. Geotech. Geoenviron. Eng.,* 124(7):617–627.

Ghaly, A. and Hanna, A. (1994). Model investigation of the performance of single anchors and groups of anchors. *Can. Geotech. J.,* 31:273–284.

Ghaly, A. and Hanna, A. (2003). Response of anchors to variations in displacement-based loading. *Can. Geotech. J.,* 40:694–701.

Ghaly, A., Hanna, A., and Hanna, M. (1991). Uplift behaviour of screw anchors in sand. I: Dry sand. *J. Geotech. Eng.,* 117(5):773–793.

Meyerhof, G.G. and Adams, J.I. (1968). The ultimate uplift capacity of foundations. *Can. Geotech. J.,* 5(4):225–244.

Mitsch, M.P. and Clemence, S.P. (1985). The uplift capacity of helix anchors in sand. *Proc. Uplift Behavior of Anchor Foundations in Soil,* S.P. Clemence, Ed., ASCE, 26–47.

7

HELICAL ANCHORS IN CLAY

This chapter summarizes the existing theories relating to the prediction of the net ultimate uplift capacity of helical anchors embedded in clay under undrained condition. Recently, numerical modeling techniques have been used to investigate the behavior of multi-helix anchors in clay. This study also is briefly described in this chapter.

7.1 INTRODUCTION

Helical anchors are effective in resisting uplift forces in clay. They are usually installed into the clayey soil in an economical manner by using truck-mounted augering equipment. At the present time, only a few studies are available on this topic, the results of which can be used to estimate the ultimate uplift capacity of helical anchors in clay. This chapter presents the details on helical anchors embedded in clayey soil.

7.2 FAILURE MODE

Figure 7.1 shows a helical anchor embedded in a saturated clay with undrained cohesion c_u. The diameter of the top helix is D_1 and that of the bottom helix

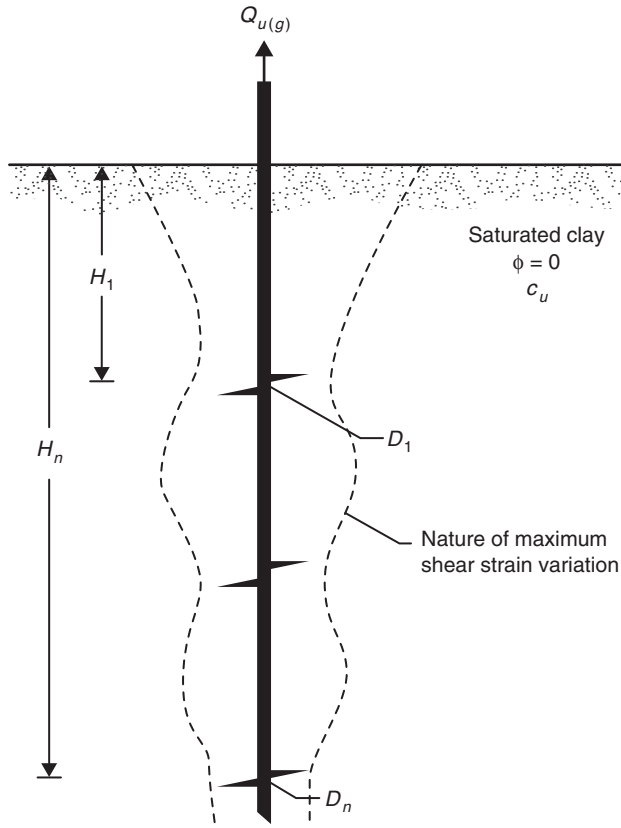

FIGURE 7.1 Failure mode in clay for shallow anchor condition

is D_n. The distance between the ground surface and the top helix is H_1, and, similarly, the distance between the bottom helix and the ground surface is H_n. If the H_1/D_1 ratio is relatively small (that is, *shallow anchor condition*), then at ultimate load, the failure surface located above the top helix extends to the ground surface. Laboratory model test results of Mooney et al. (1985) showed that the nature of the maximum shear strain variation along the length of the anchor will be as shown in Figure 7.1. However, if the H_1/D_1 ratio is relatively large, the failure surface in soil above the top helix does not extend to the ground surface (that is, local shear failure takes place). This is referred to as the *deep anchor condition*. Thus, following the recommendations of Mooney et al. (1985),

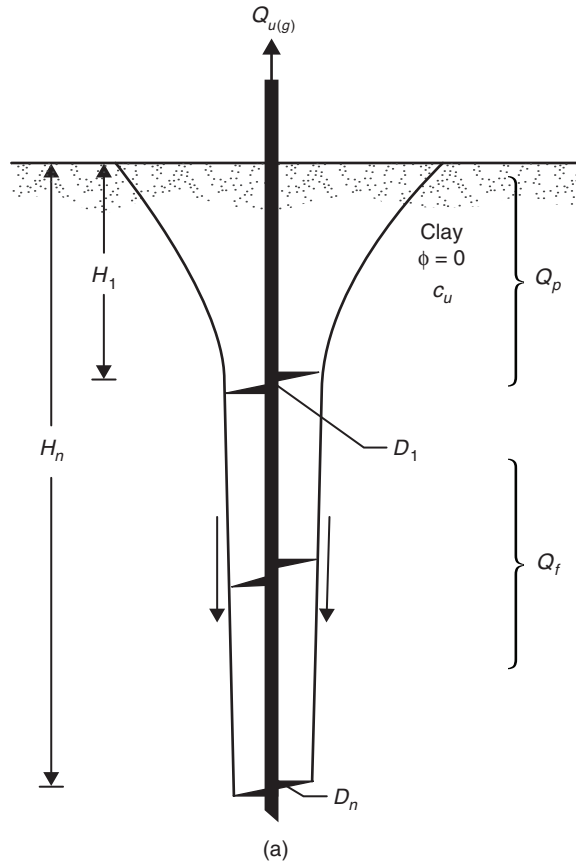

FIGURE 7.2 Idealized failure surface in clay at ultimate load: (a) shallow condition and (b) deep condition

the idealized failure surfaces in soil for shallow and deep anchor conditions are shown in Figures 7.2a and 7.2b, respectively.

7.3 NET ULTIMATE UPLIFT CAPACITY

The net ultimate uplift capacity of a helical anchor can be given as (Equation 6.4):

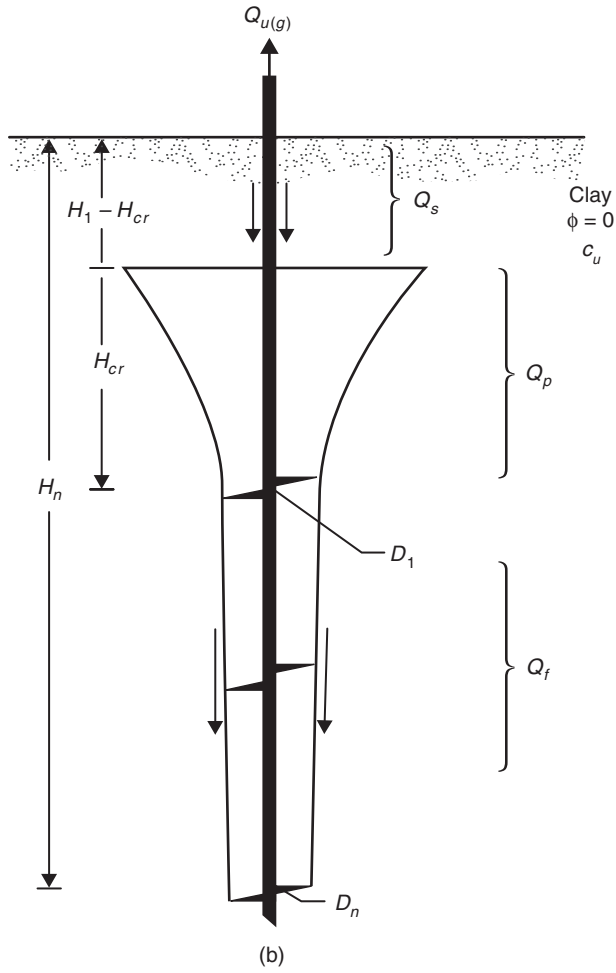

FIGURE 7.2 (continued)

$$Q_u = Q_{u(g)} - W_a \tag{7.1}$$

where

Q_u = net ultimate uplift capacity
$Q_{u(g)}$ = gross ultimate uplift capacity
W_a = effective self-weight of the anchor

For shallow anchors:

$$Q_u = Q_p + Q_f \tag{7.2}$$

where

Q_p = bearing resistance of the top helix
Q_f = resistance due to cohesion at the interface of the interhelical soil

Following the procedure for estimation of the uplift capacity of shallow plate anchors in clay, we can say that

$$Q_p = A(c_u F_c + \gamma H_1) \tag{7.3}$$

where

A = area of the top helix = $\frac{\pi}{4}(D_1^2)$
F_c = breakout factor
γ = unit weight of soil
H_1 = distance between the top helix and the ground surface

The magnitude of F_c increases with the H_1/D_1 ratio up to a maximum value of 9 at $(H_1/D_1)_{cr}$. The critical value of H_1/D_1 is a function of the undrained cohesion and can be expressed as (Das, 1980):

$$\left(\frac{H_1}{D_1}\right)_{cr} = 0.107c_u + 2.5 \leq 7 \tag{7.4}$$

where c_u is in kN/m^2.

The variation of the breakout factor F_c can be estimated from Figure 7.3, which is a plot of F_c versus $(H_1/D_1)/(H_1/D_1)_{cr}$.

The resistance due to cohesion at the interface of the interhelical soil can be approximated as (Mooney et al., 1985):

$$Q_f = \pi\left(\frac{D_1 + D_n}{2}\right)(H_n - H_1)\, c_u \tag{7.5}$$

Thus, combining Equations 7.2, 7.3, and 7.5, for the shallow anchor condition:

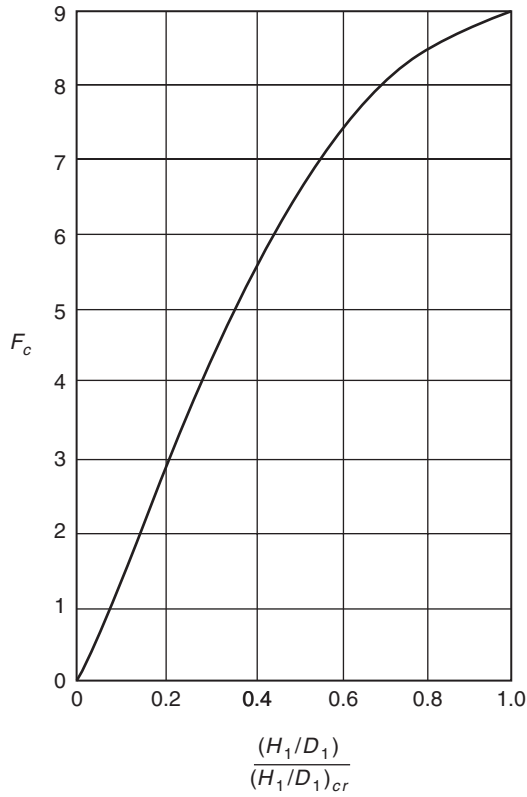

FIGURE 7.3 Variation of F_c versus $(H_1/D_1)/(H_1/D_1)_{cr}$

$$Q_f = \frac{\pi}{4}(D_1^2)(c_u F_c + \gamma H_1) + \pi\left(\frac{D_1 + D_n}{2}\right)(H_n - H_1)c_u \quad (7.6)$$

In a similar manner, for the deep anchor condition:

$$Q_u = Q_p + Q_f + Q_s \quad (7.7)$$

where

Q_s = resistance due to adhesion at the interface of the clay and the anchor shaft located above the top helix

The bearing resistance is

$$Q_p = \frac{\pi}{4}(D_1^2)(9c_u + \gamma H_1) \tag{7.8}$$

The expression for Q_f will be the same as given for the shallow anchor condition (Equation 7.5). The resistance due to adhesion at the interface of the clay and the anchor shaft located above the top helix can be approximated as:

$$Q_s = p_s H_1 c_a \tag{7.9}$$

where

p_s = perimeter of the anchor shaft
c_a = adhesion

The adhesion c_a may vary from about $0.3c_u$ for stiff clays to about $0.9c_u$ for very soft clays. Now, combining Equations 7.5, 7.7, 7.8, and 7.9, for the deep anchor condition:

$$Q_u = \frac{\pi}{4}(D_1^2)(9c_u + \gamma H_1) + \pi\left(\frac{D_1 + D_n}{2}\right)(H_n - H_1)c_u + p_s H_1 c_a \tag{7.10}$$

In all cases, a factor of safety of at least 3.0 is recommended for determination of the net allowable uplift capacity.

Example 7.1

Consider a multi-helix anchor embedded in a saturated clay where:

For the clay: $\gamma = 18.5$ kN/m^3
$c_u = 35$ kN/m^2
For the anchor: $D_1 = 0.4$ m, $D_n = 0.25$ m
$H_1 = 3$ m, $H_n = 7$ m
Diameter of the anchor shaft = 50 mm

Estimate the net ultimate uplift capacity.

Solution

$H_1 = 3$ m and $D_1 = 0.4$ m:

$$\frac{H_1}{D_1} = \frac{3}{0.4} = 7.5$$

From Equation 7.4, it can be seen that the maximum value of $(H_1/D_1)_{cr}$ is 7. Since the value of H_1/D_1 is 7.5, it is a deep anchor condition. Hence, from Equation 7.10:

$$Q_u = \frac{\pi}{4}(D_1^2)(9c_u + \gamma H_1) + \pi\left(\frac{D_1 + D_n}{2}\right)(H_n - H_1)\,c_u + p_s H_1 c_a$$

$$p_s = (\pi)\left(\frac{50}{1000}\right) = 0.157 \text{ m}$$

Assume $c_a \approx 0.5c_u = (0.5)(35) = 17.5$ kN/m^2. Therefore:

$$Q_u = \left(\frac{\pi}{4}\right)(0.4)^2\,[(9)(35) + (18.5)(3)] + (\pi)\left(\frac{0.4 + 0.25}{2}\right)(7 - 3)(35) + (0.157)(3)(17.5)$$

$$= 47.6 + 142.9 + 8.24$$

$$= \mathbf{197.74\ kN}$$

7.4 NUMERICAL MODELING SOLUTION

Merifield (2011) presented a numerical study based on ABAQUS displacement finite element software to understand the behavior of the multi-helix anchor in

clay. The ABAQUS model consisted of two parts: the anchor and the soil. An axisymmetric stress state was adopted to model the circular helices with a vertical line of symmetry existing through the center of the anchor shaft. For a fully bonded or deep helix, the ABAQUS finite element solution for the anchor breakout factor was found to be 12.61. The results indicate that there is only a small reduction in the capacity of the shallowest helix owing to the presence of helices below it. However, for practical design purposes, the breakout factor for the uppermost helix is largely unaffected by the location of the helices below. The capacity of helices below the shallowest helix is largely independent of the embedment ratio H/D (H = depth of top helix from the ground surface, D = helix diameter), provided $H/D > 2$. The ultimate capacity of each helix along the shaft increases linearly with overburden pressure up to a limiting value. At a given embedment depth, an anchor may behave as either shallow or deep, depending on the dimensionless overburden ratio $\gamma H/c_u$. If all the helices are deep and act independently of each other, then the ultimate pullout capacity can be given as:

$$Q_u = 3n\pi(1 + \pi)\left(\frac{D^2}{4}\right)c_u \tag{7.11}$$

where

n = number of helices
D = helix diameter

The critical anchor spacing $(S/D)_{cr}$, where S is the spacing of helices along the shaft, at which the transition between overall and individual deep anchor failure occurs can be given by:

$$\left(\frac{S}{D}\right)_{cr} = \frac{6(1 + \pi)}{5\pi} \tag{7.12}$$

Merifield (2011) compared the numerical results for the ultimate capacity with the ultimate capacities estimated by Narasimha Rao et al. (1991, 1993) based on the cylindrical shear method. This comparison shows that the cylindrical failure surface method overestimates the capacity by as much as 70%. However, according to Narasimha Rao et al. (1993), the cylindrical failure surface method incorporating spacing ratios ($S/D \leq 1.5$) results in good estimates of capacities. Therefore, in view of the lack of a more realistic understanding, the

authors suggest that a minimum factor of safety of 3.0 should be used to estimate the net allowable capacity from the ultimate capacity based on the cylindrical failure surface method, which was mentioned in the previous section.

7.5 USE OF *IN SITU* TESTS TO PREDICT UPLIFT PERFORMANCE

Lutenegger et al. (1988) conducted various types of *in situ* tests to determine the soil shear strength parameters for prediction of the net ultimate uplift capacity of multi-helix anchors. These tests included the following:

- Electric cone penetrometer
- Piezocone penetrometer
- Marchetti dilatometer
- Borehole shear test
- Pencel pressuremeter
- Menard three-cell and mono-cell pressuremeters
- Vane shear

Based on their tests, Lutenegger et al. concluded that in sand and clay, the best results were obtained from the cone penetrometer and dilatometer tests.

7.6 OTHER STUDIES

Narasimha Rao et al. (1993) described an experimental program carried out to investigate the behavior of multi-helix anchors at different embedment ratios (H_1/D_1 values) in soft marine clays. The results indicate that the anchor capacity increases with increasing embedment ratio. At any depth of embedment, the components contributing to uplift capacity are cohesive resistance between top and bottom helices, bearing on the top helix, and shaft adhesion above it. The anchors were classified as shallow anchor ($H_1/D_1 \leq 2$), transition anchor ($2 < H_1/D_1 \leq 4$), and deep anchor ($H_1/D_1 > 4$). The study shows that the spacing of helices affects the uplift capacity significantly. The cylindrical failure surface method, incorporating spacing ratios ($SR \leq 1.5$), results in good estimates of uplift capacities. (Note: SR is the spacing between any two adjacent helices divided by their average diameter.) In the case of anchors with helices at spacing ratios higher than 1.5 to 2.0, the individual helix bearing method gives a nominal underestimate of the uplift capacities.

7.7 SUMMARY OF MAIN POINTS

1. Helical anchors are effective in resisting uplift forces in clay.
2. Shallow and deep anchor conditions occur with small and large values, respectively, of the embedment ratio H_1/D_1.
3. The anchor capacity increases with increasing embedment ratio H_1/D_1.
4. The critical value of the embedment ratio H_1/D_1 of a helical anchor in clay is a function of the undrained cohesion of the clay.
5. For practical design purposes, the breakout factor for the uppermost helix is largely unaffected by the location of the helices below.
6. The ultimate capacity of each helix along the shaft increases linearly with overburden pressure up to a limiting value.
7. The numerical study by Merifield (2011) shows that the cylindrical failure surface method overestimates the uplift capacity by as much as 70%.
8. A factor of safety of at least 3.0 is recommended for determination of the net allowable uplift capacity.

SELF-ASSESSMENT QUESTIONS

Select the most appropriate answer to each multiple-choice question

7.1. The failure surface located above the top helix of a multi-helix anchor extends to the ground surface under:
   a. shallow anchor condition
   b. deep anchor condition
   c. both a and b
   d. none of the above

7.2. The magnitude of the breakout factor increases with embedment ratio H_1/D_1 to a maximum value of:
   a. 3
   b. 6
   c. 9
   d. 12

7.3. If the undrained cohesion of clay is approximately 10 kN/m^2, then the embedment ratio H/D of a helical anchor in that clay will be approximately:
   a. 2.6
   b. 3.6
   c. 4.6
   d. 5

7.4. The cylindrical failure surface method results in good estimates of uplift capacities of helical anchors with helix spacing ratios:
   a. $SR = 1$
   b. $SR > 1.5$
   c. $SR > 5$
   d. $SR \leq 1.5$

7.5. For a fully bonded or deep helix, the ABAQUS finite element solution for the anchor breakout factor is found to be:
   a. 8.61
   b. 10.61
   c. 12.61
   d. 6.12

Answers

7.1: a 7.2: c 7.3: b 7.4: d 7.5: c

REFERENCES

Das, B.M. (1980). A procedure for estimation of ultimate uplift capacity of foundations in clay. *Soils Found.,* 20(1):77–82.

Lutenegger, A.M., Smith, B.L., and Kabir, M.B. (1988). Use of in situ tests to predict uplift performance of multi-helix anchors. *Special Topics in Foundations,* Geotech. Spec. Tech. Publ. 16, B.M. Das, Ed., ASCE, 93–110.

Merifield, R.S. (2011). Ultimate uplift capacity of multiplate helical type anchors in clay. *J. Geotech. Geoenviron. Eng.,* 137(7):704–716.

Mooney, J.S., Adamczak, S., Jr., and Clemence, S.P. (1985). Uplift capacity of helix anchors in clay and silt. *Proc. Uplift Behavior of Anchor Foundations in Soil,* S.P. Clemence, Ed., ASCE, 48–72.

Narasimha Rao, S., Prasad, Y.V.S.N., and Shetty, M.D. (1991). The behaviour of model screw piles in cohesive soil. *Soils Found.,* 31(2):35–50.

Narasimha Rao, S., Prasad, Y.V.S.N., and Veeresh, C. (1993). Behaviour of embedded model screw anchors in soft clays. *Geotechnique,* 43(4):605–614.

8

ANCHOR PILES

This chapter describes the existing theories relating to the prediction of the net ultimate uplift capacity of anchor piles subjected to both axial and inclined pull. The discussion is divided into two major parts: piles in sand and piles in saturated or near-saturated clay (undrained condition).

8.1 INTRODUCTION

In the construction of various types of foundations, piles are generally used to transmit downwardly directed load to a stronger soil at a greater depth. They are also used to resist lateral load imposed on a foundation. During the last five to six decades, several theoretical and experimental studies were conducted by various investigators to evaluate the downwardly directed and lateral load-bearing capacity of single and group piles embedded in sandy and clayey soils.

Piles can also be used in the construction of foundations subjected to uplifting forces. The uplift force is resisted by skin friction developed at the soil-pile interface (Figure 8.1). At the present time, limited studies are available to estimate the uplift capacity of piles. Only a few laboratory model study results are available regarding the efficiency of group piles subjected to uplifting forces.

The net ultimate uplift capacity of a single pile can be expressed as (Figure 8.1):

$$Q_{u(g)} = Q_u + W_p \tag{8.1}$$

where

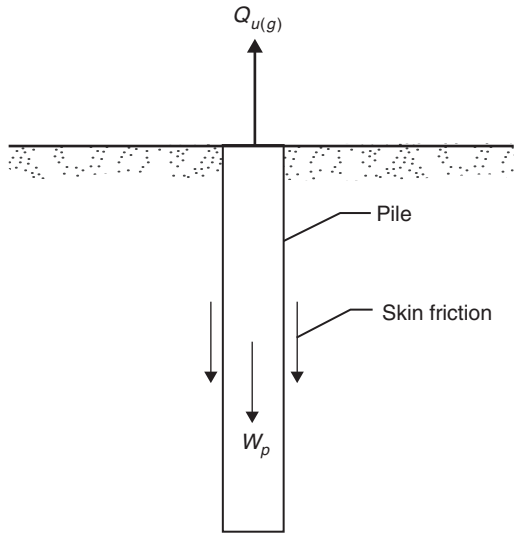

FIGURE 8.1 Pile subjected to uplifting load

$Q_{u(g)}$ = gross ultimate uplift capacity
Q_u = net ultimate uplift capacity
W_p = effective self-weight of the pile

The net ultimate uplift capacity of a pile embedded in sand is primarily a function of the following parameters:

- Length of embedment, L
- Pile diameter, D
- Roughness of the pile surface
- Soil friction angle, ϕ, and its relative density
- Nature of placement of the pile (driven, bored, or cast in place)

In a similar manner, the magnitude of Q_u for a pile embedded in saturated or near-saturated clay is a function of:

- Length of embedment, L
- Pile diameter, D
- Undrained cohesion of the clay, c_u
- Nature of placement of the pile

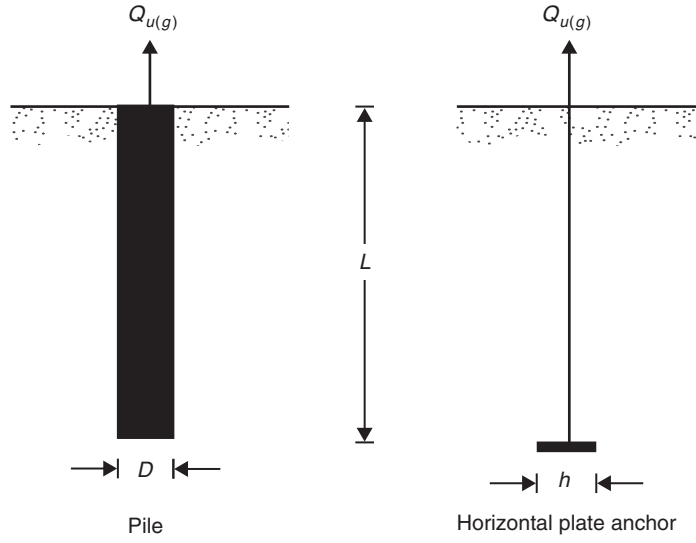

FIGURE 8.2 Comparison of a pile with a horizontal plate anchor

In any case, it has been shown from laboratory model tests that the behavior of a pile to uplift is somewhat different when compared to that of a plate anchor. This can be explained by referring to Figure 8.2, in which a pile of diameter D and a plate anchor of diameter h are embedded in a similar soil at the same depth below the ground surface (that is, L). For this case, $D = h$. If both the pile and the plate anchor are subjected to uplifting force, the nature of the net load (Q) and the uplift movement (Δ) diagrams will be like those in Figure 8.3. A comparison of these two as Q versus Δ plots shows that under similar conditions: (a) the net ultimate uplift load of the pile is somewhat lower than that of the horizontal plate anchor and (b) at ultimate load, the ratio of Δ/D is relatively less for the pile compared to the Δ/h ratio of the plate anchor.

8.2 PILES IN SAND

8.2.1 Bored Piles

Figure 8.4 shows a vertical pile embedded in a granular soil. The length of embedment and the diameter of the pile are L and D, respectively. From Equation 8.1, the net ultimate uplift capacity of the pile can be given as:

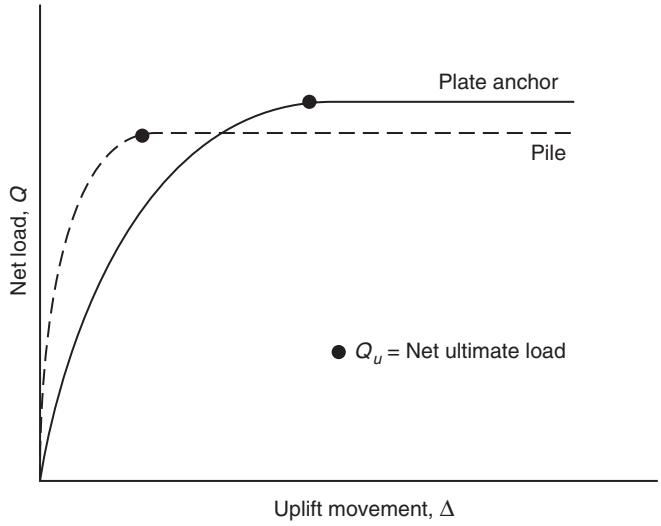

FIGURE 8.3 Comparison of the nature of net load versus uplift movement diagrams for pile and horizontal plate anchor

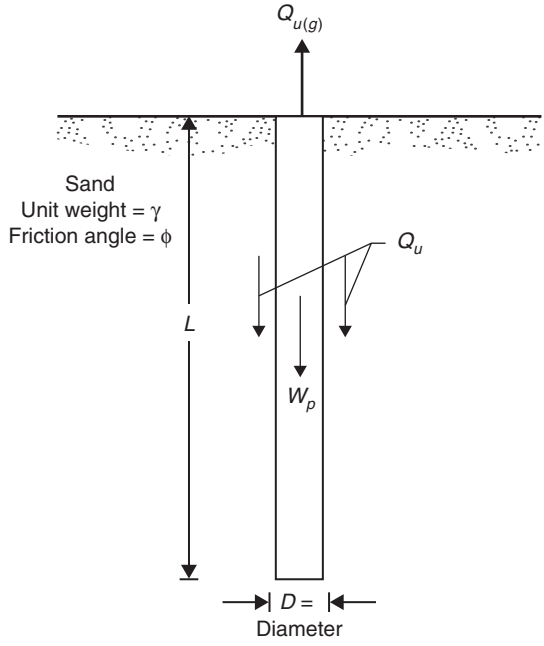

FIGURE 8.4 Bored pile in sand

$$Q_u = Q_{u(g)} - W_p \tag{8.2}$$

The net ultimate uplift capacity can be expressed as (Meyerhof, 1973a):

$$Q_u = (\sigma_0' K_u \tan \delta) A_s \tag{8.3}$$

where

σ_0' = average effective overburden pressure
K_u = uplift coefficient
δ = angle of friction at the soil-pile interface
A_s = embedded pile surface area

The average effective vertical stress is

$$\sigma_0' = \frac{1}{2} \gamma L \tag{8.4}$$

where

γ = unit weight of sand

In the case of submerged sand, the unit weight γ in Equation 8.4 should be replaced by γ' ($\gamma' = \gamma_{sat} - \gamma_w$, where γ_w = unit weight of water). For piles with a circular cross section, the embedded surface area is

$$A_s = \pi D L \tag{8.5}$$

Thus, combining Equations 8.3 to 8.5:

$$Q_u = \left(\frac{1}{2} \gamma L \right) (K_u) (\tan \delta) (\pi D L) = \frac{\pi}{2} \gamma D L^2 K_u \tan \delta \tag{8.6}$$

The preceding relationship can also be expressed as:

$$Q_u = A_s \bar{f} \tag{8.7}$$

where

$\bar{f}$ = average friction resistance per unit area of the soil-pile interface

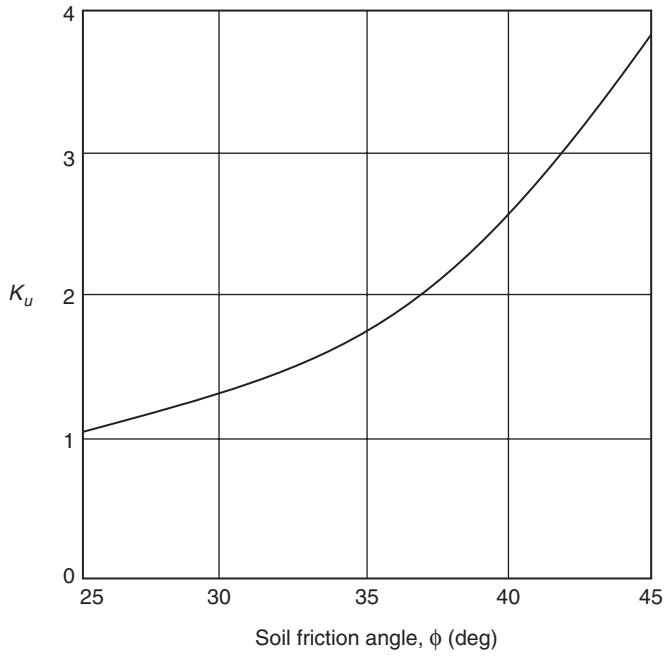

FIGURE 8.5 Meyerhof's (1973a) uplift coefficient variation

Thus:

$$\bar{f} = \frac{1}{2} K_u \gamma L \tan \delta \tag{8.8}$$

The variation of the uplift coefficient K_u with the soil friction angle ϕ suggested by Meyerhof (1973a) is shown in Figure 8.5.

Das et al. (1977a) and Das (1983) provided results of several laboratory model tests for the ultimate uplift capacity of rough piles embedded in sand. These model tests were conducted to obtain the variation of the frictional resistance per unit area f, along with embedded length of the pile. Based on Equation 8.8, it is obvious that:

$$f = \gamma z K_u \tan \delta \tag{8.9}$$

where

z = distance measured from the ground surface (Figure 8.6)

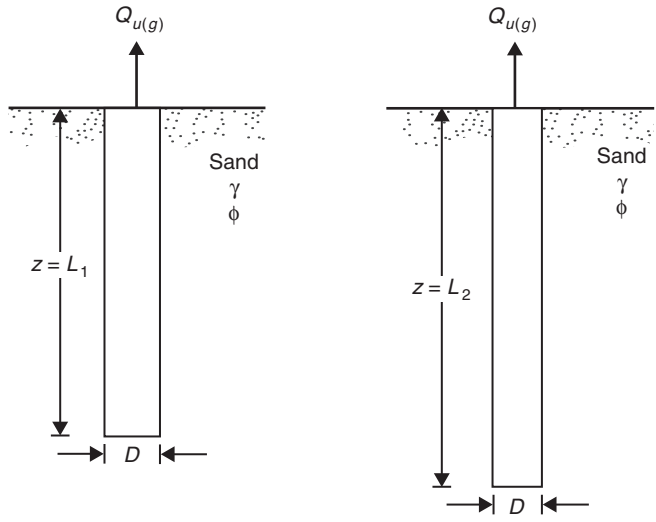

FIGURE 8.6 Determination of frictional resistance per unit area (f) from Equation 8.10

The model tests of Das et al. (1977a) and Das (1983) were conducted by changing the length of embedment L in small increments and then determining the net ultimate uplift capacity for each case. The frictional resistance per unit area f at a depth $z = (L_1 + L_2)/2$ (as shown in Figure 8.6) was calculated as:

$$f = \frac{Q_{u(z=L_2)} - Q_{u(z=L_1)}}{p(L_1 - L_2)} \tag{8.10}$$

where

$Q_{u(z=L_2)}$ = net ultimate uplift capacity of a pile with an embedment length $L_2 = Q_{u(g)(z=L_2)} - W_p$
$Q_{u(z=L_1)}$ = net ultimate uplift capacity of a pile with an embedment length $L_1 = Q_{u(g)(z=L_1)} - W_p$
p = perimeter of a cross section of the pile

The results of these tests show that for a given soil and relative density of compaction, the frictional resistance f increases linearly with L/D up to a certain value and remains constant thereafter (Figure 8.7). The embedment ratio at which the magnitude of f becomes constant can be referred to as the critical

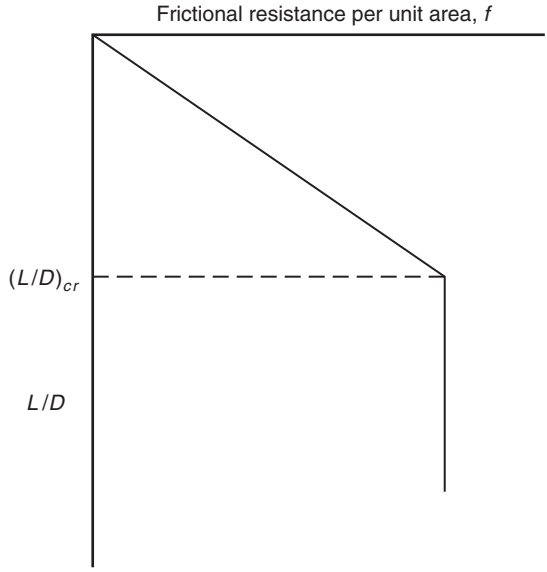

FIGURE 8.7 Nature of variation of L/D versus f

embedment ratio, $(L/D)_{cr}$. The magnitude of the critical embedment ratio can be given by the following empirical relationships (Das, 1983):

$$\left(\frac{L}{D}\right)_{cr} = 0.156D_r + 3.58 \qquad \text{(for } D_r \leq 70\%\text{)} \tag{8.11}$$

$$\left(\frac{L}{D}\right)_{cr} = 14.5 \qquad \text{(for } D_r \geq 70\%\text{)} \tag{8.12}$$

where

D_r = relative density of sand (in percent)

Figure 8.8 shows a plot of $(L/D)_{cr}$ against D_r based on Equations 8.11 and 8.12.

The nature of variation of f with L/D shown in Figure 8.7 is similar to that observed by Vesic (1970) for piles under compressive load. Based on the model test results, Das et al. (1977a) also provided the variation of δ/ϕ with D_r for rough bored piles, as shown in Figure 8.9.

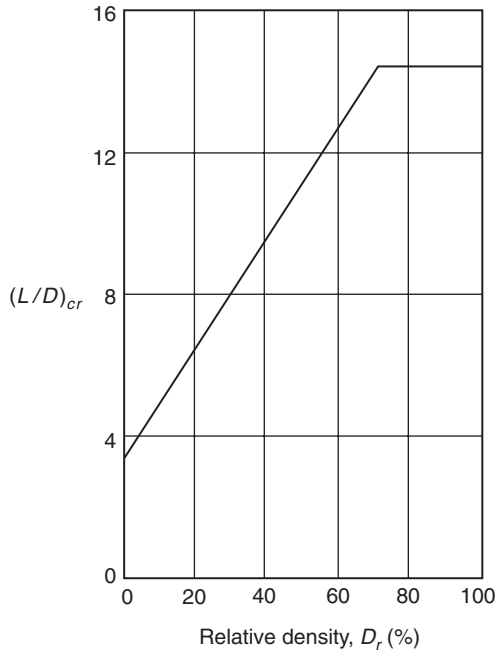

FIGURE 8.8 Plot of $(L/D)_{cr}$ versus D_r (Equations 8.11 and 8.12)

With the above theoretical and experimental results, it is now possible to develop the following step-by-step procedure for estimation of the net ultimate uplift capacity of *rough bored piles*:

1. For a given pile, obtain the embedment ratio L/D (where D = diameter of a pile with a circular cross section, and D = length of each side of a pile with a square cross section, as shown in Figure 8.10).
2. Estimate the relative density of compaction D_r of sand.
3. Determine the critical embedment ratio from Equations 8.11 and 8.12 (or Figure 8.8).
4. Compare the L/D ratio obtained in Step 1 with the $(L/D)_{cr}$ calculated in Step 3. If $L/D \leq (L/D)_{cr}$, go to Step 5. However, if $L/D > (L/D)_{cr}$, then go to Step 6.
5. If $L/D \leq (L/D)_{cr}$, then:

$$Q_u = \int_0^L pf\,dz = \frac{1}{2} p\gamma L^2 K_u \tan\delta$$

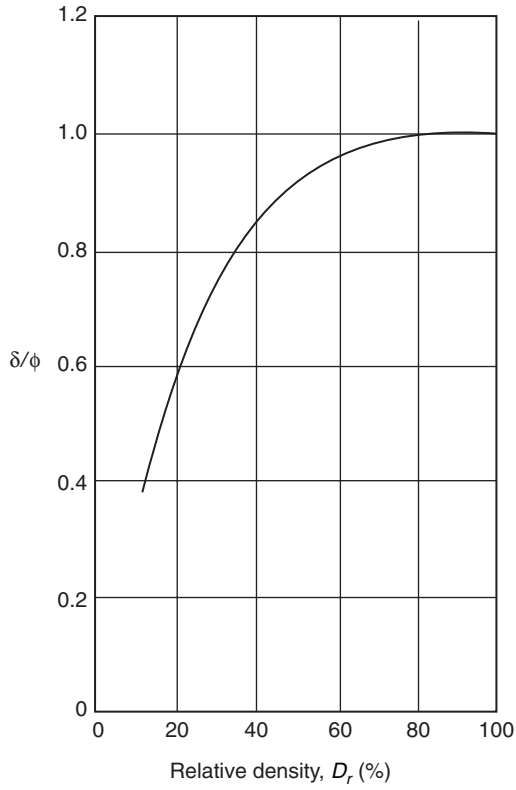

FIGURE 8.9 Variation of δ/ϕ with D_r based on the model test results of Das et al. (1977a)

For piles with a circular cross section:

$$Q_u = \frac{\pi}{2} D\gamma L^2 K_u \tan\delta \tag{8.13}$$

and for piles with a square cross section:

$$Q_u = \left(\frac{1}{2}\right)(4D)\gamma L^2 K_u \tan\delta = 2D\gamma L^2 K_u \tan\delta \tag{8.14}$$

Knowing the value of ϕ, the magnitudes of K_u and δ can be determined from Figures 8.5 and 8.9, respectively.

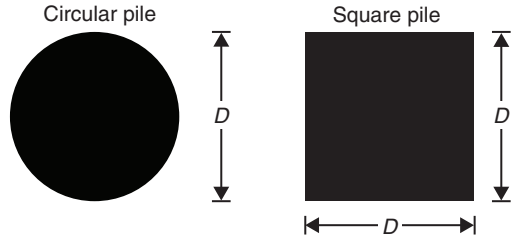

FIGURE 8.10 Cross sections of piles

6. If $L/D > (L/D)_{cr}$, then determine L_{cr}:

$$L_{cr} = \left(\frac{L}{D}\right)_{cr} D \tag{8.15}$$

$$Q_u = \int_0^{L_{cr}} pf\,dz + pf_{(\text{at } z=L_{cr})}(L - L_{cr}) \tag{8.16}$$

However (Figure 8.11):

$$f = \gamma z K_u \tan\delta \tag{8.17}$$

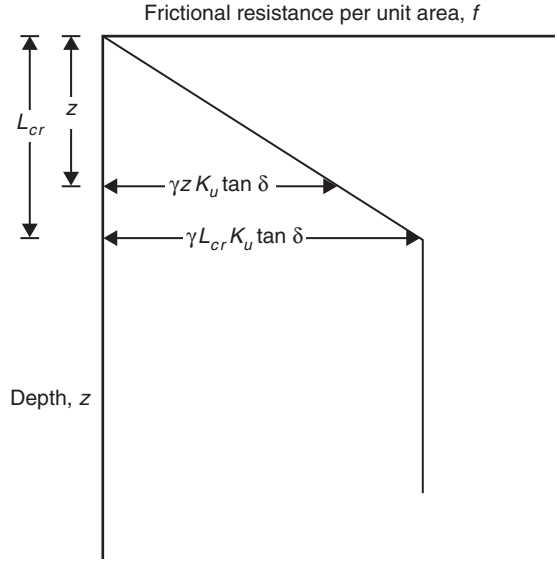

FIGURE 8.11 A typical variation of frictional resistance per unit area of depth z

$$f_{(\text{at } z=L_{cr})} = \gamma L_{cr} K_u \tan\delta \tag{8.18}$$

Substitution of Equations 8.17 and 8.18 into Equation 8.16 yields:

$$Q_u = \frac{1}{2} p\gamma L_{cr}^2 K_u \tan\delta + p\gamma K_u \tan\delta (L - L_{cr}) \tag{8.19}$$

Thus, for piles with a circular cross section:

$$Q_u = \frac{\pi}{2} D\gamma L_{cr}^2 K_u \tan\delta + \pi D\gamma K_u \tan\delta (L - L_{cr}) \tag{8.20}$$

Similarly, for piles with a square cross section:

$$Q_u = 2D\gamma L_{cr}^2 K_u \tan\delta + 4D\gamma K_u \tan\delta (L - L_{cr}) \tag{8.21}$$

Example 8.1

Consider a pile with a circular cross section with a diameter $D = 0.4$ m and length of embedment $L = 10$ m (Figure 8.12). For the sand, $\phi = 43°$, $D_r = 75\%$, and $\gamma = 17.5$ kN/m^3. Determine the net ultimate uplift capacity.

Solution

Assume $D = 0.4$ m, $L = 10$ m, $L/D = 10/0.4 = 25$, and $D_r = 75\%$. Since $D_r = 75\%$, from Equation 8.12, $(L/D)_{cr} = 14.5$. For this pile, $L/D > (L/D)_{cr}$, so Equation 8.20 will apply:

$$Q_u = \frac{\pi}{2} D\gamma L_{cr}^2 K_u \tan\delta + \pi D\gamma K_u \tan\delta (L - L_{cr})$$

$$L_{cr} = \left(\frac{L}{D}\right)_{cr} D = (14.5)(0.4) = 5.8 \text{ m}$$

From Figure 8.5, for $\phi = 43°$, $K_u = 3.35$. Again, from Figure 8.9, for $D_r = 75\%$, $\delta/\phi = 1$, so $\delta = 43°$. Now:

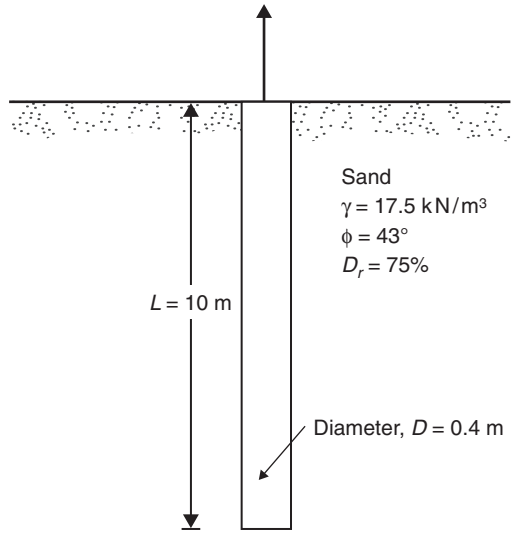

FIGURE 8.12 Example 8.1

$$Q_u = \left(\frac{\pi}{2}\right)(0.4)(17.5)(5.8)(3.35)(\tan 43°)$$
$$+ (\pi)(0.4)(17.5)(3.35)(\tan 43°)(10 - 5.8)$$
$$= 199.2 + 288.5$$
$$= \mathbf{487.7\ kN}$$

8.2.2 Driven Piles

If piles are *driven* into the ground, the lateral earth pressure coefficient will change when compared to *bored piles*. This change of lateral earth pressure coefficient at the pile-sand interface will cause a change in the skin friction f at any given depth z measured from the ground surface. For *rigid rough circular piles* embedded in sand, Meyerhof (1973b) proposed that:

$$Q_u = \frac{1}{2}\gamma L^2 D K'_u \tag{8.22a}$$

where

L = length of embedment
D = diameter of the circular pile
K'_u = modified uplift coefficient

The variations of K'_u with the soil friction angle ϕ proposed by Meyerhof (1973b) are given in Figure 8.13. It is important to keep in mind the following facts while using Equation 8.22a and Figure 8.13:

1. Equation 8.22a is for circular piles only. For piles with a square cross section:

$$Q_u = \frac{1}{2}\gamma L^2 D\left(\frac{4}{\pi}\right)K'_u = 0.637\gamma L^2 D K'_u \tag{8.22b}$$

2. Presently, no model or field test results for driven piles in sand are available to predict the magnitude of the critical embedment ratio $(L/D)_{cr}$

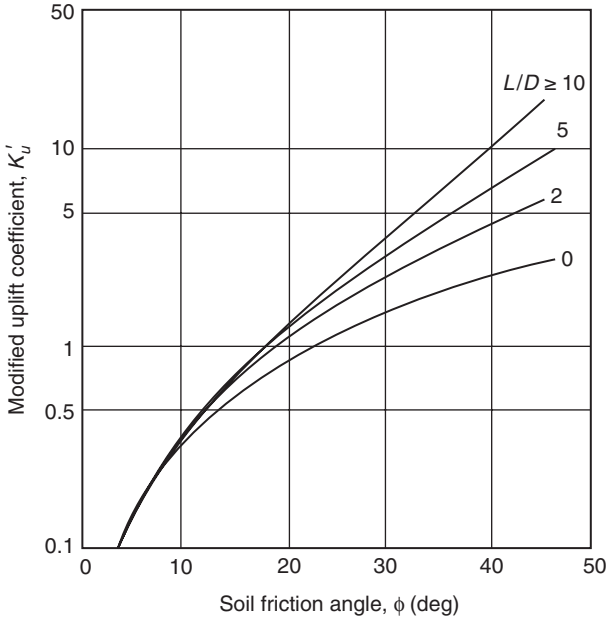

FIGURE 8.13 Meyerhof's (1973b) modified uplift coefficient K'_u

at which the unit skin friction f becomes constant as shown in Figure 8.7. For that reason, Equations 8.22a and 8.22b (and Figure 8.13) should be used for $L/D \leq 15$.

Example 8.2

Consider the pile described in Example 8.1. The only change is that L is now equal to 6 m. Estimate the net ultimate uplift capacity by assuming that:

a. It is a bored pile
b. It is a driven pile

Solution

Assume $L = 6$ m, $D = 0.4$ m, $L/D = 15$, $\phi = 43°$, and $\gamma = 17.5$ kN/m^3.

Part a. From Equation 8.20:

$$Q_u = \frac{\pi}{2} D\gamma L_{cr}^2 K_u \tan\delta + \pi D\gamma K_u \tan\delta(L - L_{cr})$$

As in Example 8.1, $K_u = 3.35$ and $L_{cr} = 5.8$, so:

$$Q_u = \left(\frac{\pi}{2}\right)(0.4)(17.5)^2(5.8)(3.35)(\tan 43°)$$

$$+ (\pi)(0.4)(17.5)(3.35)(\tan 43°)(6 - 5.8)$$

$$= 1155.5 + 13.7$$

$$= \mathbf{1169.2\ kN}$$

Part b. From Equation 8.22a:

$$Q_u = \frac{1}{2}\gamma L^2 D K_u'$$

From Figure 8.13, for $\phi = 43°$ the magnitude of K_u' is about 13.7, so:

$$Q_u = \left(\frac{1}{2}\right)(17.5)(6)^2(0.4)(13.7)$$

$$\approx \mathbf{1726\ kN}$$

Comment: Comparing the results of Parts a and b, it can be seen that Q_u is about 50% higher for a driven pile compared to a bored pile.

8.2.3 Uplift Capacity of Inclined Piles Subjected to Axial Pull

Figure 8.14 shows a rough rigid inclined pile embedded in sand with a unit weight γ and a friction angle ϕ. The length of the embedded inclined pile is equal to L. The inclination of the pile with respect to the vertical is α. The gross ultimate uplift capacity of an inclined pile can be given as:

$$Q_{u(g)\alpha} = Q_{u\alpha} + W_p \cos\alpha$$

where

$Q_{u(g)\alpha}$ = gross ultimate axial uplift capacity
$Q_{u\alpha}$ = net ultimate axial uplift capacity
W_p = effective self-weight of the pile

Thus:

$$Q_{u\alpha} = Q_{u(g)\alpha} - W_p \cos\alpha \tag{8.23}$$

Based on laboratory model test results, Tran-Vo-Nhiem (1971) proposed that:

$$Q_{u\alpha} \approx \frac{Q'_{u(\alpha=0^\circ)}}{\cos\alpha} \qquad (\text{for } \alpha \le 40\%) \tag{8.24}$$

where

$Q'_{u(\alpha=0^\circ)}$ = net ultimate pullout resistance of a similar pile with a length L' $= L\cos\alpha$

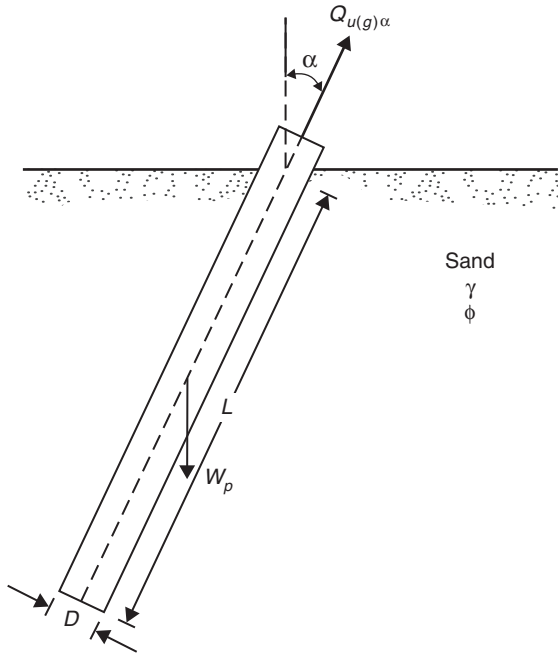

FIGURE 8.14 Geometric parameters of a rough rigid inclined pile embedded in sand

Meyerhof (1973a) also proposed a theoretical relationship for $Q_{u\alpha}$ for *bored piles* as:

$$Q_{u\alpha} \approx (\sigma_0' K_{u\alpha} \tan \delta) A_s \tag{8.25}$$

where

σ_0' = average effective overburden pressure
$K_{u\alpha}$ = uplift coefficient of inclined piles
δ = angle of friction at the soil-pile interface
A_s = embedded pile surface area

For this problem, referring to Figure 8.15:

$$\sigma_0' = \left(\frac{L'}{2}\right)\gamma = \frac{1}{2}\gamma L \cos \alpha \tag{8.26}$$

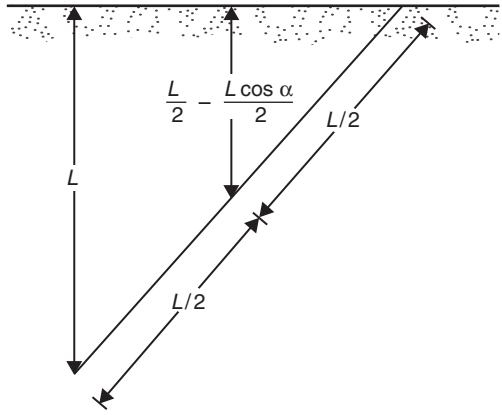

FIGURE 8.15 Geometrical parameters for the inclined plane

For *circular piles*:

$$A_s = pL = \pi DL \tag{8.27}$$

Thus, combining Equations 8.25, 8.26, and 8.27:

$$Q_{u\alpha} = \frac{\pi}{2} \gamma L^2 D K_{u\alpha} \cos\alpha \tan\delta \tag{8.28}$$

However, for piles with a *square* cross section:

$$A_s = pL = 4DL \tag{8.29}$$

Therefore, from Equations 8.25, 8.26, and 8.29:

$$Q_{u\alpha} = 2\gamma L^2 D K_{u\alpha} \cos\alpha \tan\delta \tag{8.30}$$

The variation of the uplift coefficient for inclined piles ($K_{u\alpha}$) proposed by Meyerhof (1973a) is shown in Figure 8.16. Although no theoretical or experimental results are available at this time, the authors feel that some modifications in Equations 8.28 and 8.30 are necessary in view of the fact that the unit friction f at the soil-pile interface may become constant beyond a certain depth, as shown in Figure 8.17 (similar to that for vertical piles, as shown in Figure 8.7). This modification will result in a conservative value of $Q_{u\alpha}$. The proposed modification can be done by substituting L' in Equations 8.11 and 8.12 for the critical embedment ratio, or:

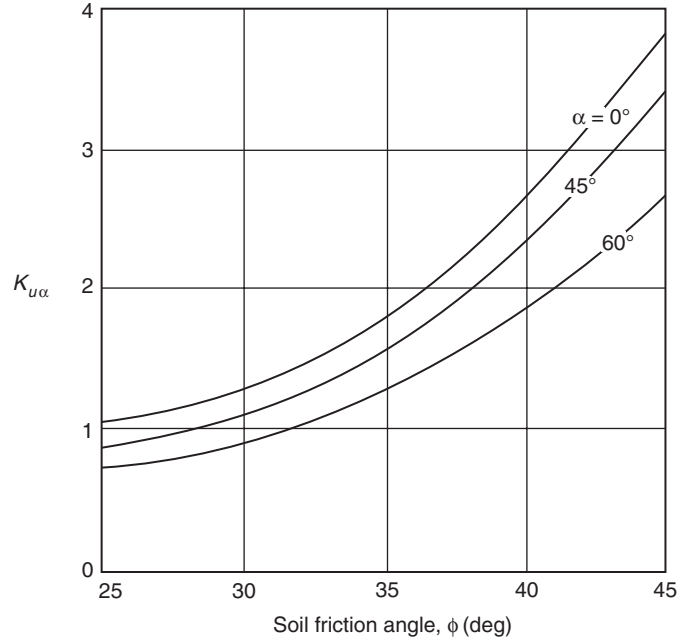

FIGURE 8.16 Meyerhof's values (1973a) of $K_{u\alpha}$

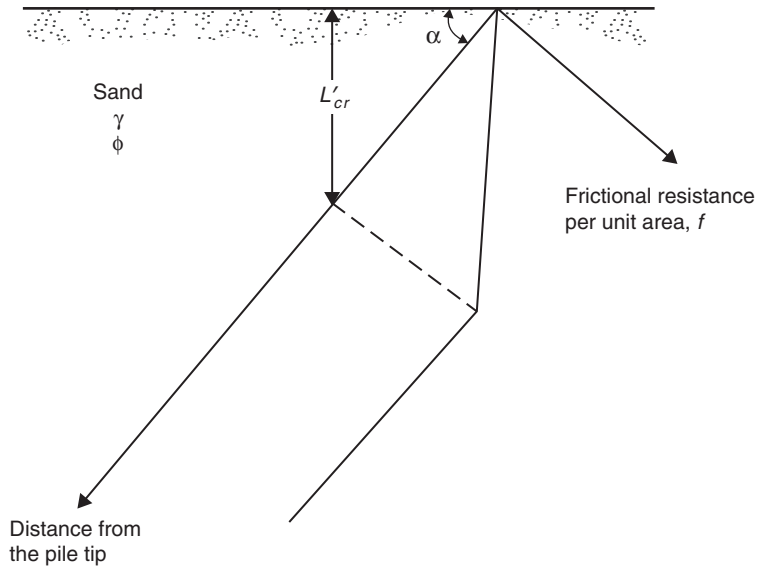

FIGURE 8.17 Variation of frictional resistance per unit area f along the surface of the inclined pile

$$\left(\frac{L'}{D}\right)_{cr} = \left(\frac{L\cos\alpha}{D}\right)_{cr} = 0.156D_r + 3.58 \qquad (\text{for } D_r \le 70\%) \qquad (8.31a)$$

and

$$\left(\frac{L'}{D}\right)_{cr} = \left(\frac{L\cos\alpha}{D}\right)_{cr} = 14.5 \qquad (\text{for } D_r > 70\%) \qquad (8.31b)$$

Proceeding in a manner similar to that shown in Section 8.2.1, we can thus obtain the following relationships.

Case 1. For $L' \le \left(\frac{L'}{D}\right)_{cr} D = L'_{cr}$:

$$Q_{u\alpha} = \frac{\pi}{2} D\gamma L^2 K_{u\alpha} \cos\alpha \tan\delta \qquad (\text{for circular piles}) \qquad (8.32)$$

and

$$Q_{u\alpha} = 2D\gamma L^2 K_{u\alpha} \cos\alpha \tan\delta \qquad (\text{for square piles}) \qquad (8.33)$$

Case 2. For $L' > \left(\frac{L'}{D}\right)_{cr} D = L'_{cr}$:

$$Q_{u\alpha} = \frac{\pi}{2} D\gamma L_{cr}^2 K_{u\alpha} \cos\alpha \tan\delta + \pi D\gamma K_{u\alpha} \cos\alpha \tan\alpha \qquad (\text{for circular piles}) \qquad (8.34)$$

and

$$Q_{u\alpha} = 2D\gamma L_{cr}^2 K_{u\alpha} \cos\alpha \tan\delta + \pi D\gamma K_{u\alpha} \cos\alpha \tan\delta (L - L_{cr}) \qquad (\text{for square piles}) \qquad (8.35)$$

In Equations 8.34 and 8.35:

$$L_{cr} = \frac{L'_{cr}}{\cos \alpha} \tag{8.36}$$

In Equations 8.32 through 8.35, the magnitudes of $K_{u\alpha}$ and δ should be obtained from Figures 8.16 and 8.9, respectively.

In light of the above derivations, it is essential to keep in mind the following general facts when estimating the net ultimate uplift capacity of inclined piles subjected to axial pullout force:

1. Equation 8.24 is recommended for use when the pile inclination α is equal to or less than 40° and L/D is equal to or less than about 20. If this empirical relationship is used for bored piles, then $Q'_{u(\alpha=0°)}$ needs to be determined by using the proper equation (Equation 8.13, 8.14, 8.20, or 8.21). However, for driven piles, $Q_{u(\alpha=0°)}$ needs to be determined using Equation 8.22a or 8.22b. In addition, note that for all calculations in Equations 8.13, 8.14, 8.20, 8.21, 8.22a, and 8.22b (if applicable), $L' = L \cos \alpha$ should be used in place of L.
2. Equations 8.32 through 8.35 are only applicable for *bored piles.*

Example 8.3

Consider the inclined bored pile embedded in sand shown in Figure 8.18. Determine the net axial uplift capacity $Q_{u\alpha}$ using Equation 8.24.

Solution

For this problem, $L = 10$ ft, $D = 1$ ft, $\gamma = 108$ lb/ft^3, $\phi = 35°$, $D_r = 60\%$, and $\alpha = 40°$. According to Equation 8.24:

$$Q_{u\alpha} \approx \frac{Q'_{u(\alpha=0°)}}{\cos 40°}$$

In order to estimate $Q'_{u(\alpha=0°)}$, we need to determine which of the two equations (either Equation 8.13 or 8.20) should be used. For this case:

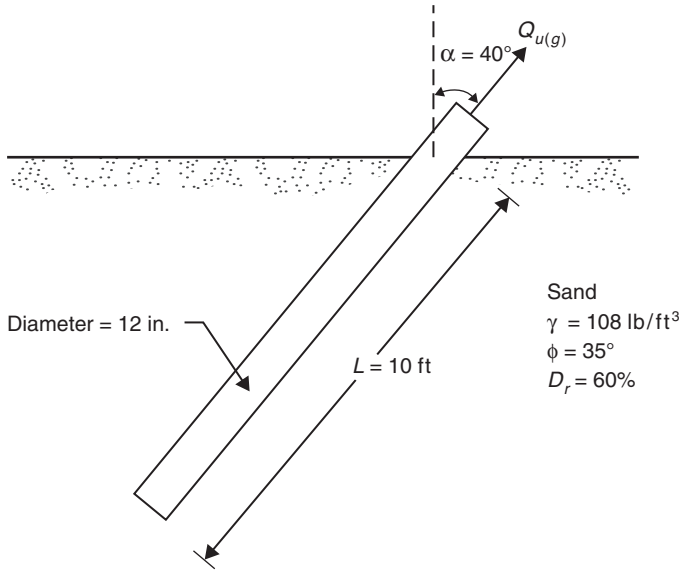

FIGURE 8.18 Example 8.3

$$\frac{L'}{D} = \frac{L\cos\alpha}{D} = \frac{(10)(\cos 40°)}{1} = 7.66$$

From Equation 8.11:

$$\left(\frac{L'}{D}\right)_{cr} = 0.156D_r + 3.58 = (0.156)(60) + 3.58 = 12.94$$

Since $L'/D \leq (L'/D)_{cr}$, Equation 8.13 will be used, with L replaced by L'. Thus:

$$Q_{u(\alpha=0°)} = \frac{\pi}{2} D\gamma L'^2 K_u \tan\delta$$

From Figure 8.5, for $\phi = 35°$, the value of K_u is about 1.83. Also, from Figure 8.9, for $D_r = 60\%$, the magnitude of δ/ϕ is about 0.97. Hence, $\delta = (0.97)(35) = 33.95°$. Thus:

$$Q_{u(\alpha=0^\circ)} = \left(\frac{\pi}{2}\right)(1)(108)(10\cos 40^\circ)^2(1.83)(\tan 33.95^\circ) \approx 12{,}265 \text{ lb}$$

$$\approx 12.3 \text{ kip}$$

Therefore:

$$Q_{u\alpha} = \frac{12.3}{\cos 40^\circ} = \mathbf{16.06\ kip}$$

Example 8.4

Solve Example 8.3 assuming that the pile is driven.

Solution

From Equation 8.22a:

$$Q_{u(\alpha=0^\circ)} = \frac{1}{2}\gamma L'^2 D K'_u$$

$$L' = (10)(\cos 40^\circ) = 7.66$$

For $L'/D = 7.66$ and $\phi = 35^\circ$, the value of K'_u (Figure 8.13) is about 5. Hence:

$$Q'_u = \left(\frac{1}{2}\right)(108)(7.66)^2(1)(5) = 15{,}842 \text{ lb} \approx 15.8 \text{ kip}$$

Therefore:

$$Q_{u\alpha} = \frac{15.8}{\cos 40^\circ} \approx \mathbf{20.63\ kip}$$

Example 8.5

Solve Example 8.3 assuming the pile is a bored pile and using either Equation 8.32 or 8.34, whichever is applicable.

Solution

From Equation 8.31a:

$$\left(\frac{L'}{D}\right)_{cr} = 0.156D_r + 3.58 = (0.156)(60) + 3.58 = 12.94$$

For the present problem:

$$L' = (L)(\cos 40°) = (10)(\cos 40°) = 7.66$$

Since $L' < L_{cr}$, Equation 8.32 will apply. Thus:

$$Q_{u\alpha} = \frac{\pi}{2} D\gamma L^2 K_{u\alpha} \cos\alpha \tan\delta$$

As in Example 8.3, $\delta = 33.95°$. From Figure 8.16, for $\phi = 35°$ and $\alpha = 40°$, the value of $K_{u\alpha} \approx 1.65$. Therefore:

$$Q_{u\alpha} = \left(\frac{\pi}{2}\right)(1)(108)(10)^2(1.65)(\cos 40°)(\tan 33.95°) = 14{,}436 \text{ lb}$$

$$\approx \mathbf{14.4 \text{ kip}}$$

8.2.4 Uplift Capacity of Rigid Vertical Piles Under Oblique Pull

Under certain circumstances, rigid piles embedded in sand may be subjected to oblique pull, as shown in Figure 8.19. The oblique pull to the pile is applied at an angle θ to the vertical. The gross ultimate uplift capacity of the pile measured in the direction of the load application $Q_{u(g)\theta}$ can be given as:

$$Q_{u(g)\theta} = Q_{u\theta} + W_p \cos\theta \tag{8.37}$$

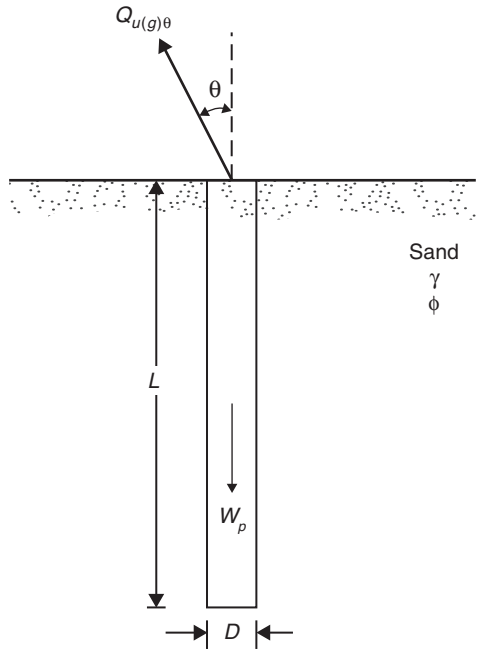

FIGURE 8.19 Rigid vertical pile subjected to inclined pull

where

$Q_{u\theta}$ = net ultimate uplift capacity
W_p = effective self-weight of the pile

For *rigid piles* (that is, $L/D \approx 15$ or less), the plot of net load versus pile displacement in the direction of the pull (Δ_θ) will be of the nature shown in Figure 8.20 (Das, 1977b). From this figure it can be shown that for vertical pull (that is, $\theta = 0°$), the net load gradually increases with vertical displacement up to a maximum value ($Q_{u\theta}$) at which complete pullout of the pile occurs. However, for $\theta > 0°$, the net load increases with Δ_θ rather rapidly up to a certain value beyond which the load-displacement plot becomes practically linear. The point at which the load-displacement plot becomes practically linear is defined as the net ultimate load ($Q_{u\theta}$).

Based on laboratory model test results, Meyerhof (1973b) suggested a semi-empirical relationship to estimate the gross ultimate uplift capacity, $Q_{u(g)\theta}$, which is of the form

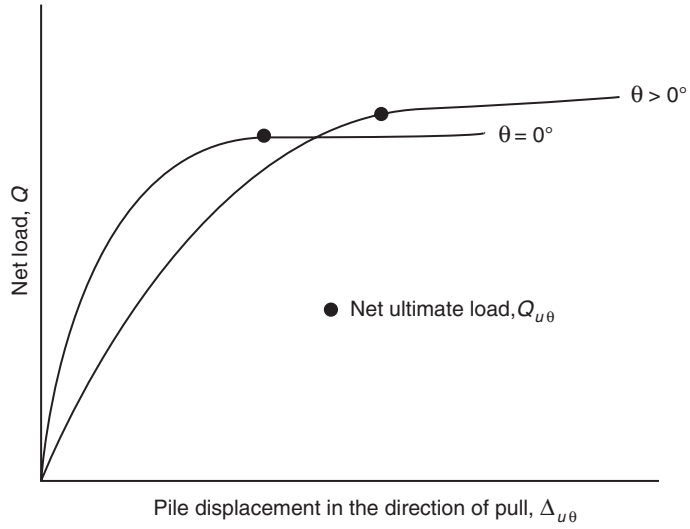

FIGURE 8.20 Nature of net load versus pile displacement for rigid pile subjected to oblique pull

$$\left[\frac{Q_{u(g)\theta}\cos\theta}{Q_{u(g)V}}\right] + \left[\frac{Q_{u(g)\theta}\sin\theta}{Q_{u(g)H}}\right]^2 = 1 \tag{8.38}$$

where

$Q_{u(g)V}$ = gross ultimate uplift capacity of the pile with $\theta = 0°$
$Q_{u(g)H}$ = gross ultimate lateral resistance of the pile with $\theta = 90°$

It is important to realize that $Q_{u(g)V} = Q_{u(g)}$ (that is, the gross ultimate uplift capacity of the pile with $\theta = 0°$, as discussed in Sections 8.2.1 and 8.2.2). For $L/D \leq 15$, without loss of much accuracy, the following relationships may be used to estimate the magnitudes of $Q_{u(g)V}$ and $Q_{u(g)H}$.

8.2.4.1 Bored Piles with Circular Cross Section

$$Q_{u(g)V} = \underbrace{\frac{\pi}{2} D\gamma L^2 K_u \tan\delta}_{\text{Equation 8.13}} + W_p \tag{8.39}$$

$$Q_{u(g)H} = G\gamma D^3 \tag{8.40}$$

where

$$G = \frac{Q_{u(g)H}}{\gamma D^3} \tag{8.41}$$

The variation of the nondimensional parameter G with L/D and soil friction angle ϕ is shown in Figure 8.21. These values are based on the analysis of Broms (1965).

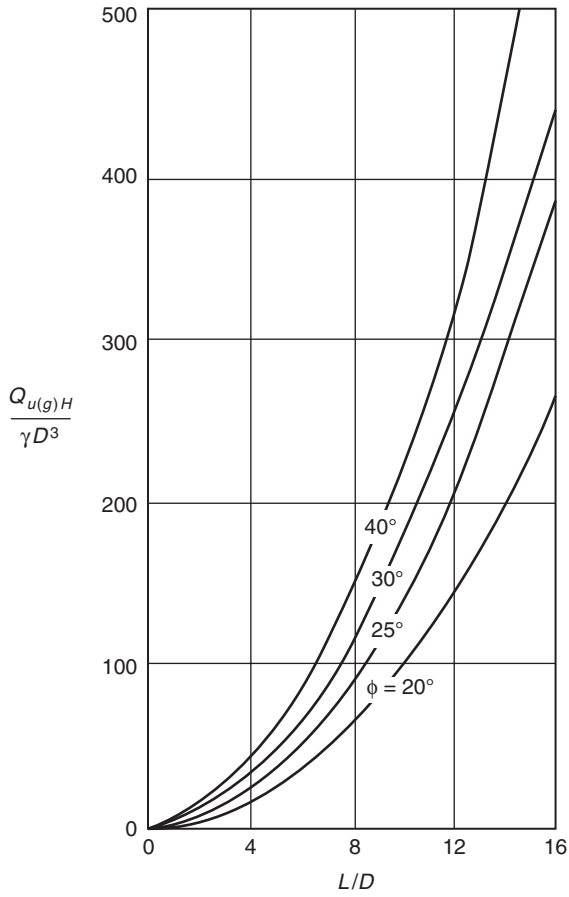

FIGURE 8.21 Plot of $G = Q_{u(g)H}/\gamma D^3$ based on Broms's analysis (1965)

8.2.4.2 Bored Piles with Square Cross Section

$$Q_{u(g)V} = \underbrace{2D\gamma L^2 K_u \tan\delta}_{\text{Equation 8.14}} + W_p \tag{8.42}$$

and

$$Q_{u(g)H} = \underbrace{G\gamma D^3}_{\text{Figure 8.21}} \tag{8.40}$$

Das et al. (1977b) suggested the use of Equation 8.40 for determination of $Q_{u(g)H}$ for bored piles.

8.2.4.3 Driven Piles

$$Q_{u(g)V} = \underbrace{\frac{1}{2}\gamma D L^2 K'_u}_{\text{Equation 8.22a}} + W_p \qquad \text{(for piles with circular cross section)} \tag{8.43a}$$

$$Q_{u(g)V} = \underbrace{0.637\gamma D L^2 K'_u}_{\text{Equation 8.22b}} + W_p \qquad \text{(for piles with square cross section)} \tag{8.43b}$$

and

$$Q_{u(g)H} = \frac{1}{2}\gamma D L^2 K'_h \qquad \text{(for piles with circular and square cross section)} \tag{8.44}$$

where

K'_h = coefficient of lateral resistance

The variation of K'_h with soil friction angle ϕ and L/D is shown in Figure 8.22. These value of K'_h were proposed by Meyerhof (1973b).

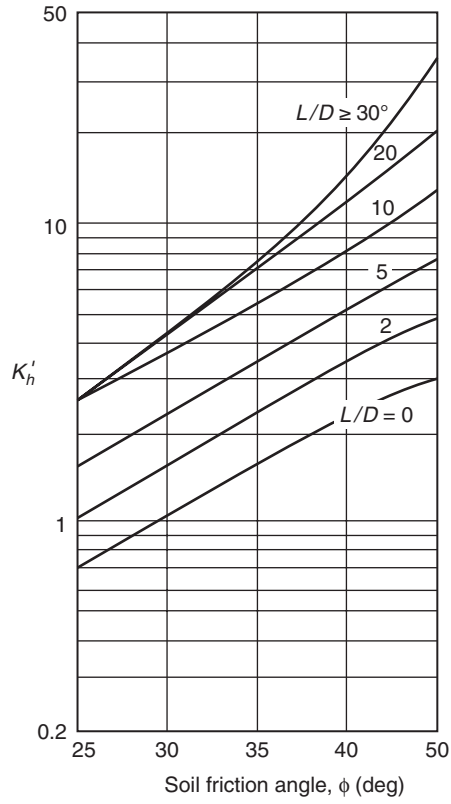

FIGURE 8.22 Variation of Meyerhof's (1973b) K_h' with soil friction angle ϕ

Example 8.6

Refer to Figure 8.19. For the concrete pile, length $L = 12$ ft and diameter $D = 12$ in. For the soil, friction angle $\phi = 35°$, relative density $D_r = 60\%$, and unit weight $\gamma = 110$ lb/ft^3. Calculate $Q_{u(g)\theta}$ for $\theta = 30°$. Assume that the pile is a bored pile

Solution

$L/D = 12/1 = 12 < 15$. Hence, from Equation 8.39:

$$Q_{u(g)V} = \frac{\pi}{2} D\gamma L^2 K_u \tan\delta + W_p$$

From Figure 8.5, for $\phi = 35°$, the magnitude of K_u is about 1.83. Also, for $D_r = 60\%$, the value of δ/ϕ is about 0.97.

$$W_p = \left(\frac{\pi}{4} D^2 L\right) (\text{unit weight of concrete})$$

$$= \left[\left(\frac{\pi}{4}\right) (1)^2 (12)\right] (150 \text{ lb/ft}^3) = 1413.7 \text{ lb}$$

$$Q_{u(g)V} = \left(\frac{\pi}{2}\right) (1) (110) (12)^2 (1.83) \tan(0.97 \times 35°) + 1413.7$$

$$\approx 32{,}068 \text{ lb} \approx 32.07 \text{ kip}$$

Again, from Equation 8.40:

$$Q_{u(g)H} = G\gamma D^3$$

For $L/D = 12$ and $\phi = 35°$, from Figure 8.21, the magnitude of G is 242. Therefore:

$$Q_{u(g)H} = (242) (110) (1)^3 = 26{,}620 \text{ lb} = 26.6 \text{ kip}$$

Now, from Equation 8.38:

$$\left[\frac{Q_{u(g)\theta} \cos\theta}{Q_{u(g)V}}\right] + \left[\frac{Q_{u(g)\theta} \sin\theta}{Q_{u(g)H}}\right]^2 = 1$$

or

$$[Q_{u(g)\theta}] \left(\frac{\cos 30°}{32.07}\right) + [Q^2_{u(g)\theta}] \left(\frac{\sin 30°}{26.6}\right)^2 = 1$$

or

$$0.027Q_{u(g)\theta} + 0.00035Q^2_{u(g)\theta} = 1$$

or

$$Q_{u(g)\theta}^2 + 77.14Q_{u(g)\theta} - 2857.14 = 0$$

or

$$Q_{u(g)\theta} \approx \mathbf{27\ kip}$$

8.2.5 Uplift Capacity of Group Piles

Foundations subjected to uplifting loads may sometimes be constructed on a group pile (Figure 8.23). For the group pile shown in Figure 8.23, the length and

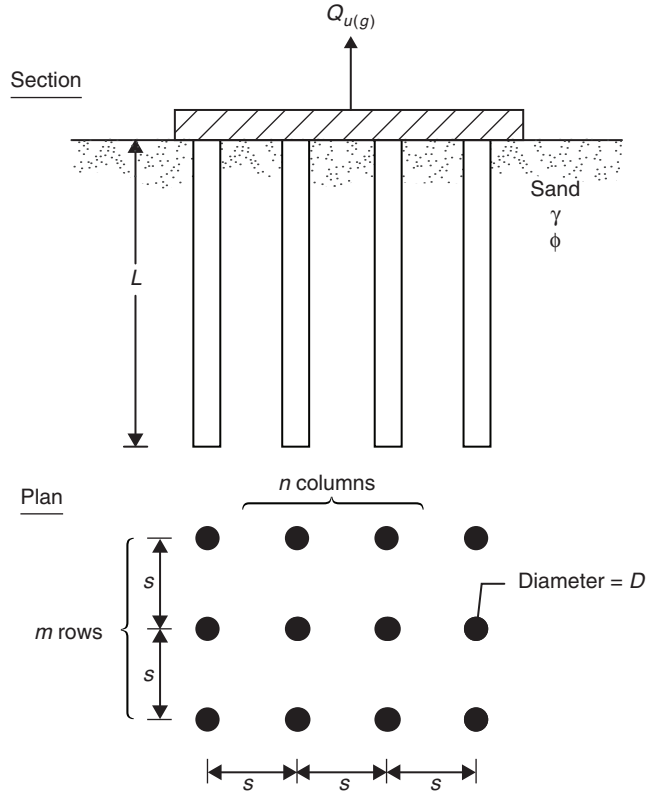

FIGURE 8.23 Group piles in sand

diameter of all piles are L and D, respectively. All piles are placed at a center-to-center spacing of s. The numbers of rows and columns in the group plan are m and n, respectively. The gross and net ultimate uplift capacities of the group pile are related as:

$$Q_{ug(g)} = Q_{ug} + W_{gp} \tag{8.45}$$

where

$Q_{ug(g)}$ = gross ultimate uplift capacity of the pile group
Q_{ug} = net ultimate uplift capacity of the pile group
W_{gp} = effective self-weight of the piles in the group and the pile cap

In the conventional sense, the group efficiency η can be defined as:

$$\eta = \frac{Q_{ug}}{mnQ_u} \tag{8.46}$$

In order to evaluate the parameters that affect the group efficiency of piles, Das (1989) provided a number of model test results in loose sand with L/D = 15 and 20. For these tests, the relative density of compaction was kept at 47.6%. The variation of the group efficiency with s/D is shown in Figures 8.24 and 8.25. Based on these model test results, the following conclusions can be drawn:

1. For a given soil (relative density, D_r) and number of piles in a group, the group efficiency increases almost linearly with s/D up to a maximum value of 100%.
2. For a given soil and s/D, the group efficiency decreases with the increase in the number of piles in a group.
3. For a given soil, s/D, and the number of piles in a group, the efficiency decreases with the increase in L/D.

More laboratory and field test results are necessary to quantify the group efficiency and develop a parametric relationship.

8.2.6 Factor of Safety

In all cases, it is recommended that a factor of safety F_s of at least 2 be used to obtain the net uplift capacity; that is:

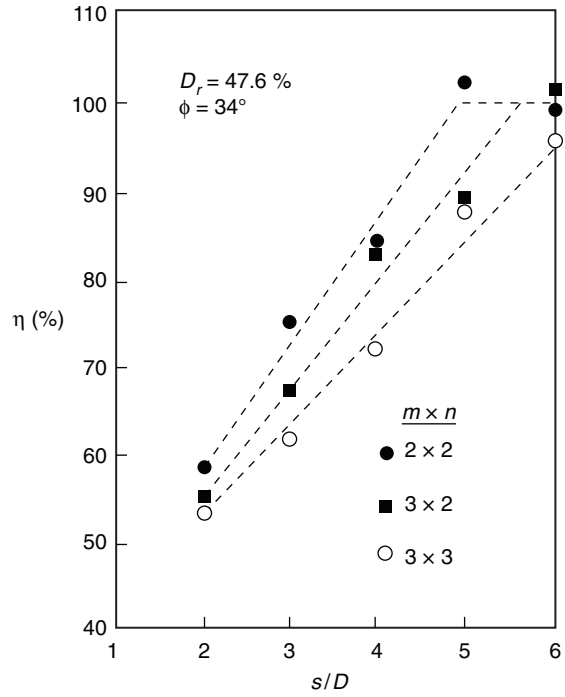

FIGURE 8.24 Model test results of Das (1989) for variation of η versus s/D (for $L/D = 15$)

$$\text{Net allowable uplift capacity} = \frac{\text{Net ultimate uplift capacity}}{F_s}$$

For a group of piles with conventional spacing of $s = 3D$ to $4D$, the net allowable uplift capacity can be assumed as:

$$Q_{ug} = \frac{mnQ_u}{F_s}$$

where

Q_u = net allowable uplift capacity of a single pile
Q_{ug} = net allowable uplift capacity of a group pile
F_s = factor of safety ≈ 2 to 2.5

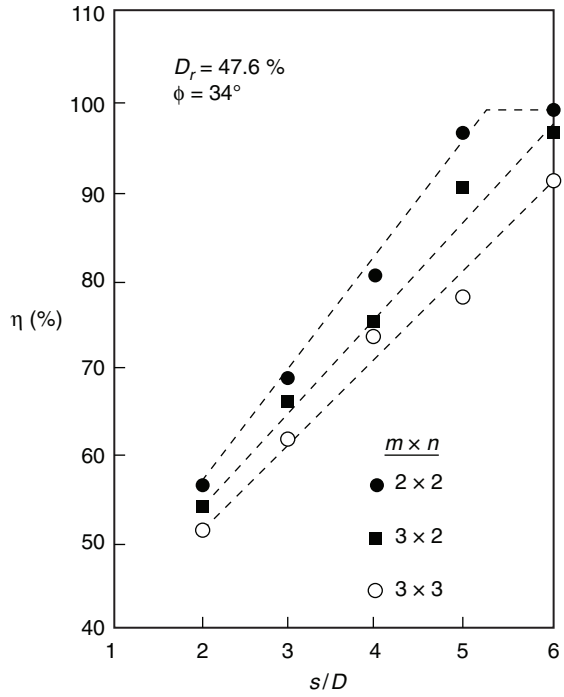

FIGURE 8.25 Model test results of Das (1989) for variation of η versus s/D (for $L/D = 20$)

8.3 PILES IN CLAY ($\phi = 0$ CONDITION)

8.3.1 Vertical Piles Subjected to Axial Pull

Figure 8.26 shows a vertical pile embedded in a saturated or near-saturated clay with an undrained cohesion of c_u. The pile is being subjected to an uplifting force. As in Equation 8.1, the gross and net ultimate uplift capacity can be expressed as:

$$Q_{u(g)} = Q_u + W_p$$

For this case, however, the net ultimate uplift capacity is a function of the undrained cohesion c_u, the pile length L, and the perimeter of the pile cross section, or:

$$Q_u = pLc_a \tag{8.47}$$

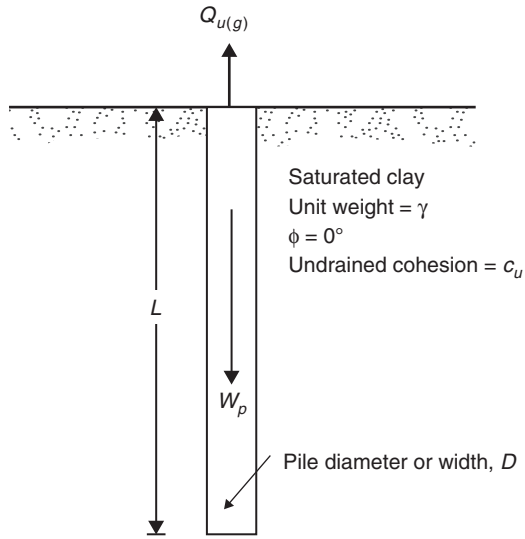

FIGURE 8.26 Pile embedded in saturated clay

where

p = perimeter of the pile cross section
c_a = adhesion at the pile-clay interface

The adhesion is a function of the undrained cohesion. Thus:

$$c_a = f(c_u)$$

or

$$c_a = \beta c_u \tag{8.48}$$

where

β = nondimensional adhesion factor

Thus, combining Equations 8.1, 8.47, and 8.48:

$$Q_{u(g)} = \pi D L \beta c_u + W_p \qquad \text{(for circular piles)} \tag{8.49}$$

and

$$Q_{u(g)} = 4DL\beta c_u + W_p \qquad \text{(for square piles)} \tag{8.50}$$

The important parameter in the preceding two equations is the adhesion factor β that needs to be determined for estimation of the ultimate uplift capacity. Available published results are summarized in the following sections.

8.3.1.1 Cast In Situ Piles

A number of field test results for the ultimate uplift capacity of cast *in situ* concrete piles have been reported by Patterson and Urie (1964), Turner (1962), Mohan and Chandra (1961), and Sowa (1970). Based on these field test results, the adhesion factors have been calculated and are shown in Figure 8.27. The average plot of the variation of β with c_u can be expressed as (Das and Seeley, 1982):

$$\beta = 0.9 - 0.00625c_u \geq 0.4 \tag{8.51}$$

where

c_u = undrained cohesion in kN/m^2

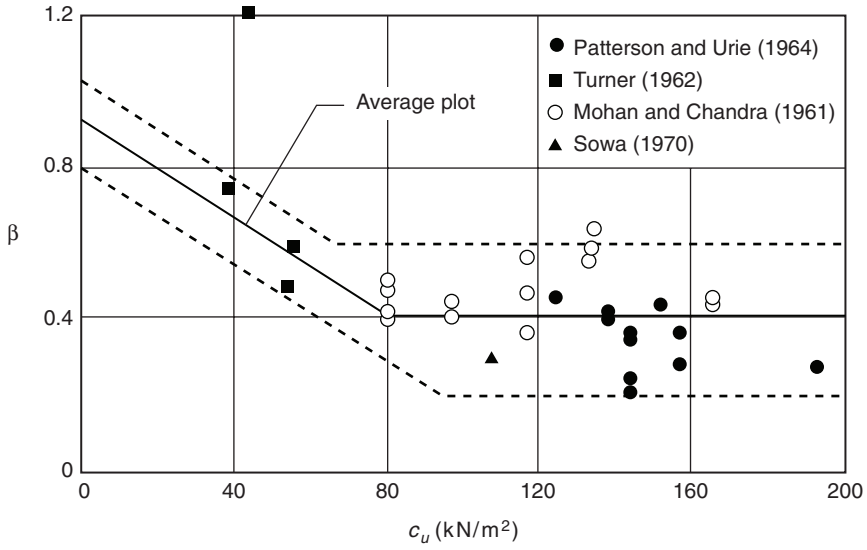

FIGURE 8.27 Variation of β versus c_u for cast *in situ* concrete piles

For a given value of c_u, the magnitude of β determined from Equation 8.51 is slightly lower than that recommended by Tomlinson (1957) for calculation of the skin resistance of concrete piles under compressive loading.

8.3.1.2 Metal Piles

Das and Seeley (1982) reported several laboratory model test results for the ultimate uplift capacity of metal piles in saturated clay. Based on their observations, it appears that for metal piles:

$$\beta = 0.715 - 0.0191 c_u \geq 0.2 \tag{8.52}$$

where c_u is in kN/m^2.

Figure 8.28 shows a comparison between Equations 8.51 and 8.52. It can be seen that for all values of c_u, the β factor for metal piles is lower than that for cast *in situ* concrete piles.

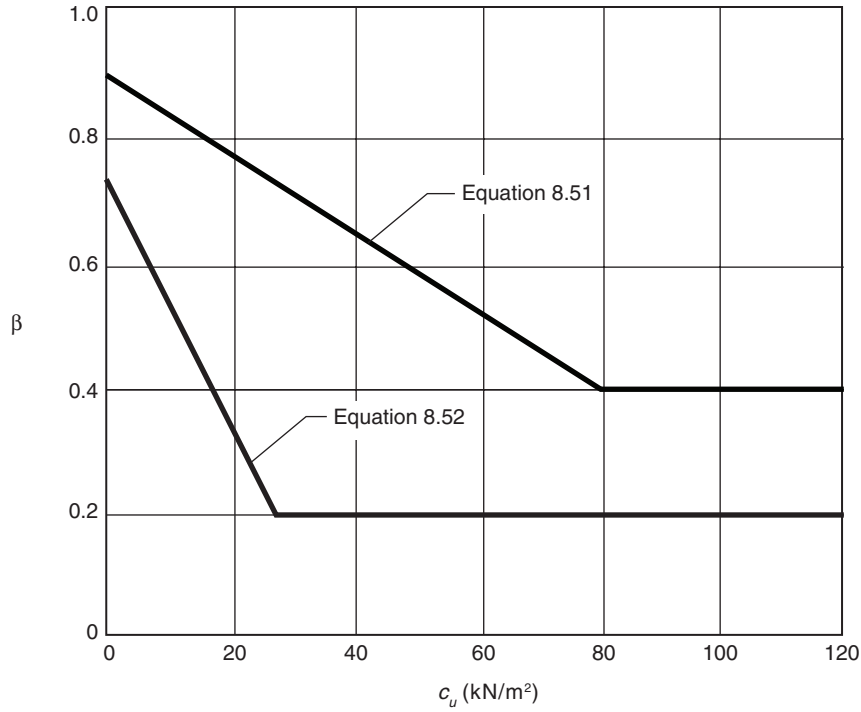

FIGURE 8.28 Comparison of Equations 8.51 and 8.52

8.3.2 Load-Displacement Relationship for Vertical Piles Subjected to Axial Uplift

Das and Seeley (1982) reported that for metal piles with $L/D \leq 16$, the net ultimate uplift capacity is realized when the pile undergoes an axial uplift of about $0.05D$ ($\approx \Delta_u$). Based on their model test results, they suggested a nondimensional relationship between the net load Q and vertical displacement Δ, which is of the form

$$\overline{Q} = \frac{\overline{\Delta}}{a + b\overline{\Delta}} \tag{8.53}$$

where

$$\overline{Q} = \frac{Q}{Q_u} \tag{8.54}$$

where

Q = net load at an axial displacement Δ
Q_u = net ultimate load at an axial displacement Δ_u
a, b = constants

Equation 8.53 can be used to make preliminary estimation of the axial displacement of a pile for a net allowable load Q. The average values of the constants a and b can be taken as 0.2 and 0.8, respectively.

Example 8.7

A vertical concrete pile with a square cross section of 0.3 m × 0.3 m and a length of 8 m is embedded in a saturated clay with an undrained cohesion of 60 kN/m^2. Estimate the net ultimate uplift capacity.

Solution

From Equation 8.50:

$$Q_u = 4DL\beta c_u$$

$D = 0.3$ m, $L = 8$ m, and $c_u = 60$ kN/m^2. From Equation 8.51:

$$\beta = 0.9 - 0.00625c_u = 0.9 - (0.00625)(60) = 0.525$$

Therefore:

$$Q_u = (4)(0.3)(8)(0.525)(60) = \mathbf{302.4\ kN}$$

Example 8.8

Refer to Example 8.7. For an allowable net uplift load of 100 kN, estimate the vertical displacement of the pile.

Solution

From Equation 8.54:

$$\overline{Q} = \frac{Q}{Q_u} = \frac{100}{302.4} = 0.331$$

From Equation 8.53:

$$\overline{Q} = \frac{\overline{\Delta}}{a + b\overline{\Delta}}$$

$a \approx 0.2$ and $b \approx 0.8$. Therefore:

$$0.331 = \frac{\overline{\Delta}}{0.2 + 0.8\overline{\Delta}}$$

or

$$0.662 + 0.2648\overline{\Delta} = \overline{\Delta}$$

or

$$\overline{\Delta} = \frac{0.662}{0.735} = 0.9$$

However:

$$\overline{\Delta} = \frac{\Delta}{\Delta_u}$$

Therefore:

$$\Delta = (\overline{\Delta})(\Delta_u) \approx (0.9)(0.05D) = (0.9)(0.05)(0.3)$$

$$= 0.0135 \text{ m} = \mathbf{13.5 \text{ mm}}$$

8.3.3 Inclined Pile Subjected to Axial Pull

Figure 8.29 shows an inclined pile subjected to axial pull. The inclination of the pile with respect to the vertical is equal to α. For this condition, the gross uplift capacity can be given by Equation 8.23, or:

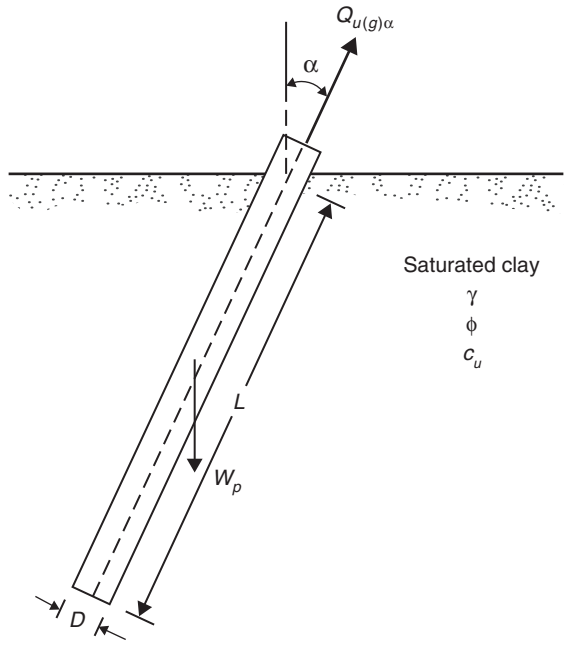

FIGURE 8.29 Inclined pile embedded in clay subjected to axial pull

$$Q_{u(g)\alpha} = Q_{u\alpha} + W_p \cos\alpha \tag{8.55}$$

The magnitude of the net ultimate uplift capacity $Q_{u\alpha}$ can be given as:

$$Q_{u\alpha} = pL\beta c_u \tag{8.56}$$

where

p = perimeter of the pile, which is equal to πD for circular piles and $4D$ for square piles

The magnitude of the adhesion factor can be estimated from Equation 8.51 or 8.52 depending on the pile type.

8.3.4 Uplift Capacity of Vertical Pile Subjected to Inclined Pull

As in Section 8.2.4, Figure 8.30 shows a vertical pile embedded in saturated clay which is subjected to an inclined pull. The ultimate uplift capacity of the pile measured in the direction of the pull can be given by Equation 8.37, or:

$$Q_{u(g)\theta} = Q_{u\theta} + W_p \cos\theta$$

For rigid piles (that is, $L/D \leq 15$ to 20), the gross ultimate uplift capacity $Q_{u(g)\theta}$ can also be given by Equation 8.38 (Meyerhof, 1973b). Hence:

$$\left[\frac{Q_{u(g)\theta}\cos\theta}{Q_{u(g)V}}\right] + \left[\frac{Q_{u(g)\theta}\sin\theta}{Q_{u(g)H}}\right]^2 = 1$$

The magnitude of $Q_{u(g)V}$ can be estimated from Equation 8.49 or 8.50, or:

$$Q_{u(g)V} = pL\beta c_u + W_p \tag{8.57}$$

where

$p = \pi D$ for circular piles and $4D$ for square piles

The gross ultimate lateral load $Q_{u(g)H}$ can be estimated as (Meyerhof, 1973b):

$$Q_{u(g)H} = c_u K_h'' \tag{8.58}$$

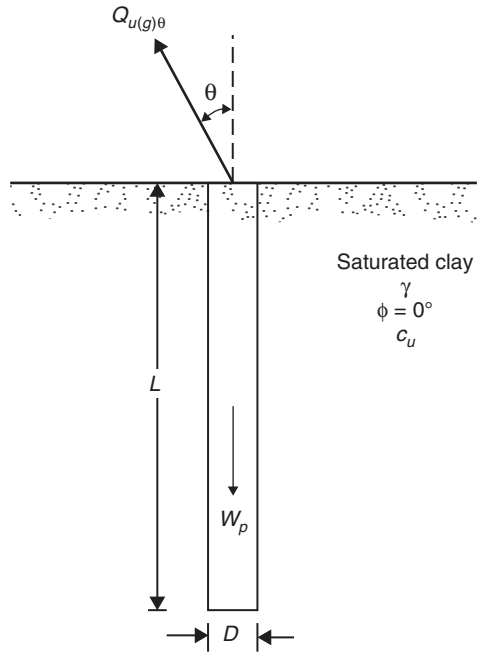

FIGURE 8.30 Vertical pile embedded in saturated clay subjected to inclined pull

where

K''_h = coefficient of lateral resistance

Based on experimental results, Meyerhof (1973b) proposed that:

$$K''_h = 1 + 0.8\left(\frac{L}{D}\right) \leq 3 \tag{8.59}$$

8.3.5 Uplift Capacity of Group Piles in Clay

Research relating to the uplift capacity of group piles (Figure 8.23) is rather scarce at the present time. The gross and net ultimate uplift capacities of group piles can be related by Equation 8.45, or:

$$Q_{ug(g)} = Q_{ug} + W_{gp}$$

Also, the group efficiency can be expressed by Equation 8.46:

$$\eta = \frac{Q_{ug}}{mnQ_u}$$

Das (1990) provided several model test results for group efficiency of piles in soft clay with $L/D = 15$ and 20 and $c_u = 10.06$ and 22.5 kN/m^2, and these results are shown in Figures 8.31 to 8.34. From these figures, the following conclusions can be drawn:

1. For a given clay (that is, c_u), L/D, and number of piles in a group, the magnitude of η increases linearly with s/D.

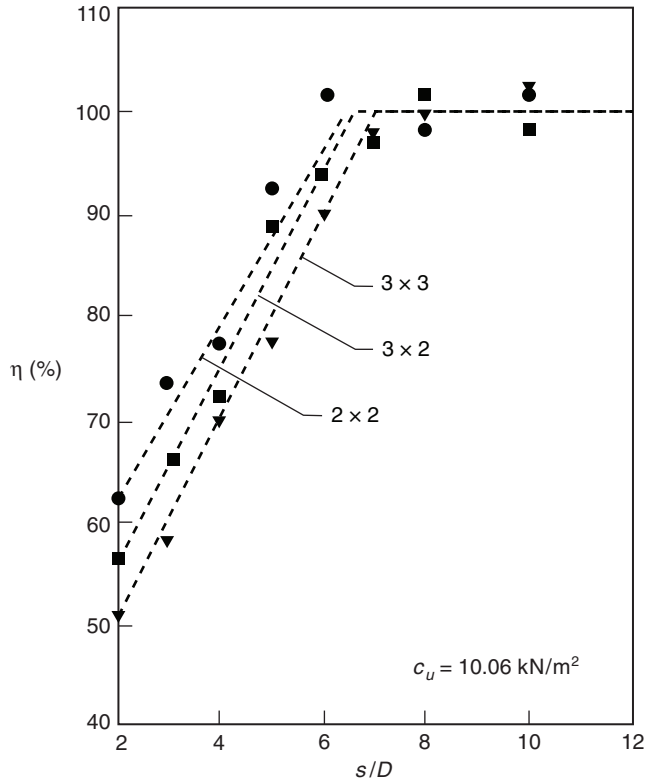

FIGURE 8.31 Model test results of Das (1990) for variation of η versus s/D ($L/D = 15$, $c_u = 10.06$ kN/m^2)

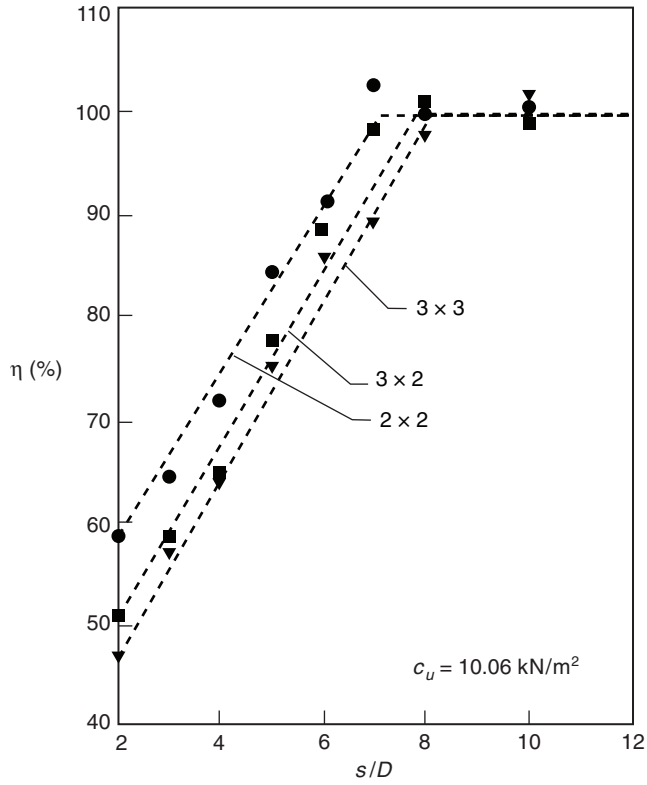

FIGURE 8.32 Model test results of Das (1990) for variation of η versus s/D (L/D = 20, c_u = 10.06 kN/m^2)

2. For a given s/D ratio and clay, the group efficiency decreases with the increase in the number of piles ($m \times n$) in the group.
3. For a given clay soil (that is, c_u) and number of piles in the group, the efficiency decreases with the increase in the L/D ratio.
4. For a given L/D ratio, number of piles in a group, and s/D, the increase in c_u results in a decrease in the magnitude of the group efficiency.
5. For short piles (that is, $L/D \leq 20$), it appears that:

$$\left(\frac{s}{D}\right)_{\eta = 100\%} \approx 0.4 \text{ to } 0.5 \left(\frac{L}{D}\right)$$

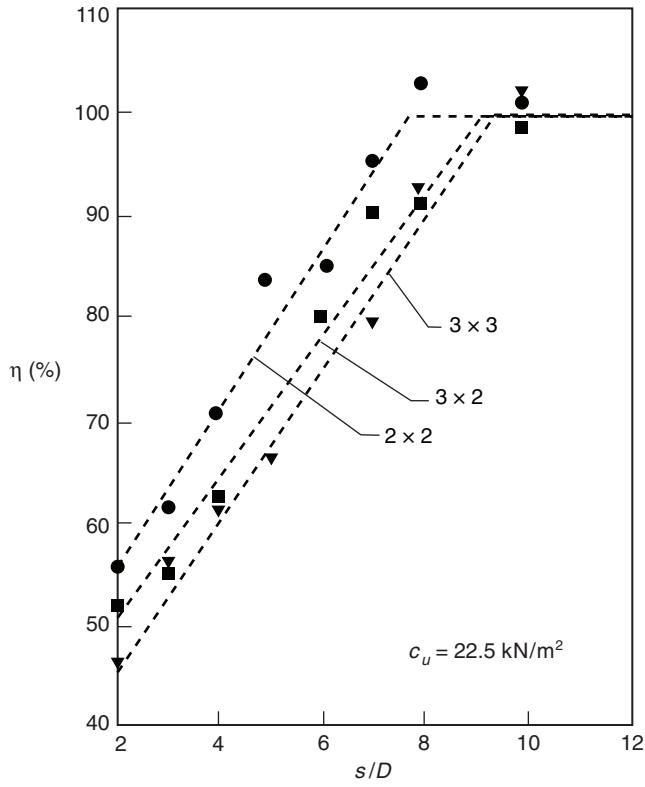

FIGURE 8.33 Model test results of Das (1990) for variation of η versus s/D (L/D = 15, c_u = 22.5 kN/m^2)

8.4 SUMMARY OF MAIN POINTS

1. The net ultimate uplift capacity of a pile embedded in sand is primarily a function of the following parameters: length of embedment, pile diameter, roughness of the pile surface, soil friction angle, soil relative density, and nature of placement of the pile (driven, bored, or cast in place).
2. The net ultimate uplift capacity of a pile embedded in clay is primarily a function of the following parameters: length of embedment, pile diameter, undrained cohesion, and nature of placement of the pile (driven, bored, or cast in place).

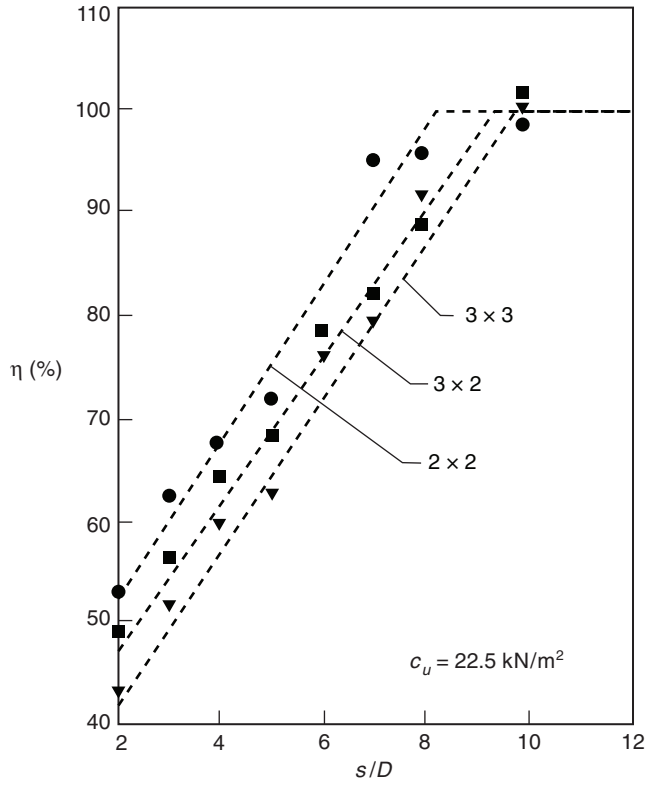

FIGURE 8.34 Model test results of Das (1990) for variation of η versus s/D (L/D = 20, c_u = 22.5 kN/m^2)

3. Under similar conditions, the net ultimate uplift load of a pile is somewhat lower than that of a horizontal plate anchor.
4. For a given sand and relative density of compaction, the unit frictional resistance increases linearly with length-to-diameter ratio (also called embedment ratio) up to a certain value and remains constant thereafter.
5. For vertical pull, the net load gradually increases with vertical displacement up to a maximum value, at which complete pullout of the pile occurs. However, for inclined pull, the net load increases with inclined displacement rather rapidly up to a certain value, beyond which the load-displacement plot becomes practically linear.
6. For a given sandy soil, its relative density, and number of piles in a group, the group efficiency increases almost linearly with pile spacing-to-diameter ratio up to a maximum value of 100%.

7. For a given clay, embedment ratio, and number of piles in a group, the magnitude of the group efficiency increases linearly with pile spacing-to-diameter ratio.

SELF-ASSESSMENT QUESTIONS

Select the most appropriate answer to each multiple-choice question

8.1. Piles are used to:
   a. transmit downwardly directed structural load to a stronger soil at a greater depth
   b. resist lateral load imposed on a foundation
   c. resist uplift force imposed on a foundation
   d. all of the above

8.2. The critical embedment ratio of an anchor pile in dense sand is about:
   a. 3.5
   b. 10.0
   c. 14.5
   d. none of the above

8.3. Select the incorrect statement:
   a. for a given soil, its relative density, and number of piles in a group, the group efficiency increases almost linearly with pile spacing-to-diameter ratio up to a maximum value of 100%
   b. for a given soil and pile spacing-to-diameter ratio, the group efficiency increases with the increase in the number of piles in a group
   c. for a given soil, pile spacing-to-diameter ratio, and number of piles in a group, the efficiency decreases with the increase in embedment ratio
   d. none of the above

8.4. The net ultimate uplift capacity of an anchor pile in clay is directly proportional to the:
   a. perimeter of the pile cross section
   b. pile length
   c. adhesion at the pile-clay interface
   d. all of the above

8.5. The ratio of the angle of friction at the soil-pile interface to the soil friction angle is unity (1) for soil relative density equal to about:
   a. 80%
   b. 60%
   c. 40%
   d. 20%

Answers

8.1: d 8.2: c 8.3: b 8.4: d 8.5: a

REFERENCES

Broms, B.B. (1965). Design of laterally loaded piles. *J. Soil Mech. Found. Div. ASCE,* 91(3):79–97.

Das, B.M. (1983). A procedure for estimation of uplift capacity of rough piles. *Soils Found.,* 23(3):122–126.

Das, B.M. (1989). Ultimate uplift capacity of piles and pile groups in granular soil. *Proc. Int. Conf. Piling and Deep Found.,* DFI, London, 241–246.

Das, B.M. (1990). Group efficiency of metal piles in clay subjected to uplifting load. *Proc. OMAE Conf.,* ASCE, Houston, 415–420.

Das, B.M. and Seeley, G.R. (1982). Uplift capacity of pipe piles in saturated clay. *Soils Found.,* 22:91–94.

Das, B.M., Seeley, G.R., and Pfeifle, T.W. (1977a). Pullout resistance of rough rigid piles in granular soils. *Soils Found.,* 17(3):72–77.

Das, B.M., Seeley, G.R., and Raghu, D. (1977b). Uplift capacity of model piles under oblique loads. *J. Geotech. Eng. Div. ASCE,* 1202(9):1009–1013.

Meyerhof, G.G. (1973a). Uplift resistance of inclined anchors and piles. *Proc. VIII Int. Conf. Soil Mech. Found.,* Moscow, 167–172.

Meyerhof, G.G. (1973b). The uplift capacity of foundations under oblique loads. *Can. Geotech. J.,* 10(1):64–70.

Mohan, D. and Chandra, S. (1961). Frictional resistance of bored piles in expansive clays. *Geotechnique,* 11(4):294–301.

Patterson, G. and Urie, R.I. (1964). Uplift resistance of full size tower foundations. *Proc. Conf. Int. Grande Reseaux Electrique a haute Tension,* Paper No. 203, Paris.

Sowa, V.A. (1970). Pulling capacity of concrete cast-in-situ piles. *Can. Geotech. J.,* 7:482–493.

Tomlinson, M.J. (1957). The adhesion of piles driven in clay soils. *Proc. IV Int. Conf. Soil Mech. Found. Eng.,* London, 2, 66–71.

Tran-Vo-Nhiem (1971). Ultimate uplift capacity of anchor piles. *Proc. IV Budapest Conf. Soil Mech. Found. Eng.,* Arpad Kezki, Ed., Budapest, 829–836.

Turner, E.A. (1962). Uplift resistance of transmission tower footing. *J. Power Div. ASCE,* 88(2):17–33.

Vesic, A.S. (1970). Tests on instrumented piles, Ogeechee River site. *J. Soil Mech. Found. Div. ASCE,* 96(2):561–584.

9

SUCTION CAISSON AND DRAG ANCHORS

The offshore developments in oil and gas production industries to move into deeper waters require anchored floating structures. This chapter summarizes the basic concepts of two types of deep-water anchors, suction caisson and drag anchors, and describes the basic theories relating to their applications.

9.1 INTRODUCTION

Offshore floating structures in oil and gas production industries are generally placed in their positions using mooring systems (steel wire/chain, synthetic rope, steel tendons, etc.) connected to suitable anchors installed in the seabed. As introduced in Chapter 1, suction caisson and drag anchors have been the two most common types in use in recent years, and therefore they are described here; details of other anchor types used in offshore applications can be found in the book by Randolph and Gourvenec (2011).

9.2 SUCTION CAISSON ANCHORS

Although concrete caisson anchors have been used, the vast majority of modern suction caisson anchors consist of large-diameter, typically in the range of 3 to 8 m, internally stiffened thin-walled steel cylindrical cells, open at the bottom

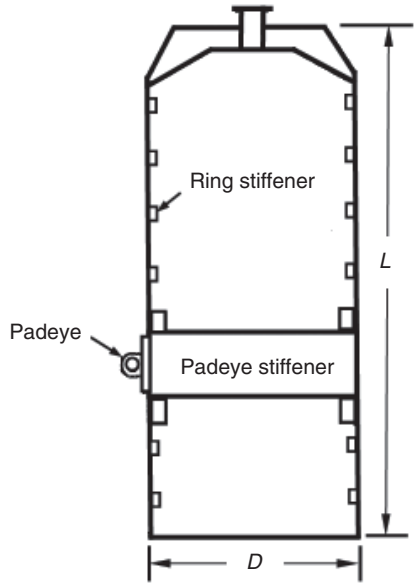

FIGURE 9.1 Suction caisson anchor (adapted from Randolph and Gourvenec, 2011)

and closed on the top (Chen and Randolph, 2007; Randolph and Gourvenec, 2011) (Figure 9.1). The length/embedment depth (L) to diameter (D) ratio of the cylindrical cells is generally in the range of 3 to 6. The cylindrical cells form a skirt system, which gets penetrated into the seabed initially by the self-weight of the cells, with further penetration achieved by pumping the water out through the opening in the top lid of the caisson, thus developing suction/underpressure inside the skirt compartments to force the caisson downward. The main reason for using suction anchors instead of traditional fixed-jacket or gravity-based structures is the significant savings in construction and installation cost (Dyvik et al., 1993).

There is currently a lack of established theoretical analysis and design guidelines for the applications of suction caisson anchors. Any attempt at realistic analysis and design requires soil data from advanced laboratory testing because the soil beneath the caisson experiences combined static and cyclic loads caused by wind or water currents (Dyvik et al., 1993; Ehlers et al., 2004; Randolph and Gourvenec, 2011). The calculation of shaft capacity of suction caisson anchors is currently based partly on conventional design methods for open-ended driven piles and also on field experience. Chen and Randolph (2007) report that,

compared with driven tubular piles, suction caissons have lower wall thickness and thus a much larger ratio of diameter (D) to wall thickness (t), with D/t values in the range of 60 to 200 rather than the typical range of 30 to 50 for piles. Even if the full volume of steel can be accommodated entirely by outward soil movement, it can be expected that the resulting stress and pore water pressure changes for suction caissons should be lower than during pile installation. The low embedment ratio and relatively high stiffness of suction caisson anchors lead to failure by rigid body motion compared with an anchor pile, which forms plastic hinges during failure.

Design issues for suction caisson anchors are divided into two groups (Randolph and Gourvenec, 2011):

1. Design for installation
2. Design for operational conditions, principally capacity

The installation design issues consider external and internal resistance during penetration of caissons, and they are commonly analyzed using conventional soil mechanics principles. Limit equilibrium methods are commonly used to estimate vertical, horizontal, and inclined anchor capacities. The vertical uplift capacity of a suction caisson anchor is governed by the weight of the caisson, frictional resistance over the caisson shaft, and upward or reverse end bearing.

With passive suction (Figure 9.2), the vertical uplift capacity Q_u is calculated as (Randolph and Gourvenec, 2011):

$$Q_u = W' + A_{se}\alpha_e \bar{c}_{u(t)} + N_c c_u A_e \tag{9.1}$$

where

W' = submerged weight of the caisson
A_e = external cross-sectional area
A_{se} = external shaft surface area
α_e = coefficient of external (steel to soil) shaft friction
c_u = representative undrained soil shear strength at the tip level
$\bar{c}_{u(t)}$ = average undrained soil shear strength over penetrated depth at time t after installation
N_c = reverse end-bearing factor ($\approx$9)

Without passive suction, the vertical uplift capacity Q_u is calculated as (Randolph and Gourvenec, 2011):

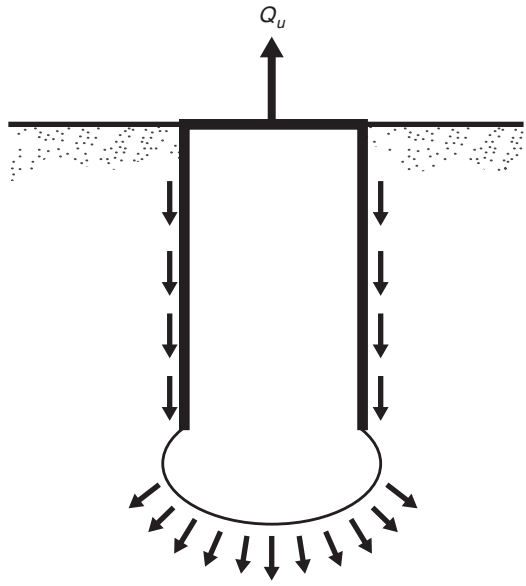

FIGURE 9.2 Caisson anchor with passive suction under reverse end-bearing failure mode

$$Q_u = W' + A_{se}\alpha_e \bar{c}_{u(t)} + A_{si}\alpha_i \bar{c}_{u(t)} \tag{9.2}$$

for caisson pullout failure mode (Figure 9.3) where

A_{si} = internal shaft surface area
α_i = coefficient of internal (steel to soil) shaft friction

or

$$Q_u = W' + A_{se}\alpha_e \bar{c}_{u(t)} + W'_{\text{plug}} \tag{9.3}$$

for caisson and plug pullout failure mode (Figure 9.4), where

W'_{plug} = effective weight of the soil plug

It should be noted that the actual value of the ultimate uplift capacity can be much lower than those calculated by using Equations 9.1 to 9.3. This may be mainly because of the damaging effects of combined cyclic loading and the oscillating horizontal component of load (Clukey et al., 1995).

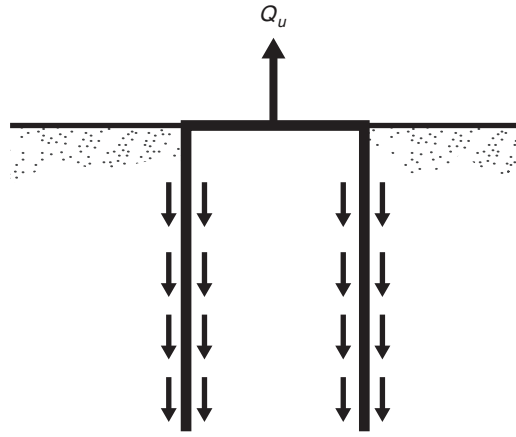

FIGURE 9.3 Caisson anchor without passive suction under caisson pullout failure mode

The failure modes of suction caisson anchors loaded horizontally at the seabed are similar to those for laterally loaded piles (Murff and Hamilton, 1993). The padeye location is calculated by moment equilibrium so that the suction caisson anchor is designed to translate horizontally and not rotate under lateral loading to achieve the maximum lateral load-carrying capacity. With no rotation of the caisson, the maximum lateral load capacity $Q_{h\,\max}$ is calculated as (Randolph and Gourvenec, 2011):

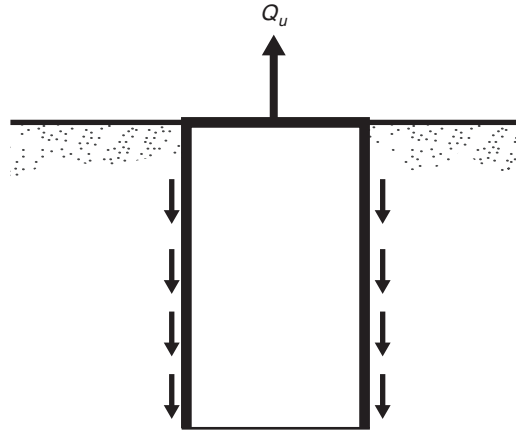

FIGURE 9.4 Caisson anchor without passive suction under plug pullout failure mode

$$Q_{h\max} \approx LD_e N_p \bar{c}_u \tag{9.4}$$

where

L = embedded length of caisson
D_e = external diameter of caisson
N_p = lateral bearing capacity factor
$\bar{c}_u$ = undrained shear strength averaged over penetration depth

It is important to note that for general loading conditions with combinations of vertical and horizontal loading, the pure vertical and pure horizontal capacities reduce by the presence of loading in the orthogonal direction. Interaction at the base of the caisson leads to a reduction in the vertical reverse end-bearing capacity as the caisson is simultaneously displaced laterally or rotated. The inclined load capacity of a suction caisson anchor also depends on whether a crack develops along the trailing edge of the caisson.

9.3 DRAG ANCHORS

A traditional drag anchor (also called fixed fluke plate anchor) consists of a broad fluke rigidly connected to a shank, as shown in Figure 9.5. The angle between the shank and the fluke is predetermined, though it may be adjusted prior to anchor placement on the seabed. The traditional drag anchors have a limitation of taking large vertical loads; therefore, vertically loaded anchors (also called drag-in plate anchors) also have been developed.

Historically, the design of drag anchors has been empirically based, but some recent approaches have been proposed to predict the entire drag trajectory and

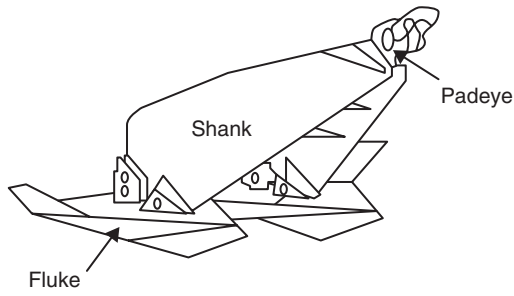

FIGURE 9.5 Conventional drag anchor (fixed fluke plate anchor) (adapted from Randolph and Gourvenec, 2011)

the holding capacity of anchors in clays (O'Neill et al., 2003). Most approaches are based on limit equilibrium analyses to identify the loads acting on the anchor and kinematic analyses to assess the movement of the anchor with some degree of empiricism. As a drag anchor approaches its ultimate holding capacity in soft undrained soils, failure of soil can be assumed to consist of localized plastic flow around the anchor fluke and shank. Owing to the relatively complex geometry of modern drag anchors, the anchor failure loads (forces parallel and perpendicular to the top face of the fluke and negative moment) are the result of very complicated three-dimensional (3D) soil displacements. A detailed investigation of these displacements would require a full 3D analysis, incorporating the complete 3D geometry of the anchor. Such an analysis can be extremely time consuming, computationally expensive, and anchor specific. To avoid working on a complex analysis, it is general practice to assume that the fluke provides a large proportion of the anchor's holding capacity and governs much of the anchor's kinematics. Considering this fact, O'Neill et al. (2003) presented a 2D finite element analysis of fluke-soil interaction in clay in an attempt to develop a design tool.

After the initial set of the drag anchor in the seabed, an increase in tension in the mooring system, say a chain, results in the anchor moving down at a slightly shallower angle than that of the fluke, dragging the end of the chain down into the soil with it. Figure 9.6 shows the motion of a drag anchor during penetration. Because of the resistance afforded by the soil to the downward movement of the chain, the chain takes up an inverse catenary, with the result that the direction of the force at the anchor shackle becomes steeper. As a result of this change in direction, the anchor gets rotated so that the fluke becomes more nearly horizontal. As penetration proceeds, the fluke eventually becomes close to horizontal and no further penetration occurs (Thorne, 1998).

The motion of the anchor shown in Figure 9.6 results in the soil around the shank failing in bearing capacity on the underside and in shearing on the base

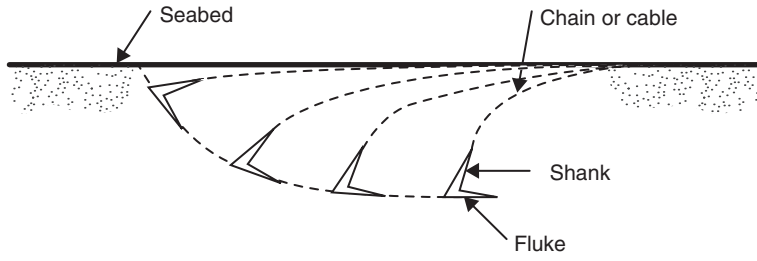

FIGURE 9.6 Penetration of drag anchor (adapted from Thorne, 1998)

and sides, exerting on the shank the maximum force of which the soil is capable. This is also true for other elements (such a anchor shackles, palms, etc.) of the anchor that have to be dragged through the soil. These forces are calculated for an anchor installed in undrained clays as follows (Thorne, 1998):

$$\text{Drag force} = DA_i DF_i c_u \tag{9.5}$$

where

DA_i = area for the ith component
DF_i = drag factor for the ith component
c_u = undrained shear strength

A drag force is shown in Figure 9.7, along with the major elements of the anchor. In the case of a long shank of rectangular cross section, there can be three drag force components (Thorne, 1998):

1. Base bearing
2. Skin adhesion of the base
3. Skin adhesion of the sides

The drag factor for base bearing is taken as the conventional value for a long footing; the area is the base area, and this force is taken as acting at right angles

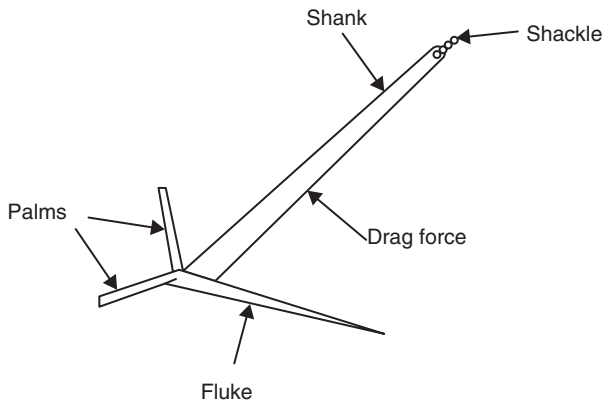

FIGURE 9.7 A drag force with basic elements of traditional drag anchor (adapted from Thorne, 1998)

to the shank. The area for side adhesion is taken as the sum of the two side areas, the drag factor as an adhesion factor of 1.0, and the force is assumed to act parallel to the fluke because this is in the direction of movement. The area for base adhesion is taken as the base area, the drag factor as an adhesion factor of 1.0, and the force is assumed to act parallel to the shank and toward the fluke end. All forces are assumed to act at the centers of the respective areas, and the undrained shear strength is taken as that at the center of area. Forces on the back of the shank are ignored on the basis that the material in contact with it will be very disturbed and softened.

The drag factors for several shapes are discussed by Thorne (1998). The drag factor (DF_i) for the specific component may be equivalent to some suitable bearing capacity factor N_c. For the most part, anchor components can be considered as either cylinders, wedges, flat plates pulled at some angle through the seabed, or long rectangular bars.

The drag forces are added to give the total drag force components normal and parallel to the fluke and the moment about the fluke center of area. In a properly designed anchor in soft clay, uplift capacity failure normal to the fluke rarely takes place. The fluke may fail the surrounding soil by rotating about its horizontal axis without pulling out; this usually occurs in the early stages of penetration but not thereafter.

Anchor forces for a given depth and fluke angle are calculated by considering two force and one moment equilibrium equations and one equation coming from chain behavior. All four of these equations involve four unknowns:

1. Moment (M)
2. Chain tension (T_a) at the attachment point
3. Normal force (F_n) on the fluke from the soil, acting through the geometric center of the fluke
4. Angle (θ_a) of the chain at the anchor attachment to the horizontal

An iterative method is used to solve the chain equations. Neubecker and Randolph (1996) suggested a simplified closed-form solution as:

$$\theta_a = \sqrt{\frac{2Z\overline{Q}}{T_a}} + \theta_0^2 \tag{9.6}$$

where

$\overline{Q}$ = average normal force per unit length of the chain
Z = depth from the mud line to the anchor shackle
θ_0 = angle of the chain at the mud line to the horizontal

Equation 9.6 ignores the self-weight of the chain, but this has been shown to incur errors of less than 2.5%. With four equations with four unknowns, it is possible to calculate the shackle load and mud line tension to move an anchor if the depth and fluke angle are known. Based on the field data reported in the past, Thorne (1998) has found that the method of analysis described above works well. For routine designs, the anchor manufacturer's design charts also help greatly.

9.4 SUMMARY OF MAIN POINTS

1. Suction caisson and drag anchors are the two most common anchor types used in deep waters for offshore floating structures.
2. The vast majority of modern suction caisson anchors consist of large-diameter, internally stiffened, thin-walled, steel cylindrical cells, open at the bottom and closed on the top.
3. The suction caisson anchors get penetrated into the seabed initially by their self-weight, with further penetration achieved by creating underpressure inside the skirt compartments.
4. The calculation of shaft capacity of a suction caisson anchor is currently based partly on conventional design methods for open-ended driven piles and also on field experience.
5. The failure modes of suction caisson anchors loaded horizontally at the seabed are similar to those for laterally loaded piles.
6. A traditional drag anchor consists of a broad fluke rigidly connected to a shank.
7. As penetration of a drag anchor proceeds, the fluke eventually becomes close to horizontal and no further penetration occurs.
8. When a drag anchor approaches its ultimate holding capacity in soft undrained soils, failure of the soil can be assumed to consist of localized plastic flow around the anchor fluke and shank.
9. Anchor forces for a given depth and fluke angle of the drag anchor are calculated by considering two force and one moment equilibrium equations and one equation coming from the chain behavior.

SELF-ASSESSMENT QUESTIONS

Select the most appropriate answer to each multiple-choice question

9.1. The diameter of suction caisson anchors is typically in the range of:
   a. 1 to 2 m
   b. 2 to 5 m
   c. 3 to 8 m
   d. 10 to 20 m

9.2. The initial settlement of the suction caisson anchor is by:
   a. its self-weight
   b. underpressure created by pumping water out
   c. underpressure created by pumping air out
   d. both a and b

9.3. The ratio of diameter to wall thickness of suction caisson anchors is typically in the range of:
   a. 3 to 5
   b. 6 to 20
   c. 30 to 50
   d. 60 to 200

9.4. The vertical uplift capacity of a suction caisson anchor is governed by:
   a. the weight of the caisson and frictional resistance over the caisson shaft
   b. frictional resistance over the caisson shaft and upward end bearing
   c. the weight of the caisson, frictional resistance over the caisson shaft, and upward end bearing
   d. none of the above

9.5. In the case of a long shank of rectangular cross section, the drag force may have:
   a. only one component
   b. two components
   c. three components
   d. four components

9.6. The angle made by the drag force against the base bearing with the shank of a drag anchor is:
   a. 0°
   b. 30°
   c. 60°
   d. 90°

9.7. In a properly designed drag anchor, uplift capacity failure:
   a. rarely takes place normal to the fluke
   b. is caused by soil bearing capacity failure
   c. both a and b
   d. always takes place normal to the fluke

9.8. Anchor forces for a given depth and fluke angle are calculated by solving four equations, out of which how many equations are force equilibrium equations:
   a. 1
   b. 2
   c. 3
   d. 4

Answers

9.1: c 9.2: b 9.3: d 9.4: c 9.5: c 9.6: d 9.7: c 9.8: b

REFERENCES

Chen, W. and Randolph, M.F. (2007). External radial changes and axial capacity for suction caissons in soft clay. *Geotechnique.* 57(6):499–511.

Clukey, E.C., Morrison, M.J., Garnier, J., and Corte, J.F. (1995). The response of suction caisson in normally consolidated clays to cyclic TLP loading conditions. *Proc. Offshore Tech. Conf.,* Houston, Paper OTC 7796.

Dyvik, R., Andersen, K.H., Hansen, S.B., and Christophersen, H.P. (1993). Field tests of anchors in clay. I: Description. *J. Geotech. Eng.,* 119(10):1515–1531.

Ehlers, C.J., Young, A.G., and Chen, J.H. (2004). Technology assessment of deep water anchors. *Proc. Offshore Tech. Conf.,* Houston, Paper OTC 16840.

Murff, J.D. and Hamilton, J.M. (1993). P-ultimate for undrained analysis of laterally loaded piles. *J. Geotech. Eng.,* 119(1):91–107.

Neubecker, S.R. and Randolph, M.F. (1996). The performance of drag anchor and chain systems in cohesive soil. *Mar. Georesour. Geotechnol.,* 14:77–96.

O'Neill, M.P., Bransby, M.F., and Randolph, M.F. (2003). Drag anchor fluke-soil interaction in clays. *Can. Geotech. J.,* 40:78–94.

Randolph, M. and Gourvenec, S. (2011). *Offshore Geotechnical Engineering,* Spon Press, Taylor and Francis, Abingdon, Oxon.

Thorne, C.P. (1998). Penetration and load capacity of marine drag anchors in soft clay. *J. Geotech. Geoenviron. Eng.,* 124(10):945–953.

10

GEO-ANCHORS

Geo-anchors are used in several geotechnical applications. This chapter summarizes the concepts of two types of geo-anchors, namely geotextile-wrapped anchors and trench anchors, and describes the basic theories relating to their analysis and design.

10.1 INTRODUCTION

Two forms of geo-anchors (geotextile-wrapped anchors and trench anchors) were introduced in Chapter 1. A geotextile-wrapped anchor consisting of a permeable core of coarse sand, gravel, or crushed stone wrapped in one or several layers of high-strength woven geotextiles can be used to increase the stability of steep slopes, to reduce the lateral earth pressures on retaining structures, or to stabilize embankments constructed on soft clay (Broms and Wong, 1986; Broms, 1993; Shukla and Yin, 2006; Shukla, 2012). The trench anchor is commonly used for firmly securing a geosynthetic layer installed as a pond/canal liner or slope surface protection so that geosynthetic movement or pullout does not occur (Hullings and Sansone, 1997; Shukla and Yin, 2006; Shukla, 2012) during installation and operation of the system. This chapter presents the fundamentals of these two anchors.

10.2 GEOTEXTILE-WRAPPED ANCHORS

Figure 10.1 shows geotextile-wrapped anchors installed along slopes (Broms and Wong, 1986; Shukla and Yin, 2006; Shukla, 2012). The drains reduce the pore

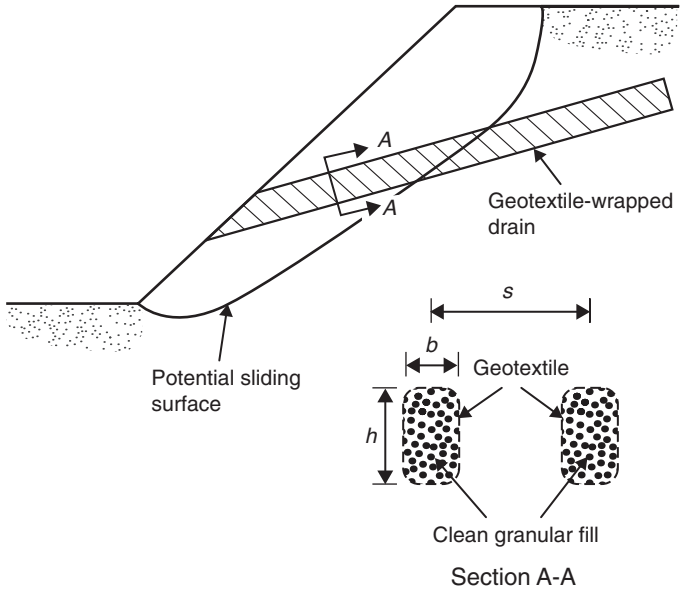

FIGURE 10.1 Schematic of slope stabilization using geofabric-wrapped drains (adapted from Broms and Wong, 1986)

water pressure within the slopes during the rainy season, and thereby the shear strength is increased. The geotextile layer acts as a filter around the drains, and therefore it prevents the migration of soil (internal erosion) within the slope into the drains. It also reinforces the soil along potential sliding zones or planes. One additional advantage of installing geotextile-wrapped anchors is that the temporary decrease in the stability of the slope is only marginal during the construction of the deep trenches required for their installation.

The required spacing of the anchors and their dimensions depend on the pore water pressure in the slope, which can be evaluated by means of a flow net (Figure 10.2). The granular material used in the anchor is considered to be infinitely pervious in relation to the slope material. The pore water pressure in the slope is reduced considerably by the drainage function both above and between the anchors, as can be seen from the flow net. For general situations, 0.5-m-wide and 1.0-m-high anchors spaced 3.0 m apart are reasonable.

The anchors should be located deep enough so that they intersect potential slip surfaces in the soil. The maximum depth is about 4 m. For slopes in residual soils or weathered rocks, this depth is usually sufficient because most slope

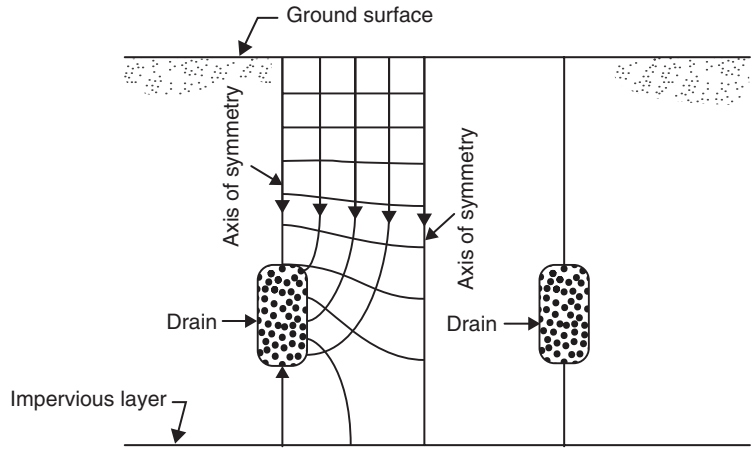

FIGURE 10.2 Flow net showing steady-state seepage toward a geofabric-wrapped drain (adapted from Broms and Wong, 1986)

failures in these materials are shallow, with a maximum depth of failure surface less than 3 to 4 m.

The required tensile strength of the geotextile can be calculated by considering the force polygon for the sliding soil mass above possible sliding surfaces in the soil (Figure 10.3). The sliding surface is often located at the contact between the completely weathered and the underlying partially weathered material.

For a planer sliding surface, the orientation of the geotextile-wrapped anchor should be perpendicular to the resultant of the normal reaction force and the force that corresponds to the mobilized shear strength along the potential failure surface, as shown in Figure 10.3, in order to utilize the geotextile effectively.

The required number of layers (N) of the geotextile in an anchor can be determined as follows:

$$N = \frac{F_s R s}{a T} \tag{10.1}$$

where

R = force per unit width to be resisted by the geotextile
s = anchor spacing

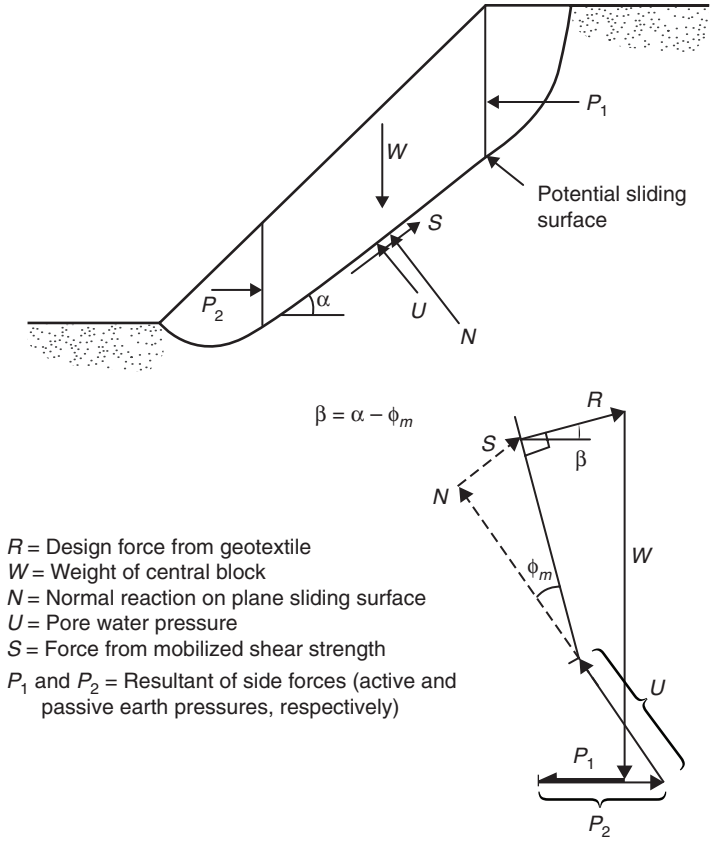

FIGURE 10.3 Computation of design tensile reinforcement to be provided by the geotextile in a geofabric-wrapped drain (adapted from Broms and Wong, 1986)

T = tensile strength per unit width of the geotextile
a = effective perimeter of the drain
F_s = factor of safety

The geotextiles available on the market generally require an elongation of 14 to 50% before the ultimate tensile strength of the geotextile is mobilized. The strain required to mobilize the ultimate strength is much less for woven geotextiles than for nonwoven geotextiles. Only woven geotextiles should therefore be used. In view of the large strain required at failure, a factor of safety of at least 3 should be used in the design.

The length L that is required to transfer the load in the geotextile to the surrounding soil can be calculated as follows:

$$L = \frac{Rs}{2(hK\sigma'_v + b\sigma'_v)\tan\delta'} \tag{10.2}$$

where

σ'_v = vertical effective stress at mid-height (center) of the anchors
K = lateral earth pressure coefficient for the compacted granular material in the anchors
h = height of the anchors
b = width of the anchors
δ' = effective interface friction angle between the geotextile and the soil

The deformation δ of the geotextile to mobilize the required tensile force can be calculated from the following equation:

$$\delta = L \times \frac{e}{100} \tag{10.3}$$

where

e = percent elongation needed to mobilize the required tensile resistance of the geotextile

During the construction of the granular fill drains, it is important to compact the fill carefully. The compaction will increase the lateral earth pressure, and therefore the interface friction between the geotextile and the soil results in reduced transfer length L. For a well-compacted fill, a value of K equal to at least 1.0 can be used in the calculation of transfer length. The lateral earth pressure is highly dependent on the degree of compaction of the granular fill. A second important point, with respect to compaction of the granular fill in anchors, is that the compaction should be done in the downhill direction in order to pretension the geotextile. In this way, the elongation of the geotextile, which is necessary to mobilize the required tensile force as well as the required displacement of the slope, will be reduced.

Geotextile-wrapped anchors were used successfully in Singapore to stabilize a steep slope in residual soil and weathered rock (Broms and Wong, 1986). Following similar concepts, geotextile-wrapped anchors can also be used to stabilize embankments constructed on weak grounds (Figure 10.4) and to reduce the lateral earth pressure on retaining structures (Figure 10.5), as described by Broms (1993).

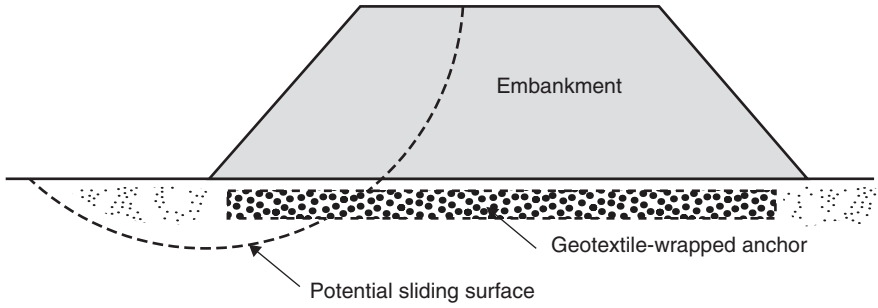

FIGURE 10.4 Stabilization of an embankment resting on weak ground with geo-anchors (adapted from Broms, 1993)

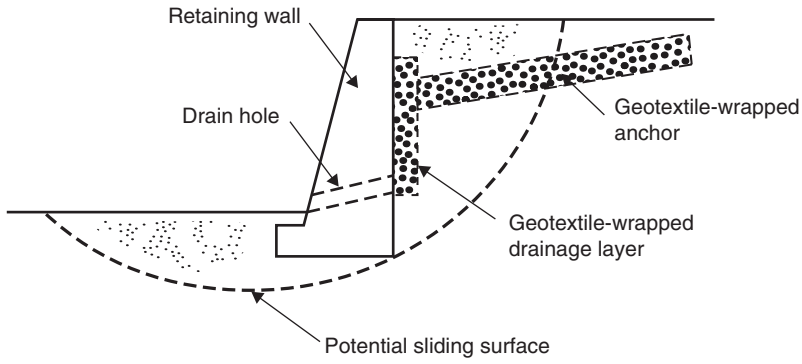

FIGURE 10.5 Stabilization of a retaining wall with geo-anchors and drains (adapted from Broms, 1993)

10.3 TRENCH ANCHORS

To maintain the position of a geosynthetic layer in several field applications before covering with soil/fill, the edges of the layer must be weighted or anchored in trenches (Figure 10.6), thereby providing the significant pullout resistance. Anchorage selection greatly depends on site conditions. In the case of unpaved roads, the geosynthetic should be anchored on each side of the road. The bond length (typically around 1.0 to 1.5 m) can be achieved by extending the geosynthetic beyond the required running width of the road (Figure 10.7a)

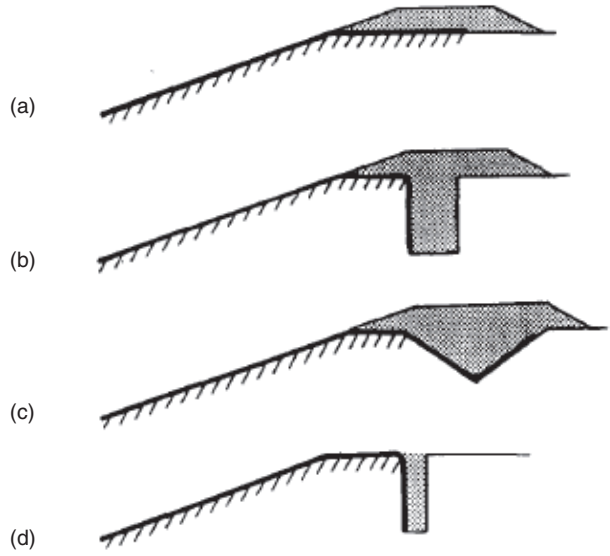

FIGURE 10.6 Simple runout anchor (a) and anchor trenches: rectangular trench (b), V-trench (c), and narrow trench (d) (after Hullings and Sansone, 1997; Shukla and Yin, 2006; Shukla, 2012)

or by providing an equivalent bond length by burying the geosynthetic in shallow trenches (Figure 10.7b) or by wraparound (Figure 10.7c). Similar approaches can also be adopted in other applications.

Hullings and Sansone (1997) presented the design details of trench anchors with a focus on geomembranes, specifically high-density polyethylene (HDPE) geomembranes; the concepts described can also be applicable to other types of geosynthetics. As a basic design principle, the trench anchor resistance should not exceed the allowable stress in the geosynthetic layers at any stage of construction and operation during the design life of trench anchors. As shown in Figure 10.6, different types of trench anchors may be used depending on required anchorage resistance, available space, construction access, and available construction equipment. A simple type of trench anchor is the runout (which is not actually a trench anchor) (Figure 10.6a), which generally requires a large runout length to produce significant pullout resistance. A rectangular trench (Figure 10.6b), typically 0.5 to 0.7 m wide and a maximum of 1 m deep with

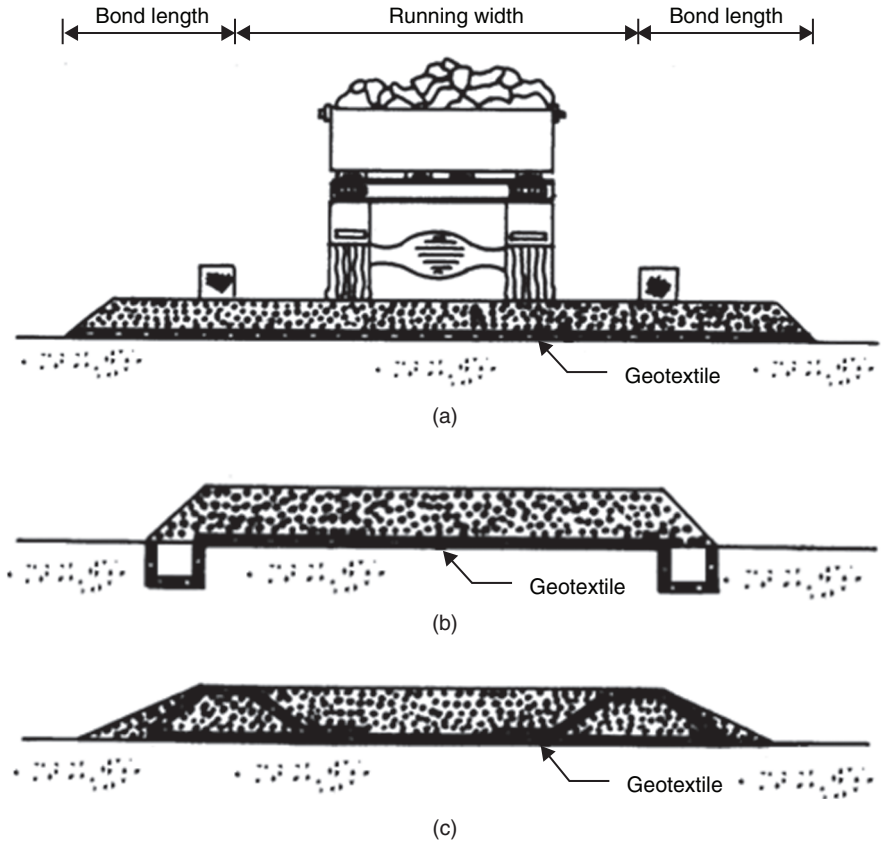

FIGURE 10.7 Use of geosynthetics in unpaved road construction (adapted from Ingold and Miller, 1988)

some runout length, can result in significant pullout resistance. The rectangular trench anchors do not require a lot of room, and they can be constructed with a small backhoe. A V-trench anchor (Figure 10.6c) can be an intermediate choice between rectangular trench and runout anchors. In confined areas, narrow trench anchors (Figure 10.6d) with self-compacting and erosion-resistant backfills may be a better choice.

The simple runout anchor resistance (or ultimate pullout capacity) Q_u may be calculated as the product of weight of the overlying soil multiplied by the tangent of the interface friction angle of the geosynthetic layer. Since the over-

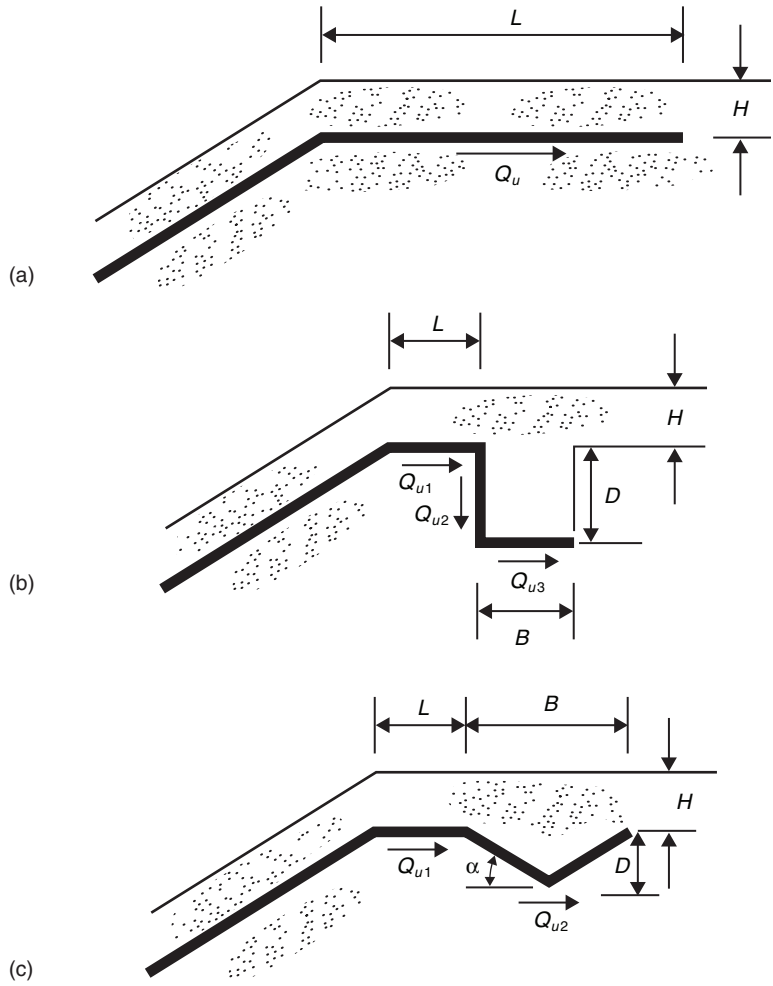

FIGURE 10.8 Notations used to develop design equations for anchor resistance (or ultimate pullout capacity): (a) simple runout, (b) rectangular trench, and (c) V-trench (adapted from Hullings and Sansone, 1997)

lying soil may crack and move along with the geosynthetic layer, Q_u should be calculated considering only the resistance on the underside of the geosynthetic layer (Figure 10.8a). Thus:

$$Q_u = W \tan \delta_L = LH\gamma \tan \delta_L \tag{10.4}$$

where

W = weight of overlying soil
L = runout length
H = height of overlying soil
γ = unit weight of soil
δ_L = interface friction angle of the lower side of the geosynthetic layer

For a rectangular trench anchor (Koerner, 2005; Hullings and Sansone, 1997) (Figure 10.8b):

$$Q_u = Q_{u1} + Q_{u2} + Q_{u3} = (LH\gamma \tan \delta_L) + \left[(1 - \sin \phi)\gamma \left(H + \frac{D}{2}\right)\right](\tan \delta_L + \tan \delta_U)D + [B(H + D)\gamma(\tan \delta_L + \tan \delta_U)] \quad (10.5)$$

where

D = depth of the trench
B = width of the trench
δ_U = interface friction angle of the upper side of the geosynthetic layer
ϕ = friction angle of the soil

For a V-trench anchor (Hullings and Sansone, 1997) (Figure 10.8c)

$$Q_u = Q_{u1} + Q_{u2} = (LH\gamma \tan \delta_L) + \left[\gamma B \left(H + \frac{D}{2}\right)(\tan \delta_L + \tan \delta_U)\right] \quad (10.6a)$$

with no movement of soil back over the V-trench portion, and

$$Q_u = Q_{u1} + Q_{u2} = (LH\gamma \tan \delta_L) + \left[\gamma B \left(H + \frac{D}{2}\right)(\cos \alpha \tan \delta_L + \sin \alpha)\right] \quad (10.6b)$$

with movement of soil back over the V-trench portion, where

B = depth of the trench
α = inclination of the side slope of the trench to the horizontal

It should be noted that Equations 10.4 to 10.6 consider the frictionless pulley assumption partially, and they have resulted from stress-based analyses. They are not ideal solutions; their validation is required with the data obtained from suitable laboratory and/or field tests. Figure 10.9 illustrates the variation in ultimate pullout capacity (or anchorage resistance) of various trench anchors for HDPE geomembranes with interface friction angle, considering interface strength on one side only.

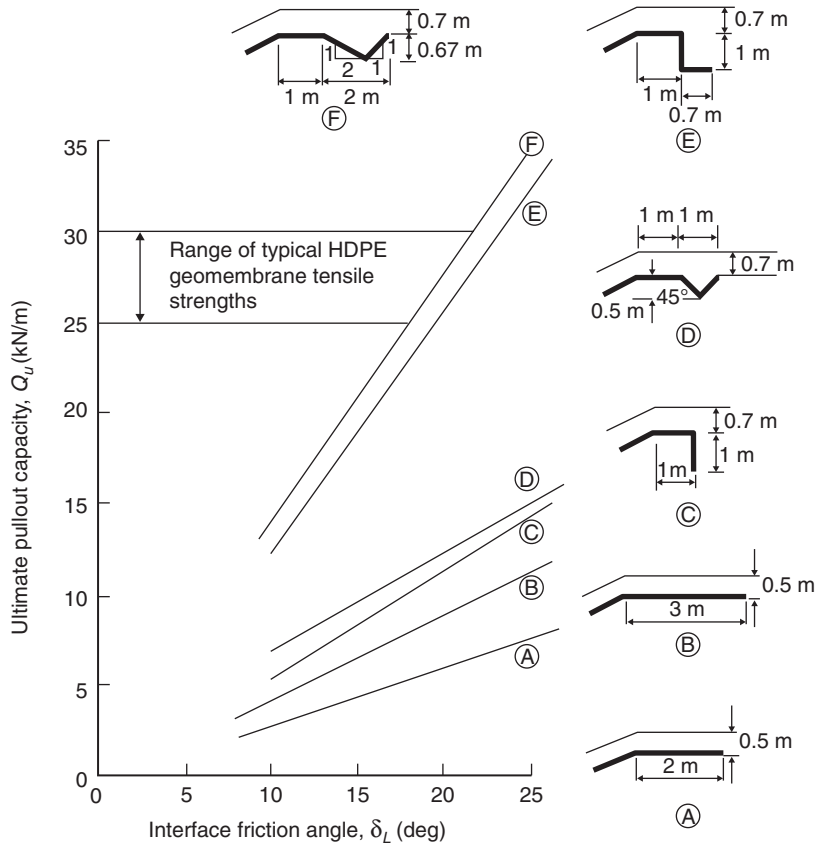

FIGURE 10.9 Ultimate pullout capacity (or anchor resistance) of some typical runout and trench anchors for HDPE geomembranes (adapted from Hullings and Sansone, 1997)

10.4 SUMMARY OF MAIN POINTS

1. A geotextile-wrapped anchor consists of a permeable core of coarse sand, gravel, or crushed stone wrapped in one or several layers of high-strength woven geotextiles. When installed within an unstable soil system, this anchor also works as a drain during the rainy season.
2. The required spacing of geotextile-wrapped anchors and their dimensions depend on the pore water pressure in the slope, which can be evaluated by means of a flow net. The required tensile strength of the geotextile can be calculated by considering the force polygon for the sliding soil mass above possible sliding surfaces in the soil.
3. Compaction of the granular fill in geotextile-wrapped anchors should be done in the downhill direction in order to pretension the geotextile layer.
4. The trench anchor is commonly used for firmly securing the geosynthetic layer installed as a pond/canal liner or slope surface protection. Anchorage selection greatly depends on site conditions.
5. As a basic design principle, the trench anchor resistance should not exceed the allowable stress in the geosynthetic layers at any stage of construction and operation during the design life of trench anchors.
6. Rectangular trench anchors do not require a lot of room, and they can be constructed with a small backhoe. A V-trench anchor can be an intermediate choice between runout and rectangular trench anchors.
7. Since the overlying soil may crack and move along with the geosynthetic layer, the ultimate pullout capacity of runout and trench anchors should be calculated considering only the resistance on the underside of the geosynthetic layer.

SELF-ASSESSMENT QUESTIONS

Select the most appropriate answer to each multiple-choice question

10.1. A geotextile-wrapped anchor can be used to:
   a. increase the stability of steep slopes
   b. reduce the lateral earth pressures on retaining structures
   c. stabilize embankments constructed on soft clay
   d. all of the above

10.2. The geotextile layer in geotextile-wrapped anchors acts as:
   a. a filter
   b. a reinforcement

c. both a and b
d. a drain

10.3. For practical applications of geotextile-wrapped anchors, their maximum installation depth can be:
a. 1 m
b. 2 m
c. 4 m
d. 10 m

10.4. Which of the following geosynthetics is commonly used in geotextile-wrapped anchors:
a. woven geotextile
b. needle-punched nonwoven geotextile
c. thermally bonded nonwoven geotextile
d. geogrid

10.5. Which of the following anchors requires a large runout length to produce significant pullout resistance:
a. runout anchor
b. rectangular trench anchor
c. V-trench anchor
d. narrow trench anchor

10.6. Which of the following anchors does not require a lot of room:
a. runout anchor
b. rectangular trench anchor
c. V-trench anchor
d. both a and c

Answers

10.1: d 10.2: c 10.3: c 10.4: a 10.5: a 10.6: b

REFERENCES

Broms, B.B. (1993). Geo-anchors. *Geotext. Geomembr.,* 12(3):215–234.

Broms, B.B. and Wong, I.H. (1986). Stabilization of slopes in residual soils with geofabric. *Proc. 3rd Int. Conf. Geotextiles,* Vienna, 295–300.

Hullings, D.E. and Sansone, L.L. (1997). Design concerns and performance of geomembrane anchor trenches. *Geotext. Geomembr.,* 15(4–6):403–417.

Ingold, T.S. and Miller, K.S. (1988). *Geotextiles Handbook,* Thomas Telford, London.

Koerner, R.M. (2005). *Designing with Geosynthetics,* Pearson, Prentice Hall, Upper Saddle River, NJ.

Shukla, S.K. (2012). *Handbook of Geosynthetic Engineering,* second edition, ICE Publishing, London.

Shukla, S.K. and Yin, J.-H. (2006). *Fundamentals of Geosynthetic Engineering,* Taylor and Francis, London.

INDEX